2024

Revealing Structures in Data:
Understanding Innate Behaviors and Neural Representations Using Latent Variables

Oihane Horno Garcia

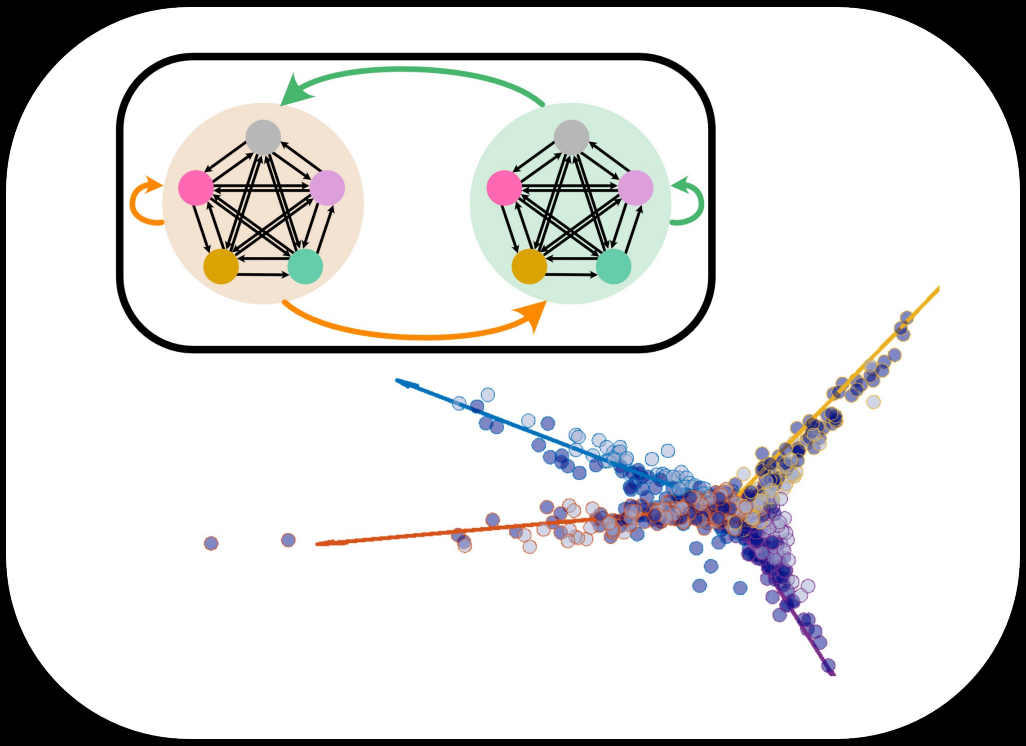

Dissertation presented to obtain the **Ph.D degree in Neuroscience**

International Neuroscience Doctorate Program

Oeiras, February 2024

INSTITUTO DE TECNOLOGIA QUÍMICA E BIOLÓGICA ANTÓNIO XAVIER | UNIVERSIDADE NOVA DE LISBOA

REVEALING STRUCTURES IN DATA: UNDERSTANDING INNATE BEHAVIORS AND NEURAL REPRESENTATIONS USING LATENT VARIABLES

OIHANE HORNO GARCIA

A DISSERTATION
PRESENTED TO THE UNIVERSIDADE NOVA DE LISBOA
IN CANDIDACY FOR THE DEGREE
OF DOCTOR OF PHILOSOPHY IN NEUROSCIENCE

SUPERVISED BY: DR. CHRISTIAN MACHENS
CO-SUPERVISERD BY: DR. LEOPOLDO PETREANU & DR. SUSANA LIMA
INTERNATIONAL NEUROSCIENCE DOCTORAL PROGRAMME
CHAMPALIMAUD RESEARCH
LISBON, PORTUGAL

2024

I feel, therefore I can be free.

- *Audre Lorde*

Acknowledgements:

It takes a village to write a thesis. This journey wouldn't have been possible without the help, encouragement, support, mentorship, and joy of an enormous amount of people, who have been fundamental not only throughout my PhD but also during the many years before.

First of all, I would like to thank the jury members, Cindy, Enrique, Alice, and Jorge for accepting to be part of this last step and for taking the time to read through these pages.

I would also like to thank FCT for the financial support and ITQB for their logistical support and patiently replying to my emails. And to everyone in the GSO: Thanks for your help!

Thanks to my thesis committee Megan and Alfonso for your help, guidance, and advice over the years.

This work would not have been possible without my supervisors: Christian Machens, Leopoldo Petreanu, and Susana Lima.

To Christian, your lab has been my home for over six years. Thank you very much for taking me in. You taught me a lot about how to present data and ideas. In your lab I learned about computational neuroscience in all its different aspects, even if I have never worked with spiking neural networks, reinforcement learning, or zebrafish. I believe that, thanks to being present in all the different lab meetings, along with your insights, I have gained some understanding of the breadth of the field, which has helped me to create my own map of Neuroscience. Thank you very much for all the knowledge you provided me with.

To Leopoldo, thank you for patiently and generously letting me learn about the experimental aspects of the project. While my success in doing experiments was not what either of us thought it would be, I learned so many things that I never thought I would learn, or even knew existed, so I can only thank you for the experience. I also learned to value the immense amount of work, knowledge, and skills that doing experiments require. Thank you for sharing a bit of that with me.

To Susana, thank you very much for trusting me and taking me in. When I started my PhD, I was afraid of behavioral experiments, because I was not sure that what we were teaching the animals to do was what they were learning. However, in your lab I learned about innate behaviors and that completely changed my perspective on behavior, so thank you for letting me widen my view. I would also like to thank you for your support, positivity, and the effort you have put into it so the project would work out. I believe that you had a big role in this thesis having a happy ending, so thank you very much for that.

I would like to give a huge thank to Gabi and Banas for letting me use your data. My PhD wouldn't have been possible without all the work, effort, pain, and success your put into it. From the bottom of my heart thank you very much. With this, I would also like to thank the mice, who unwillingly gave their freedom and life so we could understand their world and ours a little better, and I hope one day we can make up for it.

To the people in the labs past present and newest members, many of whom have become friends over sharing hardship, frustration and, also, happiness. To the people in the Machens lab, thanks for being my lunch buddies and being there to listen to me complain or bring up whatever has been occupying my brain. Thank you: Nuno, Michael, Allan, Sander, Adrien, Severin, Joana, Bill, Guille, Caroline, Francesca, Matthijs, and Ildelfonso. To the people in the Petreanu lab, thanks for the support with experiments, for your help, patience, time, and wisdom. Also my kudos for putting up with all the troubleshooting, failed experiments and many other challenges along the way. Thanks to: Tiago, Gabi, Marina, Hedi, Rodrigo, Radhika, Solene, Camille, Beatriz, Margarida, Flora, Gonçalo, and Pedro. Finally, to the people in the Lima lab who took an old PhD student and made them feel at ease in a new lab. You were always so nice, warm, and encouraging. Thanks for that and for everything I learned from you, about mouse sexual behavior, and all of those brain areas under the cortex. Thanks to: Margarida, Antonio, Baylor, Basma, Nico, Ana Rita, Bertrand, Inês, Liliana, and Jonathan.

In particular, I would like to take a bit more space to thank Marina, for being my bench neighbor and helping me when I was stuck extracting calcium traces or did not know how to plot something; also for taking me in, and opening the door of your place. I missed you when you were gone. To

Gabi, you always comforted me and taught me patiently how to best do surgeries and experiments and analysis and so many things... To Rodrigo, who taught me how to do my first surgery and hold me while I freaked out… To Radhika, for being my companion since we met in the interviews. I do not know how I would have done all of this without you. Thanks for being there, being my friend, and talking me out of my loops. I believe I grew so much thanks to you. To Severin, Nun, and Thandie, for letting me be part of your family. I look forward to seeing you grow older. To Baylor, your friendship has kept me fed and well over all this time. I am very happy to have met you. Thank for coming up with this project, you were so generous to share it with me. To Nico, you helped me in the last part of my thesis when I was the most lost, thanks a lot for taking the lead. To Bertrand for your advice, help, and happiness. To Francesca, for giving me hope that some people actually get what they deserve, I am very happy to see you flourish.

To my other CCU friends, Jaime for always listening to my crazy ideas and views and encouraging me to pursue them. To Razvan for encouraging and supporting me to write about hierarchies and Aristotle. To Kristin for being my library buddy and lunch buddy. To Ece, for your kindness and friendship and making the effort of being there, I am very grateful one day you decided I was going to be your friend.

I would also like to thank my friends outside of work that helped me and support me over the years. To Catia, Miss Brown sugar, for holding a space in the studio so we can leave the outside world behind and do something different, fun, and challenging. With you I have learned that I was stronger than I thought, and you gave the strength to face many challenges; thanks a lot for sharing that space with us. To Michael, for being the first person doing a PhD I've ever met. I believe that without having met you, my life would have been so different. Thanks for being there and sharing your life with me over all these years, and always visiting me wherever I go.

Thanks to my friends of my Cuadrilla and extended cuadrilla. Thanks to: Ainara, Andrea, Arrate, David, Garazi, Kris, Leire, Maitane, Zumaia, Imanol, Aner, Silvia… I am so happy at some point our path crossed and we got to grow up together. You all taught me so much. I am built of pieces of you, that's why I can leave home and not feel homesick; I always feel you with me. I cannot wait

to keep getting to know you. I hope that one day we will live closer and can share a day-to-day life. Eskerrikasko hor egoteagatik, maite zaituztet.

To Bill, for being you and going through life with me, thanks for your kindness and support. Thanks for being there when I need you, even right now as I press send bottom while freak out.

To the first people that taught me what it was to be part of a lab or to be a Graduate student. Thank you: Shiva, Mehran, Shahrazad, Athina, and Damian for all the adventures, parties and teaching me how to be an adult.

To Carla, Berta, Katy, Dortxi, Chelli, Bobby, Dimitri, Gato Luna, Luna, Dora, and all the animal friends, thank you for being.

To all my teachers whose work has allowed me to be here, in particular to Maite Landatxe, Xabier Lezeta and Izaskun Aldaz. There were many times while I was writing this thesis that I was thinking of you and everything I learned from you – thank you.

To the people that hold the vigils every Wednesday, take the streets and use their voice, their bodies, their life so this world can be a better tomorrow. Thank you.

To the seventeen-year-old me, for one day thinking that you wanted to study the brain using computers, and even though you did not know about neuroscience you just went and found out for yourself, this thesis is for you.

Finally, and foremost, I would like to thank my parents: Amaia y Javier. Gracias por los enormes esfuerzos que habeis hecho durante tantos años para que yo hoy pueda estar escribiendo este texto. Gracias Ama por siempre estar ahi, por hacerme compañia a traves del telefono cada vez que voy o vuelvo de trabajar. Gracias Javier por ser mi botillero. Um abrazo enorme os quiero mucho.

And to you reader.

THANK YOU ALL!!! ☺

Titulo

Revealing structures in the data: Understanding innate behaviors and neural representations using latent variables

Sumário

Esta tese compreende dois projectos distintos. O primeiro projeto utiliza a Análise de Componentes Principais (PCA, em ingles), uma técnica de redução de dimensionalidade, para investigar como uma população de neurónios no córtex visual primário de murganho (V1) representa estímulos visuais na presença e ausência de feedback cortico-cortical direto (FB) das Áreas Visuais Superiores (HVA, em ingles). Especificamente, examinámos a representação de dois estímulos distintos: grelhas flutuantes e um filme naturalista. Os nossos resultados demonstram que as alterações na representação são específicas do estímulo. No caso das grelhas flutuantes, a ausência de feedback leva a um aumento do ganho populacional, enquanto no caso do filme naturalista, altera a geometria de representação. Estes resultados apoiam a noção de que o feedback fornece informação contextual aos neurónios V1.

No segundo projeto, investigamos a estrutura organizacional do comportamento sexual do murganho, uma área que carece de uma caraterização abrangente. Utilizando um modelo de hidden Markov (HMM, em ingles), fornecemos provas de que os períodos pré-copulatórios e copulatórios previamente identificados estão de facto presentes na organização do comportamento. No entanto, a transição entre esses períodos não pode ser definida apenas pela presença de um motivo comportamental específico. Além disso, exploramos a influência da experiência do macho na organização do comportamento e descobrimos que os intervalos entre montas são os mais afectados. A

nossa análise revela que é necessário um mínimo de três sessões para que a organização do comportamento se estabilize.

Palavras-chave

PCA, V1, FB, comportamento sexual, HMM, murganho

Abstract

This thesis comprises two distinct projects. The first project employs Principal Component Analysis (PCA), a dimensionality reduction technique, to investigate how a population of neurons in the mouse primary visual cortex (V1) represents visual stimuli in the presence and absence of direct cortico-cortical Feedback (FB) from the Higher Visual Areas (HVA). Specifically, we examine the representation of two distinct stimuli: drifting gratings and a naturalistic movie. Our findings demonstrate that changes in representation are stimulus specific. In the case of drifting gratings, the absence of feedback leads to an increase in population gain, while for the naturalistic movie, it alters the representational geometry. These results support the notion that feedback provides contextual information to V1 neurons.

In the second project, we investigate the organizational structure of mouse sexual behavior, an area that lacks comprehensive characterization. Utilizing a Hidden Markov Model (HMM), we provide evidence that previously identified pre-copulatory and copulatory periods are indeed present in the behavior organization. However, the transition between these periods cannot be solely defined by the presence of a particular behavioral motif. Furthermore, we explore the influence of male experience on behavior organization and find that inter-mount intervals are the most affected. Our analysis reveals that a minimum of three sessions is required for the behavior organization to stabilize.

Keywords

PCA, V1, FB, Sexual behavior, HMM, mouse

Author Contributions

Author contributions are detailed at the beginning of every chapter. Overall, In the first chapter Gabriela Fioreze and Leopoldo Petreanu designed the experiment. Gabriela Fioreze did the experiments and the single neuron analysis. Oihane Horno did the population level analysis and wrote the chapter. Christian Machens supervised the analysis.

In the second Chapter Silvana Araujo and Susana Lima designed the experiments. Silvana Araujo did the experiments and annotated the videos. Bertrand Lacoste did the pre-processing of the data. Oihane Horno did the analysis and modeling and wrote the chapter. Christian Machens supervised the analysis.

Financial Support

The work described in this monograph was performed under the International Neuroscience Doctoral Programme (INDP 2017), funded by the Fundação para a Ciência e Tecnologia (FCT) with a doctoral fellowship (PD/BD/128303/2017) and the Champalimaud Foundation.

Overview

This thesis is divided into 4 chapters. Chapter 1 provides a general introduction to the different concepts and literature relevant to the work presented in this thesis. It delves into the historical evolution of neurophysiology, behavior, and the notion of latent variables, all of which are intricately linked to the subsequent discussion of the two projects

Chapter 2 describes the results of using dimensionality reduction techniques in a calcium imaging dataset of area V1 in the mouse visual cortex. The dataset contains imaging data of the same set of cells when they receive feedback inputs from higher-order visual areas (HVA) and when such feedback is silenced in the terminals. The results of this chapter focus on understanding the link between previously described results using single cell analysis and the populational level analysis using principal components analysis as a dimensionality reduction method. Finally, it describes a metric that distinguishes gain modulation changes and coding changes to precisely understand how the complexity of the stimulus influences the population response.

Chapter 3 describes the application of stochastic models to describe behavioural data. In particular, using a longitudinal dataset of mouse sexual behavior, it describes how a hidden Markov Model (HMM) can be used to accurately identify the different stages of behavior as well as the relationship between different motivational states. Lastly, taking into advantage that it is a longitudinal study, the role of experience is explored.

Finally, Chapter 4 is a general discussion of all the work presented in the thesis. We also discuss some future directions considering our findings.

Table of Content

List of Figures

List of Abreviation

A	Anterior - chapter 2
A	Anogenital Investigations – chapter 3
aCSF	Artificial cerebrospinal fluid
AI	Artificial Intelligence
AL	Anterolateral
AM	Anteromedial
AOB	Accessory olfactory bulb
AOE	Accessory olfactory epithelium
BNST	Bed nucleus of the stria terminalis
CNNs	Convolutional Neural Networks
CNO	Clozapine-N-oxide
CoA	Cortical amygdala
cpd	cycles per degree
Ctrl	Control group of axonal silencing experiment
DREADD	Designed Receptors Exclusively Activated by Designer Drugs
E	Ejaculation
FB	Feedback connections
FF	Feedforward connections
G	Self-Genital Grooming of the male
gOSI	Global orientation selectivity index
hM4D(Gi)-FB	Chemogenetically silenced HVA axonal group
HMM	Hidden Markov model
HVA	Higher visual areas
Hz	Hertz
IMI	Inter-mount intervals
ITI	Inter-trial interval – chapter 2
ITI	Inter-thrust interval – chapter 3
L1	Layer 1
L2/3	Layer 2/3
L4	Layer 4
L5	Layer 5

L6	Layer 6
LI	Laterointermediate
LM	Lateromedial – chapter 2
LM	Last mount – chapter 3
MeA	Medial amygdala
MI	Mounts with Intromission
MM	Markov model
MOB	Main olfactory bulb
MOE	Main olfactory epithelium
MPOA	Medial preoptic area
MT	Middle-temporal area
MwoI	Mounts without Intromission
OS	Orientation Selective
OSN	Olfactory sensory neurons
P	Posterior
PAG	Periaqueductal gray area
PCA	Principal Component Analysis
pdMeA	posterior dorsal Medial amygdala
PETH	Peri-event time histogram
PM	Posteromedial
PMv	ventral Premammillary nucleus
POR	Postrhinal
PPC	Posterior parietal cortex
PR	Progesterone receptor
PTV	Postero-temporal visual
RF	receptive field
RL	Rostrolateral
rm	Repeated measures
ROI	Region of interest
SVD	Singular value decomposition
V1	Primary visual cortex
VMH	Ventromedial hypothalamus
VNO	Vomeronasal organ
VSN	Vomeronasal sensory neurons

Chapter 1 – General Introduction

Gure zuhaitza landatu dugu,
amildegi muturrean.
Adarrak daude ertzetik haruntz,
Sustraiak, berriz, lurrean.

-Benito Lertxundi eta Jon Maya;
Itsasoari begira[1]

1.1 The question of being

[1] We planted our tree at the edge of the cliff.
The branches are beyond the edge.
The roots, on the other hand, on the soil.

''Once there were many stories for the world [2],…

We wonder because we are profoundly influenced by the world around us. When we witness a beautiful sunset, we may question what the mechanisms of vision are. When we fall in love, we might.ponder how our feelings and actions relate. Engaging and wondering about the world, around and within ourselves, is an intrinsic aspect of the human experience. The questions that we ask, how we answer them, and even their interpretation is intimately related to the socio-historical context, the analysis tools available, and the technology we have available (Haraway, 1988). To describe the interdependence of technology, science, and society in the field of philosophy of science, Gilbert Hottois (1980) coined the term 'techno-science' (see Vincent & Loeve, 2018 for a historical perspective on the term).

Some questions (What being a human means, why do we behave in a given way, etc.) have been around for longer than we can account for, and we may not be closer to answering them today. Every era focuses on questioning particular aspects of human experience, and their answers are then used to shape the way we understand ourselves. In this way, the way we view ourselves nowadays is influenced by the way we explain ourselves using neuroscience. This epistemology follows a lineage of thought that I will summarize in the following sections.

…, now only a few remain.''

[2] Sam Winston, One and Everything, p1

1.2 The birth of Man a Machine[3]

In Europe, the renaissance was a period of change. It was a break from the believed dark past of the Middle Ages and a welcome to a progressive future inspired by Ancient Greek civilization and values, bringing a renewed belief in reason. Mathematics and physics were revolutionizing the way people understood the world, with Copernicus, Harvey, Kepler, Galileo, and Newton spearheading this change. Machines were becoming more sophisticated, including the inventions of Leonardo da Vinci and letterpress printing by Johannes Gutenberg. Such machines intertwined craftsmanship and mechanical knowledge, providing them with a new meaning and position in society (Snider, 2022). René Descartes (1596-1650), father of primitive neuroscience and one of the fathers of modern science and philosophy, admittedly based his explanations of the physiological bases of behavior on the moving statues found in royal gardens (Brown, 2023), liminal machines merging artifice and humanity—a reminder that since the conception of modern science, technology and science have always had an intertwined development.

Descartes, and previously William Harvey (Harvey, 1657), proposed the workings of animals and humans as analogous to that of the hydraulic-powered mechanical statues (Descartes,1998, V). Further, he argued that the only difference between human or animal behavior, and that of the machine is the complexity of the mechanism. As we will see later, this human-machine analogy had implications that have resonated until nowadays. Importantly, he further distinguished humans and animals by the unique existence of a soul for humans, located in the pineal gland (Descartes,1998, I). Therefore, while humans were capable of thought, animals were not.

[3] Julien Offray de La Mettrie, first published in 1747.

Understanding humans (to some extent) and animals as machines had two fundamental consequences for the development of neuroscience research (Cobb, 2002): (1) the study of human behavior could be done through analogous animal behaviors, and (2) since those behaviors were mechanical in nature, they must obey the laws of nature and, thus, could be studied through the scientific method.

These game changing ideas inspired Swammerdam, who, in the 1670s, studied the movement of frog legs (Swammerdam, 1758, p122–132). Taking a reductionist approach, he was convinced he would be able to learn something fundamental about behavior. The results of his experiments he delineated the first principles of reflex movements. According to which, the movement was an outcome of muscular contraction in response to an external 'irritation' of the nerve. Interestingly, he generalized this notion to the contraction or dilation of the pupil in the presence or absence of light, which also, in his view, causes irritation to the nerve (for a review see Cobb, 2002).

As we have seen, the ideas of Descartes opened the door to the incipient study of nerve function. However, the distinction between animals and humans - The fundamental differentiation between the entity that engages in thought and the object that is the subject of thought (Harrison, 1992) - delimited what could and could not be scientifically studied. While the renaissance and the enlightenment promoted the study of science, Christianity had a fundamental role (and power) in shaping people's beliefs and understanding of the word. The division of each human into animal-like and god-like aspects agreed with Christian beliefs, while promoting the study of science. In this sense, the study of the physiology of movements (reflexes) was scientific. It did not involve the soul; thus it could be studied in animals and then be extrapolated to humans. On the other hand, ideas, their associations, and their relationship with actions

(what we nowadays refer to as psychology, behavior and neuroscience) was not thought to be measurable, as they belonged to the soul. Philosophers interested in this topic, such as Hume (1711 - 1776), kept a safe distinction between the thought process and neurophysiology (Baggini, 2002). This split has been a key pillar of Western thought.

1.3 A brief history of neurophysiology

The discoveries made by Swammerdam were groundbreaking. However, how this 'irritation' translated into movement was still a mystery. Further advancements of this research would not have been possible without the parallel advances in electromagnetism. In 1791, Luigi Galvani discovered that electrical stimuli elicited a response in the leg muscles of the frog using a similar preparation to Swammerdam. He concluded that animals have what he called 'animal electricity'. In his view, the muscles acted as electrical reservoirs and by applying external conductors he was able to induce contractions as the internal electricity flowed.

This finding created a big commotion in the scientific community, and a long debate ensued with Alessandre Volta about the existence or not of the so-called 'animal electricity' (for detail see Piccolino, 1997). The debate ended with Volta discovering the battery and Galvani retracting his findings. However, nowadays we know he was the first one to describe the electrophysiological properties of biological tissue (Piccolino, 1997).

In the 1860s Julius Bernstein, following up on the experiments of Emil Du Bois-Reymond and Hermann von Helmhotz, measured what he called the 'action potential' of the nerves (Bernstein, 1971). However, an important question was still in the air: were the nerves composed of individual cells or was it a continuous substance? The answer to this question was only possible due to the development of the Golgi staining method (Golgi,

1873), which allowed Ramon y Cajal (1888) to identify the neuron and its morphological properties. This discovery was ground-breaking and gave rise to the neuron doctrine, or the view of the neuron as the fundamental unit of the nervous system (Bullock et al., 2005). This doctrine has dominated neuroscience for over a hundred years, providing substantial understanding of neural properties and their communication. As we will see in section 2.1.6, recent theoretical formulations have started to shake the stablished neuron doctrine, giving rise to the network doctrine, or the understanding of neurons as part of a network rather than individual units (Yuste, 2015). Moreover, recent advancements in electrophysiology and imaging have allowed us to simultaneously record hundreds of neurons, allowing to prove such theories.

We are able to collect an amount of neural data that has not been possible until very recently, suggesting that we might be closer than ever to gaining a comprehensive understanding of neural computations. However, the immensity of the data has brought new challenges. How can we deal with such big datasets and gain meaningful insights about the neural computations? As we will see, mathematical techniques to reduce the dimensionality of the data while keeping it major characteristics intact have become indispensable to understanding big datasets.

How the neuron doctrine applies to vision neuroscience and the insights we have gained so far will be covered in Chapter 2. Additionally, dimensionality reduction techniques will be applied to understand the relationship between single neuron activity and population coding.

Advances in Neurophysiology have gone hand in hand with advances in technology. However the understanding of behavior has mostly been shaped by changes in the theoretical understanding of what life is.

1.4 A brief history of Behavior

As mentioned earlier in this chapter, the origins of 'neuroscience' research were fundamentally dualist in nature. Thus, what nowadays is termed *higher cognitive* abilities pertained to the soul, which in turn was also thought to play a role in behavior. However, not everyone agreed with this view. In the mid-18th century, David Hartley emerged as one of the first monist Western philosophers. He took a novel physiological approach in the way he understood the formation of 'ideas', perceptions, thoughts, and emotions. In his view, 'association'' was seen as the physiological process by which these mental functions would either connect and merge or separate and disperse (1749). Moreover, he rejected the idea that humans were any different than animals or that there was something beyond the body.

In the realm of behavior, Hartley stressed the role of experience or 'association'. In his view, certain movements could be classified as 'originally automatic' (Hartley, 1749, prop. 19). This includes internal body movements such as heart rate or bowel movements. Interestingly, movements that may begin as automatic. can turn voluntary through the process of association. This would be the case of walking for instance: a child may try to walk innately ('originally automatic' movement) and then through the association of his movement with other outcomes (reaching for a toy, for example), this movement would transform into a 'volitional' movement (Hartley, 1749, prop. 20). Further, he reinforced the role of experience through repetition of the same action, making it second nature or 'secondarily automatic' (Hartley, 1749, prop. 21). Nowadays, we refer to this term as muscle memory and it is what allows performers to play an instrument in front of an audience without having to think of every movement. Particularly, Hartley's work was foundational in understanding

the association between the mind and the body without the interference of the soul and acknowledging how the environment or the outcome of our actions may shape our future behavior.

During the following century, many researchers including Paul Broca (Broca, 1861; Finger, 2004), and Carl Wernicke (Wernicke, 1874; Pillman, 2003) were eager to understand the relationship between different brain areas (particularly the cortex, the outermost layer of the brain) and human behavior. In 1848 the case of Phineas Gage showed the dark side of the brain-behavior relationship (Ratiu et al., 2004). Gage's personality completely transformed after he suffered a terrible workplace accident. While laboring on the railroad tracks, an iron rod penetrated his skull, resulting in the ablation of several brain areas. This tragic incident served as a poignant demonstration of the profound influence that the brain exerts over our behavior.

While different findings started to shed light on how behavior was manifested, several questions were still unresolved. On one hand, it was unclear whether there was a difference between humans and animals and what that difference (if any) entailed. On the other hand, the field of taxonomy, which identified the different animal species, families, and genus, struggled to gain scientific credibility, as it seemed like a collection of facts and descriptions rather than hypothesis driven (Cronquist, 1969). All of this changed in 1859, when Charles Darwin published "On the Origin of Species". His theory of evolution provided an explanation for the field of taxonomy and placed humans as just another animal (with the consequent repercussions of the time (Glick, 1988)). Darwin's groundbreaking work introduced the concept of adaptation, providing a framework to comprehend animal behavior within the context of natural selection. This transformative theory, coupled with Mendel's insights into trait inheritance, offered a coherent framework that began to provide

answers to the until then mysterious characteristics of animal behavior, laying the foundation for the field of ethology (Ellis et al., 2015).

Ethology is the study of animal behavior, generally innately present. In ethology the understanding of the behavior becomes the central scientific question, which is often addressed through ethograms – an objective description of the behavioral motifs displayed by the animal and their organization. It aims to study the interplay between genetic, adaptative and environmental factors and the organization of the behavior. The field of ethology slowly emerged after Darwin's proposal of evolutionary theory, however, Konrad Z. Lorenz, Nikolaas Tinbergen, and Karl von Frisch are considered the fathers of modern Ethology after being awarded the Nobel Prize in 1973 (Marlen & Griffin, 1973; Font, 2023).

Nowadays the development of video cameras, genetic tools and optogenetic approaches have made it possible to dissect behaviors and gain insights into their neural underpinning. Perhaps ironically, sexual behavior is one of the least studied innate behaviors (Ågmo & Ellingsen, 2003; Ventura-Aquino, 2017). A detailed understanding of each behavior is fundamental to gain meaningful insights into its neural underpinnings. In this light, in Chapter 3, we will analyze the organization of mouse sexual behavior and what the role of male experience might be.

1.5 The latent variable approach

The understanding of how a network of neurons operates or how behaviors are organized is a complex task. In both cases, as in many others in science, the data that we deal with is multivariate and has a degree of redundancy. Distinguishing a meaningful characteristic from redundancy or noise can be a great challenge. A way to solve this issue is to transform the data into linear combinations of the observed variables,

resulting in a model of latent variables or factors that accurately reflect the predominant association patterns within the dataset (Kvalheim, 2012). This strategy is called the latent variable approach, as the high dimensional data is replaced by a few latent summarizing factors that are sufficient to represent the data. These factors are then used for plotting, further analysis, and understanding the data.

Psychology research pioneered the development of latent variables, as since its early beginning it faced the challenge of how to validate the association between covarying variables. This obstacle was beautifully stated by Spearman (1904):

''In psychology, more perhaps than in any other science, it is hard to find absolutely inflexible coincidences; occasionally, indeed, there appear uniformities sufficiently regular to be practically treated as laws, but infinitely the greater part of the observations hitherto recorded concern only more or less pronounced tendencies of one event or attribute to accompany another. (…) One after another, laborious series of experiments are executed and published with the purpose of demonstrating some connection between two events, wherein the otherwise learned psychologist reveals that his art of proving and measuring correspondence has not advanced beyond that of lay persons.''

The earliest and simplest form of a latent variable is correlation, proposed by Galton (1886). Correlation provides a qualitative measure of the extent to which a series of measurements relate or correspond with each other. Particularly, Galton proposed a quantification tool to relate the length of the arms and the length of the legs. This work was later extensively developed by Pearson and Spearman. The latter went further and proposed that the covariation between the two variables suggested a

hidden underlying source of variation (Spearman, 1904). The idea of having a hidden source that would explain the observed covariation changed the paradigm of psychometrics and led to the development of Factor Analysis (Bartholomew, 1995).

Around this time, Pearson (1901) proposed a more mathematics-oriented approach: the Principal-axis method. This was a matrix factorization technique that allowed to decompose a number of correlated data variables into uncorrelated (orthogonal) factors. The solution proposed by Pearson had two drawbacks that made it hard to use at the time (Kvalheim, 2012).

The first was the complicated computations one had to do to factorize the matrix. In a time without computers this was indeed a major challenge. The second was that the extracted latent variables, while uncorrelated, were not necessarily interpretable. A few years later, Thurston proposed the centroid method (Thurston, 1931; 1947). This method proposed an approximation to the principal-axis which facilitated its computation. More importantly, it utilized a linear combination of the computed orthogonal latent variables to favor interpretability of the data (Thurstone, 1947). Currently, thanks to the advances in graphical interfaces, rotating the obtained graph to make sense of the data may seem trivial. However, at the time when such visual aids were not possible, departing from the orthogonal framework to create an interpretable reference frame was a big breakthrough. Thus, it rapidly gained popularity and acceptance and was later developed into more sophisticated and rigorous methods (Ahmavaara & Thurstone, 1954; Kaiser, 1958; Hurley, & Cattell,1962; Hendrickson, & White, 1964).

In the 90s, thanks to the development and availability of computers, Spearman's principal-axis method, or currently better known as Principal

Component Analysis (PCA) has gained the popularity it originally lacked (Hotelling,1933). Due to its descriptive and 'hypothesis free' approach, it has become a common technique to reveal the hidden structure of neuroscience data (McClurkin et al., 1991; Kjaer et al., 1994; Chapin et al., 1999; Chapin & Nicolelis, 1999). This method will be extensively covered in section 2.1.7 and used to analyze the data in chapter 2.

The above methods and their later developments are appropriate to describe stationary data. However, how could one deal with *changes over time*? As advanced, the 20th century was the century of information technology. The theoretical and technical pillars were laid out for the development of computation and cybernetics. In parallel it was a time of geopolitical unrest, which made many scientist's research orient towards war and defense strategies. This was the case for Norbert Wiener, who developed a time-series analysis to predict the target of aircraft bullets. This forecasting analysis was based on the foundational work of Andrei Andreevich Markov, a mathematician that set the foundations of the probability theory known as Markov Models (Markov, 1906, pp. 143–158).

The development of sequential analysis, and Markov Models in particular, initiated a prolific time in ethology (Altman, 1965; Sebeok, 1965; Dingle, 1969) and psychology (for a review written at the time see Mosteller, 1957) for the understanding of the temporal patterns of behavior (particularly learning) and communication. Probabilistic analysis of patterns provided a unique chance to describe what was becoming more and more clear to both fields: while the behavior of an individual depends on previous actions, future actions do not follow a deterministic rule, rather they behave in a seemingly stochastic manner (Altman, 1965).

A Markov Model is a probabilistic model in which each of the states is an observable and the current state is sufficient to determine the transition

probability to the next observables. This is a powerful model to characterize non-deterministic behavior, as we will see in section 3.1.8. However, it has an underlying assumption that is violated in most biological applications. It assumes that there is no internal or hidden parameter that would determine the transition from one state to another. The development of more advanced computers and algorithms (Kouemou & Dymarski, 2011) allowed Markov Models to become more sophisticated. Particularly, in the 60s the statistician Leonard E. Baum published a series of seminar papers describing the Hidden Markov Model (HMM) (Baum, & Petrie, 1966; Baum, & Eagon, 1967; Baum & Sell, 1968; Baum et al., 1970; Baum, 1972). HMM models were initially used for speech recognition within the United States Defense Institute (Baker, 1975; Jelinek et al., 1975). While initially it was an obscure technique (Rabiner et al., 1986), after the publication of an accessible tutorial (Rabiner, 1989) its use expanded beyond the forecast of the authors (Rabiner, 2015).

The particularity of the Hidden Markov Model is that transitions between the different observables is a stochastic process given by hidden factors. Therefore, they model observables in two distinct layers: an observable layer and an hidden layer. This characteristic is very appealing in behavioral data. A detailed description of this model is given in Section 3.1.8, and it will be applied to behavioral data in Chapter 3.

The use of latent variables has become a fundamental feature of the study of complex systems. In a time where science has become more fragmented and specialized than ever, data analysis methods employing latent variables have become a common thread between fields (Kvalheim, 2012). From a mathematical point of view, latent variables allow for the creation of a reduced space that makes a complex problem much more tractable and easily depictable (Kvalheim, 2012). Further, one cannot

forget the role of the personal computer. Without such a powerful computing machine at one's disposal, it would be hard to imagine the widespread use of such complex algorithms. Finally, is interesting to consider that there might be something inherently human about using a latent reduced space to understand complex data. In fact, John Stuart Mill (1843) suggested that the latent variable approach generally connects to how humans absorb information, creating patterns and associations between ideas (Kvalheim, 2012).

In the opening of this chapter, I discussed how Descartes introduced a metaphor that paved the way for a mechanistic understanding of human and animal functioning. Just as he saw aspects of humanity mirrored in the movements of mechanical statues, today we see our resemblance to Artificial Intelligence and, more broadly, computing systems. Nowadays, we conceptualize brain processing as a complex and sophisticated analogue of computer operations. However, whereas Descartes believed the mind's hidden states and motivations were beyond scientific reach, through the development of mathematical techniques, we have enabled their rigorous and systematic exploration. Almost four hundred years later, the description, characterization, and comprehension of hidden variables is at the forefront of Neuroscience research. In this thesis this approach will be used to make sense of neural data responding to visual stimuli and to find the organizational structure of ethological behavior.

Chapter 2 - Changes in visual stimuli representation upon silencing feedback from Higher Order Visual Areas to V1

2.0 Autor contribution

Experimental conception and design Leopoldo Petreanu (L.P.) and Gabriela Fioreze (G.F.). Experiments G.F.. Data pre-processing G.F. Data analysis G.F, Marina Fridman and Oihane Horno (O.H.). Supervision and mentoring for Population-level analysis Christian Machens. Population-level analysis O.H. Writing O.H.

2.1 Introduction

2.1.1 The act of seeing

As living organisms, we are embedded in and interact with the external world. These interactions are possible because of the sensing organs of our bodies. Since modernity, sight has gained a privileged position in Western cultures (Levin, 1993; Ong & Hartley, 2013). Notably, most metaphors we use daily are based on visual evocations: ‘envisioning something’, ‘to bring light to a matter’, ‘bright future’, ‘at first glance’, etc. Due to its cultural importance, it is not surprising that much of the body of sensory processing in Neuroscience has focused on vision (Hutmacher, 2019).

Although the process of seeing may seem passive and camera-like — photons arrive at a sensor, in our case the retina, and an image is recreated — in reality, it is nothing of the sort. First, we actively position our bodies and heads to improve our perception (De Winkel et al., 2021; Oie et al., 2002; Peterka, 2002). We also constantly move our eyes with saccades and micro-saccades to gain full access to what is in front of us (Deubel & Schneider, 1995; Martinez-Conde et al., 2013). Even when we perceive an image, this perception is not *perfect* or immutable. Optical

illusions are great examples of how our brains use contextual and expected information to recreate and interpret what we see (Figure 2-1 A). Thus, what is the process that allows us to see?

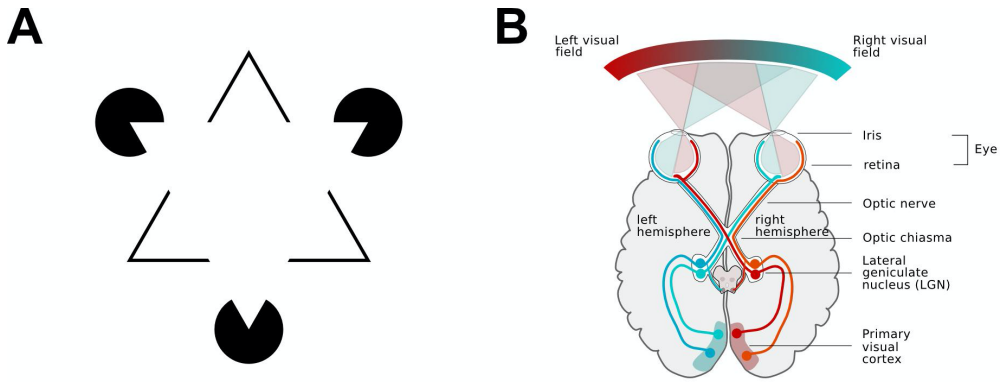

Figure 2-1 Visual Illusion and Visual Pathways

A. Kanizsa Triangle visual illusion. An illusory contour is created by the three pacman shapes (Kanizsa et al., 1979). The resulting triangle seems brighter and closer to the observer than the rest.
B. Schematic of the visual pathway from the eyes to the primary visual cortex. The visual field is captured by the retina on each of the eyes and further sent to the primary visual cortex. The optic chiasm is the place where the left and the right visual fields separate.

In most mammals, the visual process starts when photons hit the eye (Illustration in Figure 2-1 B, from top to bottom). They enter through the iris into the retina, a light-sensitive tissue located in the innermost layer of the eye. The photosensitivity of the retina is attributed to two types of photoreceptor cells: rods and cones. When photons activate these cells, they trigger a cascade of electrical and chemical signals, ultimately generating an action potential in the retinal ganglion cells. The axons of the retinal ganglion cells form the optic nerve. The optic nerve transmits the visual information from each of the eyes to both brain hemispheres. The path crosses in the optic chiasm. The crossing allows for the separation of the right and the left visual fields into the left and right brain

hemispheres respectively. The optic nerve primordially reaches the brain through the thalamus, a brain structure located at the top of the forebrain. Specifically, it projects into the lateral geniculate nucleus (LGN). While other areas are also innervated, visual flow is believed to initiate in LGN. The LGN then transmits the information to the visual cortex.

2.1.2 The hierarchical organization of the visual cortex

The cortex is the outermost portion of the brain in mammals, though analogous structures to the cortex can be found in other animals (Güntürkün, & Bugnyar, 2016). The cortex was first characterized by Edinger in 1899, while he was looking for a brain structure that would explain the cognitive capabilities of humans (Patton, 2015). It is believed that the cortex plays a fundamental role in sensory, motor, and cognitive processes such as learning and decision-making. Starting in 1903 to 1914, Brodmann published a series of articles characterizing the distinct cortical areas, including the occipital lobe or the visual cortex (Brodmann,1903a; Brodmann ,1903b; Brodmann 1905a; Brodmann, 1909; for more information about his extensive research see Zilles, 2018). Each of these cortical areas have a specific sensory, motor, or cognitive function. Since then, the cortex has remained one of the main areas of study in neuroscience.

The mammalian visual cortex is composed of many different areas, and it is thought to be hierarchically organized. This means that the visual information follows a sequentially organized pathway, where each level of the hierarchy processes more complex information than the preceding one. It was the experimental work of Hubel and Wiesel in 1962 that proposed the notion of hierarchy to describe cortical organization. They presented a cat with a visual stimulus composed of edges with different

orientations while they recorded single units along different locations of the visual field. They found that many units, called simple cells, responded if the edge was present in their receptive field (RF) and if it had a particular orientation. The RF is the region in visual space which elicits a reliable response from the neuron (Sherrington, 1906). They also found a second class of cells, named complex cells, that did not need the stimulus to be in their RF to respond, and some could also respond to moving stimuli (Hubel & Wiesel, 1962). Additionally, the response latency of complex cells was larger than that of simple cells. They explained the complex cell responses as a result of a serial feedforward architecture. In this framework, several lower-order neurons (simple cells) innervate higher-order neurons (complex cells). The complex cells integrate the simple cells' responses to simpler features and generate a more complex response. This concept sparked the idea that the different visual cortical areas could be hierarchically organized.

The cortex is composed of six stacked laminae or layers (L1-L6) (Baillarger, 1840). Foundational work tracing the laminar projections across the different visual areas of the non-human primate revealed an intricate architecture of hierarchical connections, most of which are excitatory connections (Rockland & Pandya, 1979). The Feedforward connections (FF) originate from L2/3 in the lower areas and terminate most densely in L4 of the higher areas. The reciprocal Feedback connections (FB) originate in L5 and L6 of the higher areas and terminate in L1 and L6 of the lower areas (Figure 2-2 A). Following this organizational principle, Maunsell and Van Essen, and later Felleman and Van Essen, proposed an anatomy-based hierarchically organized map of all the primate visual areas (Illustration of the simplified map, Fig 2-2 B) (Maunsell & Van Essen, 1983; Felleman & Van Essen, 1991). One should notice that while useful, this hierarchical organization of the visual cortex is an oversimplification. The anatomical structure is not strictly

hierarchical, nor the visual processing rigorously follows the anatomical hierarchy (Hegdé & Felleman, 2007).

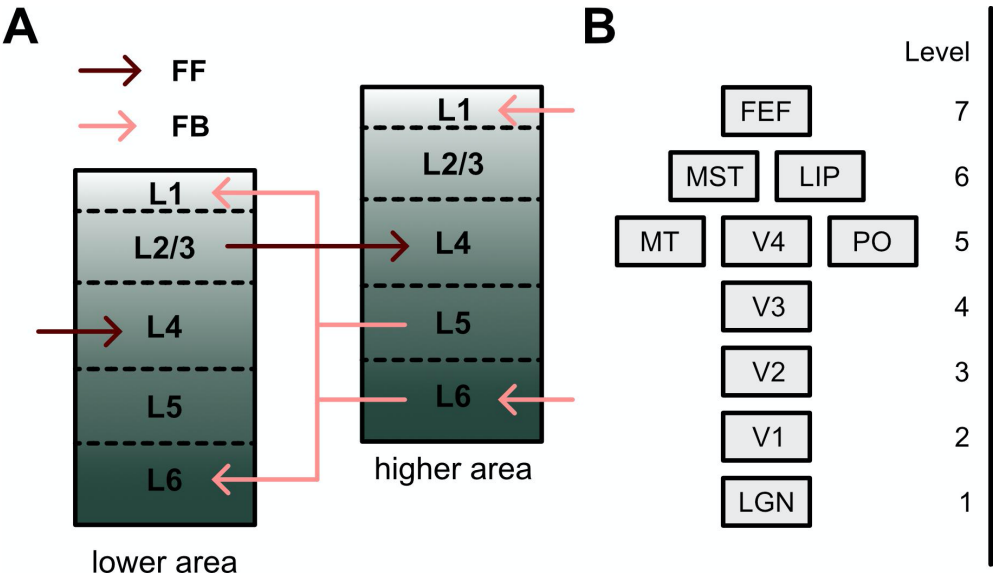

Figure 2-2 Organization of primate visual cortex

A. Illustration of the feedback and feedforward projections between a lower and a higher area. Pink lines illustrate feedback connections and dark red lines feedforward connections.
B. Illustration of the simplified map of Felleman and Van Essen. Each square represents an area and its location the level in the hierarchy, adapted from (Capalbo et al., 2008)

While the anatomical connections between the areas have been well studied and a role for FF connections was proposed after Hubel and Wiesel's studies, what the role of feedback may be was (and is) still unclear. Thus, some researchers turned to the area of theoretical neuroscience in the search for answers.

2.1.3 Models of visual perception

The fields of Experimental Neuroscience, Theoretical Neuroscience, and Artificial Intelligence (AI) have maintained a continuous dialogue over time (MacPherson et al. 2021). Despite pursuing distinct objectives, their communication has been instrumental to their advancement. Experimental neuroscience contributes biological findings to theoretical neuroscience, which in turn aims to systematize and formalize these insights. Meanwhile, AI prioritizes the practical application of its concepts. Although not inherently tethered to biological fidelity or biologically plausible solutions, AI frequently draws inspiration from Neuroscience's progress (Hassabis et al. 2017). Concurrently, Theoretical Neuroscience is influenced by the mathematical innovations of AI (Marblestone et al. 2016). Considering this ongoing exchange, it is easy to see how the results of Hubel and Wiesel transformed the field of computer vision.

Hubel and Wiesel's main conclusion relied on a core computational idea: that complex visual perception of an image can be reduced to local and simple features – lines and edges - that are integrated through a serial hierarchy through the visual pathway. This idea provided a computational role to feed-forward connections that was incorporated into the already existing perceptron model (Rosenblatt, 1958, 1961, 1962). Several layers that mimic the computations done in the visual pathway were added, giving birth to the Neocognitron algorithm (Fukushima 1980; Fukushima et al., 1983). This algorithm was further developed and formalized into feed-forward Convolutional Neural Networks (CNNs) (LeCun, 1998) (Illustration on the relationship between visual pathways feedforward connections and Convolutional Neural Networks Figure 2-3 A). Such models were successful at differentiating handwritten digits and brought high hopes to the artificial intelligence community (Cox & Dean, 2014). However, their performance was limited, as they were hard to train and

were based on a large parameter space. The architectures incorporated backpropagating error signals, (Werbos in 1974; LeCun et al.,1989), which sent back the errors of the higher layers into the lower ones, with the aim to increase their performance. As computer power increased, this approach later gave rise to what is known nowadays as deep learning (For a review see LeCun et al., 2015) — a powerful approach in computer vision and image generation (Voulodimos et al., 2017), however known for its limited interpretability and questionable biological plausibility (Saxe et al., 2021).

Interestingly, state of the art neuroscience models of the visual hierarchy are currently made of deep convolutional neural networks, whose activity can be directly compared to the brain (Yamins & DiCarlo, 2016). On the other hand, current state of the art machine learning models have diverged from this direct connection to the visual hierarchy (e.g., vision transformers; Dosovitskiy et al., 2020) but they do use an attention-like mechanism which is vaguely related to perceptual attention (see Lindsay 2020). In the recent years, deep neural networks have proven useful to generate stimuli that would elicit a maximal response in different areas of the cortex (Bashivan, et al., 2019) or to predict responses (Cadieu, et al., 2014; Yamins el al., 2014; Cadena et al., 2019). However, understanding and developing best practices to make use of this algorithms to uncover the principles of visual computations in the brain is still in the making (Saxe et al., 2021). Despite its potential use in understanding experimental neuroscience data, perhaps it was the birth of deep learning that diverged the paths of AI and Theoretical Neuroscience. While AI focused on leveraging computational power and developing mathematical tools to enhance algorithmic performance (Rahwan et al., 2019), Theoretical Neuroscience aimed to elucidate normative principles governing brain function.

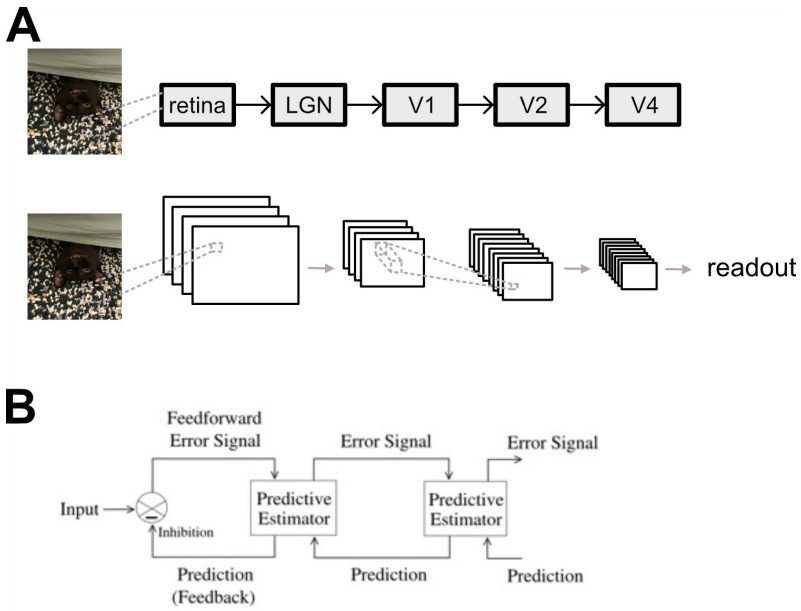

Figure 2-3 Illustration of different models of visual perception

A. illustration of the forward model and its correspondence with the forward pathway of the cortex. Adapted from (Cox & Dean, 2014)
B. Architecture of predictive coding model. From Rao & Ballard, 1999.

As mentioned, primitive perceptual models were based on the feedforward picture from Hubel & Wiesel (1962). However, feedback, an equally ubiquitous connection type was mostly left out of the picture. The framework of normative approaches aimed to elucidate the functional role to feedback connections. Olshausen and Field's seminal work in 1996 demonstrated that a set of neurons could develop bandpass RFs that were localized and oriented, akin to the ones measured by Hubel and Wiesel. Two key computational principles were necessary for this: sparsity in neuronal representation, and minimal discrepancy between the ensemble representation of neurons and the true image – ensuring the preservation of information. Highlighting that optimizing the right cost function resulted in a biologically plausible network implementation. However, this was limited to one hierarchical stage.

A few years later, Rao and Ballard (1999) incorporated a third principle: predictive coding. In their framework, neuronal ensembles learn the statistical patterns of their environment and only signal deviations from these patterns. This approach assigns functional roles to each element in the visual pathway. At each hierarchical stage, feedforward inputs convey error signals from lower areas, while feedback inputs convey predictions from higher areas. Each area's role is to compute the predicted estimation based on these inputs. (See Figure 2-3 B for an illustration). This hierarchical architecture explains the increase in receptive field (RF) size with the hierarchical level. Consequently, it elucidates the phenomenon of surround suppression observed in Hubel and Wiesel's experiments (Hubel & Wiesel, 1968; Boltz & Gilbert, 1986). In surround suppression, when an oriented bar exceeds a neuron's RF, its response decreases. According to the predictive-coding framework, the neuron reduces its firing rate because the prediction from the higher area aligns with the feedforward input, resulting in no prediction error and thus no signal sent upwards.

Building upon the concept of feedback inputs as both generative and predictive, Lee and Mumford (2003) proposed a theory of hierarchical Bayesian inference for visual perception. This framework is part of a genealogy of work started by Helmholtz in 1867 of understanding the brain as an unconscious inference machine. According to this framework, the visual system leverages prior experiences to continually infer and disambiguate between conflicting stimuli, thus shaping perception. In this context, visual illusions like the illusory contour depicted in Figure 2-1 A can be understood as the brain's attempt to reconcile conflicting inputs by generating the simplest perceptual interpretation: for instance, inferring the presence of a white triangle occluding black circles in the background, resulting in the hallucination of a contour.

While there have been great advances in the understanding of visual processing, the theoretical frameworks are still in their infancy. One of the main reasons is that the role of feedback connections and how they shape the stimulus representation on each of the areas is still unknown. Perhaps, more experimental data from an animal model that allows for genetic manipulations and experiments may help to gain more knowledge about the role of FB.

2.1.4 Mouse visual cortex

Although primates and cats have been the main subjects of study in the field of visual perception, nowadays the usage of mice has become widespread. The study of the mouse visual system offers several advantages (Huberman & Niell, 2011). The genetic tools available in mice surpass the ones available in any other mammals. Additionally, their size and fast reproductive cycle makes them a much more accessible model organism to study. It is worth noting that there are several differences between mice, and primates or cat visual systems, both because of the mouse's ethology and its much-reduced brain volume. Perhaps, the most important difference is that mice have poorer visual acuity (for a review see, Niell & Scanziani, 2021). However, key anatomical and functional similarities indicate that the computational principles may be preserved across species.

Primary visual cortex (V1) is one of the most studied brain areas in humans, primates, cats, and mice. It is located in the dorsal area of the posterior cortex, and it is the main receiver of LGN input (See Figure 2-1 B). Mouse V1 is retinotopically organized (Wang & Burkhalter, 2007). This means that neighboring locations in the visual field will be represented by

neighboring locations in V1. This organization preserves the spatial information from the visual field, maintaining the topographic mapping of visual input. Furthermore, as in primates and cats, neurons in mouse V1 are finely tuned to oriented edges (Niell & Stryker, 2008). However, there is a notable distinction. Cat and primate V1 neurons follow a columnar organization, where neurons tuned to similar orientations are topographically arranged (Hubel and Wiesel, 1962, 1963, 1968; Ts'o & Guilbert, 1988; Leventhal et al., 1995; for a historical view on the developments of the organizational models see Dow, 2002). On the contrary, mice V1 lacks such organization, following what is called a salt-and-pepper organization (Ohki et al., 2005).

V1 sends afferent projections to higher visual areas (HVA), which will in turn send efferent projections to V1. The number, arrangement, and nomenclature of the mouse HVA has evolved through the years, becoming more precise thanks to technological advances (Caviness, 1975; Wagor et al., 1980; Olavarria & Montero,1989, Wang & Burkhalter, 2007; Garrett et al., 2014. For a review see Glickfeld & Olsen, 2017). The latest studies of Garrett et al. (2014) identified nine HVAs using intrinsic imaging; anterior (A), anterolateral (AL), anteromedial (AM), laterointermediate (LI), lateromedial (LM), posterior (P), posteromedial (PM), postrhinal (POR), and rostrolateral (RL). (Figure 2-4 A). Two-photon imaging experiments have shown functional specialization of such areas (Andermann et al., 2011 and Marshel et al., 2011).

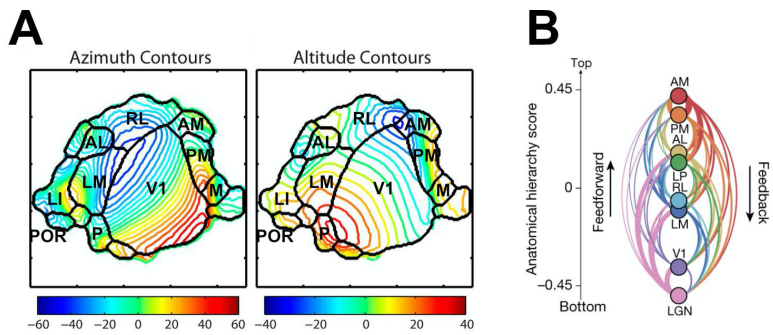

Figure 2-4 Mouse visual cortex

A. Topographic organization of the mouse visual cortex. Average azimuth (altitude) contours, in degrees, show progression of the horizontal (vertical) retinotopy from temporal (lower) fields in red to the nasal (upper) field in blue. Area boundaries are shown in black. Modified from Garrett et al., 2014.
B. Hierarchical organization in the mouse visual cortex. Anatomical hierarchy scores of the different areas and the feedback and feedforward connections between them. From Siegle et al., 2021.

Cortico-cortical connections in the mouse have the same anatomical stereotypes as those described earlier in primates (Figure 2-2 A). The response latency and size of RFs increases along the visual hierarchy as it does for cats and primates (Siegle et al., 2021). However, the hierarchy in the mouse visual cortex is shallower (Harris et al., 2019; D'Souza et al., 2022). As an example, while in the primate visual pathway eight levels are needed for a RF to integrate 40 degrees of the visual field, in the mouse only four are needed (D'Souza et al., 2022). In addition, feedback projections to mouse V1 are not limited to visual areas. V1 receives a vast array of feedback inputs from other cortical areas (Leinweber et al., 2017; Mazo et al., 2022), perhaps suggesting that visual perception is a more integrative process than previously thought of (Pennartz et al., 2023).

In primates, two pathways of visual information can be identified, the ventral or 'what' stream and the dorsal or 'where' stream. In the mouse, such streams are also identifiable, although with more diverse properties

(Han, et al., 2022). The analogues to the ventral stream compose areas LM, LI, P and POR. The dorsal stream analogue areas are AL, RL, PM, AM and A (Oh et al., 2014; Zingg et al., 2014). HVAs preferentially encode different spatial-temporal properties of the visual stimulus. AL and RL neurons preferentially encode fast speed (Andermann et al., 2011; Marshel et al., 2011; Tohmi et al., 2014) LM, AM, and LI prefer medium speeds (Marshel et al., 2011; Tohmi et al., 2014), and PM prefers slow moving stimuli (Andermann et al., 2011). For a review see Burkhalter et al., 2023. The functional specializations observed in HVAs could arise from the functionally specific patterns of information sent from V1 neurons to each HVA (Glickfeld et al., 2013).

Neuronal responses within the mouse HVAs are complex, as measured through the representations of natural images and movies (Vries et al., 2020). Additionally, they exhibit diverse encoding properties such as mixed selectivity, where neurons can encode various parameters, such as stimuli from different sensory modalities (for a review refer to Glickfeld & Olsen, 2017). The complexity of signals in HVA neurons prompts the question of whether their feedback projections to V1 convey essential information to modulate the activity of V1 neurons. To answer this question, one has to first understand the main properties V1 responses to visual stimuli.

2.1.5 Stimulus representations in mouse V1

Oriented gratings and moving dots have been the main stimuli used to characterize V1 responses across species. As mentioned, it has been canonically believed that V1 neurons were primarily driven by oriented edges of a particular orientation, static or drifting. Neurons that are driven by such stimuli are called orientation selective (OS). Although mice have

poor vision acuity, V1 neurons have high precision coding of stimulus orientation, and they can discriminate stimuli with a 0.35º threshold (Stringer et al., 2021b). For a review on how orientation selectivity arises refer to Ferster & Miller, 2000. OS neurons respond to oriented bars or gratings in their RFs. Notably, when the stimulus extends beyond their RFs their responses are reduced. This effect is called surround suppression, or context modulation, and it has been experimentally shown to be mediated by feedback projections (mice: Vaiceliunaite et al., 2013; Self et al., 2014; monkeys: Angelucci & Bullier, 2003; Angelucci & Bressloff, 2006). For a review refer to Angelucci et al., 2017. Interestingly, the opposite effect can also be true. In the presence of an oriented grating with an occlusion, orientation-selective neurons in V1 with a RF in the occluded location will respond to the grating (Schnabel et al., 2018; Keller et al., 2020; Kirchberger et al., 2023).

Another approach to probe the functional role of V1 is to use naturalistic images. The main reason for such an approach is that naturalistic images conserve the spatial and temporal frequencies present in nature, and for which the visual cortex has evolved to process. Thus, neural responses to such images are also more similar to the ones naturally occurring and can provide valuable insight into the underlaying computations (Kayser et al., 2003; Nastase et al., 2020). V1 responses to naturalistic images are reliable and sparse, both for static (Yoshida & Ohki, 2020) and moving images (Froudarakis et al., 2014), aligning with the sparse coding hypothesis. This hypothesis states that given the brain's limitations (the number of neurons, the energy consumption, and maximal number of spikes per neuron, among others) in order to efficiently code for the external world, the brain has to code for each stimulus sparsely by ignoring the redundant information and only representing the informative bits (Field, 1987;1994). Interestingly, it seems that sparse representation of stimulus a broad characteristic of other sensory modalities (Rinberg et

al., 2006; Hromádka et al., 2008; Poo & Isaacson, 2009; Sachdev et al., 2012; Mayrhofer et al., 2015; Liang et al., 2019)

In science, to have accurate measurements, the same experiment must be conducted several times. In vision neuroscience, this translates to repetition of the same stimulus over several trials. However, due to the nature of the brain, each repetition is not independent, and several factors can affect the trial-to-trial variability, including the lack of control of all the experimental conditions. A major source of change over repetitions is adaptation (Gibson, 1933; Barlow, 1989; for a review see; Kohn, 2007 and for theoretical mechanisms underlying adaptation Weber et al., 2019 and Carandini & Heeger, 2012). On longer timescales, when longitudinally tracking the response to a stimulus over days, researchers found that the tuning of V1 neurons was not stable (Deitch et al., 2021; Marks & Goard, 2021; Xia et al., 2021). This phenomenon is called representational drift. The stability of the representation is stimulus dependent; the representation of natural images is less stable than that of drifting gratings (Marks & Goard, 2021), suggesting that OS may be more of an intrinsic property of the neurons. Importantly, while single neuron representations were not stable, the population coding was (Deitch et al., 2021, Xia et al., 2021). Thus, even if individual responses varied day-to-day, the manifold in which the stimulus representation was located was stable. This finding highlights how population analysis can be very useful to further understand the functionality of the visual cortex.

2.1.6 Beyond the Neuron doctrine

Since its initial description by Ramon y Cajal (1888), the neuron has been thought to be the main functional unit of the brain. The reduction of brain function to the single neuron led to the belief that if we understand the

single neuron, we will be able to describe the functions of different brain areas and their relationships. This enterprise began with the previously mentioned mapping of receptive fields and tuning properties of the neurons in different areas. The identification of the 'bug detector' neuron (Lettvin, 1959), and later the 'Jennifer Aniston' neuron also known as 'grandmother cell' (Quiroga et al., 2005) led to the idea that neurons might be the perceptual units of the brain (Barlow, 1972). In fact, stimulation of very few (Salzman, 1994) or even single neurons (Brecht et al., 2004; Houweling & Brecht, 2008) could elicit measurable behavioral changes in primates and rodents. The assumption of the single neuron as the fundamental unit of perception and behavior naturally raises other questions (Yuste, 2015): If every person or concept that we know of is represented by a single neuron, how likely is the researcher to record exactly from that neuron in a given experiment? And further, what happens if this neuron dies? Would the person or concept itself be forgotten?

Perhaps it is more likely that groups of neurons code for these concepts in coordination instead (Yuste, 2015; Saxena & Cunningham, 2019; Ebitz & Hayden, 2021). Such network-level coding would explain other phenomena, including trial-to-trial variability measured when recording responses to the same stimulus. Anatomical data supports this network-level coding idea, demonstrating that each neuron receives inputs from many neighboring neurons, simultaneously sending outputs to many, partially overlapping neurons (Shepherd, 1990; Braitenberg, & Schüz, 1998). Recent technological developments in electrophysiology and in neuronal imaging — multi-array electrodes and the more recent neuropixel probes (Steinmetz et al., 202), plus calcium microscopy and novel mesoscope (Sofroniew, 2016) techniques — allow researchers to simultaneously record from hundreds of cells. As the increase in the number of neurons being recorded becomes more feasible, a new

challenge arises: how do we make sense of this high-dimensional data (the recording of hundreds of neurons over many trials)?

One solution is to use dimensionality reduction techniques. Such tools combine the activity of the recorded neurons into a smaller set of latent variables that summarizes the data. The advantage of these methods is that they can help to find interpretable descriptions of neuronal representations, while providing information about their structure as well.

2.1.7 Principal Component Analysis

A common unsupervised dimensionality reduction technique is Principal Component Analysis (PCA) (Pearson, 1901). Depending on the discipline, this technique can be referred to as the Karhunen-Loève transformation (Karhunen & Joutsensalo, 1995), the Hotelling transformation (Hotelling, 1933), the method of empirical orthogonal functions, and singular value decomposition (SVD). This approach remaps the data into orthogonal axes that maximally explain the variance of the data. This analysis can be very insightful because it shows how the variance is distributed along the dimensions of the data, and the properties of such dimensions.

To illustrate this method, we can use the simplest case where we have the activity of two neurons (x_1, x_2) over some trials. Figure 2-5 A shows an example of how the activity looks for the different trials in the neural space. PCA extracts the direction along which the activity varies the most; this direction is the first principal component. Since we have two neurons, we can have a maximum of two principal components. The second, and last component is then orthogonal to the first one and captures the remaining variance. Once we have obtained the mapping from the neuronal to the principal components space, we can plot the activity in this space instead

(Figure 2-5 B). PCA is not only useful because it can reveal structure in the data, but it is also a very powerful tool to visualize the data.

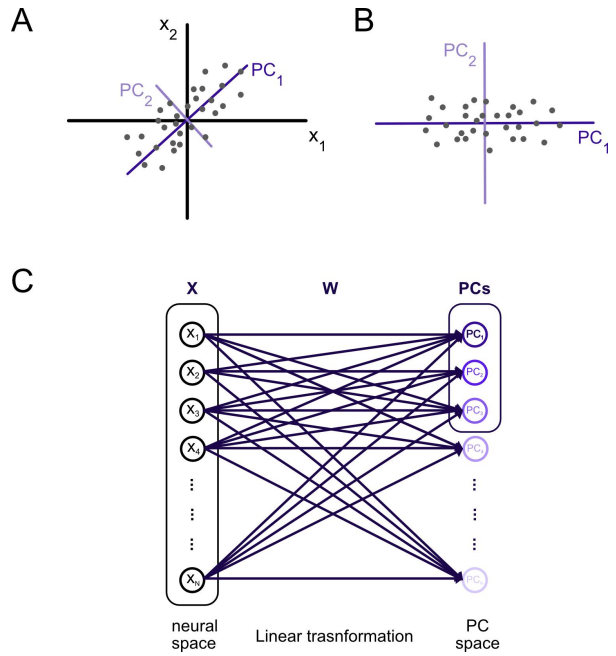

Figure 2-5 Illustration of PCA analysis

A. Activity in neuron space. Single trial activity of neurons x_1 and x_2 for the individual trials (gray dots). The axes along which the data varies the most are the principal component axes. The main principal component is depicted in purple and the second principal component in light purple.
B. Activity in principal component space. Single trial activity is projected into the PC axis (gray dots). The co-fluctuation of activity disappears as this is being captured by the PC. The main principal component is depicted in purple and the second principal component in light purple.
C. Illustration of the linear transformation done by PCA. The activity in the neural space **X** is transformed by the matrix **W**, creating the principal component space. The arrows indicate the weights of each of the neurons to the different PC. The lightness of the purple represents the degree of the variance explained by each of the PCs.

As mentioned, PCA works by extracting the principal axes along which the data varies the most, while keeping the components orthogonal between each other. Let's say that we have recorded *N* neurons over *K* trials, creating a matrix $\boldsymbol{X}_{N \times K}$. We want to obtain a linear transformation of

the neurons ($\boldsymbol{w_1}$) so when we project the data into it ($\mathbf{X}^T \cdot \mathbf{w_1}$), it keeps the maximum variance of the data; this is the first principal component. Further, we want to find a second linear transformation of the neurons ($\boldsymbol{w_2}$) that maximally captures the variance that is remaining (removing the variance explained by the first component) when we project the data into it (second principal component), thus this linear combination is orthogonal to the previous one ($\mathbf{w_1} \cdot \mathbf{w_2} = 0$). We can continue doing this up until the last component (the N^{th}), which is orthogonal to the previous N-1 components. The combination of all the components would keep all the variance of the data, as it is just a rotation of the axes. There are many ways to derive the principal components of a data set. Here we will explain the eigenvalue decomposition as it is the approach that has been taken in the project.

To start, it is important to center the data before going forward with the analysis. This means that the mean value of every neuron across trials should be equal to zero.

$$\tilde{X} = X - \frac{\sum_{i=1}^{N} x_i}{N} \quad (1)$$

There are multiple reasons for doing this. The main one is that we are interested in understanding the structure of the data with respect to the different stimuli; thus, if we fail to center the data, we are at risk of the principal components capturing instead, the absolute variance of the neurons with respect to zero, rather than their mean activity (if they have different means).

As we mentioned, we are interested in keeping the variance of the data, therefore, we need to understand the relationship between the different

neurons. The covariance matrix of the data provides this information. Since the data is centered, this is the covariance:

$$V = cov(\tilde{X}, \tilde{X}) = \frac{\tilde{X}\,\tilde{X}'}{n-1} \qquad (2)$$

This matrix has the dimensions N x N and reflects how the different neurons co-fluctuate. If the covariance between the neurons i and j is positive ($\mathbf{V}_{i,j} > 0$), it means that the two neurons are correlated. Similarly, if it is negative ($\mathbf{V}_{i,j} < 0$), the two neurons are anti-correlated; while one increases in value the other one decreases and vice-versa. Lastly, if the covariance is equal to zero ($\mathbf{V}_{i,j} = 0$), then their activities are not related. Importantly, this matrix is symmetric ($\mathbf{V}_{i,j} = \mathbf{V}_{j,i}$) and positive semi-definite.

One of the most important tools in linear algebra is the eigen-decomposition of a matrix. The decomposition factorizes the matrix into its eigenvalues (λ) and eigenvectors (**w**). 'Eigen' in German means 'its own'; one can understand the eigenvectors and eigenvalues as the characteristic or latent properties of the matrix. Importantly, the eigen-decomposition of a positive semi-definite matrix such as the covariance matrix **V** reveals the latent structure of the data and has useful properties. First, the eigenvectors are orthogonal between each other. Second, the eigenvalues are real, and greater than or equal to zero. In other words, the eigenvectors create an orthogonal basis of the covariance matrix, and each of the eigenvalues reveals the 'score' of each of the bases, or how much variance they explain. Generally, we assemble the eigenvectors **w** of matrix **V** into a matrix denoted as **W**. Each column of **W** represents an eigenvector of **V**. The corresponding eigenvalues λ are arranged in a diagonal matrix denoted $\boldsymbol{\Lambda}$, where the diagonal elements contain the eigenvalues, while all other elements are zeros. The eigen-decomposition of a matrix has to meet the following constraint:

$$\boldsymbol{VW} = \boldsymbol{W\Lambda} \tag{3}$$

Since **V** is a positive semi-definite matrix, the eigenvectors create an orthogonal basis and they fulfill $\boldsymbol{W}^{-1} = \boldsymbol{W}^{T}$, and if normalized $\boldsymbol{WW}^{T} = \boldsymbol{I}$, where **I** is the identity matrix. This allows one to rewrite the equation in the following form:

$$\boldsymbol{V} = \boldsymbol{W\Lambda W}^{T} \tag{4}$$

In summary, calculating the covariance matrix of the centered data and then performing its eigen-decomposition, allows us to find orthogonal linear relations between the neurons ($\boldsymbol{w}_i$). The variance explained by each of the linear combinations is given by their eigenvalue λ_i. As we will see later, the distribution of the variance explained along the different principal components provides important information about the structure of the data. A flat distribution, where every component explains similar variance, indicates that there is not much structure — e.g., perhaps the noise is too big in relation to the signal. On the contrary, a very sharp distribution that rapidly decays to zero indicates that the data lies in a low dimensional manifold and therefore, understanding what those dimensions represent can give important insights into the neural coding.

The eigenvectors $\mathbf{w}_i$ indicate the weight or contribution of each of the neurons to the i^{th} principal component. Thus, the principal component (PC) is obtained by projecting the data $\tilde{X}$ into the eigenvector:

$$PC_i = \tilde{X}^{T} \boldsymbol{w}_i \tag{5}$$

Each of the principal components has the dimensionality of the stimulus (1xK). Additionally, the number of non-zero principal components will be limited by the number of stimuli or the number of neurons, whichever is smaller. Therefore, the Principal Components can be understood as 'super neurons' that encapsulate shared properties of the actual neurons to represent the stimulus (Figure 2-5 C). One can then focus the analysis on a particular set of principal components, reducing the dimensionality of the data while keeping the desired amount of variance.

2.1.8 Population analysis of stimulus representation

In the context of neuroscience, dimensionality reduction such as principal components analysis (PCA) has become a common tool to investigate population representations. One of the first studies in vision neuroscience to employ PCA was Hagerty et al., in 1982, where they applied PCA to a number of physiological properties of the responses to visual stimuli, with the aim of summarizing the response properties. Much more recently, employing PCA has proven useful to cluster neural responses from different cortical areas, providing an unsupervised characterization of the areas and their boundaries (Kumar et al., 2021). Along similar lines, it has also served to characterize the aforementioned dorsal and ventral processing streams in the mouse cortex (Wang et al., 2012). For a review on the use of PCA in other Neuroscience areas and its benefits see Cunningham, & Yu, 2014.

An additional benefit of PCA is that it helps to reveal the dimensionality of neural representations. When a large number of neurons are recorded, the existence of a high dimensional manifold on which the dynamics are bounded is a sign of an efficient representation (DiCarlo et al., 2012; Rigotti et al, 2013; Chung et al., 2018). However, a sizable number of

studies show that the representational manifold is bounded inside of a low dimensional plane (Chapin, & Nicolelis, 1999; Mazor & Laurent 2005; Machens et al., 2010; Churchland et al., 2012; Mante et al., 2013; Cunningham & Yu, 2014; Archer et al., 2014; Sadtler et al., 2014; Kobak et al., 2016). An important caveat of all the aforementioned studies is that the stimulus, or task complexity was low and it is know that the encoding dimensionality is dependent on the dimensionality of the stimulus (Gao et al., 2017). Stringer et al. (2019) demonstrated that when the dimensionality of the stimulus increases, the representational dimensionality in V1 increases with it, bounded by an upper limit to ensure that the representation is still smooth. This suggests that the stimulus representation lies on a maximally high dimensional manifold while still allowing for a smooth transition from one representation to another when they are similar enough. In other words, the stimulus representation balances the representation of fine and coarse stimulus features, being able to distinguish between different stimuli, while preserving their distance when coarse features are similar.

2.1.9 The role of HVA in stimulus representations

Collectively, feedback inputs from HVAs represent the major source of FB to V1 (Leinweber et al., 2017; Morimoto et al., 2021), suggesting that they may play a major role in V1 stimulus representation. One can therefore try to elucidate the role of FB by understanding how the HVAs shape the stimulus representation in V1. Traditionally this has been studied by silencing HVAs and assessing how the coding of V1 changes. One can think of V1 (or any brain area) as an integrator of information of many sources. In order to see how one given source affects the carried

computation in the target area (V1), one can silence the source and investigate how this affects the target area V1.

There are at least three different ways in which HVA can affect stimulus representations: modulation of neural activity (e.g., attention; is FB inhibitory or excitatory?), enhancement of visual perception, and providing contextual information. HVA silencing experiments show evidence for all of these hypotheses.

Modulation: Studies in squirrel monkeys (Sandell & Schiller, 1982) and cats (Bardy et al., 2006, 2009; Huang et al., 2007, 2004; Mignard and Malpeli, 1991; Wang et al., 2010, 2000) have shown that silencing areas such as the homologues of V2, V4, and PTV cortex can lead to a decrease in V1 neuron responsiveness to visual stimuli. In monkeys, cooling the middle-temporal area (MT) also reduced V1 neuron activity (Hupe et al., 1998; Hupé et al., 2001). However, the effects of inhibiting V2 and V3 found both suppressing and facilitating effects (Bullier et al., 1996; Nassi et al., 2013). In mice, inhibiting certain areas like posterior parietal cortex (PPC) led to increased V1 activity (Hishida et al., 2019), whereas optogenetic inhibition of AL or PM resulted in decreased V1 responses (Oude Lohuis et al., 2022). Additionally, optogenetic silencing of LM neurons showed mixed effects depending on the precise silencing timing (Javadzadeh, & Hofer, 2022). Furthermore, there is evidence suggesting that direct feedback inputs also influence changes in V1 neuron firing rates (Nurminen et al., 2018). However, the overall effect of HVA top-down signals on V1 — whether excitatory or inhibitory — remains unclear due to significant variability across studies, including differences in species, methods of inactivation, visual areas silenced, visual stimuli used, number of recorded neurons, and the animal's physiological state.

Perception: HVAs can improve visual perception by sharpening the tuning curves of V1 neurons or increasing their selectivity to stimulus properties such as spatial or temporal frequencies. Unfortunately, due to the small number of studies that silenced a HVA or a direct FB projection, and the contradictory results between the existing studies, it is hard to reach a consensus on whether or how HVAs play a role in enhancing V1 perception.

In the monkey literature there seems to be a bigger agreement that while neurons do not change their tuning curves in response to silencing HVAs, they do increase their selectivity to the prefer or the anti-preferred stimulus (Sandell & Schiller, 1982; Nassi et al., 2013). The cat literature also suggests no change in the tuning profiles of neurons upon silencing area 17 or 21. However, individual neurons may broaden (Wang et al., 2000; 2007) or sharpen their tuning curves (Huang et al., 2007). Mice studies show the biggest disagreement in this regard. In one study, optogenetic inhibition of area LM reduced the selectivity of V1 neurons to their preferred stimulus (Pafundo et al., 2016). Along similar lines, following a inactivation of PPC (A, AM and RL), V1 neurons lost their selectivity to particular motion direction (Hishida et al., 2019). Contrary to this, another study showed that optogenetic silencing of AL and PM decreased V1 neurons' responses to their non-preferred stimulus (Oude Lohuis et al., 2021), suggesting that FB reduces the discrimination accuracy. A similar study found that upon optogenetic inactivation of AL and PM neurons projecting to V1, V1 neurons decreased their selectivity to the preferred spatial frequencies of the silenced areas (Huh et al., 2018).

Context: Lastly, it has been suggested that HVAs may provide contextual information to V1. Therefore, they may enhance or suppress neuronal responses depending on the stimulus properties beyond the RFs of the V1 neurons. The classical phenomenon to study contextual effects on V1

is to elicit surround modulation. Surround modulation is the change (typically a decrease) of the response to a stimulus when it expands beyond the RF of the neuron. In monkeys, it has been suggested to be mediated through FB projections (Angelucci & Bullier, 2003; Angelucci et al., 2017; for a review see Angelucci & Bressloff, 2006). In mice, it is believed that it is mediated primarily by FB projections coming from area LM (Keller et al., 2020b; Vangeneugden et al., 2019). suppression has classically been studied with oriented gratings. However, stimuli of natural scenes are also able to modulate the activity of V1 neurons (Guo et al., 2005). Notably, the surround not only modulates an existing V1 response. In the mouse, it can also generate a response when there is no stimulus in the RF of the neuron, eliciting a second RF (Keller et al., 2020a). This response is dependent on HVA activity, as optogenetic inhibition of HVA reduces the response to the second RF, highlighting again the role of HVA in bringing extra-RF information to V1. The mediation of HVA in contextual modulation can be explained by their relay of surrounding information into V1. Monkey FB projections to V1 are retinotopically organized and cover a spatial range that is equivalent to the entire range involved in center-surround interactions (Angelucci, et al., 2002; Angelucci & Bullier, 2003). Recent studies in mouse visual cortex show similar results (Marques et al., 2018; Keller, et al., 2020a).

Many optical illusions function because of center-surround interactions. Illusory contours, as in the Kanizsa triangle shown in Figure 2-2 A, are also perceived by mice. Neurons with RFs in the area of the illusory contour respond even if there is no stimulus present (Pak et al., 2020). This effect is also mediated by HVAs, shown by the decreased response of V1 to illusory contours when LM neurons are optogenetically silenced. Another type of perception mediated by the presence of the surround is the figure ground segregation. This happens when an object has a different property than the background (contrast, orientation, phase or

texture), thereby making it more salient than if the background was not present. V1 neurons are thought to play a role in this effect, as they respond stronger to the figure than to the background, particularly during the delayed phase of the neural response (Poort et al., 2016). Optogenetic silencing of the HVA resulted in a decreased response to the figure in the delayed phase of the neural response (Kirchberger et al., 2021). Importantly, a follow up study showed that recurrent processes within V1 also play an important role in figure-ground segregation, suggesting a circuit within V1 that integrates FB signals in order to give rise to contextual information (Kirchberger et al., 2023). Overall, while there seem to be multiple lines of evidence of HVA FB conveying extra-RF information to V1 neurons, it is still unclear what is being sent or how this information is integrated within V1.

All these studies have help to elaborate on how HVAs and concordantly FB may affect stimulus representation on V1. However, the study of silencing HVAs in confounded when one aims to study the role of FB, as one measures the perturbation of silencing the area and the projection. Focusing on FB connections we may be able to get a clearer picture of their role.

2.1.9 Role of cortico-cortical feedback projections

Several studies have shown that the activity of lower areas can successfully predict the activity of higher areas, suggesting that bottom-up projections are large drivers of the higher-order areas activity (Nowak et al., 1999; Roberts et al., 2013; Semedo, et al., 2018). Anatomical examinations show that cortico-cortical FB projections are as dense as the reciprocal FF projections (Van Horn et al., 2000), advancing the idea that they may have an important role in visual perception. However, little

is known about their functional role. Anatomical studies of FB projections show that there is an organizational structure in the information that is transmitted. Ji et al. (2015) showed that HVAs project their FB into V1 following a patchy organization with different spatial-temporal sensitivities, allowing for a broad stimulus selectivity in V1. Furthermore, FF signals coming from V1 to HVA and reciprocal HVA FB projections to V1 follow specific loop patterns (Young et al., 2021). Specifically, these projections typically establish stronger connections with neurons in L5/6 (infragranular) layers, which then loop back to the originating source, compared to neurons that project elsewhere. However, such specificity for looped connectivity was not observed in the superficial layers. The specificity of the organizational principle governing the superficial and deep layers of the cortex hints at an intricate role of cortico-cortical FB in computations.

In fact, a functional study of FB projections from LM to V1 showed that they follow a precise organizational principle (Marques, et al., 2018). Area LM is the area that projects the most FB to V1 (Morimoto et al., 2021). Marques et al. showed that the projections, on average, send information about the same visual field area that the V1 neurons care about; i.e., they are retinotopically matched on average. Importantly, they also carry a significant amount of input from distal RFs, hinting that HVA axonal projections to V1 can be a source for contextual information.

2.1.10 Aim of the study

Visual areas do not represent stimuli in isolation. While looking at single neuron responses can be very informative, it can also be misleading. Moreover, equating neural coding solely with a neuron's firing in response to a stimulus may be overly narrow or simplistic. Instead, neuronal function encompasses various aspects: the specific timing, whether it

synchronizes its firing with other neurons, or contributes to the formation of dynamic patterns, and even if it stays silent (Fairhall, 2014). In fact, neurons across the mammalian brain and particularly in V1 are strongly interconnected (Shepherd, 2003; Braitenberg, & Schüz, 2003). As a result, individual neurons within the mammalian brain are unlikely to be significant for the overall circuit function. Instead, the circuit function is likely to rely on interactions among a multitude of neurons (Yuste, 2015; Saxena and Cunningham 2019).

Therefore, in order to understand the function of an area one may not need to focus on a single neuron, but rather on a selected ensemble. The phenomenon referred to as representational drift, the instability of single neurons' responses to a stimulus over multiple days, serves as a clear example of this concept. When looking at single neuron responses, one observes that the neurons do change their preferred stimulus and therefore one may conclude that the stimulus representation is not stable. However, looking at the population activity, one realizes that in the population such representation is stable (Deitch et al., 2021, Xia et al., 2021). The same is true when a manipulation is inflicted. Looking solely at single neuron responses may lead to the wrong conclusion as we are not aware how the population, as a whole, changes or does not, its response to the manipulation.

Additionally, from the previous section it was clear that there is a lot of conflicting evidence on what the role of the HVA in V1 stimulus representation might be. However, those studies do not tell us much about what the role of FB might be, as they silenced both the areas and the FB projections. Uniquely silencing FB projections is a much more challenging task that has only been possible recently (Nurminen et al., 2018). In this study they optogenetically silenced V2 projections onto V1 and found that

the RF of the V1 neurons increases and the surround suppression effect is reduced for the proximal surround.

Taking advantage of the technological developments of simultaneously imaging large numbers of cells and targeted genetic advances, we aim to elucidate the role of direct cortico-cortical FB from HVA to V1 in the stimulus representation of artificial gratings and naturalistic stimuli. We use a chemogenetic approach to silence all the direct cortico-cortical FB projections from the HVA to V1, while we image V1 neurons. This approach allows us to isolate the precise role that direct-FB projections from HVA have in V1 when presenting artificial and naturalistic stimuli. From previous studies of silencing HVA we expect the role of FB to be linked with contextual modulation. In order to characterize this effect further, we employ PCA to understand the population representation of the presented stimulus in V1 and how this representation is affected by FB.

2.2 Results

2.2.1 Experimental setup and approach

We developed a procedure for assessing the impact of direct cortico-cortical FB projections from HVAs on V1 visual stimulus representations. The goal is that by presenting both artificial and naturalistic stimuli with very different characteristics in terms of spatial statistics and dimensionality, a direct comparison can be drawn between the V1 representations of such stimuli with and without FB. The experiments were done using a two-photon microscope in awake head-fixed transgenic mice that were able to run at will on a linear treadmill that allowed us to measure their speed (Figure 2-6 A). The treadmill data was used to remove the running bouts to control as much as possible that the

animal was in the same state. The neural responses were measured by imaging GCaMP6s-expressing neurons in the left hemisphere of V1 while the mouse was presented with the visual stimulus monocularly in the right eye.

To assess the contribution of direct cortico-cortical HVA FB projections in V1, the same neurons were measured with intact FB and with silenced FB projections. We employed a chemogenetic approach. We used hM4D(Gi), a type of inhibitory Designed Receptors Exclusively Activated by Designer Drugs (DREADDs) (Armbruster and Roth, 2005; Armbruster et al., 2007). hM4D(Gi) acts in combination with clozapine-N-oxide (CNO) injection, and together they suppress the activity of axon terminals. For details on the surgical protocols, see Methods and Figure 2-18. Two experimental groups were employed, the control group (Ctrl), which did not express hM4D(Gi), and the experimental group (hM4D(Gi)-FB) injected with hM4D(Gi) (Figure 2-6 B). Each animal from either group was imaged for two consecutive days. On the first day, artificial cerebrospinal fluid (aCSF) was injected into V1 L2/3 to measure the baseline activity level when the direct cortico-cortical FB projections from HVA to V1 were intact. On the second day, CNO was injected into V1 L2/3, silencing the axonal terminals of the experimental group (hM4D(Gi)-FB). Injecting CNO in the Ctrl group allowed us to control for the mechanical damage of axons, off-target effects of CNO, and visual stimulus repetition. We imaged the neurons in L2/3 a layer rich in pyramidal neurons. We matched the two-photon field of view across the two imaging days and identified the neurons present on both days by their morphological features (Figure 2-6 C) (Methods).

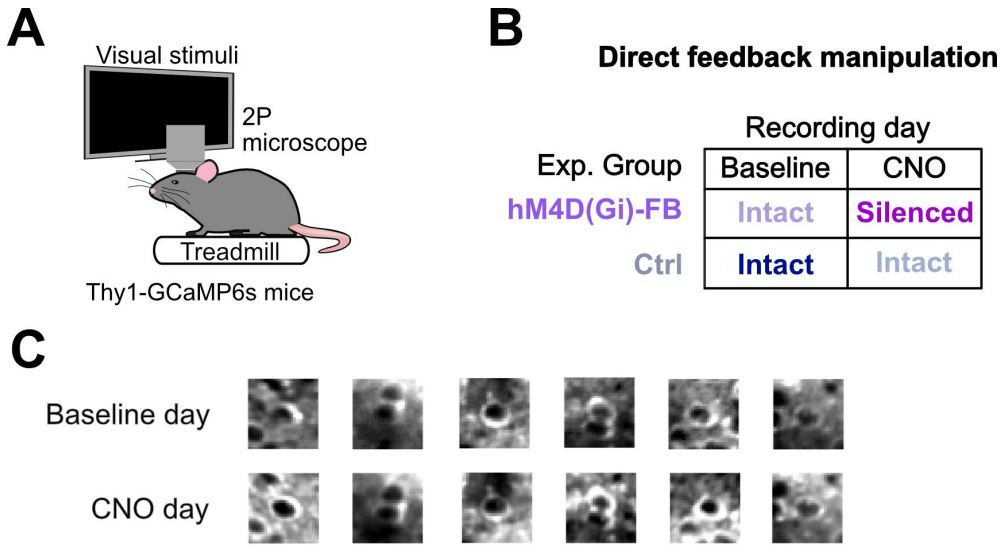

Figure 2-6 Experimental protocol and experimental groups

A. Schematic of the recording setup. To acquire the neural recordings, mice were head-fixed under a two-photon microscope while they were awake and able to run at will on a treadmill. A monitor presented visual stimuli to the mouse's right eye and the two-photon microscope recorded the V1 in the left hemisphere. Modified from Fioreze, 2022.
B. Summary of the experimental groups and recording days. Awake non-behaving mice from the hM4D(Gi)-FB and Ctrl group underwent two days of consecutive two-photon imaging immediately after an injection of aCSF or CNO in V1 (Baseline or CNO day, respectively).
C. Example tracked neurons across recording days. Two-photon imaging field of view was matched across two days of consecutive imaging and neurons present on both days were identified based on their morphology. Modified from Fioreze, 2022.

2.2.2 Feedback modulates the orientation selectivity of single neurons to drifting gratings

Gratings have been a classically studied stimulus to characterize V1 neuron response properties. Their low dimensionality and response characterizability make them a good candidate to elucidate the representational changes resulting from the silencing of the HVA FB terminals to V1. Previous studies that silenced HVAs have reported conflicting effects on V1 selectivity for drifting gratings (Oude Lohuis et al.,

2021; Pafundo et al., 2016). Using our novel experimental approach, we were able to uniquely silence the axonal projections from HVAs to V1. This protocol is less confounded because it enables testing the direct FB contribution alone, rather than both indirect and direct effects that may occur when silencing the entire area.

The full-screen drifting gratings consisted of two spatial (0.02 and 0.04 cycles per degree (cpd)) and two temporal (0.5 and 1 Hz) frequencies and four orientations moving in two opposite directions, making a total of eight directions (+/-0º, +/-45º, +/-90º, +/-135º). Each of the stimuli was repeated 20 times and presented for 0.5s after a 0.5s inter-trial interval (ITI). After preprocessing the two-photon images, we computed the normalized fluorescence $\Delta F/F0$, (Figure 2-7 A in gray) for every neural region of interest (ROI). To mitigate potential contamination from decaying GCaMP6s traces across subsequent trials, we deconvolved the $\Delta F/F0$ traces to identify events (Figure 2-7 A in black).

The tuning preference of a neuron is defined by the direction/orientation that elicits the maximum response. Figure 2-7 C illustrates the mean response of an example neuron to each of the orientations in the two days for the hM4D(Gi)-FB group. For each neuron, we combined the responses to the different spatial and temporal frequencies and the two drifting directions to calculate the orientation tuning curve for each of the days. This calculation was done taking into account the circular nature of the data, and thus computing the circular mean of the responses to the four orientations (Berens, 2009). We did not observe any significant change in the tuning curve after silencing direct cortico-cortical FB (Figure 2-7 B, hM4D(Gi)-FB group, Baseline vs. CNO, Watson-Williams test, p=1). Single neuron analysis revealed no change in the preferred orientation derived from silencing direct cortico-cortical HVA FB to V1.

We then wondered whether, while maintaining the preference for a particular orientation, the lack of HVA FB broadens or sharpens the tuning curve of the neurons. To quantify this, we computed the global orientation selectivity index (gOSI) (Mazurek et al., 2014). This index is bounded between zero and one. Values close to one suggest that the neuron has a very sharp selectivity to a particular orientation. On the contrary, values closer to zero indicate that the tuning curve is broad, and the neuron is equally selective to all orientations. We found that on the CNO day of the hM4D(Gi)-FB group, the gOSI increased compared to the baseline day (Paired t-test, p=0.0001; hM4D(Gi)-FB: 622 cells). To control for off-target effects of CNO and adaptations based on repetition of the stimulus in the second day, we calculated the per neuron difference in gOSI index: ΔgOSI ($gOSI_{baseline}$ - $gOSI_{CNO}$). Positive values indicate a decrease in the gOSI on the CNO day, negative values an increase, and close to zero values no change. We found a significant increase in the ΔgOSI hM4D(Gi)-FB vs Ctrl group (t-test, p=6x10−8; hM4D(Gi)-FB: 622 cells, Ctrl: 870 cells) when looking across all the neurons. To control that such an effect was not driven by outliers (neurons or animals), we computed the per session ΔgOSI metric (Figure 2-7 D, Hierarchical bootstrap, p=0.039; hM4D(Gi)-FB: 7 sessions from 4 mice, maximum 2 sessions per mice (51 (mouse 1),110 (mouse 1),84 (mouse 2),69 (mouse 2),124 (mouse 3),88 (mouse 3),96 cells (mouse 4)). Ctrl: 6 sessions from 4 mice, maximum 2 sessions per mice (221 (mouse 1),126 (mouse 1), 160 (mouse 2),89 (mouse 2),107 (mouse 3),167 (mouse 4) cells)). These results indicate that the neurons become more selective for specific orientations.

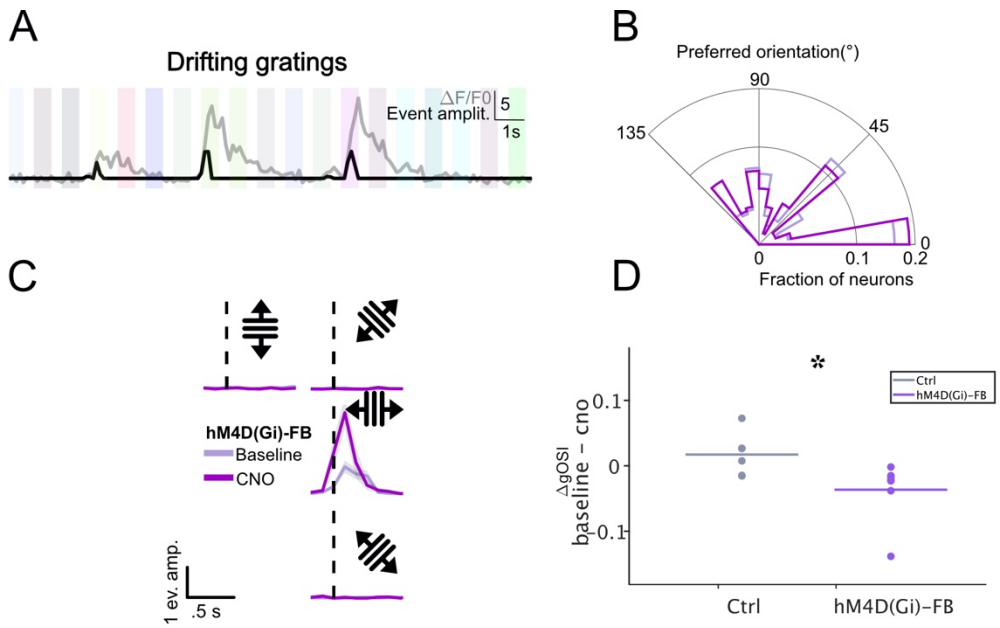

Figure 2-7 Direct cortico-cortical feedback decreases the orientation-selectivity of V1 neurons through selective inhibition of responses to the preferred orientation.

A. Traces of an ROI example. Vertical bars illustrate the different visual stimuli. The computed ΔF/F0 trace is shown in gray and the deconvolved events are in black.
B. Circular histogram of the distribution for the preferred orientation for the hM4D(Gi)-FB group**.** Dark purple indicates the distribution for the CNO day and light purple for the baseline day.
C. Example of mean responses of an ROI in the hM4D(Gi)-FB group. Dark purple indicates the mean responses for the CNO day and light purple for the baseline day.
D. ΔgOSI per session for each of the groups. Circles indicate individual sessions and horizontal lines the mean. In gray is the Cnt group and in purple is the hM4D(Gi)-FB group. Star indicates significance (ns: p>0.05, *: p<0.05, **: p<0.01, ***: p<0.0001). hM4D(Gi)-FB group n=7 sessions from 4 mice, Cnt group n=6 sessions from 4 mice.

2.2.3 Geometry of intact feedback on V1 population response to gratings

We then looked at how direct cortico-cortical feedback from HVA affected the V1 population coding of the oriented gratings. For this, we used PCA as a dimensionality reduction method. We performed PCA on the mean activity for each of the four orientations for the control and CNO days simultaneously to obtain a shared reduced space (see Methods). We started by looking into the Ctrl group. We saw that the first three components explained 75±4% of the variance, indicating that the encoding occurs in a low dimensional manifold. Additionally, the explained variance for each of the components was not significantly different between the two days (Figure 2-8 A, 2-way rm ANOVA: CNO vs Baseline p=0.42, post-hoc PC comparison p= (0.36; 0.39; 0.52; 0.53; 0.90)).

We looked at the projections of the single trial responses onto the first three eigenvectors (Figure 2-8 B). We observed that the single-trial projections landed along a one-dimensional axis that extended from the origin. We named this vector the tuning axis. In Figure 2-8 B, this vector is indicated by a line corresponding to the color of the orientation. The position in which a single trial lies is proportional to the population activation of that trial. Thus, trials with low activation laid close to the origin, and trials with more activation laid further away. Notably, very few points were found between two tuning axes. The combination of the four tuning axes created a tetrahedral geometry in which each of the vectors represents the line that goes from the center to the vertex of the tetrahedra, suggesting that each of the stimuli is well separate and distinguishable from each other.

We then proceeded to characterize the obtained geometry. We projected all the trials of the same orientation for both days on the first three PC axis and computed their SVD decomposition (see Methods). This approach allowed us to study the dimensionality of the single stimulus representation and the further characterize its structure. We first computed how much of the variance each of the tuning axes explained for the trials of a given orientation (Figure 2-9 A). We found no significant difference between the Baseline and CNO days (2-way repeated measures (rm) ANOVA: CNO vs Baseline p=0.45, post hoc tuning axis comparison p= (0.03; 0.98; 0.99; 0.85)). Interestingly, each of the tuning axes explained an average of 76% of the variance (per orientation axis: 0º: 75±5%, 45º: 76±6%, 90º: 81±7%, 135º: 75±6%), reinforcing the notion that each stimulus representation is highly one-dimensional.

We then proceed to calculate the angle between the tuning axes. We sorted the different orientations according to their distance from each other in degrees –for instance, the tuning axis of 0 and 45, 45 and 90, and 90 and 135 are all at a 45º distance from each other. We found that regardless of their angular distance, they were all close to orthogonal from each other. Again, we found no significant difference in the measurements between Baseline and CNO days (Figure 2-9 B, 2-way rm ANOVA: CNO vs Baseline p=0.98, post hoc angle difference comparison p= (0.52; 0.34; 0.37)).

Finally, we calculated the strength of each of the tuning axes, by calculating the mean across the trial projections for a particular orientation on each of the days. We found that, on average, drifting gratings oriented at 90º generated the strongest value. However, we found no significant difference between the Baseline and CNO days. (Figure 2-9 C, 2-way rm ANOVA: CNO vs Baseline p=0.66, post hoc tuning axis comparison p= (0.40; 0.37; 0.11; 0.47)).

Overall, we saw that the population representation of the four oriented drifting gratings is embedded into a three-dimensional manifold. Further, we could define a tuning axis for each of the orientations that were arranged creating an orthogonal tetrahedron. The coding of a single orientation was bounded to a single dimension as the tuning axis explained around 70% of the variance. Finally, off-target CNO effects and/or stimulus repetition effects do not seem to affect the orthogonal tetrahedral geometry that the representation of the four drifting gratings forms.

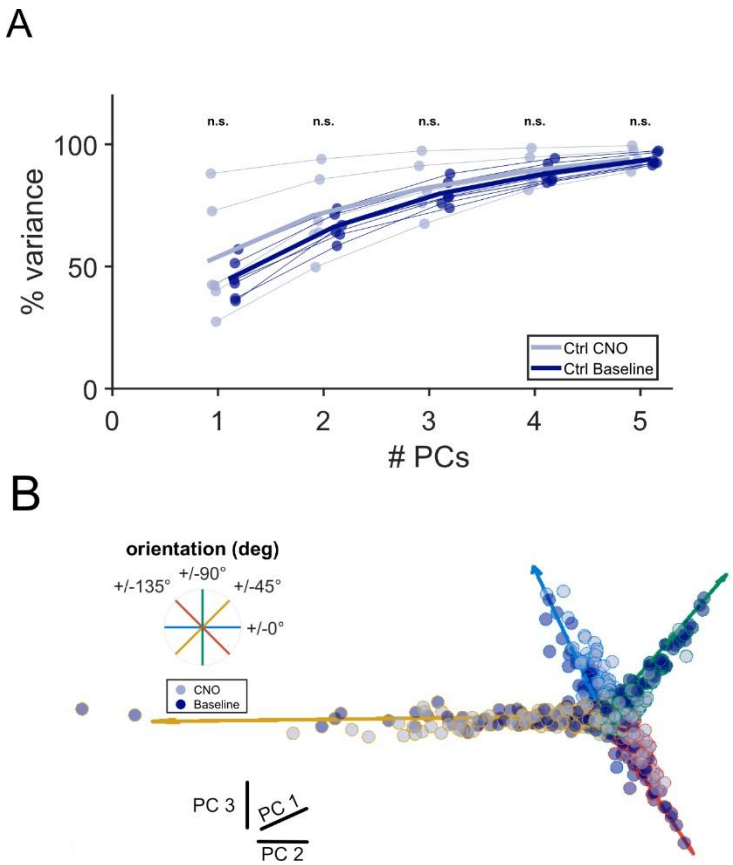

Figure 2-8 Geometry of drifting gratings in the control group.

A. Variance explained by the first five principal components in the Ctrl group. Light blue indicates the variance for the CNO group and dark blue for the Baseline group. Star indicates significance (ns: p>0.05, *:

p<0.05, **: p<0.01, ***: p<0.0001). hM4D(Gi)-FB group n=7 sessions from 4 mice, Cnt group n=6 sessions from 4 mice.
B. Geometrical representation of the populational response to the drifting gratings using the first three PCs. Dark dots represent individual trials of the Baseline group and light dots for the CNO group. The outline of the dots indicates the orientation of the drifting grating on the given trial. The lines represent the orientation axis for each of the orientations.

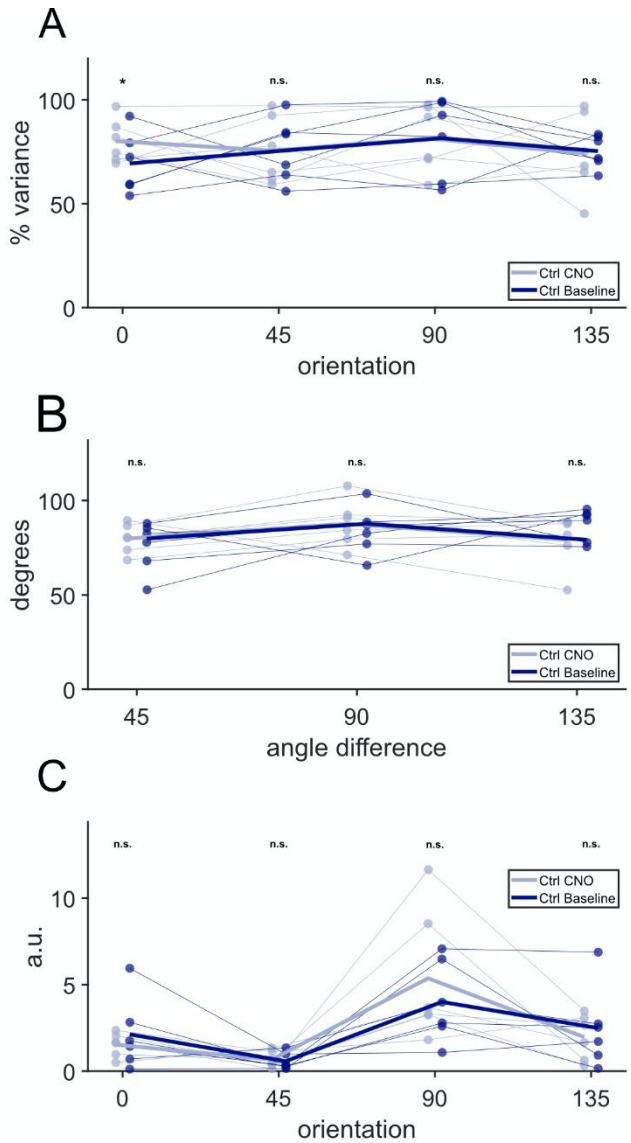

Figure 2-9 Characterization of the tetrahedral geometry and changes in the Ctrl group.

A. Variance explained by each of the tuning axes. Light blue represents the variance explained for the CNO day trials and dark blue for the Baseline trials. The lines represent the overall mean and the circles the mean over each of the sessions. Star indicates significance (ns: p>0.05, *: p<0.05, **: p<0.01, ***: p<0.0001). hM4D(Gi)-FB group n=7 sessions from 4 mice, Cnt group n=6 sessions from 4 mice.
B. Angle between the tuning axes across the orientation's angular distances. Light blue represents the angle in degrees for the CNO day trials and bark blue for the Baseline trials. The lines represent the overall mean and the circles the mean over each of the sessions. Star indicates significance (ns: p>0.05, *: p<0.05, **: p<0.01, ***: p<0.0001). hM4D(Gi)-FB group n=7 sessions from 4 mice, Cnt group n=6 sessions from 4 mice.
C. Mean projection value across each of the tuning axes for the trials of each orientation. Light blue represents the mean for the CNO day trials and dark blue for the Baseline trials. The lines represent the overall mean and the circles the mean over each of the sessions. Star indicates significance (ns: p>0.05, *: p<0.05, **: p<0.01, ***: p<0.0001). hM4D(Gi)-FB group n=7 sessions from 4 mice, Cnt group n=6 sessions from 4 mice.

2.2.4 Direct cortico-cortical FB from HVA to V1 decreases the gain of the population response to drifting gratings

Once we understood the geometrical properties of the drifting gratings representation, we set out to study how this representation changed in the absence of direct cortico-cortical FB from HVA. We used the same approach of building a shared, reduced PC space with the Baseline responses and the CNO responses. Figure 2-10 A shows a sample session, similar to Figure 2-8 B. In this case, the light purple circles indicate the Baseline day, and the dark purple circles the CNO day. The diamonds of each color represent the mean population response for that day, and the black arrows indicate the position of the diamonds. A tetrahedral-shaped representation was formed. We then explored whether any of the quantifications we described above suggested a change in the representation.

We did not observe any change in the variance explained by the axis for the Baseline or CNO groups (Figure 2-10 B left, 2-way rm ANOVA: CNO vs Baseline p=0.17, post hoc tuning axis comparison p= (0.92; 0.44; 0.37; 0.13)). In fact, the values obtained were very similar to those obtained for the Ctrl group (Figure 2-8 A). Leveraging that we had a paired experiment, we subtracted the CNO day responses from their corresponding baselines for each of the recorded sessions. Although the variance explained by the absence of FB was slightly less, it was not significantly different (Figure 2-10 B right, t-test p=0.13).

In the same way as we did for the Ctrl group, we calculated the angles between the different orientation axes. Again, we saw that they created an almost orthogonal tetrahedral whose shape did not change in the absence of direct cortico-cortical FB from HVA (Figure 2-10 C 2-way rm ANOVA: CNO vs Baseline p=0.17, post hoc angle difference comparison p= (0.72; 0.94; 0.06), t-test p=0.56).

Finally, we explored whether, in line with the single-cell analysis results, there was an increase in activity along the orientation axis. We computed the mean value along the orientation axis in the CNO and baseline day separately for each of the presented orientations. Indeed, we verified that there was a significant increase in the CNO day relative to baseline for the hM4D(Gi)-FB group (Figure 2-10 D left, 2-way rm ANOVA: CNO vs Baseline p=0.005, post hoc tuning axis comparison p= (0.006; 0.15; 0.69; 0.05)). This is also visible in Figure 2-10 A when looking at the mean responses (represented as diamonds) for each of the orientations. For all the orientations except 90º, the mean response of the CNO day was farther away from the origin than the Baseline day response. When we subtracted the mean CNO day response from the Baseline response, we measured a significant decrease in the hM4D(Gi)-FB group compared to the Ctrl group (Figure 2-10 D right, t-test p= 0.033). In summary, silencing

direct cortico-cortical FB from HVA to V1 increases the population response to the drifting gratings but conserves its geometry.

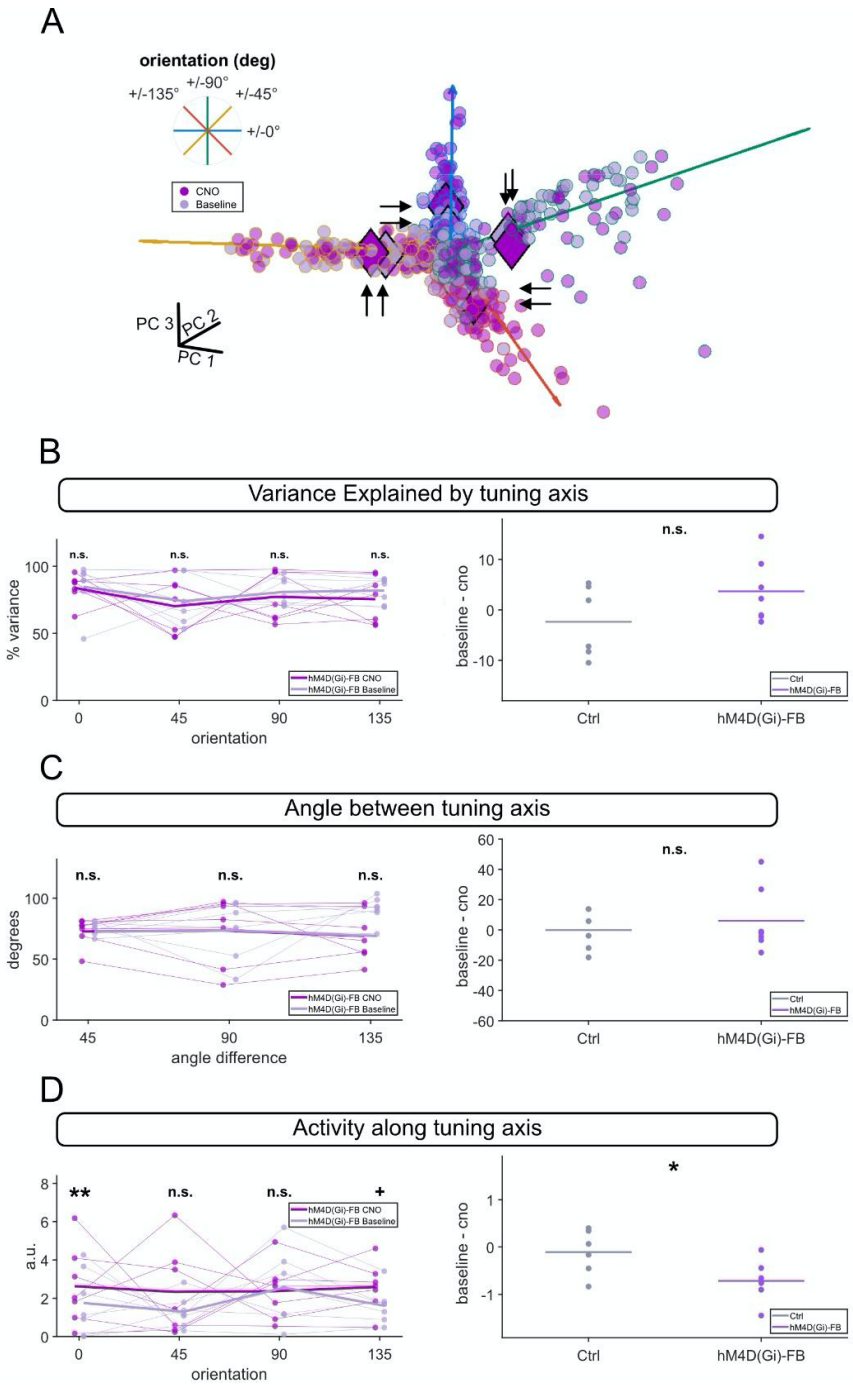

Figure 2-10 Population representation of drifting gratings in the hM4D(Gi)-FB group.

A. Geometrical representation of the populational response to the four drifting gratings in the hM4D(Gi)-FB group using the first three principal components. Light dots represent individual trials of the Baseline group and dark dots of the CNO group. The outline of the dots indicates the orientation of the drifting grating on the given trial. The lines represent the orientation axis for each of the orientations. Diamonds represent the mean for each of the groups (light Baseline and dark CNO) for each of the four orientations.
B. Variance explained by the tuning axis. Left: Variance explained by each of the tuning axes. Dark blue represents the variance explained for the CNO day trials and light blue for the Baseline trials. The lines represent the overall mean and the circles the mean over each of the sessions. Star indicates significance (ns: $p>0.05$, *: $p<0.05$, **: $p<0.01$, ***: $p<0.0001$). Right: Mean subtraction (baseline – CNO) for the two groups Ctrl and hM4D(Gi)-FB. Star indicates significance (ns: $p>0.05$, *: $p<0.05$, **: $p<0.01$, ***: $p<0.0001$). hM4D(Gi)-FB group n=7 sessions from 4 mice, Cnt group n=6 sessions from 4 mice.
C. Geometrical shape of the representation. Left: Angle between the tuning axes across the orientation's angular distances. Dark blue represents the angle in degree for the CNO day trials and light blue for the Baseline trials. The lines represent the overall mean and the circles the mean over each of the sessions. Star indicates significance (ns: $p>0.05$, *: $p<0.05$, **: $p<0.01$, ***: $p<0.0001$).
Right: Mean subtraction (baseline – CNO) for the two groups Ctrl and hM4D(Gi)-FB. Star indicates significance (ns: $p>0.05$, *: $p<0.05$, **: $p<0.01$, ***: $p<0.0001$). hM4D(Gi)-FB group n=7 sessions from 4 mice, Cnt group n=6 sessions from 4 mice.
D. Strength of the representation along the axis. Left: Mean projection value across each of the tuning axes for the trials on each orientation. Dark blue represents the angle for the CNO day trials and light blue for the Baseline trials. The lines represent the overall mean and the circles the mean over each of the sessions. Star indicates significance (ns: $p>0.05$, *: $p<0.05$, **: $p<0.01$, ***: $p<0.0001$).
Right: Mean subtraction (baseline – CNO) for the two groups Ctrl and hM4D(Gi)-FB. Star indicates significance (ns: $p>0.05$, *: $p<0.05$, **: $p<0.01$, ***: $p<0.0001$). hM4D(Gi)-FB group n=7 sessions from 4 mice, Cnt group n=6 sessions from 4 mice.

2.2.5 Direct cortico-cortical FB from HVA changes the single neuron preferred epoch in a naturalistic movie

Once we assessed how the lack of direct cortico-cortical FB from HVA to V1 affected the representation of the well-established stimulus set of

drifting gratings, we went on to study a more complex visual stimulus, namely a naturalistic movie.

The naturalistic movie consisted of a 30s movie clip extracted from the movie “1984”, repeated ten times with an ITI of 5s. As before, after preprocessing the two-photon images, we computed the normalized fluorescence $\Delta F/F0$, (Figure 2-11 A in gray) for every neuron region of interest (ROI). Following the same methodology as in the preprocessing of the drifting gratings, we deconvolved the $\Delta F/F0$ traces to identify events (Figure 2-11 A in black), to mitigate potential contamination from decaying GCaMP6s traces across subsequent movie frames.

Every neuron had its particular response pattern to the movie. Due to previous observations of representational drift, we wondered how stable this pattern was over the two days of recordings. To visually quantify it, we averaged the response to the movie across the repetitions of the Baseline day. We sorted their response according to the frame of maximum response. To cross-validate the sorting, we only used half of the trials in the Baseline day to do the sorting. We used this same sorting for the remaining half of the Baseline day trials to visualize them, along with the full CNO day trials. Doing this for both the Ctrl (Figure 2-11 C) and hM4D(Gi)-FB (Figure 2-11 D) groups, we saw that while the preferred frame was maintained in the Ctrl group, this was not the case for the hM4D(Gi)-FB group. Figure 2-11 B shows an example ROI in the hM4D(Gi)-FB for the Baseline day in light purple and CNO day in dark purple where the change in the response pattern can be observed.

To quantify the observed dissimilarity in response patterns, we computed the cosine similarity between the mean response to the movie clip on the Baseline day and the CNO day for each of the neurons. Namely, we computed how similar the mean activity of the Baseline and CNO days

were for each of the neurons. Cosine similarity is bounded between zero and one. Values close to one indicate that the responses between the two days are similar, and values close to zero indicate that the responses between the two days are maximally different. We found that the cosine similarity in the hM4D(Gi)-FB group was significantly smaller than in the Ctrl group, meaning that the mean activities between the two days were more dissimilar for the hM4D(Gi)-FB group than the Ctrl (Figure 2-11 E, Hierarchical bootstrap, p=0.01). Confirming the visual inspection that the response patterns to the same movie clip with and without direct cortico-cortical FB from HVA to V1 significantly changed.

Tetzlaff et al., 2012, proposed that FB projections diversify the neurons' responses. Therefore, we wanted to analyze whether part of the observed change in response pattern due to lack of HVA FB was due to V1 neurons becoming more similar to each other. We calculated the signal correlations between the neurons on each of the days and subtracted the mean results per session (Baseline day – CNO day) to quantify how much the signal correlations changed when there was no direct cortico-cortical FB from HVA to V1. We measured a significant increase in the signal correlation in the CNO day of the hM4D(Gi)-FB group (Figure 2-11 F. Hierarchical bootstrap, p=0.0025). Thus, tuning curves of different V1 neurons become more similar after silencing direct cortico-cortical feedback, as neurons tend to gain responses to similar movie epochs.

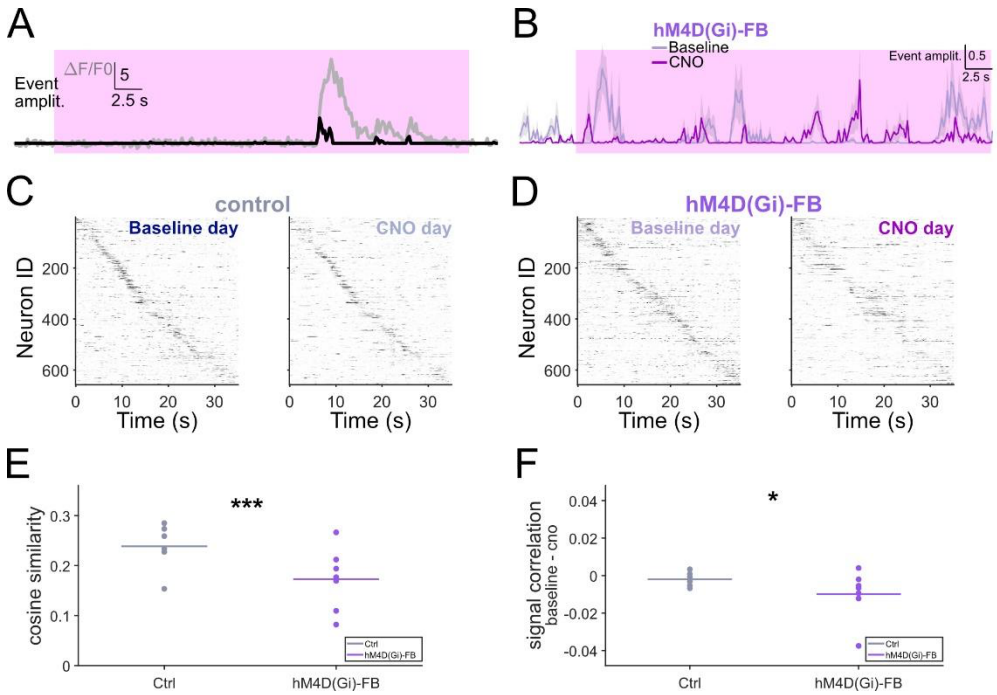

Figure 2-11 Tuning of V1 neurons to natural movie changes upon silencing of direct cortico-cortical feedback inputs.

A. Traces of an example ROI. Pink shadow illustrates the presentation of the naturalistic movie. The computed ΔF/F0 trace is shown in gray and the deconvolved events are in black.
B. Example mean response of a single V1 neuron from hM4D(Gi)-FB group. Each trace corresponds to the mean evoked activity to multiple natural movie presentations on Baseline (light purple) and CNO (dark purple) imaging days. Shaded areas represent standard deviation.
C. Heatmap of tuning curves of all neurons from the Ctrl group for Baseline (left) and CNO (right) imaging days. Tuning curves were sorted by their preferred movie epoch in the Baseline day and cross-validated on half the trials. The same sorting was applied to the CNO day.
D. Heatmap of tuning curves of all neurons from the hM4D(Gi)-FB group for Baseline (left) and CNO (right) imaging days. Tuning curves were sorted by their preferred movie epoch in the Baseline day and cross-validated on half the trials. The same sorting was applied to the CNO day.
E. Cosine similarity values between Baseline and CNO day per each of the sessions for both hM4D(Gi)-FB and Ctrl groups. For each neuron, cosine similarity was calculated between the tuning curve vectors of Baseline and CNO imaging days. Circles indicate the mean per session and lines overall mean. Star indicates significance (ns:

p>0.05, *: p<0.05, **: p<0.01, ***: p<0.0001). hM4D(Gi)-FB group n=7 sessions from 4 mice, Cnt group n=6 sessions from 4 mice.
F. Subtraction of signal correlation values (Baseline – CNO day) per each of the sessions for both hM4D(Gi)-FB and Ctrl groups. For each neuron, cosine similarity was calculated between the tuning curve vectors of Baseline and CNO imaging days. Circles indicate the mean per session and lines overall mean. Star indicates significance (ns: p>0.05, *: p<0.05, **: p<0.01, ***: p<0.0001). hM4D(Gi)-FB group n=7 sessions from 4 mice, Cnt group n=6 sessions from 4 mice.

2.2.6 Dimensionality and geometry of naturalistic movie in V1

Naturalistic stimuli are known to create a high-dimensional manifold, as the stimulus itself is high-dimensional (Stringer et al., 2019). Indeed, when we computed a shared reduced space in the Ctrl group for the Baseline and CNO days, we saw that we needed 25 components to capture 89±1% of the variance of the stimulus (Figure 2-12 A). There was no significant difference between the variance explained in the Baseline and CNO days for the individual PC components (2-way rm ANOVA: CNO vs Baseline p=0.82, post-hoc p= (0.90; 0.32; 0.88; 0.77; 0.91; 0.78; 0.86; 0.86) for PC: 1, 5, 10, 15, 20, 25, 30, 35 respectively).

Next, we wanted to explore the shape of the components. The neurons recorded on the same session shared the same RFs, but this varied across different sessions. Since the temporal and spatial statistics also varied across the visual field, the principal components computed on different sessions could code for very different things. However, since the recorded neurons were the same in the Baseline and Ctrl days, we could still compare them. Upon visual inspection, we saw that the projections of the first PC of the Baseline and CNO days aligned to a large extent. Figure 2-12 B-D shows the first to third projections of an example session as an illustration. From this example, one can see that each of the PCs highlights a particular time band of the movie clip. The consistency in the

population coding projections from Baseline to CNO days aligns with the observation of highly similar response patterns exhibited by single neurons on both days.

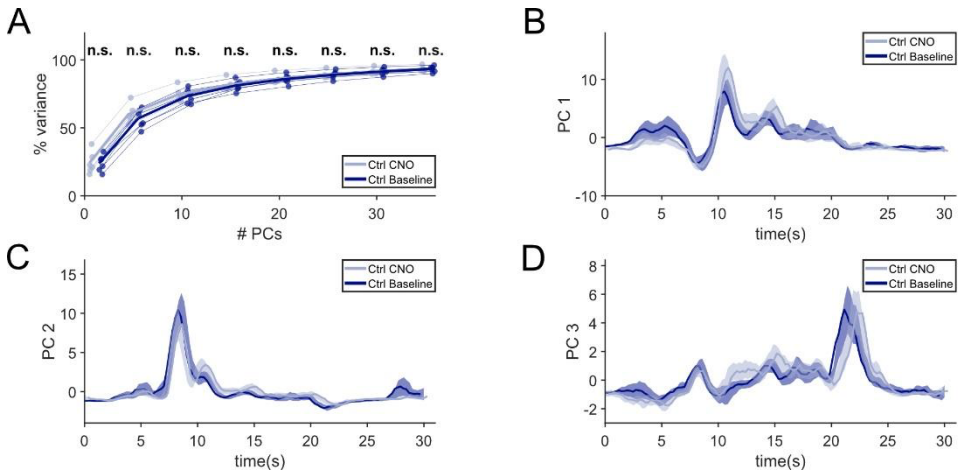

Figure 2-12 PC space of Naturalistic Movie in Ctrl group.

A. Variance explained of Ctrl group. Cumulative variance explained per PC for the CNO day in light blue and Baseline day in dark blue. Circles represent sessions and lines mean. Star indicates significance (ns: p>0.05, *: p<0.05, **: p<0.01, ***: p<0.0001). hM4D(Gi)-FB group n=7 sessions from 4 mice, Cnt group n=6 sessions from 4 mice.
B. Mean of the activity projected onto the first Principal Component. Projection over time of the first PC in dark blue for the Baseline day and light Blue for the CNO day. Shade represents the standard error of the mean and solid line mean.
C. Mean of the activity projected onto second Principal Component. Projection over time of the second PC in dark blue for the Baseline day and light Blue for the CNO day. Shade represents the standard error of the mean and solid line mean.
D. Mean of the activity projected onto third Principal Component. Projection over time of the third PC in dark blue for the Baseline day and light Blue for the CNO day. Shade represents the standard error of the mean and solid line mean.

2.2.7 Direct cortico- cortical FB from HVA to V1 changes the population representation to the naturalistic movie

Once we characterized the population representation for the group with intact FB and we made sure there was no representational drift, we explored the population representation for the manipulated group. The cumulative variance between the Ctrl and hM4D(Gi)-FB groups was quite similar (Figure 2-13 A, C, 2-way rm ANOVA: CNO vs Baseline $p=0.02$, post-hoc $p= (0.05; 0.98; 0.40; 0.78; 0.39; 0.48; 0.45; 0.55)$ for PC: 1, 5, 10, 15, 20, 25, 30, 35 respectively). However, the first component explained, on average, more variance in the CNO day than it did for the Baseline day. One explanation for this can be the increase of signal correlation for the CNO day in the hM4D(Gi)-FB group.

Upon visual inspection of the principal components for each of the sessions, we realized that contrary to the Ctrl group, the projections did not overlap. Figures 3-13 B to D represents the projections of the first to third components for an example session. As one can see, the projections overlap to a larger extent for the first component, but they are increasingly different for the second and third components.

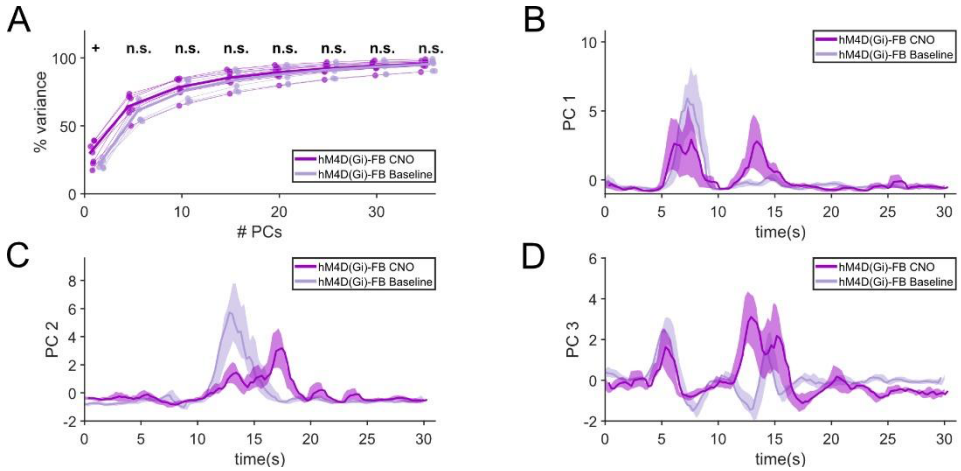

Figure 2-13 PC space of Naturalistic Movie in hM4D(Gi)-FB group.

A. Variance explained of hM4D(Gi)-FB group. Cumulative variance explained per PC for the CNO day in dark purple and Baseline day in light purple. Circles representant sessions and lines mean. Star indicates significance (ns: p>0.05, *: p<0.05, **: p<0.01, ***: p<0.0001). hM4D(Gi)-FB group n=7 sessions from 4 mice, Cnt group n=6 sessions from 4 mice.
B. Mean of the activity projected onto the first Principal Component. Projection over time of the first PC in dark purple for the CNO day and light purple for the Baseline day. Shade represents the standard error of the mean and solid line mean.
C. Mean of the activity projected onto the second Principal Component. Projection over time of the second PC in dark purple for the CNO day and light purple for the Baseline day. Shade represents the standard error of the mean and solid line mean.
D. Mean of the activity projected onto third Principal Component. Projection over time of the third PC in dark purple for the CNO day and light purple for the Baseline day. Shade represents the standard error of the mean and solid line mean.

Comparing the 3D projections of the example sessions shown in Figure 2-12 B-D for the Ctrl group and Figure 2-13 B-D for the hM4D(Gi)-FB group shows how different the coding geometry is when direct cortico-cortical FB from HVA to V1 is silenced.

We then set out to quantify the observed difference. We concluded that this quantification was best done by two non-overlapping measures: The length difference between the projections and the angle between the

projections (Illustration in Figure 2-14 A). Figure 2-14 B shows an example projection of the mean activity in the Baseline and CNO day, the differences between these two trajectories were done time-bin by time-bin. When a time-bin point is projected into n PC dimensions, this point creates a vector from its location to the origin. In Figure 2-14 A two points are depicted in a three-dimensional space, one for each of the days. The vectors are denoted as $\mathbf{v}_{\mathbf{CNO}}$ and $\mathbf{v}_{\mathbf{Baseline}}$. Once the vectors are identified, one can calculate the length difference of the vectors as the difference between the modulus of the two vectors. In addition, one can calculate the angle between the two vectors as the inverse cosine of their normalized dot product (See methods for details). These two non-overlapping measures indicate whether the difference can be described as gain modulation, as in the drifting gratings response, or a change in the geometry. Additionally, we created an artificial control – same-day control - in which we measured the length and angle difference between two halves of the Baseline trials for the hM4D(Gi)-FB group to control for changes that arise from trial-to-trial fluctuation (see methods for details).

We looked at how these two measures changed as we added dimensions. In the case of the length difference, while in the hM4D(Gi)-FB group was slightly larger than the one obtained in the Ctrl group or the same-day control, we did not find any significant difference between the Ctrl and the hM4D(Gi)-FB groups (Figure 2-14 C, two-way ANOVA: CNO vs Baseline $p=0.50$, post hoc $p= (0.84; 0.38; 0.49; 0.53; 0.51; 0.50; 0.48; 0.46)$ for PC: 1, 5, 10, 15, 20, 25, 30, 35 respectively). The lack of an effect of the length difference could be explained because we were averaging over the whole duration of the stimulus. Therefore, while some points during the stimulus presentations could have a higher strength and others less strength, when averaging, this difference would sum close to zero. To make sure this was not the case, we looked at the length difference over time for the tenth PC (doing the same for other PCs did not change the result). We found that

at no time the length difference between the two groups was significantly different (Figure 2-14 D, two-way ANOVA: CNO vs Baseline p=0.45).

When we looked at the angle between the projections in the Baseline and CNO we saw that this angle systematically increased for all the conditions as we added dimensions (Figure 2-14 E, two-way ANOVA: CNO vs Baseline p=0.015, post hoc p= (0.25; 0.01; 0.01; 0.009; 0.01; 0.02; 0.02; 0.03) for PC: 1, 5, 10, 15, 20, 25, 30, 35 respectively). This result makes sense since, as we increase the dimensionality, small differences in position can result in big angular differences. Importantly, this difference was significantly larger for the hM4D(Gi)-FB group than any of the two control groups. Interestingly, for the case of two dimensions, the difference between the hM4D(Gi)-FB and Ctrl group was not significant, similar to what we saw in Figure 2-13 B where the projections of the first PC component were the most similar to each other.

Finally, looking at the over-time angular difference between the CNO and Baseline projections for the first ten PCs, we identified the time points in the movie where the angular difference was the biggest (Figure 2-14 F, one-way ANOVA: CNO vs Baseline p=0.03, only reporting the times of significant difference with more than two consecutive instances; post hoc p= (0.06, 0.004, 0.043,0.008,0.04) for t= (2.8s : 3.8s), p= (0.001, 0.04) for t= (8.3s : 8.6s), p= (0.005, 0.004 ,0.003, 0.01, 0.01, 0.01, 0.02, 0.001) for t= (17.9s : 19.7s), p= (0.05, 0.08, 0.0008, 0.26, 0.01, 0.04) for t= (20.7s : 21.9), p= (0.02, 0.03, 0.01) for t= (29.5s : 30s)). Although different sessions were recorded over different RFs, these periods of biggest angular difference were maintained, suggesting that global scenery properties were coded following different geometries with and without direct cortico-cortical FB from HVA.

Overall, the population analysis results conveyed that the population coding for the stimulus changes its geometry but not how strongly it responds to a stimulus, in agreement with the results we obtained when comparing single cells. Additionally, the population analysis showed which periods of the movie the geometry diverged the most.

The naturalistic movie was composed of a single sequence with four different parts (manually identified). Figure 2-15 is an attempt to convey the main characteristics of each of the parts. The movie starts with a close shot that lasts for the first 3s, in this period the camera slightly zooms into the scene and focuses on the character and the column that is on the right. The next sequence's (3-14s) primary characteristic is the column and the camera moving from its left to its right. This sequence is thus dominated by a movement that could resemble a vertical oriented bar moving from the right to the left of the screen. In the next scene (14-20s), we see the same scene as in the beginning of the movie, but from another angle. Larger features of the image are more present; the face and the background, while the camera does a zoom out. Finally, the last scene (20-30s) is a zoom out of the room where a lot of small items are present.

From Figure 2-14 F, we see that the biggest angular difference elicited by a lack of direct FB from HVAs to V1 was in the second half of the movie. Additionally, pronounced differences are observed at the beginning and at the end of the column scene, particularly as the column becomes prominent in the visual field, and as its transitions away from the screen, revealing a new scene.

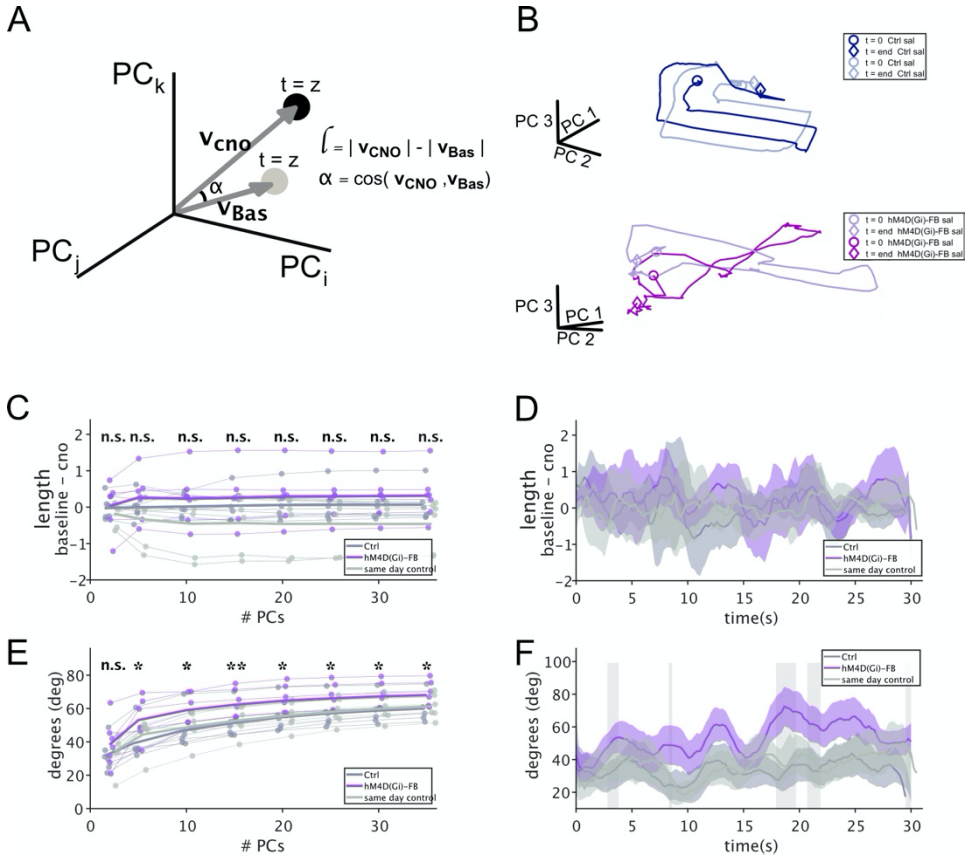

Figure 2-14 Silencing direct cortico-cortical FB from HVA to V1 changes the representational geometry but not the strength of the naturalistic movie.

A. Schematic of the analysis done to compare PC projections. The black dot represents the value of the PC projection at a given time t for the PCs i,j, and k on the CNO day. The gray dot represents the value of the PC projection at the same time t and for the PCs i,j, and k, on the Baseline day. Each of the dots creates one vector going from the origin to the value of the projection ($\mathbf{v_{CNO}}$ and $\mathbf{v_{bas}}$). The difference between the vectors is calculated by two measures: Length difference, the length of the two vectors is subtracted, and their angle, the angle between the two vectors is calculated.
B. Example of the coding trajectory for the first three PCs. Top: Ctrl group. Dark blue for the Baseline day and Light blue for the CNO day. Bottom: hM4D(Gi)-FB group. Dark purple for the CNO day and light purple for the baseline day. The circle represents the beginning of the movie and the diamond the end.
C. Length difference between the CNO and baseline projection as the number of PCs increases. hM4D(Gi)-FB group in purple, control group in dark grey and same day control in light grey, where the projection differences are calculated by halving the repetitions of the same control

baseline group (methods). Circles indicate session and lines overall mean. Star indicates significance (ns: p>0.05, *: p<0.05, **: p<0.01, ***: p<0.0001). hM4D(Gi)-FB group n=7 sessions from 4 mice, Cnt group n=6 sessions from 4 mice.
D. Length difference between the CNO and baseline projections for the tenth PC along the movie presentation. hM4D(Gi)-FB group in purple, control group in dark grey and same day control in light grey, where the projection differences are calculated by halving the repetitions of the same control baseline group (methods). Solid lines represent mean and shaded region standard error of the mean. Grey rectangles indicate significance ((ns: p>0.05, *: p<0.05, **: p<0.01, ***: p<0.0001).
E. Angle between the CNO and baseline projection as the number of PCs increases. hM4D(Gi)-FB group in purple, control group in dark grey and same day control in light grey, where the projection differences are calculated by halving the repetitions of the same control baseline group (methods). Circles indicate session and lines overall mean. Star indicates significance (ns: p>0.05, *: p<0.05, **: p<0.01, ***: p<0.0001). hM4D(Gi)-FB group n=7 sessions from 4 mice, Cnt group n=6 sessions from 4 mice.
F. Angle between the CNO and baseline projections for the tenth PC along the movie presentation. hM4D(Gi)-FB group in purple, control group in dark grey and same day control in light grey, where the projection differences are calculated by halving the repetitions of the same control baseline group (methods). Solid lines represent mean and shaded region standard error of the mean. Grey rectangles indicate significance (ns: p>0.05, *: p<0.05, **: p<0.01, ***: p<0.0001).

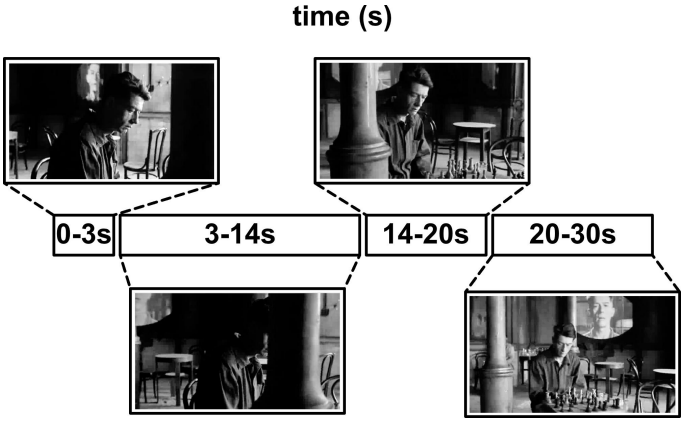

Figure 2-15 Breakout of the natural movie scenes.

0-3s: Zoom in: Close shot of face.
3-14s: Column passing from left to right of the screen.
14-20s: Zoom out: Medium shot of the face with some background.
20-30s: Long shot with a lot of background.

2.3 Discussion

In the present study, we investigated how the stimulus representations of V1 neurons changes with the absence of direct cortico-cortical FB from HVAs in the awake non-behaving mouse. We characterized the changes for a low dimensional stimulus, full-screen drifting gratings, and for a high dimensional stimulus, a naturalistic movie. We showed that while the gain of the drifting gratings was affected by the FB contribution from HVA, in the case of the movies it resulted in change in the geometry of the population representation, but not in the gain.

2.3.1 Experimental protocol

The results of this study rely on a novel experimental technique that allows for the selective silencing of direct cortico-cortical FB coming from all HVAs into V1, while maintaining the activity of the HVAs intact. The effectivity of this experimental protocol to silence FB axonal projections from HVA to V1 has been extensively detailed in Fioreze (2022). Therefore, here we will only highlight that this experimental design allows for simultaneous imaging and tracking of a large number of neurons over the span of two days, including the measurement of their calcium activity both with intact FB and with silenced direct cortico-cortical FB. Additional axonal imaging experiments of higher area LM showed that CNO application reduced around 33% of their visually evoked activity (Fioreze, 2022). This measure provides a lower bound estimate to the extent of FB silencing in the experiments analyzed for this study.

Another important caveat of the experimental protocol is the stabilization of the system once the perturbation occurs (Wolff & Olveczky, 2018). The brain operates in a tight Excitatory and Inhibitory (E/I) balance (Renart,

2010). Any perturbation leads to a temporary instability and potential adjustment to a new E/I balance equilibrium point. In our case, this transient state was not measured, as CNO injections were done 30 minutes prior the imaging session started. Axonal silencing using DREADDs lasts for several hours (Stachniak et al., 2014). The stimulus presentation reported in this study lasted for 15 minutes and was done in the beginning of the session, therefore we believe that it is safe to assume that the whole session was recorded under stable FB silencing conditions.

We have grounds to believe that a new E/I balance point was reached due to the silencing of direct cortico-cortical FB projections. While the overall mean activity of the neurons was unchanged with and without direct cortico-cortical FB from HVA to V1, there was a significant difference in the ratio of neurons being both more and less active when compared to the Ctrl group (Fioreze, 2022). Therefore, when looking at the reduced representational space, we z-scored individual neural responses each day independently, to avoid any confounds in our analysis.

Finally, in this studied we included the individual sessions rather than the individual mice to increase the power of the statistical tests. Due to the challenging nature of the experiments only four mice were recorded on each groups, statistical analysis between four points is underpowered, to avoid this we included the individual sessions instead.

2.3.2 Direct FB from HVA to V1 affects the population representation in a stimulus dependent manner

In the present study, we showed that the properties of the visual stimuli have a strong influence on the type of change exhibited by the population

representation. The schematic in Figure 2-14 A, shows that, in any given trial, two types of differences can occur, independently or in combination. (1) The gain can change, identified by a difference in distance from the origin. (2) The geometry of the representation can change, i.e., the angle between the two points changes.

Utilizing the same dimensionality reduction analysis for gratings and movie stimulus, we showed that the population representation changed in a stimulus dependent manner. We saw that for the drifting gratings the gain increased when direct FB from HVAs to V1 was silenced (Figure 2-10 D). Additionally, we did not see such a change for the naturalistic movie, as the length was maintained in the two conditions (Figure 2-14 C). On the contrary, the silencing of FB changed the coding geometry of the naturalistic movie (Figure 2-14 E). Importantly, both results generally agreed with the single cell analysis.

In the case of the drifting gratings, we observed that single cells increased their gOSI when direct cortico-cortical FB from HVAs to V1 was silenced (Figure 2-7 D). An increase of gOSI means that the single neurons sharpened their tuning to oriented gratings. In a similar manner, this sharpening was observed in the population with an increase in the gain when FB was silenced (Figure 2-10 D). In the case of the naturalistic movie, we measured that the single cells mean response's cosine similarity between Baseline and CNO day increased in the absence of FB (Figure 2-11 E), which means that the cells mean response shape to the naturalistic movie is not conserved when FB is being silenced. In the population level, this translated in a change on the coding geometry, particularly for certain movie epochs.

Overall, these results do not agree with FB having a role in sharpening the coding of the visual stimulus. If this would be the case, we probably

would have measured a decrease in the gain for the drifting gratings in the absence of FB – the population representation of the drifting grating would be weaker. In the case of the movie, we probably would have seen time points in which the gain of the population was increased and others in which perhaps it was decreased. However, as mentioned the gain modulation for the naturalistic movie was unchanged (Figure 2-14 D). We thus conclude that, the results of the present study agree more with FB bringing contextual information to V1.

The integration of contextual information happens in the following manner. V1 integrates several FF inputs coming from LGN, creating a larger RF (Hubel and Wiesel, 1963). Additionally, in the case where FB projections are intact, V1 receives local and contextual information coming from the HVA (Marques et al., 2018). The two inputs (FF from LGN, and FB from HVAs) provide V1 with unique information that combines both local and contextual information. In the case where FB projections are silences, V1 has only access to the local information, and therefore it only represents an integration of FF inputs coming from LGN. In this case, LGN and V1 represent *similar* information. As we will see in the following sections, this framework can explain the stimulus dependent difference we observed when silencing direct cortico-cortical FB from HVA to V1.

2.3.3 Lack of direct cortico-cortical FB sharpens the representation of the full-field drifting gratings

We found that drifting gratings in two cardinal and two oblique (0º,90º,45º, 135º) orientations were represented in a nearly orthogonal tetrahedral shape. Each orientation is coded along a one-dimensional vector that we called tuning axis (Figure 2-8 B), where the distance from the origin

determines how strong the population response is. We believe that the elongation along the tuning axis is due to joining the responses to different spatial and temporal frequencies. We presented two spatial (0.02 and 0.04 cpd) and two temporal frequencies (0.5 and 1 Hz). While the population responses to the two temporal frequencies were no different from each other, we observed that the responses to the lower spatial frequency were further away from the origin (data not shown). Therefore, combining the response of the low and the high spatial frequency when creating the subspace probably contributed to the elongation of the tuning axis. Importantly this distribution did not change when FB was silenced.

We found that the geometrical representation to full screen drifting gratings was unchanged upon silencing direct cortico-cortical FB from HVA to V1. This is consistent with V1 neurons developing their tuning properties to drifting gratings through FF connections (Ferster & Miller, 2000), and with previous reports where no relationship was found between the activation of the HVA and the tuning curve of the single neurons (Oude Lohuis et al., 2021; Pafundo et al., 2016). Instead, we saw that the length difference between the FB intact representation, and FB silenced representation changed. We measured an increase in the distance from the origin when direct cortico-cortical FB from HVA to V1 was silenced. These results are consistent with reports that link the activity of HVA and surround suppression (Nassi et al., 2013; Nurminen et al., 2018; Vangeneugden et al., 2019; Keller et al., 2020b). Figure 2-16 illustrates how in the case where the FB is intact (Figure 2-16 A), the redundant information coming from HVA suppresses the response of V1. In contrast, for the case of silenced FB (Figure 2-16 B), V1 responds to the drifting gratings as if they were only present in its RF area.

In order to verify that surround suppression changes the population representation of the drifting gratings by decreasing the length of the

tuning axis, it would be informative to perform PCA on surround suppression experiments. Such experiments consist of recording the activity of an ensemble of V1 neurons while presenting drifting gratings confined to the RF of the V1 neurons and flanked drifting gratings, where in addition, a same orientation drifting grating appears on both sides. For such a stimulus protocol, we would expect to see an increase of the population gain when the flanked surround is absent (the drifting grating is only present in the RF of the V1 neurons), similar to the result we obtained when silencing direct FB from HVAs to V1. Further, when the flanking stimulus is present (the drifting grating is present in the RF of the V1 neurons and their surround) we would expect to measure a reduced gain on the population activity, similar to FB being intact. Additionally, presenting flanked gratings with non iso-oriented surround (different orientations in the surround than in the center) would be informative on how the surround information shapes the representational geometry of the drifting gratings. Further, it would also be interesting to present RF-confined drifting gratings in addition to full-field drifting gratings in future FB silencing experiments. If the reason why the population response to the gratings increases in the absence of FB is indeed an effect of surround suppression, when the stimuli is confined to the RF of V1 there should not be such an increase.

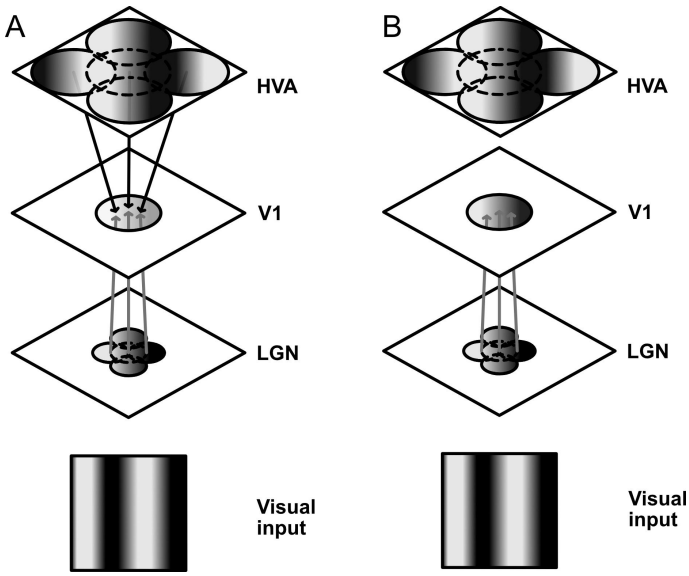

Figure 2-16 Illustration: Lack of FB from HVA to V1 increases the response to full field drifting gratings.

A. FB from HVA is intact. When full field drifting gratings are presented, V1 incorporates the FF information coming from LGN and the FB information coming from the HVA. The LGN neurons that have an overlapping RF with the V1 neurons send the response to the gratings through FF projections. Neurons in the HVA also respond to the full field gratings. Since there are full field both the neurons in the HVA that have an overlapping RF with V1 neurons and the ones that have a RF in the surrounding areas send redundant information to V1. V1 incorporates the FF and the FB signals and responds less to the grating showing a surround suppression effect. In the image each plane represents an area, and the circles represent the size of the RF and 'what they see'. The gray arrows indicate the FF connections and the black arrows the FB connections.

B. FB from HVA is silenced. When full field drifting gratings are presented, V1 only incorporates the FF information coming from LGN. The LGN neurons that have an overlapping RF with the V1 neurons send the response to the gratings through FF projections. This information activates the Neurons in V1 that are tuned to the gratings creating a response. Neurons in the HVA also respond to the full field gratings, however they do not send this information back to V1. In the image each plane represents an area, and the circles represent the size of the RF and 'what they see'. The gray arrows indicate the FF connections and the black arrows the FB connections.

2.3.4 Lack of direct cortico-cortical FB affects the representation of the naturalistic movie

Using naturalistic images or movies to understand the visual system can be a difficult choice. On the one hand, naturalistic images provide a more accurate picture of how the visual system processes information, as its statistics are close to what is seen in nature. On the other hand, compared to artificial stimuli, naturalistic stimuli are much harder to parametrize, and it is therefore harder to use metrics to quantify response and compare with other studies. Overall, however, we believe that using a high dimensional naturalistic stimulus supplements the understanding that we gain from drifting gratings alone.

Importantly, even if responses to oriented edges seem to be the foundational response of V1 (Hubel & Wiesel, 1968), V1 computations appear to be non-linear, and using normative models to predict V1 responses to naturalistic stimuli is a hard task (Carandini et al., 2005; Festa, et al., 2021). Furthermore, V1 responses to naturalistic images are sparse and reliable (Froudarakis et al., 2014; Yoshida & Ohki, 2020). This is a reflection of the redundancy that exists in the natural world, and the distribution of the statistics in such images (Field, 1987; Field, 1994). Our results agree with these findings. Single neurons are selectively activated at different epochs in the movie and these epochs are consistent across days (Figure 2-10 D). Because of the complexity of the natural scenes, the population representation lies in a high dimensional manifold (Gao et al., 2017; Stringer et al., 2019). This is supported in our results by the fact that around 25 components are needed to capture 89±1% of the variance (Figure 2-12 A and Figure 2-13 A). From our results however, how direct cortico-cortical FB from HVA to V1 affects the dimensionality of the representation is not clear.

If FB would carry a modulatory or visual attention signal, one possibility is that removing it could cause a drop in the dimensionality, as this, presumably one dimensional, signal would be absent when FB is being silenced. However, we did not see clear evidence of this. We did find that the first component carried a larger variance when FB was absent than in the Baseline level (Figure 2-13 A). One explanation of this is that in the single neuron level the signal correlation increases (Figure 2-11 F). The first component in PCA normally carries the overall activity fluctuation, of the population. It is also known that the first component of the PCA can carry information about the internal state of the animal (Saleem et al., 2013), which would affect the overall correlations of the cell ensemble. In our study, however, we removed the running bouts for the analysis and did PCA on the mean activity (averaging out the differences in the internal state), therefore the first component should solely carry information about the stimulus. If such a fluctuation is more shared (high signal correlation), it makes sense that the first component explains more of the variance than in a scenario where signal correlations are lower. Alternatively, the bigger variance explained by the first component could be related to the decay rate of the eigenvalues (the variance explained by each of the components). It is known that the spectrum of the eigenvalues reflects the dimensionality of the stimulus (Stringer et al, 2019). The eigenvalues should decay faster than a power law of $n^{-\alpha}$ where $\alpha = 1 + 2/d$ and d is the dimensionality of the stimulus. Fitting a power law to the eigenvalue spectrum of the drifting gratings and naturalistic movie with silenced and intact FB, would be a good approach to determine whether the dimensionality of the naturalistic movie decreases in the absence of FB. This decrease would point towards a role of FB increasing the complexity of the stimulus.

Our analysis revealed that, in contrast to the drifting gratings, the lack of direct cortico-cortical FB from HVA to V1 changed the geometry of the

representation to the naturalistic movie. In this case, we did not see that the obtained subspaces were maintained with a change in gain (Figure 2-14 C), but rather that the whole representation changed (Figure 2-14 E). This became particularly apparent as the dimensions increased, suggesting that the first two dimensions (which carry the most variance) are kept intact. The FF information in the two cases (with and without FB) is presumed to be the same, and therefore, it makes sense that there is a subspace that is invariant to the presence of FB and a subspace that is shaped by it.

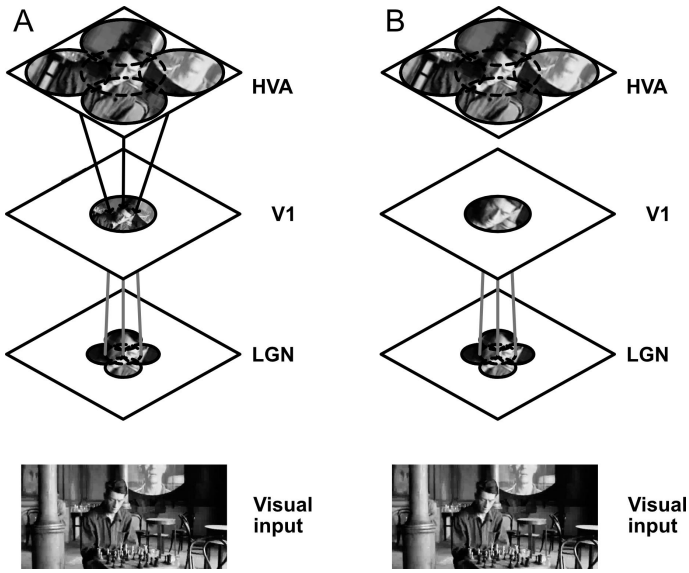

Figure 2-17 Illustration: Lack of FB from HVA to V1 changes the response to naturalistic movie.

A. FB from HVA is intact. When the naturalistic movie is presented, V1 incorporates the FF information coming from LGN and the FB information coming from the HVA. The LGN neurons that have an overlapping RF with the V1 neurons send the response to the patch of the image they have access to through FF projections. Neurons in the HVA also respond to the patch of the image they have access to. Since they send FB projections from HVA neurons that have overlapping and non-overlapping RF, V1 incorporates the FF and the FB signals and responds to the image in its RF but incorporating the surround information. In the image each plane represents an area, and the

circles represent the size of the RF and ‘what they see’. The gray arrows indicate the FF connections and the black arrows the FB connections.
B. FB from HVA is silenced. When the naturalistic movie is presented, V1 only incorporates the FF information coming from LGN. The LGN neurons that have an overlapping RF with the V1 neurons send the response to the patch of the image they have access to through FF projections. This information activates the Neurons in V1 creating a response to only the patch of the image in the RF of V1 neurons. Neurons in the HVA also have access to the image patch in their RF, however they do not send this information back to V1. In the image each plane represents an area, and the circles represent the size of the RF and ‘what they see’. The gray arrows indicate the FF connections and the black arrows the FB connections.

Figure 2-14 F showed how the angular difference was dependent on the time of the movie. In this figure, the biggest angular difference comes from the latter half of the movie. This part corresponds to the spatial statistics being larger, as more items of the room become visible. Additionally, both the beginning of the column scene and the end of the column scene have a larger angular difference. These two points indicate a somehow drastic change in the visual field. According to the predictive error framework (Shipp, 2016; Leinweber et al., 2017), this change could elicit some prediction error responses as the expectations of the environment change. Alternatively, from the point of view of adaptation (Carandini & heeger, 2012), one could also expect larger responses to novel stimuli. In addition, the contextual information becomes more similar to the local information, this could lead to some effect of surround suppression. However, we do not see such an affect when looking at the difference in length in that period (Figure 2-14 D). To better understand and characterize the relationship of the changes and the visual flow, one should measure the energy of the visual flow (Horn & Schunck, 1981) and the spectrum of the spatial and temporal frequencies and investigate whether any dependencies are found. In addition, because each of the session was recorded on a different location in V1, the neurons on each

of the sessions have access to different visual field. Therefore, it would be important to find a method to assess what is the RF of the V1 neurons on each of the sessions (Liu, et al., 2016).

We believe that while further characterization may be needed, our results are consistent with FB carrying surround information and therefore changing the information that V1 receives. An illustration of this idea can be seen in Figure 2-17. In Figure 2-17 A the FB from HVA carry surround information, therefore V1 has information not only what is on its RF but also the statistics of the near context. When HVA FB is silenced (Figure 2-17 B), this information is lost, therefore V1 only receives the visual information corresponding to its RF. This illustration shows how the same stimulus can be represented by V1 very differently on the absence of FB giving rise to a change in the geometrical representation but not in its gain.

Naturalistic stimulus, bring diversity to the neural representation but are unconstrained. Responses to drifting gratings are very characterizable but lack ethological validity. Each of them teaches something about the visual system but lacks what the other one has. A third alternative is to use artificially manipulated naturalistic images (Freeman & Simoncelli, 2011; Freeman et al., 2013; Rikhye & Sur, 2015). These approaches have turned useful to prove the computations of the visual system because they allow to modify certain stimulus characteristics to prove hypothesis. This type of stimulus seems particularly useful to use in future FB silencing experiments, as it could allow to pinpoint specific characteristics that would elicit certain change, or no change at all, helping to understand the computation principles of FB.

2.3.5 Limitations of the analysis

In this study we focused on the differences in the mean responses when direct cortico-cortical FB was silenced and when it was intact. We took this approach because we were interested on the effect of FB on the stimulus representation. However, this analysis disregards other effects that FB may have in the trial-to-trial variability.

Whether there was a difference in the trial-to-trial variability in the case of the response to the drifting gratings was partially investigated with the variance explained by each of the tuning axis. We saw that this measure was unchanged in the two conditions (Figure 2-10 B). Suggesting that for this stimulus there was no structural difference in the trial-to-trial variability. However, further analysis was not done in this direction.

In order to investigate the structural changes of the trial-to-trial variability due to the absence of direct cortico-cortical FB from HVA to V1, one should employ other dimensionality reduction techniques where the temporal structure is maintained. Tensor component analysis may be a good approach as it maintains different the components: mean stimulus representation, trial-to-trial variability and neuronal activity. Allowing parse out the different components in which the response between the two conditions may vary. However, this method would require for a larger set of recorded neurons in order to be able to accurately answer this question.

Additionally, to study the interaction between internal state and the presence of direct cortico-cortical FB, an alternative FB silencing method such as optogenetic would be preferred. Using optogenetic silencing allows for interleaved trials with and without FB, allowing to have a more

reliable comparison between trials that are close together and therefore more likely to share a similar internal state.

2.4 Materials and Methods

Modified from Fioreze (2022)

2.4.1 Animals

All procedures underwent review and approval by the Champalimaud Centre for the Unknown Ethics Committee and were conducted in compliance with guidelines established by the Portuguese Direcção Geral de Veterinária. The hM4D(Gi)-FB and Ctrl groups consisted of heterozygous male mice expressing GCaMP6s in the cortex (C57BL/6J-Tg (Thy1-GCaMP6s) GP4.3Dkim/J). For all in vivo experiments, mice aged between P56 and P182 at the initiation of the study were housed with their littermates in a 12-12 hour reversed light–dark cycle.

2.4.2 Surgery protocol

Pre-imaging procedures

All mice used for the hM4D(Gi)-FB group underwent the following procedures, in order: (1) clear skull preparation, (2) intrinsic signal imaging, (3) virus injection and window implantation, and (4) intrinsic signal imaging.

All mice used for the Ctrl group underwent the following procedures, in order: (1) window implantation, and (2) intrinsic signal imaging. Animals used for in vivo functional imaging of axons underwent the following procedures, in order: (1) virus injection and window implantation, and (2) intrinsic signal imaging.

Clear skull preparation

Animals in the hM4D(Gi)-FB group were anesthetized with isoflurane (induced: 5%; sustained 1-1.5%; O2 flow: 1L/min) and injected with bupivacaine (0.15ml, 0.05%, injected under the scalp), buprenorphine (0.1mg/kg, subcutaneously), dexamethasone (2mg/kg; subcutaneously) and Cefovecin (6mg/kg; subcutaneously) to supply local and general analgesia, control inflammation and to prevent postoperative infections, respectively. Eyes were kept moist using ophthalmic ointment (Vitaminoftalmina A). While under anesthesia, body temperature was maintained at 37°C using a heating pad (Supertech). A circular cut was made on the scalp exposing the skull. After cleaning the connective tissue, a layer of cyanoacrylate was applied uniformly into the skull followed by a thin layer of clear dental cement. A custom-designed circular head-post was fixed to the skull over V1 with black dental cement. Next, the clear dental cement located inside the head-post well was polished using dental drills and a layer of transparent nail polish applied (Guo et al., 2014).

Viral injections and imaging window implantation

Animals were anesthetized with isoflurane (induced: 5%; sustained 1-1.5%; O2 flow: 1L/min) and injected with bupivacaine (0.15ml, 0.05%, injected under the scalp), buprenorphine (0.1mg/kg, subcutaneously), dexamethasone (2mg/kg; subcutaneously) and Cefovecin (6mg/kg; subcutaneously) to supply local and general analgesia, control inflammation and to prevent postoperative infections, respectively. Eyes were kept moist using ophthalmic ointment (Vitaminoftalmina A). While under anesthesia, body temperature was maintained at 37°C using a heating pad (Supertech). Viruses were injected using a polished pulled glass pipette with an opening of 10-15μm. Mineral oil was applied at the back of the pipette prior to insertion of a plunger, which was controlled by a hydraulic manipulator (Narashige, MO10).

For mice in the hM4D(Gi)-FB group, the skull surface was exposed by removing the dental cement layer within the head-post well with a dental drill. 30-40 nL of AAV5-CaMKIIa-hM4D(Gi)-mCherry (Addgene, catalog 50477-AAV5) was injected in LM, AM, RL, AL and PM (left hemisphere, 0.35 mm in depth) (Figure 3-18 A). Retinotopic maps and brain vessels obtained from intrinsic signal imaging were used to define the injection sites (Figure 3-18 B). Mice in the Ctrl group were not injected with viruses.

Animal in all groups had a circular craniotomy (4mm) drilled in the bone over the left visual cortex using a dental drill. The dura mater was kept undamaged. A custom-designed imaging window was built from two layers of glass attached with a UV-curable optical glue (Norland Optical Adhesive 61). The top glass had a torus shape with an outer diameter of 5mm and inner diameter of 3mm. The bottom layer of glass was shaped as a circle with outer diameter of 4 mm and two circular holes of 0.15 mm allowing intracerebral injection of solutions. The imaging window was carefully placed over the craniotomy and attached to the skull with cyanoacrylate and black dental cement.

Intrinsic signal imaging

Retinotopic maps of the visual cortex were acquired using intrinsic signal imaging (Kalatsky and Stryker, 2003; Marshel et al., 2011). Imaging was performed at the 'clear skull preparation' (Guo et al., 2014) or the glass imaging window. Mice were anesthetized with isoflurane (induced: 5%; sustained 1-1.5%; O2 flow: 1L/min) and injected with chlorprothixene (1mg/kg, intramuscularly) (Kalatsky and Stryker, 2003). Eyes were kept moist using silicone oil (Sigma-Aldrich) while not perturbing the animal's vision. While under anesthesia, body temperature was maintained at 37°C using a heating pad (Supertech). We used a Retiga QIClick camera (QImaging) controlled using Ephus (Suter et al., 2010) to record intrinsic

signals at 5Hz. High magnification zoom lens (Thorlabs) focused at the skull or brain surface under the glass imaging window. We illuminated the surface of the skull or imaging window with a 620nm red LED while recording the hemodynamic responses to a drifting bar stimulus being presented to the mouse's right eye. The drifting bar crossed the screen 80 (clear skull preparation) or 40 (imaging window) times for each of the four cardinal directions (12s period, 20° width, masking an alternating checkerboard pattern at 5 Hz). At the end of the experiment, a picture of the blood vessels was taken using a 535nm green LED.

Drug preparation and injections

For intracerebral injections, mice were lightly anesthetized with isoflurane (induced: 5%; sustained 0.5%; O2 flow: 0.5L/min) and injected with dexamethasone (2mg/kg; subcutaneously) to prevent bleeding. Eyes were kept moist using ophthalmic ointment (Vitaminoftalmina A). Temperature of animals under anesthesia was maintained at 37°C using a heating pad (Supertech). Solutions were injected using a polished pulled glass pipette with an opening of 10-15µm. Mineral oil was applied at the back of the pipette prior to insertion of a plunger, which was con- trolled by a hydraulic manipulator (Narashige, MO10). Mice were injected with 100 nL of aCSF (125mM NaCl, 5mM KCl, 10M glucose, 10mM Hepes, 2mM CaCl2, 2mM MgSO4) or CNO diluted in aCSF (300 µM) at 200-300 µm in depth (Stachniak et al., 2014) (Figure 3-18 C and D). Animals were taken to the imaging setup immediately after the injections and recording started after animals recovered from anesthesia (around 15-30 min). All CNO solutions were made fresh on the day of the injection.

Histology

Up to one week after the end of imaging sessions, mice were deeply anesthetized and transcardially perfused with 4% paraformaldehyde in

0.1 M phosphate buffer, pH 7.4. Brains were sliced into 50µm coronal sections. We performed immunohisto- chemistry to boost mCherry signal with a polyclonal anti-mCherry antibody (abcam, ab167453) and an Alexa Fluor 594-conjugated secondary antibody (ThermoFisher, A-11037). DAPI was used as a counterstain. We imaged all brain slices that contained cortical structures using a slide scanner with a 10× objective (Axio Scan.Z1, Zeiss). Some brain slices were also imaged with a confocal microscope with a 40× objective (LSM 710, Zeiss).

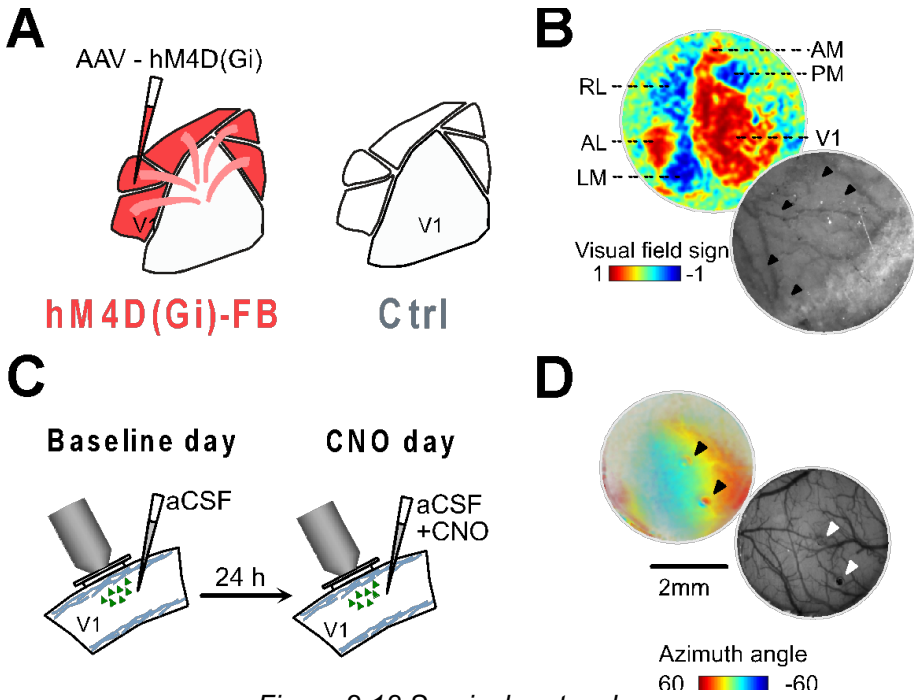

Figure 2-18 Surgical protocol.

A. Schematic of injections in the experimental groups. Thy1-GCaMP6s mice injected with *AAV5-CaMKIIa-hM4D(Gi)-mCherry* in the HVA surrounding V1 composed the hM4D(Gi)-FB group, whereas Thy1-GCaMP6s mice with no viral injections composed the Ctrl group. Modified from Fioreze, 2022.
B. Intrinsic-guided viral injections. Representative visual field sign map acquired with intrinsic imaging through the clear skull preparation and labels of the HVA and the corresponding image of vessels. Black arrows indicate injection sites. Modified from Fioreze, 2022.
C. Illustration of the recording days. Awake non-behaving mice from the hM4D(Gi)-FB and Ctrl group underwent two days of consecutive 2-

photon imaging immediately after an injection of aCSF or CNO in V1 (Baseline or CNO day, respectively). Modified from Fioreze, 2022.
D. Representative V1 retinotopic map (azimuth) and the corresponding image through the Custom-made imaging window. Windows were implanted so that holes were positioned over the V1 monocular zone (mint). Scale bar=2mm. Arrows indicate holes to allow local injections of aCSF or CNO. Modified from Fioreze, 2022.

2.4.3 Two-photon calcium imaging

We used a custom microscope (based on the MIMMS design, Janelia Research Campus, https://www.janelia.org/open-science/mimms) equipped with a resonant scanner. GCaMP6 was excited using a Ti:sapphire laser (Chameleon Ultra II, Coherent) tuned at 920nm. We used GaAsP photomultiplier tubes (10770PB-40, Hamamatsu) and a 16x (0.8 NA) objective lens (Nikon). We performed volumetric imaging by scanning in the axial direction with a piezo actuator (Physik Instrumente). Data from the time of the piezo flyback was discarded. Rubber rings in torus shape were glued to the head post to form an imaging well. Imaging well was shielded from light from the monitor with a custom-made conical shield attached to the objective lens. The microscope was controlled using ScanImage (Vidrio; Pologruto et al., 2003). The objective was perpendicularly aligned to the surface of the imaging window and kept for the two consecutive days of imaging. Imaging of calcium indicators began 3 weeks after viral injections and lasted for another 3 weeks.

For functional imaging of somas, seven planes separated by 30μm were acquired at a sampling rate of 8.32Hz per plane. Each FOV had 200×200μm (256×256 pixels). The first field of view was placed 150–180μm below the dura. For functional imaging of axons, mice were head-fixed and lightly anesthetized with isoflurane (induced:5%, sustained:1%, O2 flow: 1L/min) and injected with chlorprothixene (1 mg/kg, intramuscular) to reduce movement artifacts. Temperature of animals

under anesthesia was maintained at 37°C using a heating pad (Supertech). Four planes separated by 10μm were acquired at a sampling rate of 7.5Hz per plane. Each FOV had 80×80μm (512×512 pixels). Axons were imaged 20–100μm below the dura. Imaging positions were centered in the V1 monocular zone guided by intrinsic imaging and immediately beside the hole used for the injection of solutions.

2.4.4 Stimuli

Visual stimuli were presented on a LED (BenQ XL2411Z 24") monitor positioned 20cm from the mouse. Monitor was positioned to provide stimulation to the mouse's right eye and about 45° to the mouse's head axis.

We used Matlab and Psychophysics Toolbox (Brainard, 1997) to generate the batch of visual stimuli. Mice in the hM4D(Gi)-FB and Ctrl group were presented with drifting gratings and a natural movie. Full field, full-contrast drifting gratings moved in one of eight directions (cardinals and obliques), had a spatial frequency of 0.02 or 0.04 cpd and a temporal frequency of 0.5 or 1Hz. Each grating type (combination of direction, spatial frequency and temporal frequency) was repeated 20 times. The structure of the trials was as follows: 0.25s of gray screen, 0.5s of visual stimulation (stimulus period), 0.25s of gray screen. For the natural movie, a black and white clip (30s) from the movie Nineteen Eighty-Four (directed by Michael Radford, 20th Century Fox, 1984) was presented 10 times. The structure of the trials was as follows: 3s of gray screen, 30s of visual stimulation (stimulus period), 2s of gray screen. Animals were also recorded for 5 minutes while every pixel in the monitor was black. Mice used for functional imaging of axons were presented with drifting gratings as described before except with a spatial frequency of 0.04 cpd and a temporal frequency of 1 Hz. The structure of the trials was as follows: 0.5s of gray screen, 0.5s of visual stimulation, 2s of gray screen.

Running speed measurement

Mice speed was measured with a linear treadmill coupled to a magnetic analog rotary encoder (MAE3, US Digital). Rotation of the linear treadmill was recorded and digitized using Bpod and Analog Input Module (SamWorks, www.sanworks.io). ADD treadmill for dark.

2.5 Data Analysis Methods

2.5.1 Data pre-processing

For each recording session of somatas, we conducted image registration, identified and curated neurons, and extracted F traces (soma and neuropil) using the Suite2p toolbox (Pachitariu et al., 2017). Neuropil F traces were then subtracted from soma F traces using 70% of the total neuropil F trace detected. Following this, we determined the baseline fluorescence, F0, for each region of interest (ROI) by computing the 30th percentile of the F traces using a 60-second sliding window. Finally, the normalized fluorescence ($\Delta F/F$) was calculated as follows:

$$\Delta F/F = (F - F0)/F0$$

For somatas, to avoid contamination of tails into following trials due to the slow decay of the GCaMP signal, we deconvolved $\Delta F/F$ traces using the standard package available at the Suite2p toolbox.

Tracking of neurons across days

Neurons present in both days of imaging were identified using ROIMatchPub (source code: www.github.com/ransona/ROIMatchPub). This software utilizes the mean projection of the registered sessions along with user-defined landmarks to identify the positions of regions of interest

(ROIs) across multiple days. Subsequently, the ROIs are overlaid and compared, with additional manual curation based on anatomical features to verify the identity of neurons.

Analysis running speed

For each trial, the running speed was computed, and a trial was labeled as a 'running trial' if the animal's speed exceeded 1cm/s for more than 10% of the trial duration. During subsequent analysis, 'running trials' were excluded when drifting gratings were presented. Likewise, during the presentation of natural movies, periods of running were disregarded.

2.5.2 Data normalization

Because the silencing of HVAs feedback had mix effects on the activity levels of the cells, to avoid confounding results in the population analysis the deconvolved traces were z-scored per neuron and per session.

2.5.3 Single neuron analysis

Orientation and direction selectivity index

Orientation and direction selectivity indexes were computed using a global orientation selectivity index (gOSI) (Mazurek et al., 2014):

$$gOSI = \left| \frac{\sum_k R(\theta_k) exp(2i\theta_k)}{\sum_k R(\theta_k)} \right|$$

Where R(θk) is the response to angle θk including the stimulus period of trials at the combination of temporal and spatial frequency that elicited the

maximal response (preferred temporal and spatial frequency) for each neuron.

Cosine similarity

Cosine similarity (CS) was calculated as the follows:

$$CS(a,b) = \frac{a \cdot b}{|a|\,|b|}$$

Where a and b are tuning curve vectors of a given neuron for ’Baseline’ and ’CNO’ imaging days, respectively. For natural movies, tuning curves were obtained by averaging all trials for each 2-photon acquired frame during stimulus presentation. For natural images, tuning curves corresponded to the average response to each stimulus type.

Signal and noise correlations

Signal correlations were calculated as the Pearson’s correlation coefficient of tuning curves to all combinations of pairs of neurons modulated by the stimulus in an imaging session. For noise correlations, first ’noise’ was calculated by subtracting the average response to all trials from all trial responses for each neuron. After that, noise correlations were calculated as the Pearson’s correlation coefficient of the noise for all pairs of neurons in an imaging session. To calculate mean correlations for each animal, correlation coefficients were first averaged for each session and after for each animal.

2.5.4 Principal Component Analysis

Main PCA analysis

PCA was done following the eigen decomposition method. For that first, after normalizing the data (section 2.5.2), the Baseline day and the CNO day trials were concatenated. Thus, the data had the dimensions of the

neurons present in a given session and double the number of stimulus (one for the Baseline and one for the CNO day). This allowed us to create a shared space between the two days so the PC components would be the same.

Once that was done, the covariance matrix was calculated (**V)** and then the eigenvalue decomposition:

$$V = W\Lambda W^T$$

The variance explained was given by the diagonal entries of the Λ matrix, and each of the principal component was computed in the following manner:

$$PC_i = \tilde{X}^T \boldsymbol{w}_i$$

Tuning axis

In the case of the drifting gratings, another dimensionality reduction was done to characterize the tuning axis of a given orientation r. For this, we projected the trials of the orientation r for both days (Baseline and CNO) into the first three principal components. This created a matrix $\mathbf{Y}_r$ of 3x160, since each oriented drifting grating was repeated 160 times and the two days were included.

$$Y_r = \sum_{i=1}^{3} \tilde{X}_r^T w_i$$

We then following the same approach as before calculated its covariance matrix and performed the eigen decomposition. This provided us with the main axis which we called the tuning axis for orientation r.

Angle between tuning axes

The angle between the tuning axis of orientations r and l was calculated by multiplying the eigenvectors of each of the tuning axes and calculated the arc cosine of the value.

Length difference and angle between PC projections

In the case of the naturalistic movie stimulus, we calculated the length difference and the angle between the mean Baseline day activity projected into the first n PCs and the mean CNO day activity projected into the same first n PCs.

This was done by first projecting each of the activities into the corresponding PCs:

$$Z_{Bas} = \sum_{i=1}^{n} \tilde{X}_{Bas}^{T} w_i$$

$$Z_{CNO} = \sum_{i=1}^{n} \tilde{X}_{CNO}^{T} w_i$$

The length difference was given by the difference of the modulus of the two vectors

$$\mathbf{d}_{\text{Bas – CNO}} = |Z_{Bas}| - |Z_{CNO}|$$

This was the difference for the full naturalistic movie, and then it was averaged to calculate the mean value per PC.

The angle was calculated by the arc cosine of the multiplication of the two matrixes:

$$\mathbf{a} = \text{acos}(Z_{Bas} Z'_{CNO})$$

This again gave the angular difference for all the trials of the movie; this was again averaged to get one value for each PC.

Same day control

To control for changes in angle due to an increase of the dimensionality and trial-to-trial variability, we created a second control group for the hM4D(Gi)-FB. This group was generated by random allocation of half of the trials of the hM4D(Gi)-FB Baseline day as same day control Baseline and the remining trials to the same day control CNO group. All the measurements were done exactly the same way as the Ctrl and hM4D(Gi)-FB groups.

2.5.5 Statistics

For all the statistical analysis α was set to 0.05. Numbers of sessions and cells are stated in the text.

Single Neuron:

Tuning curve comparisons were conducted using a 2-way ANOVA, with imaging day (Baseline and CNO) or experimental groups (hM4D(Gi)-FB and Ctrl), and orientation or direction angles as grouping factors. Subsequently, Bonferroni post hoc tests were applied, with a significance level (α) set to 0.05.

For other parameters, comparisons between imaging days (Baseline and CNO) or experimental groups (hM4D(Gi)-FB and Ctrl) were performed using t-tests, with α set to 0.05. Neurons were pooled across all animals unless otherwise specified, and when not explicitly stated, the t-test was unpaired.

To control for variability across animals, comparisons between means across animals were done using hierarchical bootstrap (Saravanan et al., 2020). Neurons from different sessions but same animal were pooled. Data was resampled 10000 times and frequency of neurons for each animal was kept. To obtain the p-value with α set to 0.05, the joint probability distribution of the two groups was computed with each sample forming the two axes of a 2-D plot and the total density of the joint probability distribution on one side of the unity line was measured. The computed value will be called pboot in this thesis to differentiate from the p-value of standard statistical methods. Experimental groups are significantly different if $p_{boot} \geq 0.975$ or $p_{boot} \leq 0.025$.

Population Analysis:

Within group statistical analysis was done using a 2-way repeated measures ANOVA, the main effect was the group (CNO vs Baseline), and PCs or orientations were the group factor. Then post-hoc comparisons were done to check for significant difference between the two groups.

Between group statistical analysis was done by using a 2-way ANOVA, the main effect was the group (Ctrl vs hM4D(Gi)-FB), and PCs, orientations or frames were the grouping factors. Then post-hoc comparisons were done to check for significant difference between the two groups7

When only two measures were tested a simple t-test was performed.

Chapter 3 – Organization of mouse sexual behavior and the effect of experience

L'histoire d'un corps est l'histoire de l'oubli.

-Jaques Le Guff et Nicolas Troung[4]

[4] The history of a body is the history of an oblivion.
- J. Le Guff & N. Troung, A history of the body in the Middle Ages p.11, 2004

3.0 Author contribution

Experimental conception and design Susana Lima S.L. and Silvana Araujo (S.A.) Experiments S.A. Data pre-processing S.A. and Bertrand Lacoste (B.L.), Data analysis O.H. Modeling O.H. Writing O.H. Supervision and mentoring for project conception and structure S.L. for modeling C.M.

3.1 Introduction

In the previous chapter I mentioned the importance of moving from characterizing a single neuron to an ensemble of neurons (Yuste, 2015). The main argument is that by inspecting the ensemble we can access states that otherwise will be inaccessible. Therefore, we should leverage the technological advances of two-photon imaging and multielectrode arrays to understand neuronal populations as a whole, rather than individual neuronal properties. However, how much do we need to characterize and probe the population dynamics to understand it if we do not know how they relate to behavior, or if they relate to behavior at all?

In this chapter I take a different approach and I focus on studying and dissecting mouse sexual behavior, with the hope that its characterization may contribute to a better understanding on the various neural mechanisms required for its emergence.

3.1.1 The study of behavior in neuroscience

Neuroscience is the understanding of brain function. Because of the difficulty to define the words “brain” and “understanding”, this short sentence can be interpreted in a number of ways. When thinking about the brain one generally thinks of the mind, what makes us “*us”*. But what

does it mean? Scientifically speaking, the brain is the largest cluster of neurons in our body. For most animals, it is located in the head. It is believed to be the center of command of the nervous system. In vertebrates, the brain works closely with the spinal cord. Additionally, it sends and receives inputs from the peripheral nervous system, which expands through the whole body. In recent years, it has been shown that the nervous system has bidirectional communication with the immune and digestive systems (Quan & Banks, 2007; Cryan & Dinan, 2012; Dantzer 2018; Rutsch et al., 2020; Fung, 2020; Castellani et al., 2023). At minimum, the brain is an extremely complicated organ with diffuse boundaries. One could dare to go beyond the mind-body duality and think that due to this tight interconnection with other organs, it is impossible to sever the brain from the body function. This inevitably brings us to the question: what is the body without behavior? Before delving into this, we should think of what understanding is and what it implies for the brain.

To understand something is to grasp its meaning, to connect the dots. It involves making associations between ideas and gaining an insight that was not there by the ideas alone. Using the over-employed example of gravity, one would say that knowing that the apple will fall to the ground is not an understanding. It is a mere description of the facts. To understand it, means to know that every object, because of its mass produces a perturbation that attracts other mass objects; Knowing that this is what makes the apple fall to the ground, and at the same time, the earth to revolve around the sun. Understanding something is a complicated and never-ending process. How do we go about understanding a complex system such as the brain?

David Marr (1982) postulated that there are three levels at which a complex system operates and the three must be understood to understand the system. In brief, there is (1) the computational theory; why

it does what it does, (2) the algorithm; how it does it, and (3) the implementation: how it is applied (Marr, 1982, p. 25). Since his contribution, there have been many discussions on the topic (Schall, 2004; Bechtel, 2008; Carandini, 2012; Cooper and Peebles, 2015; Frank and Badre, 2015; Badre et al., 2015; Fetsch, 2016). However, the main idea remains.

Assuming that the brain is the driver of the body when performing a behavior, then, one could say that behavior is the main function of the brain. Therefore, to understand brain function, one must investigate how the neural processes relate to behavior (Gomez-Marin et al., 2014). In other words, to describe the particularities of how the nervous system reacts to a stimulus, or to model its reaction is not enough. In addition, one needs to have a theoretical understanding on whether and how a stimulus is relevant for the animal and why the animal behaves in response to it (Krakauer et al., 2017). To achieve this, one needs to dissect the behavior into its fundamental components to be able to pose hypotheses and theories based on their interplay (Cooper and Peebles, 2015).

This still leaves us with one difficult question: What is behavior? Indeed, it is such a broad term that behavioral biologist do not necessarily agree on what behavior entails or it does not (Levitis et al., 2009). Levitis et al. realized that both experts and novices rely on inference rather than in a definition when judging whether something is a behavior or not. After conducting a large survey among the experts on the field Levitis et al., proposed the following operational definition:

> ‘‘Behavior is the internally coordinated responses (actions or inactions) of whole living organisms (individuals or groups) to internal and/or

external stimuli, excluding responses more easily understood as developmental changes''

Notably, and most crucially for neuroscience, they concluded that while internal processing of information by the animal is a necessary condition for behavior, it is not sufficient as an action is required for it to be considered behavior. Importantly, this action may include inaction if the context requires so (i.e.: freezing upon a threat). Overall, behavior is an expansive concept that has three important attributes (Gomez-Marin, et al., 2014). First, it is relational, a behavior is a reaction to the environment and the internal state of the animal, therefore the context in which the behavior occurs needs to be addressed. Second, behavior is dynamic, it changes across time and space, acknowledging how a behavior changes over time is fundamental for its understanding. Third, behavior is high dimensional, while it has less degrees of freedom than neural activity, it is still highly complex. Different behaviors can occur simultaneously, and it is variable in the sense that is not predictable. Thus, the researcher should find a reduced space to map the behavior to be able to track it.

3.1.2 Learned vs innate behaviors

Behavioral responses are intimately linked with neural patterns of activity and vice-versa (Krakauer et al., 2017) (Figure 3-1A). Choosing the right behavior that we want to study is crucial to understand the type of neural activity that we are interested in. In neuroscience there are two broad types of behaviors in terms of how they are acquired: Learned, behaviors that are developed during the lifetime of the animal, through observation, association, or experience, and innate behaviors, which are present from birth or emerge at a certain point in the life of the animal without the need of learning.

The study of learned behavior is abundant in neuroscience, particularly in controlled and constrained settings. The most prevalent form of studied learning is instrumental learning, also referred to as operant conditioning (Skinner, 1969). It entails establishing an association between a behavior and its resulting outcome, frequently achieved through a trial-and-error approach. This process typically requires training the animal in a specific task, which it subsequently performs across numerous repeated trials (Harlow, 1949). The formalization of this type of learning has derived into the current reinforcement learning framework (Dayan & Balleine, 2002). However, training the animal can be difficult and costly (Dennis et al, 2021), and the interpretation of the neural activity underlying the behavior difficult. It has come to the attention of many researchers that often 'spurious' movements play a role and can often be a key component to interpret the neural activity during a task, particularly when the learned behavior is outside of the ethological repertoire of the animal (Figure 3-1 B) (Gilad et al., 2018; Musall et al., 2019; Stringer et al., 2019).

Innate behaviors are typically considered to be genetically hardwired and instinctive; they include hunting, escape, feeding, mating, and courtship among many others. Classically, such behaviors have been studied in the field of ethology. Ethology aims to understand behavior in natural settings, including its phenomenological, causal, ontogenic and evolutionary aspects (Lorenz, 1937; Tinbergen, 1951, 1963; Von Frisch, 1953). The study of innate behaviors has been less common in neuroscience, however in recent years there has been a call to highlight its importance to understand brain function (Anderson & Perona, 2014; Gomez-Marin et al., 2014; Krakauer et al., 2017; Brown and de Bivort, 2018; Juavinett et al., 2018; Mobbs et al., 2018; Datta et al., 2019; Gomez-Marin, 2019; Mathis & Mathis, 2020; Parker et al., 2020; Cisek & Green, 2024). The use of such behaviors constrains the neural activity to be relevant to the behavior (Figure 3-1 C) (Krakauer et al., 2017), avoiding the mentioned

problems with neural activity underlying non-behaviorally relevant tasks. Additionally, it can lead to the discovery of shared computational principles across species.

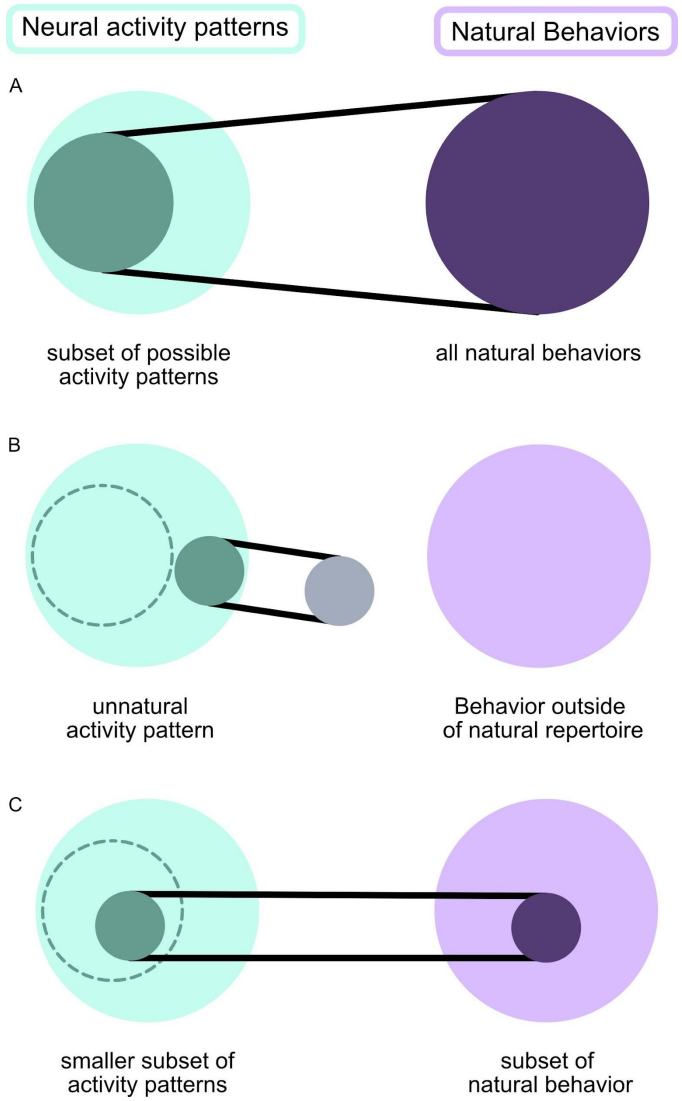

Figure 3-1 Illustration of potential mappings between neural activity and behavior.

A. Of all the potential neural activity patterns (big light blue circle), only a subset (medium dark blue circle) will be pertinent to the behavior of animals in their natural habitat (big dark purple circle). Modified from Krakauer et al., 2017.

B. The task that the animal learns in the lab (small gray circle) might be so non-ethologically relevant it elicits neural responses (small blue circle) that are non-existent in natural behaviors. Modified from Krakauer et al., 2017.
C. The use of innate behaviors (small purple circle) guaranties the identification of neural circuits relevant to the naturalistic behavior (small blue circle). Modified from Krakauer et al., 2017.

Considering the intricate interplay between behavior and neural activity, one can wonder: What makes an animal start or stop drinking water at a particular point if nothing in the environment has changed? or why does an animal chase a potential mate at a specific moment? Since this chapter of my thesis is dedicated to innate motivated behaviors, in the following section I will discuss the main frameworks and structure of motivated behaviors, for a detailed review see Berridge, 2004.

3.1.3 Structure of instinctive motivated behaviors

The concept of motivation has served behavioral scientist for over a century to frame the understanding of innate behaviors. After careful observation of various animal behaviors and following the work of Sherrington (1906), the ethologist Wallace Craig (1918) concluded that innate behaviors had a beginning point, a middle part, and an end point. In particular, he identified four different phases: Appetitive, consummatory, aversion and freedom from stimuli (Figure 3-2). Appetitive phase is characterized by an absence of the stimulus of desire (water, food, …), and by a flexible and active search and approach to it. Appetitive behaviors are characterized by their learnability (Berridge, 2004). Consummatory behaviors are initiated when the goal stimulus is at reach. Such behaviors often involved stereotypical species-specific actions (Berridge, 2004). Once the consummation of the goal stimulus ends, the

aversive phase starts. In this phase, the stimulus that once was desired becomes unwanted or undesirable and thus the animal actively tries to get rid of it (Ball & Balthazart, 2008). Eventually the phase of “being free from the stimulus” is initiated, when the stimulus does not generate a valence state to the animal. While not every innate behavior can be divided into four phases depending on the species, it has become a useful division to describe the non-stationary interaction of animals with stimuli in the environment. Currently, this four-phase division has evolved into the pleasure cycle (Krigelbach et al., 2004; Krigelbach et al., 2012; Georgiadis et al. 2012) (see section 2.2.5 for more details).

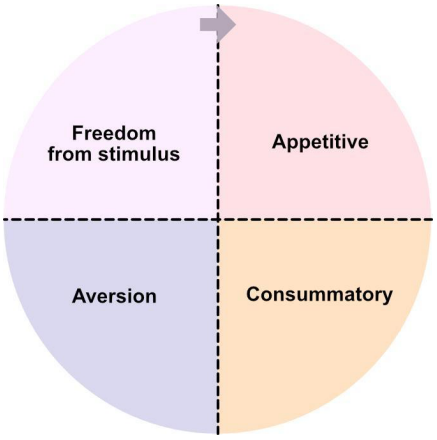

Figure 3-2 Four phase innate behavior model by W. Craig (1918).

In order to explain the transition between these phases, behavioral scientists have employed the term ‘drive’. The use of drive allows to create an intervening variable to parsimoniously explain and predict a behavior (Miller, 1971). In this context, thirst, hunger, and sexual arousal would be the drivers of drinking, eating, or mating behaviors. Thus, the drive provides a quantification that can be assessed through its associated impacts on behavioral dependent variables (Berridge, 2004).

3.1.4 Sexual behavior

Sexual behavior is present in animals that reproduce sexually. It usually entails a complex interaction between sexually mature individuals and involves the integration of external and internal cues to make adequate decisions and achieve a goal. While it is accepted that the experience of the individual animal refines the expression of the behavior (Hull and Rodríguez-Manzo, 2009; Swaney et al., 2012; Wei et al., 2021), sexual behavior falls under the umbrella of innate behaviors, as it is primarily under the influence of hormonal actions in the brain that allow for external cues to trigger sexual arousal (Xu, 2013; Rodríguez-Manzo & Canseco-Alba, 2014; Ryu & De Marco, 2017). Because of its complexity, the study and dissection of sexual behavior can elucidate many areas of neuroscience such as perception, decision making, motivation, reward, etc.

While undoubtedly one of the main goals of sexual behavior is fertilization, sex can be much more than that. In many species, including humans, engaging in sexual behavior can be a source of pleasure, social bonding, and intrinsic reward (Toates, 2009; Trezza et al., 2011; Pfaus et al., 2012; Fleischman, 2016; Werner et al., 2023). Interestingly, while animals engage in sexual behaviors often and innately, the survival of the individual animal is not necessarily tied to them engaging in such behaviors. In fact, quite on the contrary, as sex can lead to high-risk situations due to exposure to predators (Magnhagen, 1991) or parasites (Hamiltoon & Zuk, 1982). For instance, the female praying mantis would attempt to eat the male after mating. However, from the point of view of the species or the social group, reproduction is crucial for its survival across time. Therefore, for the species reproducing sexually, such as

mammals, the engagement of the individuals on sexual behavior is beneficial and explains why animals may risk their safety in doing so.

Sexual reproduction requires two different gametes (sperm and eggs) to be exchanged between the individuals. The gametes are produced in the reproductive organs or gonads. Most mammalians are gonochoristic, which means that the reproductive organs of each individual can either produce eggs or sperm. Individuals producing eggs are generally referred to as females, and individuals producing sperm are referred to as males. Individuals with atypical sex variations are referred to as intersex. In humans the percentage of intersex population is relatively low, it ranges from 0.05-1.75% of the population depending on how it is quantified (Blackless et al.,2000; Committee on Measuring Sex, Gender Identity, and Sexual Orientation, 2022, p18). This percentage is comparable to the estimated redhaired people (1-2%) (Katsara & Nothnagel, 2019). The formation and differentiation of sex is a multilayered process that goes from genes to culture. For a larger discussion on the topic, I refer the reader to the book Sexing the body (Fausto-Sterling, 2000).

Generally, sexual encounters involve two individuals. There is evidence in humans and non-human animals of male-male and female-female sexual encounters (humans: Committee on Measuring Sex, Gender Identity, and Sexual Orientation, 2022, p18. Non-human animals: Dagg, 1984; Bagemihl, 1999; Roughgarden, 2013). While such encounters do not lead to reproduction, they may fulfill a role in the societal structure of the species (Bailey & Zuk, 2009). Most sexual encounters in non-human animals, however, involve a male and a female, and thus this will be the focus of this chapter.

3.1.5 The structure of sexual behavior

Mammalian sexual behavior is highly variable across species. Nonetheless, it generally follows a simple pleasure cycle (Craig 1918; Sherrington 1906; Georgiadis *et al.* 2012). Three phases can be described: (1) appetitive or pre-copulatory (wanting), characterized by an increase in motivation and approach to the sexual partner; (2) consummatory or copulatory (liking), where the body of the sexual act occurs, there is a strong presence of genital responses and actions that may result in the climax that can take the form of orgasm and/or ejaculation; (3) satiety or refractory phase (inhibition/ learning), this phase is known by a lack of sexual interest of the animal (Figure 3-3).

The appetitive phase is the phase where we find more variations across species, mainly in courtship behaviors. They can range from elaborate dances to complex nest building (Bastock, 1967; Andersson, 1994; Hebets & Uetz, 1999; Olsson et al., 2009). This phase entails behaviors that can call for the attention of putative mates. One of its main goals is to gather information that can help individuals make a choice of a suitable partner (Lenschow et al., 2022), recognize the reproductive state of others (Hanson & Hurley, 2012), increase sexual arousal (Lee et al., 2016) and generally guide animals to encounter a partner to initiate the next phase, copulation.

The copulatory phase is unique to each animal species (Dewsbury, 1972). This phase is shaped by natural and sexual selection. For instance, the pressure of the environment (i.e.: risk of predation), may modulate the length of the copulation (Eberhard, 1996; Birkhead & Møller, 1999; Simmons, 2001; Firman et al., 2017). For a review on how genital morphology may shape copulatory behavior see Brennan & Orbach,

(2020). Despite the differences, shared solutions can be seen across various species (Anderson, 2016), suggesting that gaining understanding of the behavior for a particular model organism can help us find common generalizable principles to elucidate such an intricate behavior. In mammals, where fertilization is internal, copulatory sequences require the insertion of the male organ in the female reproductive organ (Schärer et al., 2011). Alternatively, this process can be also understood as the female reproductive organ circluding the male organ (Adamczak, 2016). Through a series of copulatory sequences, male and female arousal are thought to increase, until the male ejaculates and deposits the sperm inside the female.

After ejaculation, in many species males enter an inhibitory phase where sexual motivation is highly decreased (Masters & Johnson, 1966; Seizert, 2018). This phase is supposed to tie reproductive capacity to behavior, such that the male only engages in sexual behavior when enough sperm is available (Rojas-Durán et al., 2015; Hernandez et al., 2006). This period can vary dramatically across taxa, depending on the reproductive strategy of each species (McGill, 1963; Wilson et al., 1963; Rodriguez-Manzo, 1999; Levin, 2009; Valente et al, 2021).

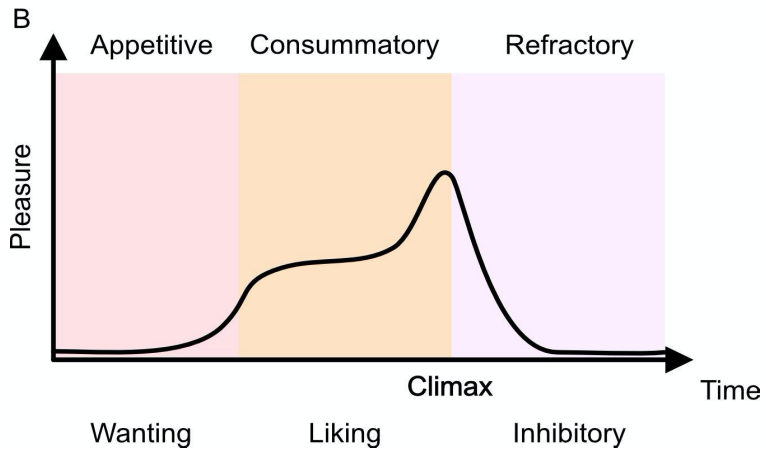

Figure 3-3 The pleasure cycle of sexual behavior.

3.1.6 Mouse sexual behavior

This chapter of the thesis focuses on sexual behavior, to the general question of understanding how the coordinated action of two individuals leads to fertilization. Because sexual behavior differs widely across taxa, this section will focus on rodents, in particular the house mouse, the object of study during this chapter of my thesis.

Rats and mice excel at generalization (Dennis et al., 2021). They display an extensive range of behavioral flexibility and the capacity to thrive in virtually any environment, regardless of its natural or artificial nature. Additionally, many aspects of rodent sexual behavior are observable and relatively easy to study in a controlled laboratory setting (Dewsbury, 1975), retaining many aspects of their expression in the wild (McGill, 1963). This makes rats and mice a commonly used model organism to study various aspects of sexual behavior. Due to rats being more complex social animals than mice, they have been predominantly used as a model organism for sexual behavior in the past. In recent years, however, in part due to the advances in genetic mouse lines and techniques, and because its behavior is closer to the one exhibited in humans (with intravaginal thrusting post penile intromission and refractory periods more similar to humans, Valente et al., 2021), the study of sexual behavior in the mouse has become more popular.

In mice, as well as in rats and other gonochoristic animals, gonadal hormones are key to the sexual dimorphism observed in the brain and the behavior. Starting in the perinatal phase of the animal (before being born), gonadal hormones guide the development of sexual dimorphisms (Wallen, 2005; Wu & Shah, 2011; de Vries & Forger, 2015; Knoedler & Shah, 2018). Later, during puberty, the same gonadal hormones trigger

the activation of these circuits, leading to the expression of relevant sex-typical behaviors (Schulz, et al., 2009; McCarthy & Arnold, 2011; Arnold, 2009). For a review see (Jennings & Lecea, 2020) and for a comparative review between mice and rats see (Bonthuis et al., 2010).

Like most species, mice only engage in sexual encounters when they are sexually receptive and there is a high chance of fertilization. Post-puberty, in the presence of the right female cues and context, male mice will become sexually aroused and initiate copulatory actions (Mosig & Dewsbury, 1972). However, male receptivity will be decreased post-ejaculation, during the refractory period (McGill, 1963). The duration of this period varies across mouse strains, as it can last from some minutes in wild mice, to a couple of days or even weeks for the C57BL/6 strain, one of the most commonly used in laboratory settings (McGill, 1963; Valente et al., 2021). In rats, it seems that dopamine and serotonin may play a role in the duration of the refractory period (Lorrain et al., 1997; 1999; Guadarrama-Bazante & Rodriguez-Manzo, 2019), and more recently the circuitry in mice also has been explored (Bayless et al., 2023). The refractory period seems therefore to tie reproductive capacity to sexual behavior (Pfaus, 2009) and in some species can also be linked to different reproductive strategies (sperm allocation for example, Rojas-Durán et al., 2015; Hernandez et al., 2006).

Female receptivity on the other hand is closely tied to the reproductive cycle (Gutierrez-Castellanos et al., 2022). It is governed by the fluctuation of Estrogen and Progesterone hormones released by the gonads, forming what is known as the Estrous cycle. The estrous cycle in mice last 4-5 days, and females are only receptive during the proestrus/estrous phase of the cycle. To avoid unwanted pregnancy of the female, and for easiness of experimental design, many studies involving sexual behavior are done with hormonally primed ovariectomized females (Uphouse et al., 1970;

Edwards, 1970; Nelson, 2005), where after removing the source of sex hormones (the ovaries) the female cycle is recreated by exogenous treatment with estrogen and progesterone.

Mouse sexual behavior begins with the encounter of the potential mate. In this initial stage, called appetitive or pre-copulatory, volatile and non-volatile olfactory cues are an essential source of information of the other individual (Calhoun, 1963; Beach, 1976; Plant & Zeleznik, 2014). Non-volatile pheromones are smelled through nose-to-nose investigations. In addition, ultrasonic vocalizations are exchanged (Nyby, 1983; Neunuebel et al., 2015). As this phase evolves, nose-to-nose investigations transition into anogenital investigations, where the male (and the female) investigates the anogenital region of the female (male). These behaviors are believed to increase the arousal level of the couple (Asaba et al., 2017; Neunuebel et al., 2015) (Figure 3-4 Pre-copulatory period). When the arousal level of the male reaches the threshold to initiate copulation, he begins to attempt to mount the female by approaching the female from behind and resting his paws on the female flanks. The male can also perform failed mount attempts, in which he fails to position himself correctly in relation to the female (these mounts may include head mounts). If the female is in her non-receptive phase of the cycle she will reject the male, displaying an array of defensive behaviors (arching of the back, active escape behavior, kicking and boxing) to prevent mating (Gutierrez-Castellanos et al., 2022). It is important to note, that even if she is non-receptive, she will engage in social interaction with the male (Nomoto and Lima 2015, Gutierrez-Castellanos et al. 2022).

If the female is receptive, she will eventually adopt the lordosis position in response to the mount attempt (Plant & Zeleznik, 2014). The beginning of the copulatory period is typically defined by the first mount with intromission (penile insertion) (Figure 3-4 Copulatory period). These

mounts are characterized by an initial variable period of shallow penile thrusts (pre-insertive thrusting). The goal of this behavior is believed to be to locate the vaginal opening of the female (McGill, 1962), however it is still underexplored. After the first intromission or penetration, a series of deep pelvic thrusts follows. In mice, similarly to humans, the copulatory phase is characterized by the presence of multiple mounts. The mounts can be mounts with intromission or mounts without intromission. This type of mounts, as indicated by the name, lack intromission, therefore they are only composed of the pre-insertive thrusting period. Mounts are often followed by self-genital grooming bouts of the male. The length of the copulatory phase is highly variable and mouse specific. The end of the sexual encounter is marked by the ejaculation of the male mice inside the female vagina and the insertion of the plug, preventing her from copulating with other males (Sutter and Lindholm, 2016). After ejaculation, the male falls to the side and stays motionless for a few minutes. This marks the beginning of his refractory period (Figure 2-2 Refractory period). The female, on the other hand, can have several other sexual encounters during the receptive cycle (Dean et al., 2006).

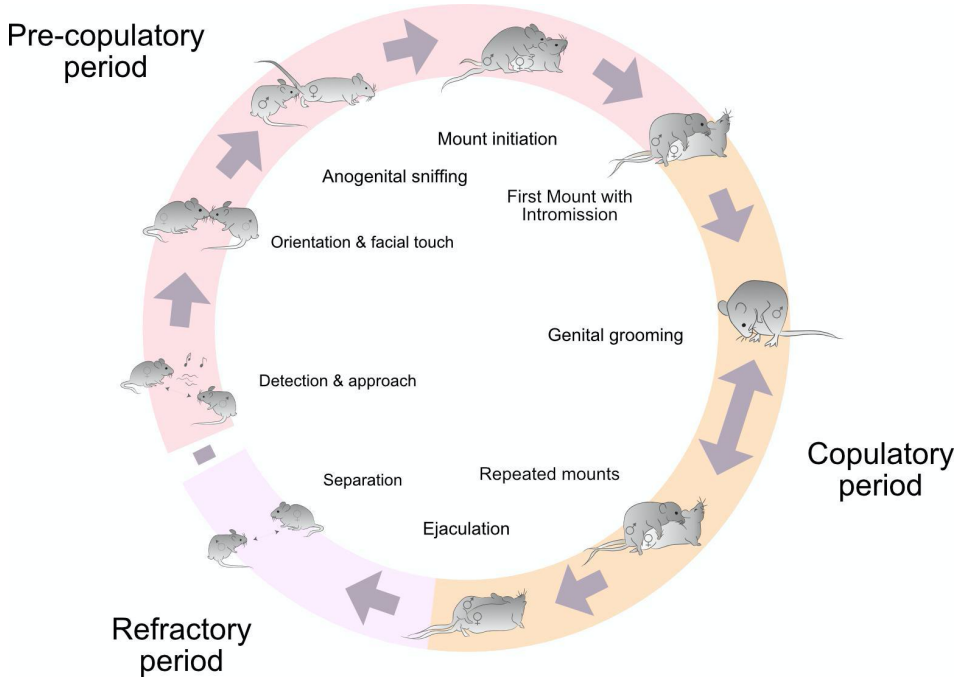

Figure 3-4 lustration of main motifs of mouse sexual behavior.

Adapted from (Lenschow & Lima, 2022)

From this description, it is apparent that mouse sexual behavior has a complex structure, suggestion that the underpinning neurobiological mechanisms are also complex and multifactorial

3.1.7 Neurobiological mechanisms of mouse sexual behavior

Chemosensory cues including pheromones, volatile and contact-dependent are fundamental for a successful sexual encounter. Airborne substances are detected and transmitted via the main olfactory pathway (Dulac & Wagner, 2006). Odor molecules are inhaled through the nasal cavities, passing through the main olfactory epithelium (MOE) where they bind to the olfactory sensory neurons (OSN) (Figure 3-5 A). Contact-dependent pheromones are transduced through the accessory olfactory pathway. They are actively pumped in through the nasal cavities reaching

the accessory olfactory epithelium (AOE), located in the vomeronasal organ (VNO) (Dulac and Wagner, 2006; Asaba et al., 2014). In the AOE non-volatile pheromones bind with to vomeronasal sensory neurons (VSN) that project to the accessory olfactory bulb (AOB) (Figure 2-5 A). Disruption of the main olfactory pathway in female mice by lesioning the MOE, reduced their tendency to approach conspecifics and the readiness to acquire the lordosis position (Keller et al., 2006). In a similar manner, impairing the accessory olfactory system in female mice by genetic or physical ablation of the AOE or AOB, reduces their interactions and the engagement in sexual behavior (Martínez-Ricós et al., 2008, Haga et al., 2010; Oboti et al., 2014; Leinders-Zufall et al., 2014), highlighting the vital role of odors in mice sexual behavior. Interestingly, while presence of male-derived non-volatile odors generates an innate attraction to sexually naïve females, the attraction to male-derived volatile odors is learned (Moncho-Bogani et al., 2002; Moncho-Bogani et al., 2005; Martinez-Garcia et al., 2009).

OSNs have downstream projections to the main olfactory bulb (MOB), the hub of the olfactory information in the brain. AOB in turn, targets several limbic areas; the medial amygdala (MeA), cortical amygdala (CoA) and the bed nucleus of the stria terminalis (BNST). All these areas are activated during the pre-copulatory phase (Ubeda-Bañon et al., 2007, Bergan et al., 2014; Li et al., 2017). The posterior dorsal part of MeA (pdMeA) responds stronger to the presence of the opposite sex and is experience dependent (Li et al., 2017).

The transition from the pre-copulatory to copulatory state is believed to be mediated by the inhibitory connections from MeA to the hypothalamic regions, including the medial preoptic area (MPOA), the ventromedial hypothalamus (VMH), and the ventral premammillary nucleus (PMv) (Raam & Hong, 2021; Bayless et al., 2023), MeA receives, in turn,

excitatory connections originating in the aforementioned hypothalamic regions (Figure 3-5 B). MPOA has been identified as one of the main areas controlling male sexual behavior in rodents (Angoa-Pérez & Kuhn, 2015; Hull & Dominguez, 2015). MPOA activation reflects mounting, thrusting and ejaculation (Kondo et al., 1990) and mediates penile erection (Hull & Dominguez, 2015; Nutsch et al., 2016). Additionally, activation of steroid receptor Esr1+ MPOA neurons through optogenetic stimulation produced comparable instances of mounting behavior and pup retrieval in both male and female mice (Wei et al., 2018; Karigo et al., 2021). The ventrolateral portion of the ventromedial hypothalamus (VMHvl), conversely, is recognized as a key component of the female sexual brain circuit. Classic studies involving electrical stimulation and lesions have demonstrated that it is essential for eliciting lordosis behavior in rats (Pfaff & Sakuma, 1979a, 1979b). Recent research in mice has reinforced the importance of the VMHvl in female sexual behavior, as the removal of its population expressing PR (progesterone receptor) significantly reduces lordosis behavior (Yang et al., 2013). Additionally, optogenetic stimulation of steroid receptor neurons such as Esr1+ of VMHvl in males (Lee, 2014) and females (Hashikawa et al., 2017) induces mounting regardless of the sex. Equally important is the Periaqueductal gray area (PAG) receiving projections from VMH. PAG brings hypothalamic information to the spinal cord, which controls activity. PAG seems to be involved in lordosis posture in rat and mice (Sakuma & Pfaff, 1979; Haga el al., 2010; Hashikawa et al., 2017; Ishii et al., 2017).

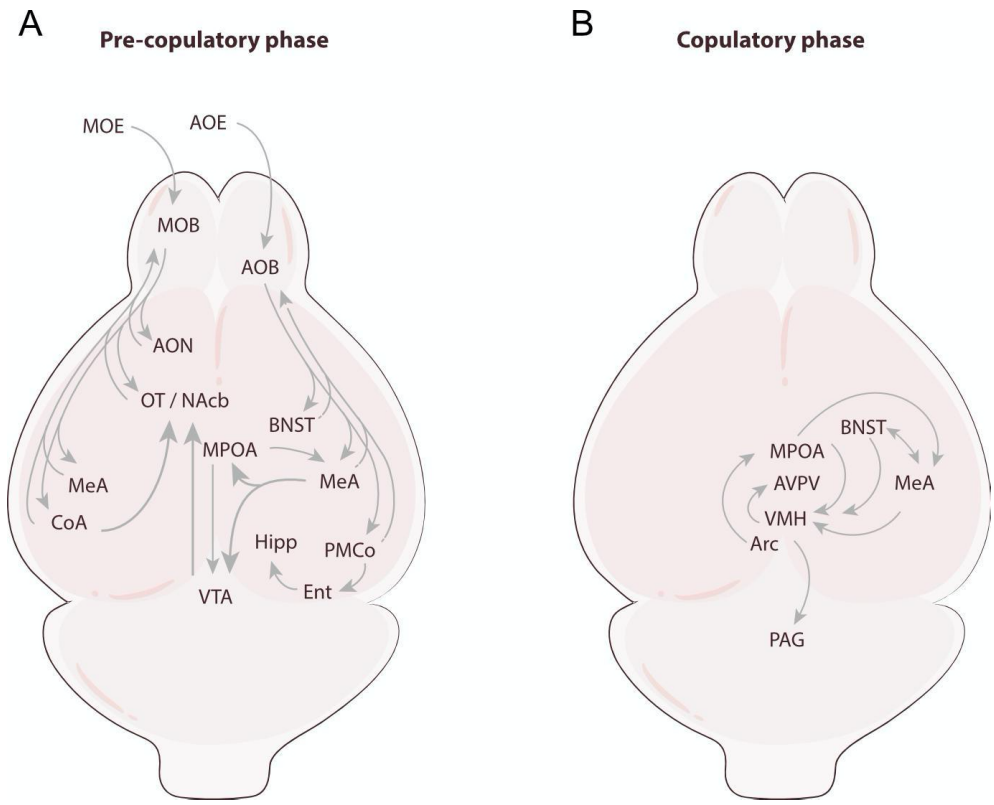

Figure 3-5 Main neural pathways of mouse sexual behavior.

A. Main neural pathways during pre-copulatory phase. Modified from Gutierrez-Castellanos et al., 2022.
B. Main neural pathways during copulatory phase. Modified from Gutierrez-Castellanos et al., 2022.

As mentioned, hormones play a pivotal role in sexual behavior. In fact, they not only trigger its initiation, but they fundamentally shape the behaviors during the sexual act. For a review on how hormones shape sexual behavior in mice see (Burns-Cusato et al., 2004, Gutierrez-Castellanos et al., 2022).

The intricacy of the neurobiological pathways and its complex relation with various aspects of the behavior, makes it clear that to understand the neurobiological relation with behavior, a detailed description of the behavior and how the different motifs relate to each other is needed.

3.1.8 Modeling sequential behavioral data

Variable behavioral sequences are often modeled as probabilistic outcomes (old: Miller, 1952; Altmann, 1965; more recent: Chen et al., 2012; Marques et al., 2020; Cury & Axel, 2023). This means that the sequence is not deterministic but follows a latent probability distribution. The goal is to find a probabilistic model that generalizes well to unseen data and captures the main properties of the behavior.

Markov Model

The most parsimonious approach to building a model that captures the stochasticity of a series of sequences is to use a Markov Model (MM). A Markov Model has the property that the next observation is uniquely dependent on the current observation, rather than the whole history (Davis, 2018, ch1). We will introduce this model with the aid of a simple example sequence of two observables A and B.

A A B A A B A A B B A A B A

First, we can define the probabilities of being in states A and B as P(A) and P(B), respectively. The empirical probability of a given state is estimated by the number of times that state occurs divided by the total number of occurrences.

$$P(A) = \frac{N(A)}{N(A) + N(B)} \quad (1)$$

Thus, a probability is always bounded between zero and one. Since there are only two possible states, the probability of one of them is complementary to the other *P(B) = 1 – P(A).* Therefore, in this example we have:

$$P(A) = \frac{9}{9+5} = 0.64$$
$$P(B) = 1 - \frac{9}{14} = 0.36 \quad (2)$$

We can now also define the transition probability between the two observables, which is the conditional probability of event A occurring given that event B has happened:

$\mathrm{P_{AA}} = \mathrm{P(A|A)}$: transition probability from A to A
$\mathrm{P_{AB}} = \mathrm{P(A|B)}$: transition probability from A to B
$\mathrm{P_{BA}} = \mathrm{P(B|A)}$: transition probability from B to A
$\mathrm{P_{BB}} = \mathrm{P(B|B)}$: transition probability from B to B

Computing the number of transitions from one observable to another, our data suggests that the transitions from A to B are equally likely as the transition from A to A.

$$\mathrm{P_{AB}} = \mathrm{P_{AA}} = 0.5 \quad (3)$$

When looking at transitions occurring from the B observable, we note that transitioning from B to A is more likely than from B to B:

$$\mathrm{P_{BA}} = 0.75$$
$$\mathrm{P_{BB}} = 0.25 \quad (4)$$

Now that we know the four transition probabilities between the two states, we have created a transition probability matrix that can be represented as a diagram (Figure 3-6).

Formalizing what we have done so far, if we have an X_1 sequence of m states, where $X_1 = \{x_1, x_2, \ldots x_n\}$ and. The transition probability between the states i and j is given by:

$$P_{i,j} = P(X_{t+1} = j | X_t = i) \quad (5)$$

Calculating the transition probability for every i and j, we get the transition probability matrix M of dimension m^2 $(m \times m)$.

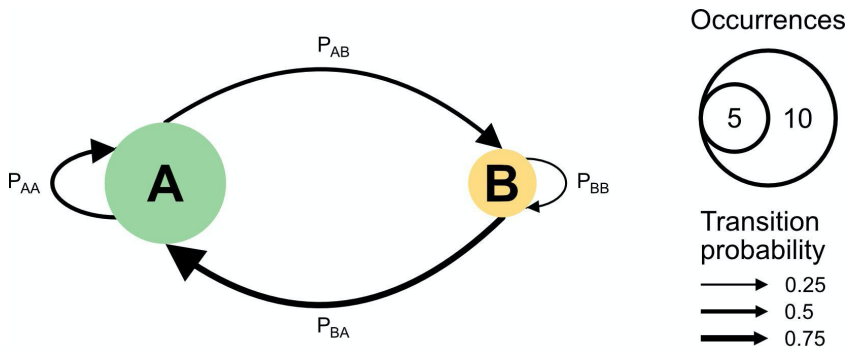

Figure 3-6 Diagram example of a Markov Model.

Left: Diagram representing the Markov model of the states A (in green) and B (in yellow) where the arrows represent the different transition probabilities. Right: Legend of the diagram where the size of the circle represents the occurrences of each of the states and the arrow thickness the transition probability.

More interestingly, by fitting the model on our initial sequence, which we will call the training data, we have created a simple generative Markov model. This model can output infinite sequences that follow the computed transition probabilities. Markov models are not only useful because they can capture and generate non-deterministic data, but they also have useful mathematical properties (for more details see Boyd & Lau, 1998). Among others, one can calculate the expected number of steps to reach a certain state, and its expected number of visits. Additionally, one can analytically calculate whether the transition probabilities between two different transition probability matrices are significantly different. This is a

very useful property when assessing behavioral differences between distinct groups.

In order to verify that the employed model is generalizable to other sequences, one has to assess its validity on additional data. Using a new sequence (test data), we can determine how likely it is that this sequence comes from the probability distribution learned from the training data. Let's assume that the newly observed sequence is the following:

A B A A B B B B A A B A A B

The likelihood of the sequence is given by multiplying the transition probabilities of each of the steps: P_{AB} x P_{BA} x P_{AA} x P_{AB} x …. Writing it formally:

$$L(X'|M) = \prod_{t=2}^{n} P_{x'_{t-1}x'_t} \tag{6}$$

Thus, we can calculate the likelihood of occurrence of each of the sequences given our model:

$$\begin{aligned} \mathrm{L}(\mathrm{P}_{\mathrm{train}}|\mathrm{M}) &= 0.00031 \\ \mathrm{L}(\mathrm{P}_{\mathrm{test}}|\mathrm{M}) &= 0.00005 \end{aligned} \tag{7}$$

We realize that there is a big discrepancy between the two likelihoods. Looking at the two sequences, one thing we notice is that while transitions from state A follow what is expected from the model, the transitions from B do not. In fact, according to our model, having a sequence of four consecutive B observables has a very low chance:

$$\mathrm{P}(\mathrm{B}|\mathrm{B}|\mathrm{B}) = \mathrm{P}_{\mathrm{BB}}\,\mathrm{x}\,\mathrm{P}_{\mathrm{BB}}\,\mathrm{x}\,\mathrm{P}_{\mathrm{BB}} = 0.016 \tag{8}$$

This explains why the likelihood of the test data is lower than for the train set.

A common approach to report the likelihood of an observation is to calculate its log-likelihood: the logarithm of the likelihood of the sequence. In a deterministic scenario, we obtain that the probability of our observation is one, in which case the log-likelihood will be zero *(log(1)=0).* In a stochastic scenario with the most unlikely outcome, the probability of our observation approaches zero, giving a log-likelihood of minus infinity *(log (0) = -∞).* Thus, the log-likelihood is always a negative number, upper bounded by zero.

The value of the log-likelihood is influenced by two factors. The first is how deterministic the model is. The bigger the probability of a certain transition, the higher the log-likelihood of this transition will be when it occurs. This becomes clear when we compare the probability of transitioning from B to A with the probability of transitioning from A to A:

$$\begin{gathered} P_{BA} > P_{AA}; \\ \log(P_{BA}) > \log(P_{AA}); \\ \log(0.75) > \log(0.5); \\ -0.12 > -0.3 \end{gathered} \tag{9}$$

The second factor is how much the observed sequence matches the highest probability transition of the model. As we saw in our example, the B to B transition is less likely than the B to A transition. However, in our observed sequence, B to B transitions were more prevalent, decreasing the probability of observing the second sequence given our model. Doing the calculation for our example we obtain:

$$L(train \vee M) = \log(0.0003)$$
$$L(test \vee M) = \log(0.00001); \quad (10)$$

$$L_{train} = -3.51$$

$$L_{test} = -4.29$$

In this case, comparing the two values we observe that there is a big drop from the train to the test data. This suggests that either the two sequences do not come from the same probability distribution, that the data used to train the model was insufficient, and/or that the model is not appropriate to capture these sequences. One must notice that the log likelihood cannot be interpreted in isolation, but in comparison to other values of the same characteristics.

Hidden Markov Models

In the previously described MM, the future outcome is solely dependent on the current observable. However, often there are hidden variables (unobservable) that may be dictating the observables. Such models are called Hidden Markov Models (HMM). These types of models are also stochastic; however, they operate in two layers (Schuster-Böckler & Bateman, 2007). The first layer is what we observe, i.e., a stochastic sequence. The second layer is also a stochastic sequence, but it is hidden. This hidden sequence is the one that dictates the outcomes of the observables.

We can use an everyday example to illustrate this. We may brush our teeth in the morning before leaving the house, or at night before going to bed. If we just had access to this behavior, when we see someone brushing their teeth, we would conclude that it is equally likely that they would leave the house or go to sleep next. In this case we are taking the observable (brushing teeth) as the cause of the future state (leave / sleep).

However, it is not the observable dictating the next state, but rather whether it is the morning or the night, a hidden variable if we do not have access to it. Therefore, at night there is a big chance that we will go to sleep and in the morning a big chance that we will leave the house.

In our world, every morning leads to a night and vice-versa, which simplifies the inference process. Imagine a word where this is not the case. There is a probability that the morning leads to another morning, and a night to another night. In this case, we would have to infer the transition probabilities between the hidden variables (night and day), and simultaneously the probabilities from the hidden variables to the observables (brushing-teeth/leaving /sleeping), which are called emission probabilities. Figure 3-7 shows a schematic where C and D are the hidden states and A and B the observables.

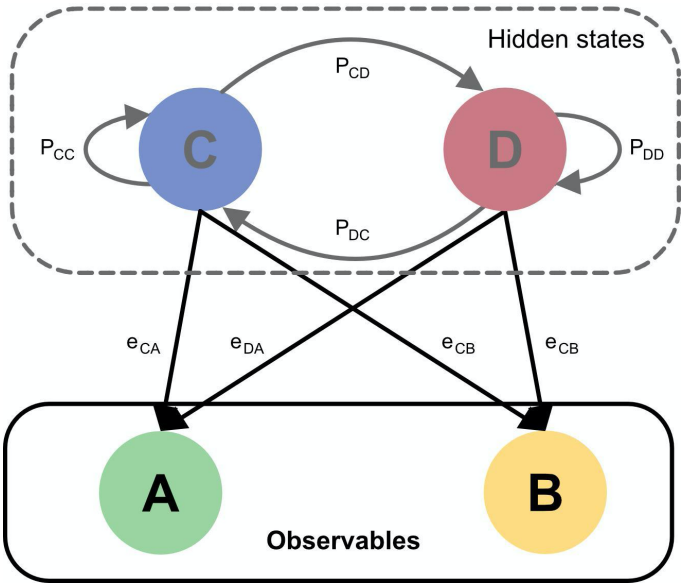

Figure 3-7 Hidden Markov Model diagram.

Diagram representing the structure of a HMM. There is a set of hidden states (C and B) that have an associated transition probability ($P_{i,j}$) between each other. Simultaneously there is a set of observables (A

and B). The observables are linked to the hidden states through the emission probabilities of the later's ($e_{k,l}$).

Learning a HMM is a more complicated process than the one of the covered MM. It is a recursive inference process that requires more data than a single sequence, as the solutions with a single sequence are degenerate, meaning that there is not a unique solution. There are several methods that can be used to train a HMM, for details see (Ramage, 2007).

HMMs are very useful models to describe sequential behavioral data. They are flexible and can be arranged in different ways, depending on the meaning of the hidden states, how many there are or other features of the data. For instance, in the example of brushing teeth, we know that it is not fully true that the observation of leaving/sleeping is only given by the fact that it is the morning or the night. There is a strong concurrency between the sequence of brushing teeth and leaving, as the opposite does not make sense. Therefore, we could extend this model with different layers or hierarchical structures to make it more plausible for the behavior we are studying.

3.1.9 Goal of the current research

Detailed descriptions of sexual behaviors can be crucial for gaining insights into evolutionary adaptations, species-specific traits, and how organisms interact with their environment, among others (Timbergen, 1963; Gomez-Marin et al., 2014; Brown & De Bivort, 2018). The microstructure of other innate behaviors of the mouse has been given a lot of attention, allowing for a better understanding of their composition, but also their neural underpinnings (Weber & Olsson, 2008; Kalueff et al., 2016; Johnson, 2018; Thompson et al., 2017; Lee et al., 2019). Similarly,

the organization of rat sexual behavior has been largely described (Chu, & Ågmo, 2014; Ågmo & Snoeren, 2015; Chu & Ågmo, 2015a; Chu, & Ågmo, 2015b; Chu, & Ågmo, 2016; Ågmo & Snoeren, 2017; Heijkoop et al.,2018; Huijgens et al., 2021). However, the organizational microstructure of mouse sexual behavior, a fundamental model organism in modern neuroscience, remains poorly understood. Even though several studies have described mouse sexual behavior in detail (McGill, 1962; 1963; Dewsbury 1972;1975; Mosig & Dewsbury, 1976; Valente et al, 2021), due to its large inter-individual variability, proper quantification of its organizational structure and how experience shapes it has not been studied in detail yet. This is important not only to understand behavior in detail, but also to guide us into what possible neuronal mechanisms control the behavior and, importantly, to guide experimental design.

While some recent efforts have been put into understanding mouse sexual behavior, most studies just investigate latencies to initiate copulatory behavior and latencies to ejaculate, ignoring the richness of the behavior (Park, 2011; Liu et al., 2020). Regarding the effect of sexual experience on the behavior, the same is true (McGill,1962; Phelps et al., 1998; Taziaux et al., 2007; Picot et al., 2014; Jean et al., 2017; 2021). Therefore, to understand if and how the structure of mouse sexual behavior evolves with experience we performed a longitudinal study of the male mouse while having successful consecutive sexual encounters with different females. Taking advantage of a large dataset, this study quantifies the main structures of mouse sexual behavior and how the experience of the male shapes them. Also, because one of the main goals of sexual behavior studies is to understand the arousal trajectory that takes a male to the ejaculatory threshold, we also focused on analyzing behavioral correlates that are associated with arousal, and how those evolve throughout sexual intercourse.

We found that, while the behavioral motifs executed during sexual intercourse are maintained across several encounters, the transition between the appetitive and consummatory phase seem to be affected by experience. The same happens for the temporal organization of the behavioral motifs. Finally, we find no evidence of arousal increase as the session progresses, contrary to what is commonly accepted. These results shed new light on the structure of mouse sexual behavior and should guide research aiming to elucidate its underlying neuronal mechanisms.

3.2 Results

3.2.1 Description of mouse sexual behavior

We recorded the sexual behavior of eleven male mice over six consecutive sessions, starting when the males were sexually naive. Both male and females were C57BL/6J, and the females were ovariectomized and supplemented with external estrogen and progesterone to induce female receptivity (Edwards, 1970). Because this study primarily intended to investigate how male mouse sexual behavior evolves with experience, the following male-centered behaviors were manually annotated from the video recordings: Initial Interaction between male and female, Anogenital Investigations from male to female (A), self-Genital Grooming of the male (G), Mounts with Intromission (MI), Mounts without Intromission (MwoI), and male Ejaculation (E). An example of an annotated session is shown in Figure 3-8. As shown in the inset of the figure, each Mount with Intromission has a pre-insertive and an intravaginal thrusting period. During the pre-insertive thrusting, the penis is not inserted in the vagina but there is shallow pelvic thrusting movements also named probing, trying to locate the female vagina. Once the first intromission occurs, the

intravaginal thrusting period begins, and the penis is inserted in the vagina repeatedly.

One marked characteristic of mouse sexual behavior is its inter and intra individual variability. Every session is different from the other sessions, as the number of elements can vary dramatically. We wondered what behavioral structure was conserved across animals and if we could build a model that could generate the observed data.

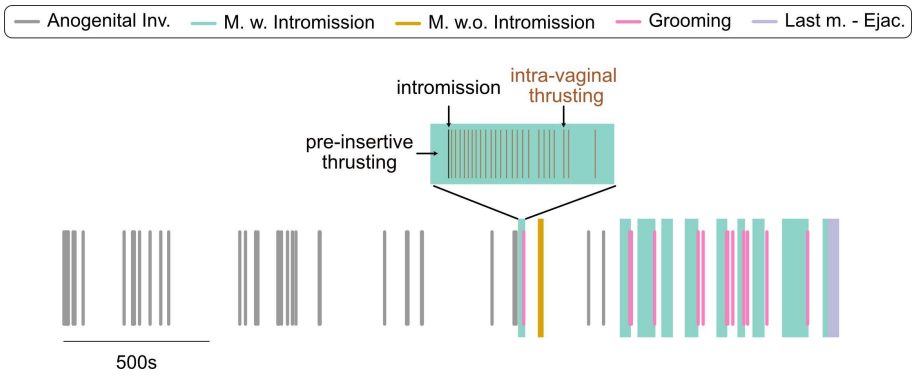

Figure 3-8 Example session of mouse sexual behavior.

Example of a sexual behavior session. Each color represents a given annotated action. Gray: Anogenital Investigation from male to female. Yellow: Mount without Intromission. Pink: Male Genital Grooming. Green: Mount with Intromission. Purple: Ejaculation. Green Inset: Zoom in on a Mount with Intromission showing the period preceding the intromission with pre-insertive thrusting movements, the penile intromission (black line), and the sequence of intra-vaginal thrusts occurring in (brown lines).

3.2.2. Structure of mouse sexual behavior

Variable behavioral sequences are often modeled as probabilistic outcomes. This means that the sequence is not deterministic but follows a latent probabilistic distribution. Our goal is to find a probabilistic model

that generalizes well and captures the main properties of the mouse sexual behavior.

We were first interested in the sequence of the events, ignoring the time interval between them. Therefore, we assumed that the transition from one event to the next would be instantaneous or timeless. For this, we used the annotated behaviors and removed the time interval between the events (Figure 3-9 A).

The most parsimonious approach is to use a Markov Model (MM) (MacKay, 2003), where the next behavior is only dependent on the current behavior – a memoryless model with a stationary probability distribution. This model assumes that only the current state influences the following one (Illustration of the model Figure 3-9 C left). Cross validating the 80% of the training data with the remaining 20% of the data (test data) we calculated the log-likelihood of the MM (Figure 3-9 G). We observed a big drop in the test data, suggesting that this model was not able to generalize well. In fact, when looking at the example trace generated by the model (Figure 3-9 C right) we noticed that unlike in the actual behavior, Anogenital Investigation occur at any stage of the behavior. However, in our data, Anogenital Investigations only occur in bouts at the beginning of the behavior while later they rarely occur or occur in isolation, as in the example trace (Figure 3-9 A). This means that the transition probabilities are not stationary. In fact, when plotting the distribution of all events across the session, we saw that the Anogenital Investigations are primarily confined to the beginning of the session. As their fraction drops, the Mounts with Intromission and Genital Grooming increase (Figure 2-9 B).

We then looked for other ways of modeling the behavior. Classically sexual behavior has been separated in two phases, pre-copulatory and

copulatory (Beach, 1956) and the copulatory phase is generally thought to be initiated by the first Mount with Intromission (Rosenthal, 2017). Therefore, we built a second model that would manually partition the data into the appetitive phase (from the first behavioral motif to the first Mount with Intromission) and the consummatory phase (from the first Mount with Intromission to Ejaculation). In a similar way to the previous model, we built a two state MM (2s MM) (Figure 3-9 D). In this case, there is one MM for the pre-copulatory period, and one for the copulatory. Both are absorbent MM, meaning that when reaching certain motif (Mount with Intromission for the pre-copulatory and Ejaculation for the copulatory model), the process terminates. When examining the log-likelihood of the train and the test data sets, we observed that they had a larger value than the one-state MM (Figure 3-9 G). This suggests that this model captures the data better, and in fact, the mating behavior is classically separated into these two different states.

Next, we asked if we could obtain the separation between the two hidden states in an unbiased manner. For that we used a Hidden Markov Model (HMM), which assumes that there is a set of hidden states that give rise to the observables and the transition probabilities capture the transition between the hidden states. However, in single-layer HMMs like described in a previous section, the emission of observables in each hidden state does not depend on the previous observable, but only on the hidden state (i.e. the transition between hidden states is markovian but the intra-state sequence of observables is just a categorical distribution). In order to capture the markovian structure of the behavior inside the hidden states, we built a two-layered HMM with two states (2l 2s HMM). The first layer is a HMM that determines the hidden state. The second layer determines the transition probability between the observables using a MM (see methods for details) (Figure 3-9 H left). Looking at the performance of this model, we saw a notable improvement with respect to the 2s MM. Both

the log-likelihood of the train and the test data increased, and their distance decreased notoriously (Figure 3-9 G). Suggesting that this was indeed a model that generalizes well to the data we had. Finally, we trained a 2l 3s HMM, now with three hidden states, to test whether perhaps there was another phase in the behavior. The log-likelihood of both the train and test set were lower than the 2l 2s HMM, suggesting that imposing three hidden states was overfitting the data (Figure 3-9 G).

Taking these results into consideration, we believe that the best model to capture the variability of the data and that generalizes well is the 2l 2s HMM. Figure 3-9 F illustrates the transition probability between the behavioral motifs and the two hidden states, where the occupation of the circles is proportional to the number of visits to a given motif and the thickness of the arrows is proportional to the transition probability. The statistical significance was calculated by computing the chance model for each session (see methods for details).

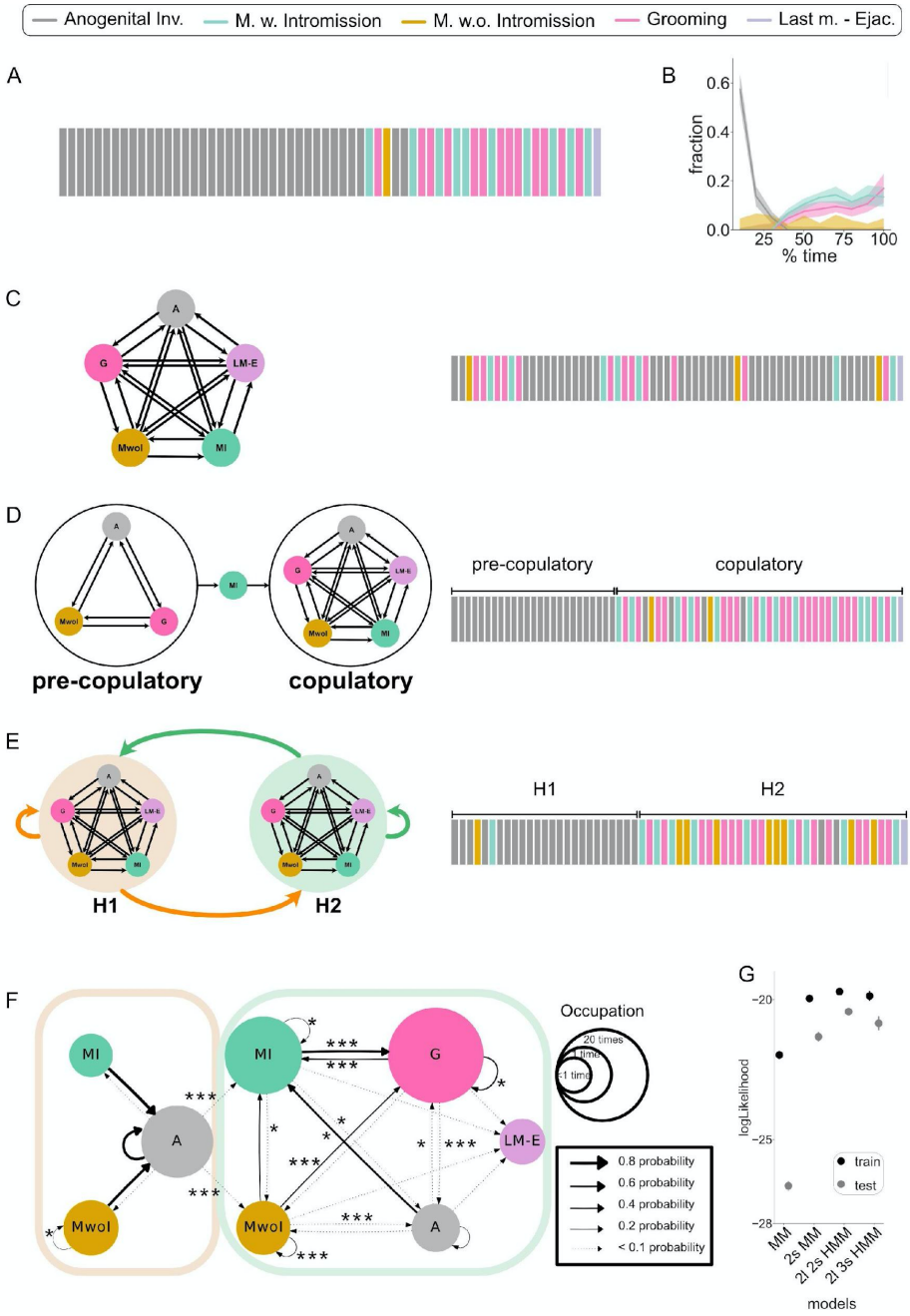

Figure 3-9 Behavioral motifs of mouse sexual behavior are well represented by a two-states HMM with two layers.

A. Example of a session used to train the model. Same session as in Figure 3-6 C removing the time between events. Only the sequence of events was used to train the model. Each color represents a given annotated action. Gray: Anogenital Investigation from male to female.

Yellow: Mount without Intromission. Pink: Male genital Grooming. Green: Mount with Intromission. Purple: Ejaculation.
B. Fraction of events per percentile in the session (10% bins). Median over all the animals in all sessions. Gray indicates anogenital investigations, pink self-genital grooming, green mounts with intromission and yellow mounts without intromissions.
C. Single MM. Left: Illustration of the employed MM to explain the data. Each circle corresponds to a behavioral motif and the black arrows represent the probability to transition from one motif to the next one. Right: Example sequence created by the model.
D. Classical transition: 2s MM. Left: Illustration of the employed model to explain the data. Two states are defined as Pre-copulatory and Copulatory and the transition between them is forced to be the first Mount with Intromission. Each circle corresponds to a behavioral motif and the black arrows represent the probability to transition from one motif to the next one. Right: Example sequence created by the model.
E. Unbiased transition: 2l 2s HMM. Left: Illustration of the employed model to explain the data. A two states HMM is trained, once in a hidden state, the transition between the behavioral motifs are assumed as an absorbent MM. Each circle corresponds to a behavioral motif, the black arrows represent the probability to transition from one motif to the next one. Light yellow circle indicates the first hidden state, and light green the second hidden state. The yellow and green arrows represent the transition probabilities between the two hidden states. Right: Example sequence created by the model.
F. Obtained transition using the 2l 2s HMM. The arrow thickness defines the probability of transitioning between two states and the size of the circle the mean occupancy per animal of that given state as depicted on the right. The transitions are calculated for all the animals in all sessions.
G. Log-likelihood calculation of the four different models: MM with no hidden state, classical model of transition between appetitive and consummatory (2s MM), 2l 2s HMM – model with unbiased transition between hidden states, and 2l 3s HMM. In black is the log-likelihood of the trained data and gray the log-likelihood of the test data.

3.2.3. Experience shapes the transition probability between behavioral motifs

We then further investigated the concurrence between the state transitions given by the 2l 2s HMM and the classical approach 2s MM. Figure 3-10 A illustrates three example sessions, each of them belonging

to a different scenario: (1) The 2l 2s HMM gives a posterior transition epoch than the classical approach (s.1) (9% of the sessions), (2) the two transition points coincide (s.2) (67% of the sessions), and (3) the 2l 2s HMM gives an anterior transition point than the classical approach (s.3) (24% of the sessions). While most mismatches between the HMM and the classical approach belong to the third scenario, we found that the mismatches of the first kind – where the HMM predicted a transition after the classical approach, were mostly confined to the early sessions (Figure 3-10 B). Recognizing the potential impact of experience on behavior, we further investigated the effect of experience on the structure of mouse sexual behavior.

The experiment followed each male of the eleven males from the first session, naïve virgin, to the sixth session, experienced (Figure 3-10 C). First, we focus on the two 2l 2s HMMs computed using only the naïve (session 1) and only the experienced (session 6) sessions (Figure 3-10 D - F). Notably, in session 6, the transitions to Mounts with Intromission do not occur in the first phase, explaining the bigger mismatch between the 2l 2s HMM and the 2s MM. Additionally, there is a change in the interaction between Mount with Intromission and Genital Grooming events. The frequency of Genital Grooming bouts decreases (analytic p= 0.002, see methods), and the probability of transitioning back to a Mount with Intromission increases (analytic p=0.00008, see methods).

The observed changes in the organization of sexual behavior raised the question of how many sexual encounters it takes for the male's behavior to stabilize, or in other words, for the male to be considered experienced. To address this, we used linear discriminant analysis (LDA) between the 2l 2s HMMs obtained from the first and the last sessions using leave-one-out cross-validation. This analysis provides an axis that maximally separates the two sessions – the experience axis. We projected the full

dataset onto this axis, including the intermediary sessions (session 2-5) (Figure 3-10 G). The results suggest that from the fourth session onward, the transition matrix between the observable behaviors does not change much, corresponding to the behavior of an experienced male.

Regarding the third case, where the 2l 2s HMM gives an anterior transition point than the classical approach (s.3) (24% of the sessions), it turns out that they correspond to sessions where the second phase of the behavior was initiated whenever the male performed a Mount without Intromission. This suggests that Mounts without Intromission have a copulatory role in behavior and should be considered when studying sexual behavior in mice as copulatory.

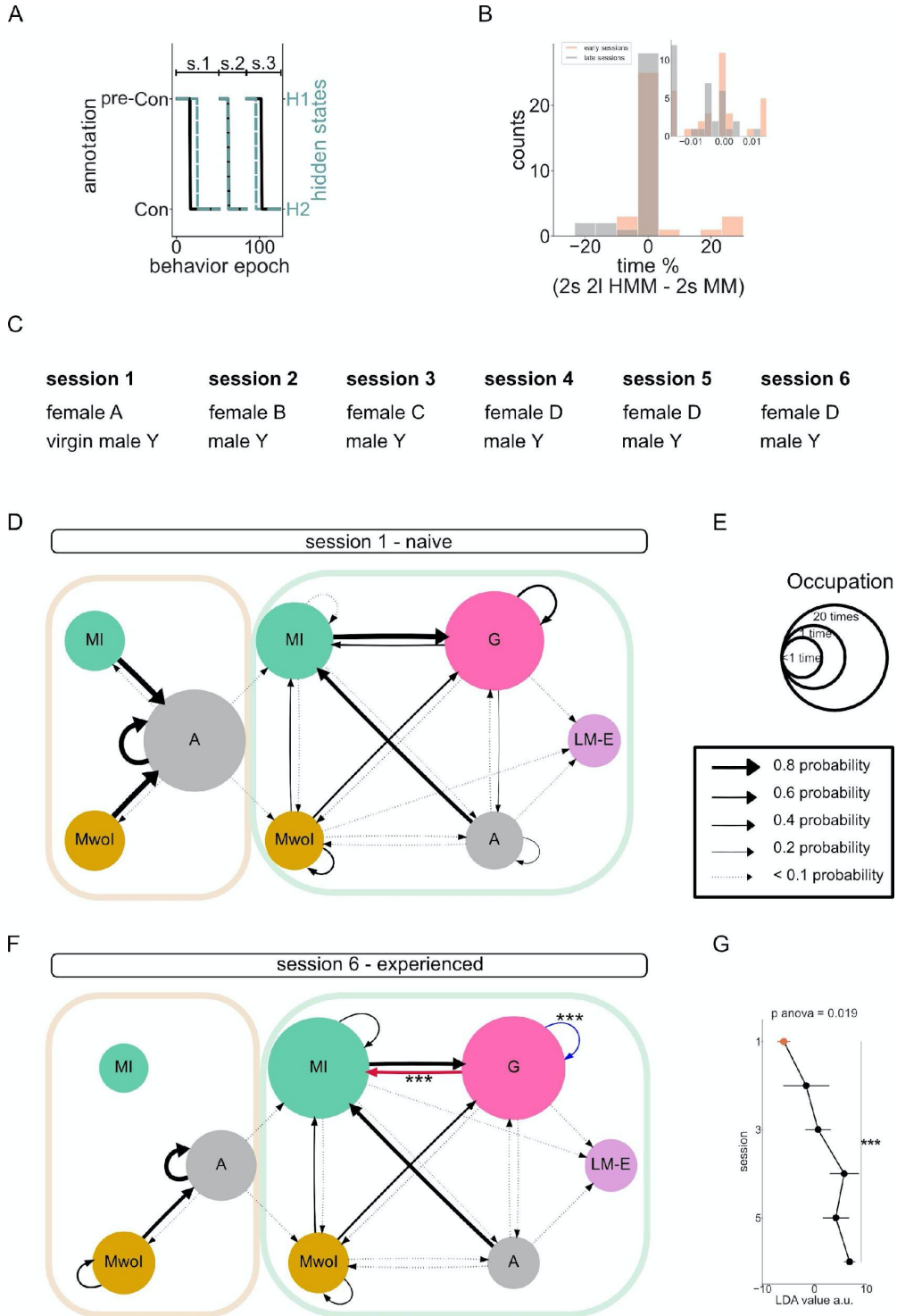

Figure 3-10 The role of experience in the structure of mouse sexual behavior.

A. Example trace of three sessions shows the correspondence between the transition in the hidden states given by the HMM (dash-blue) and the state transition based on the definition of pre-copulatory are in black.
B. Histogram of the percentual time difference between the state transition given by the two states HMM and the classical approach. Early sessions – first three - are shown in pink and late sessions – last three - are shown in gray. Negative values indicate that the classical approach gave an earlier time than the HMM, zero values indicate that both gave the same time, and positive values that the classical approach gave a later time than the HMM.
C. Illustration of the experimental sessions. Each male underwent six sessions. In the first one he was sexually naïve (virgin). In the first four sessions, he was paired with a different female (OVX) each time. In session 5 and 6 he was paired with the same female he was paired with on session 4. The females were pseudo-randomly rotated across the 11 males that took part in the experiment.
D. Transition model between behavioral motifs in session 1. Pre-copulatory (brown) and copulatory (light green) latent states are defined by the HMM and the transitions between them once in a latent state are assumed as absorbent MM. The arrow thickness defines the probability of transitioning between two states, and the size of the circle signifies the mean occupancy per animal of that given state.
E. Legend of the two models.
F. Transition model between behavioral motifs in session 6. same as D but for session 6.
G. Mean scores of Linear discriminant analysis, obtained through cross-validation method and then projected on the whole data set of the transition matrices. The more negative scores mean the higher the probability of the transition matrix belonging to session 1 and, the more positive scores to session 6.

3.2.4 Experience changes the number and timing of events

So far, we assumed that all the events were instantaneous, therefore any notion of time was absent from our analysis. Once we understood the two-phase separation in the behavior and which behaviors were the most relevant on each of the phases, we decided to incorporate the time between the events in our analysis. To visualize the statistics of the data, we plotted the peri-event time histogram (PETH) of behavioral motifs

aligned to the state transition defined by the designed 2s 2l HMM, for each of the sessions (Figure 3-11 A). The width of the PETH plots shows the large variability across animals, still, experience-dependent changes are evident. As previously reported (Zhang et al., 2021), we found that Anogenital Investigations are performed mainly during the pre-copulatory period.

In line to what has been reported by others (Jean et al., 2021) we observed a statistically non-significant but quantifiable reduction of the duration of the pre-copulatory period (one-way repeated measures (rm) ANOVA p = 0.12, Figure 3-11 B). Interestingly and contrary to what others have shown (Swaney et al., 2012; Jean et al., 2017) male sexual experience does not influence the duration of the copulatory period (one-way rm ANOVA p=0.48, Figure 3-9 C). However, we observed that the number of Anogenital Investigation events decreases with experience (one-way rm ANOVA p=0.005, post-hoc (session 1 vs session 6) p=0.006, Figure 3-11 D top panel). Interestingly, the rate of the anogenital investigations remains constant with experience (one-way rm ANOVA p=0.64, Figure 3-11 D lower panel).

In a similar manner, the number of Mounts with Intromission was unchanged (one-way repeated measures ANOVA p= 0.11, Figure 2311 E top panel). However, there was a significant effect across sessions when looking at the rate of Mounts with Intromission (one-way repeated measures ANOVA p= 0.033, post-hoc (session 1 vs session 6) p=0.1, Figure 3-11E lower panel).

In summary, we saw that that the amount of Anogenital Investigations that the male performs during the pre-copulatory period decreases with experience. Additionally, the rate of the Mounts with Intromissions was

also affected by experience, therefore we wanted to investigate this aspect further.

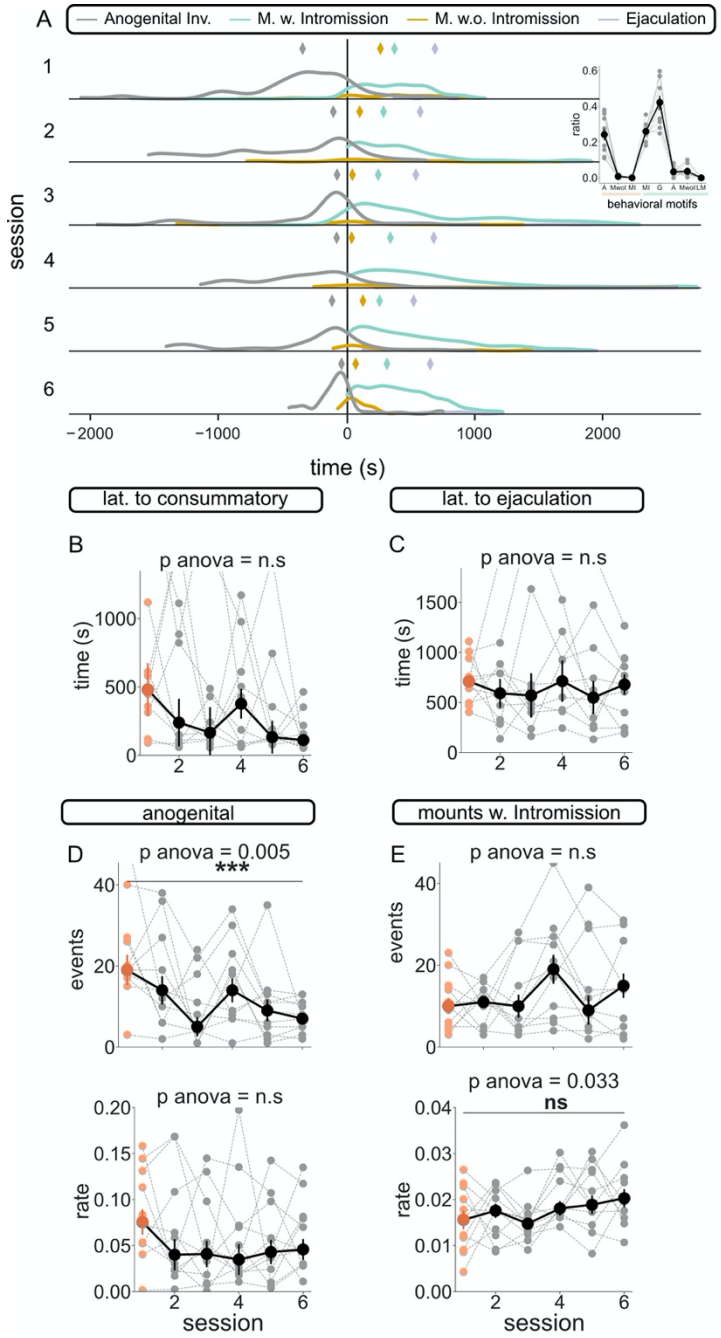

Figure 3-11The role of experience in the number and timing between events.

A. Peri-event time histogram of each of the sessions aligned to the transition given by 2s 2l HMM. In gray are noted the Anogenital Investigation, green the Mounts with Intromission and yellow Mounts without Intromission. Diamonds display the mean for all the animals in that session. Inset: ratio of each of the behavioral epoch per phase. Gray indicates mean of the animal and black the overall mean.
B. Latency to consummatory. Mean time per animal and session from the first event to the transition to the second phase given by the 2-s 2l HMM. Each animal is depicted in grey and the median across all animals in black for all the sessions except the first one. In the first session, each animal is depicted in light pink and the median in pink. One-way repeated measures ANOVA is performed across sessions and when significant post hoc test between first and last session.
C. Latency to ejaculation. Same as B for the latency to ejaculation.
D. Top panel: Number of anogenital investigation events per session. Each animal is depicted in grey and the median across all animals in black for all the sessions except the first one. In the first session, each animal is depicted in light pink and the median in pink. One-way repeated measures ANOVA is performed across sessions and when significant post hoc test between first and last session. Lower panel: Same as D for the rate of Anogenital Investigations.
E. Top panel: Same as D for number of Mounts with Intromission Lower panel: Same as D for the rate of Mounts with Intromission.

3.2.5 Experience changes the interval between mounts

The mounting rate can be affected by a change in the mount durations or a change in the inter-mount intervals. Therefore, we further scrutinized the two behavioral motifs separately to understand which one was changing with experience.

To investigate this, we looked at the duration of Mounts with Intromission only. We defined the mount duration as the time from mount onset to mount offset. We found no change with experience in the mean mount duration, even though the variance decreased significantly with experience (one-way rm ANOVA p= 0.671, Levene's variance (s1-s6) test p=0.042, Figure 3-12 A and B respectively). We defined the inter-mount interval, as the time interval between a mount offset and the next mount

onset. We found that there was a significant reduction in the inter mount interval mean and variance (one-way rm ANOVA p= 0.043, post-hoc session 1 vs 6 p=0.081 and Levene's variance (s1-s6) test p= 0.037 Figure 3-12 C and D respectively).

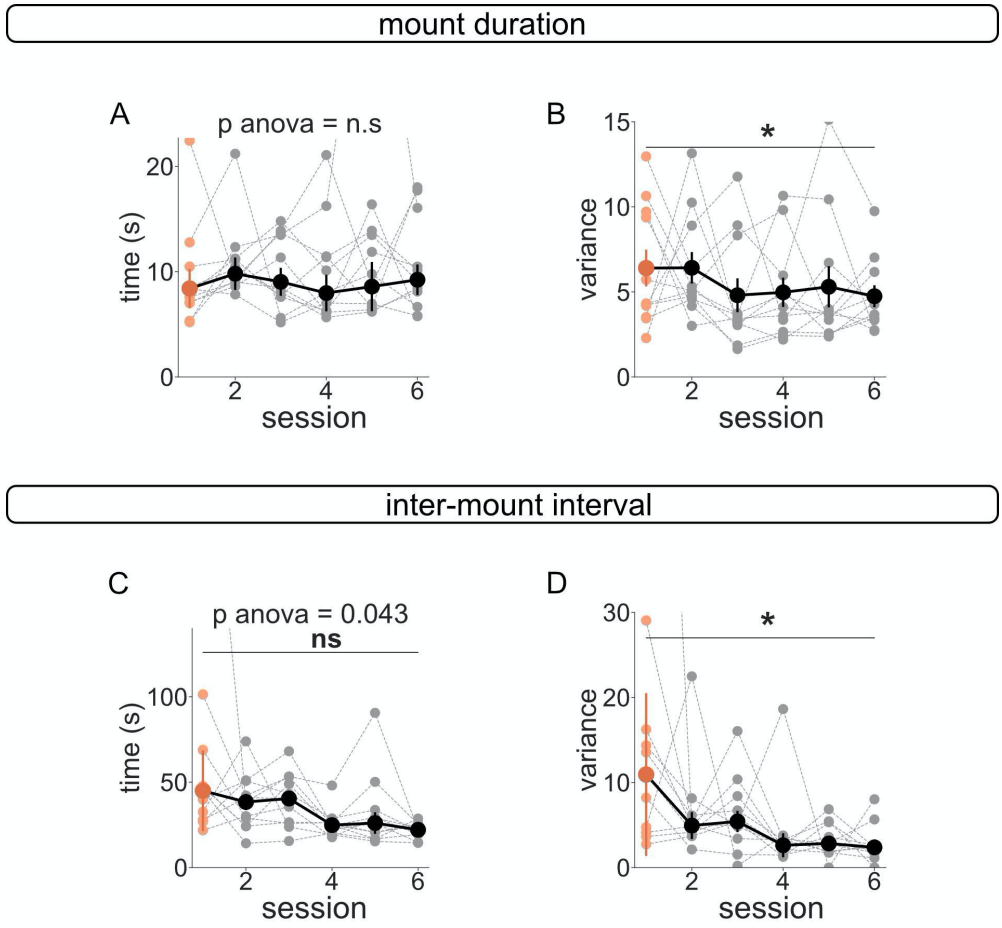

Figure 3-12 Experience changes on timing between events.

A. Session effects on effects on the mean mount duration for Mounts with Intromission. Mean inter Mount duration in seconds per animal and session. Each small circle represents the mean of an animal and a session, and the big circles represent the median of all the animals in that session. The first session is depicted in light pink for individual animals and dark pink for the median. One-way repeated measures ANOVA is calculated for all the sessions and when the test is significant a post-hoc test is calculated between the first and last session (n.s.: p > 0.05, *: 0.05 > p > 0.01, **, 0.001 > p < 0.01, *** p < 0.001).

B. Session effects on the variance of the duration of Mounts with Intromission. Within animal variance of the mount duration in seconds per animal and session. Each small circle represents the variance of an animal and a session, and the big circles represent the median of all the variances of the animals in that session. The first session is depicted in light pink for individual animals and dark pink for the median. Significance is calculated using Levene's test of variance between the first and last session. (n.s.: $p > 0.05$, *: $0.05 > p > 0.01$, **, $0.001 > p < 0.01$, *** $p < 0.001$).
C. Same as A for the session effects on the mean inter-mount interval of Mounts with Intromission and any other mount.
D. Same as B for the session effects on the variance inter-mount interval of Mounts with Intromission and any other mount.

We noticed that Mounts with Intromission were often followed by Genital Grooming (71 ± 10% of the cases). Therefore, we investigated the inter-mount interval in the two cases – after a Mount with Intromission not followed by grooming and followed by grooming. For the inter-mount interval after Mounts with Intromission followed by Genital Grooming, we found a significant difference between sessions according to ANOVA, and a tendency for decrease between the first session and last (Figure 3-13 A, one-way rm ANOVA $p= 0.029$, post-hoc session 1 vs 6 $p= 0.067$). The variance of the groups also changed (Figure 3-13 B, Levene's variance (s1-s6) $p= 0.039$). Regarding the inter-mount interval after Mounts with Intromission not followed by Genital Grooming, we found a significant difference between sessions according to ANOVA and a non-significant tendency for a decrease between the first and last session (Figure 3-13 C, one-way repeated measures ANOVA $p= 0.0049$, post-hoc session 1 vs 6 $p= 0.300$). The variance of the inter-mount intervals for both cases was found not to decrease with experience (Figure 3-13 D, Levene's variance (s1-s6) $p= 0.226$). These results suggest that there is a change in the timing between mounts, with males becoming more stereotypical with experience, in particular when the mounts are followed by Genital Grooming.

We then further scrutinized the inter-mount intervals to determine which part of the interval was being affected by experience (Illustration in Figure 3-13 E). Thus, we defined the “mount offset - grooming onset” interval, the “grooming bouts” interval (from first grooming onset to last grooming bout offset), and the “grooming offset - mount onset” interval. For this analysis we aggregated all the intervals across animals for Mounts with intromission followed by grooming (Figure 3-13 F). As already shown, the mean duration of the full inter-mount intervals after Mounts with intromission decreased significantly between sessions 1 and 6, as well as the variance decreased (t-test p= 3*10-04, and Levene’s var. test p= 1*10-05). We measured that both the “grooming bouts” interval (t-test p= 0.003 and Levene’s var. test p= 0.001), and the “grooming offset - mount onset” interval were reduced in mean and variance with experience (t-test p=0.009, and Levene’s var. test p= 3*10-04). However, the “mount offset - grooming onset” interval was less affected by experience (t-test p= 0.012, and Levene’s var. test p= 0.894).

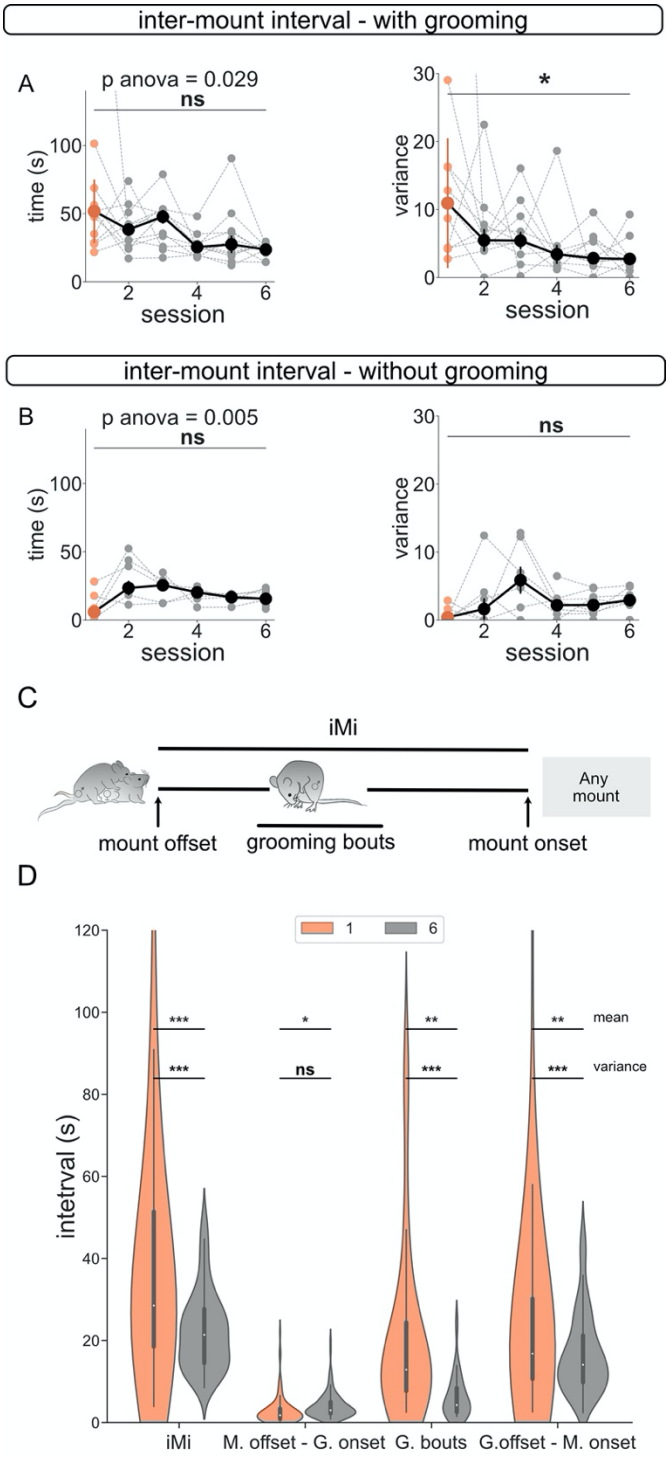

Figure 3-13 Inter-Mount interval is shortened with experience when followed by grooming.

A. Session effects on effects on the mean inter-mount interval for Mounts with Intromission followed by grooming. Left panel: Mean inter Mount with Intromission interval in seconds per animal and session. Each small circle represents the mean of an animal and a session, and the big circles represent the median of all the animals in that session. The first session is depicted in light pink for individual animals and dark pink for the median. One-way rm ANOVA is calculated for all the sessions and when the test is significant a post-hoc test is calculated between the first and last session (n.s.: $p > 0.05$, *: $0.05 > p > 0.01$, **, $0.001 > p < 0.01$, *** $p < 0.001$). Right panel: Session effects on the variance of the inter-Mount interval for Mounts with Intromission followed by grooming. Within animal variance of the inter mount interval in seconds per animal and session. Each small circle represents the variance of an animal and a session, and the big circles represent the median of all the variances of the animals in that session. The first session is depicted in light pink for individual animals and dark pink for the median. Significance is calculated using Levene's test of variance between the first and last session. (n.s.: $p > 0.05$, *: $0.05 > p > 0.01$, **, $0.001 > p < 0.01$, *** $p < 0.001$).
B. Same as A for the inter-mount intervals for Mounts with Intromission not followed by grooming.
C. Illustration of the sequence and intervals of mounts with thrusting followed by genital grooming of the male and another mount. Four intervals can be defined: Inter mount interval (IMI), the time between mount offset and mount onset of the following mount. Mount offset - Grooming onset interval, the time between mount offset and initiation of grooming bouts. Grooming bouts interval, duration of grooming bouts. Grooming offset – Mount onset interval, time between the end of grooming and the mount onset of the following mount.
D. Violin plots of all the intervals for all the animals in the session, first session (pink), and last session (gray) for each of the four different intervals described in C. Significance is calculated with a two-sample t-test and represented in the top. (n.s.: $p > 0.05$, *: $0.05 > p > 0.01$, **, $0.001 > p < 0.01$, *** $p < 0.001$), the significant difference between variance is calculated using Levene's variance test in the bottom (n.s.: $p > 0.05$, *: $0.05 > p > 0.01$, **, $0.001 > p < 0.01$, *** $p < 0.001$).

3.2.6 Behavioral changes across the session

We then proceeded to investigate the time-dependent behavioral changes during a session. The first session, notably different from the rest, was removed from this part of the analysis. Since each animal had a variable number of mounts, to ensure a fair balance between animals we focused

on specific mounts for each animal, removing the last mount leading to ejaculation – namely the first, second, third-to-last and second-to-last mount (Figure 3-14 A).

We first investigated if the mount duration of Mounts with Intromission varied across the session. We detected an increase in the mount duration as the session progressed (see Table 3.6.1 for the statistical results, Figure 3-14 B), even though we saw no change in the inter-mount interval (see Table 3.6.2 for the statistical results, Figure 3-14 C). We then went on to inspect the structure of the Mount with Intromission. As the session progresses, the latency to the first thrust – the pre-insertive period of the Mount with Intromission – decreases with the number of the mount (see Table 3.6.3 for the statistical results, Figure 3-14 D). Since mounts increased in duration over the session, we looked into the thrusting vigor, the mean of the inter-thrust interval in the first four thrusts. We saw a significant decrease from the second mount to the last one see Table 3.6.4 for the statistical results, Figure 3-14 E), however the most noticeable change was that the variability of the animals decreases as the session progresses.

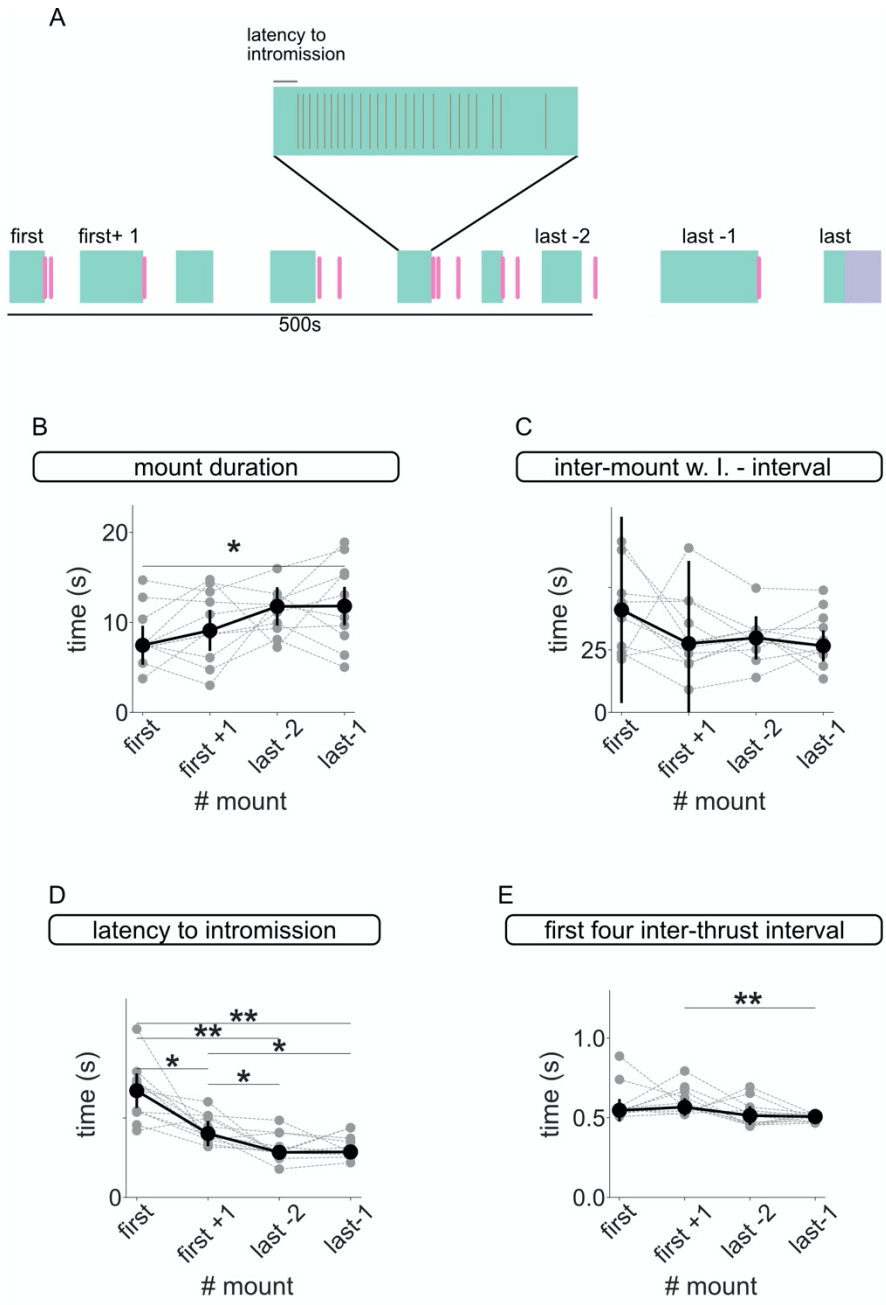

Figure 3-14 Behavioral changes across the session.

A. Schematic of the used divisions. For a given animal only four Mounts with Intromission were included in the analysis. The first mount, the second mount (first +1), the third-to-last mount (last-2) and the second-to-last mount (last-1), as indicated in the schematic. The remaining Mounts with intromission, including the last one were excluded from

this analysis. The time from the MI onset to the first thrust was defined as the latency to first thrust.
B. Mount duration in the first, second, third-to-last and second-to-last mounts. Gray circles indicate mean per animal over the five included sessions, and black circles mean over animals for that particular mount. Statistical using one-way repeated measures ANOVA and if significant post-hoc analysis with. Analysis has been done per mouse and removing the first session. (n.s.: $p > 0.05$, *: $0.05 > p > 0.01$, **, $0.001 > p < 0.01$, *** $p < 0.001$.).
C. Inter mount interval starting in the first, second, third-to-last and second-to-last mounts. Same as B for inter mount interval.
D. Latency to intromission after mount in for the first, second, third-to-last and second-to-last mounts. Same as B for inter mount interval.
E. Inter thrust interval of first four thrusts for the first, second, third-to-last, and second-to-last mounts. Same as B for inter mount interval.

3.2.7 The effect of experience in the behavioral changes across the session

We finally explored whether any of the temporal changes observed across the session were dependent on male experience, by comparing the first and the last sessions for each of the animals. Using the same metrics, we found no significant difference relating across-session-temporal changes and experience (Figure 3-15 A, Mount with Intromission duration; two-way repeated measure ANOVA main effects for session $p=0.727$, Figure 3-15 B, inter-mount interval; two-way repeated measure ANOVA main effects for session $p=0.152$, Figure 3-15 C, latency to first thrust; two-way repeated measure ANOVA main effects for session $p= 0.708$, and, Figure 3-15 D inter-thrust interval of first four thrust; two-way repeated measure ANOVA main effects for session $p=0.284$). Suggesting that the described changes across the session are not influenced by experience.

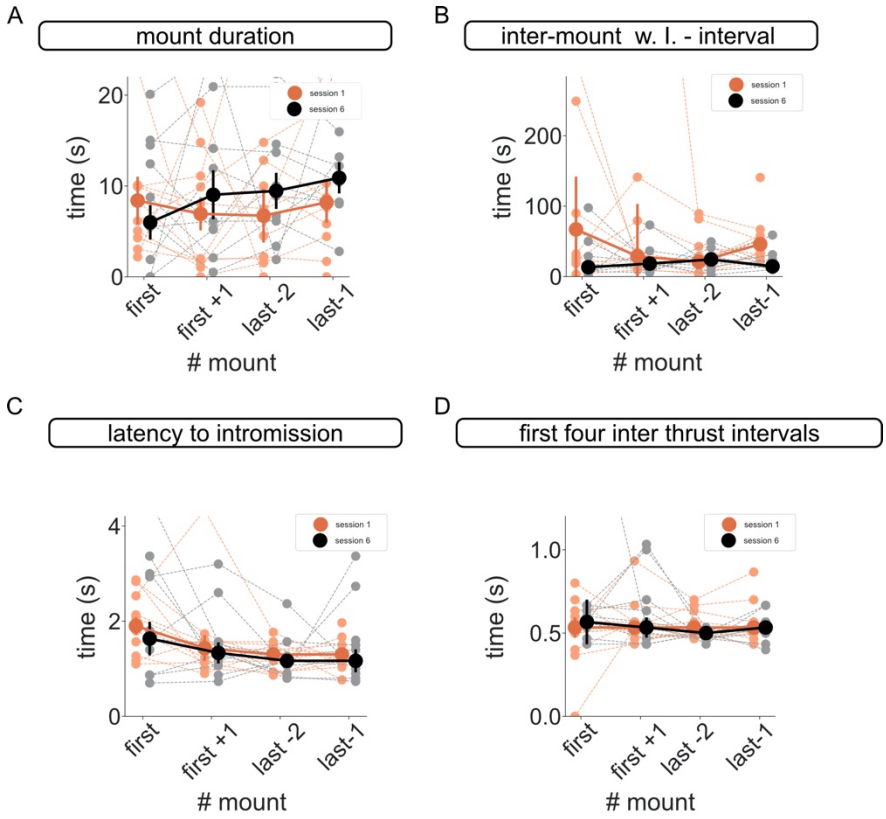

Figure 3-15 Experience does not shape the observed behavioral changes across the session.

A. MI duration for the first, second, third-to-last, and second-to-last mounts for the first session in pink and last session in black. Statistical analysis has done using two-way repeated measures ANOVA and reporting main effects for session. (n.s.: $p > 0.05$, *: $0.05 > p > 0.01$, **, $0.001 > p < 0.01$, *** $p < 0.001$.).

B. Inter-mount with Intromission interval for the first, second, third-to-last, and second-to-last for the first session in pink and last session in black. Statistical analysis has done using two-way repeated measures ANOVA and reporting main effects for session. (n.s.: $p > 0.05$, *: $0.05 > p > 0.01$, **, $0.001 > p < 0.01$, *** $p < 0.001$.).

C. Latency to intromission after mount in for the first, second, third-to-last, and second-to-last for the first session in pink and last session in black. Statistical analysis has done using two-way repeated measures ANOVA and reporting main effects for session. (n.s.: $p > 0.05$, *: $0.05 > p > 0.01$, **, $0.001 > p < 0.01$, *** $p < 0.001$)

D. Inter thrust interval of first four thrusts for the first, second, third-to-last, and second-to-last, depicted from light to dark grey, for the four mount quantiles in time percentage. Statistical analysis has done using two-way repeated measures ANOVA and reporting main effects for

session. (n.s.: p > 0.05, *: 0.05 > p > 0.01, **, 0.001 > p < 0.01, *** p < 0.001).

3.3 Discussion

The present study leverages a comprehensive dataset to examine the intricacies of mouse sexual behavior and its modulation with increasing male sexual experience. Utilizing a statistical framework, specifically a two-layered Hidden Markov Model (HMM) with two hidden states, akin to the documented stages of sexual behavior—pre-copulatory and copulatory—we were able to delineate these stages with greater precision. Our analysis, coupled with the expansive dataset, afforded a nuanced exploration of both the appetitive/pre-copulatory and consummatory/copulatory phases of sexual behavior.

Notably, our findings revealed that in sexually naive males, the demarcation between appetitive and consummatory stages is less distinct, as the execution of a Mount with Intromission did not consistently signify entry into the second hidden state. However, as male mice gained experience, this boundary became more defined, aligning with the execution of any mount type. This result supports the idea that Mounts without Intromission have a similar impact on the consummatory phase to Mounts with penile insertion. Additionally, increased experience correlated with a decreased requirement for Anogenital investigations to initiate mounting and progress to the copulatory phase.

Furthermore, the behavioral sequence within the copulatory phase exhibited greater stereotypy with experience, characterized by a heightened frequency of transitions from Mounts with Intromission to Grooming and vice versa. This transition led to a reduction in the interval between successive Mounts with Intromission, impacting both mean and

variance, making the intervals more predictable. Importantly, this interval reduction was observed exclusively for mounts followed by grooming.

Interestingly, we saw no strong evidence of sexual arousal increase across a session as, despite observed increase in mount duration and a decrease in the latency to first thrust across the session, we saw no discernible alterations in the timing of events across the session, including intermount intervals and intervals between consecutive thrusts. Therefore, our findings diverge from the conventional depiction of sexual arousal gradually escalating until reaching the ejaculatory threshold. Instead, our data suggest a relatively constant level of sexual arousal throughout the consummatory phase within a single session. This nuanced insight challenges conventional understandings and underscores the importance of empirical investigations in refining our comprehension of complex behavioral phenomena.

3.3.1 The phases of sexual behavior

The distinction between appetitive and consummatory phases provides a structured approach to studying behavior, allowing researchers to identify specific actions associated with goal-directed behavior (appetitive) versus those involved in achieving the goal (consummatory). It also aids in elucidating the neural substrates underlying different phases of behavior. For example, appetitive behaviors often involve reward anticipation and motivation, whereas consummatory behaviors entail execution and completion of the desired action. Partitioning the sexual encounter into different phases is however quite a controversial topic. It was first proposed by modern Ethology pioneers Lorentz and Tinbergen to describe behavioral phenomena (Lorentz, 1950, Tinbergen, 1952). However, since several criticisms and cautionary tales have been brought up highlighting the lack of realism of this division (Hinde, 1956; 1966;

Beer, 1964; 1983; Manning and Dawkins, 1998, p.212, Het al., 2002; 2005; Sachs, 2007). One criticism is that the division between appetitive and consummatory phases may oversimplify complex behaviors. In reality, behaviors often involve a continuum rather than discrete phases, and rigid categorization may ignore the fluidity and interplay between different components of behavior. Also, some behaviors may not neatly fit into the appetitive-consummatory framework. For instance, certain behaviors may involve simultaneous aspects of both phases, making it challenging to categorize them definitively. The expression of behaviors can be context-dependent, influenced by environmental factors, internal states, and past experiences. This complexity may not always align with a simple appetitive-consummatory dichotomy. While the appetitive-consummatory framework has proven valuable in many research contexts, it is essential to recognize its limitations and be cautious in its application, considering the diverse and dynamic nature of behavior. Researchers continue to refine and expand upon this framework to better capture the complexities of motivated behaviors. Additionally, it is worth noting that while the appetitive phase an pre-consummatory phase can be understood as synonyms, their historical baggage is different. On the one hand, appetitive refers to the buildup of the drive or desire. Originally the term included the period in which the animal was not in the presence of the object of desire, a receptive female in this case, and thus included her search and lure (Craig, 1917). While modern use of appetitive phase does not necessarily include this period of the absence of the stimuli, there is an understanding that the wanting is being generated, and thus its boundaries are unclear.

In fact, a newer model of sexual behavior, the incentive sequence model, was proposed by Pfaus (1996). This model addresses the liquid boundaries between appetitive and consummatory phases, allowing the animal for a non-sequential transition from one to the other. This model,

instead of using a sharp distinction between the two phases (Beach 1956), draws them in a partially overlapping Ven Diagram. We, inspired by this view of not imposing hard boundaries to the transition between phases we employed an unbiased approach to describe the phases, such as the HMM. HMMs are statistical models that are particularly useful for analyzing sequential data, where the underlying states are not directly observable but can be inferred from observed data. We thought to apply this statistical model to test if we could find evidence of different hidden states comparable to the classical appetitive/consummatory definition. In fact, a HMM with two hidden states was the model that best captured our behavior, supporting the common division of sexual behavior, with Anogenital Investigations being mostly performed during the first state and Mounts with Intromissions in the second one. However, even though in most of the cases the transition was aligned with the classical transition point, in several session (particularly in inexperienced males) the transition occurred after the male performed several Mounts with Intromission and involved the execution of several Anogenital investigations.

This could be because an inexperienced male does not know the sequence of events once penile insertion is achieved, because during the initial sessions his arousal needs to be boosted by Anogenital Investigations or even because naïve males do not “understand” what sexual arousal is. The question of whether naive animals understand or know what to do when they first experience sexual arousal is complex and depends on various factors, including the species, individual differences, and the definition of "understanding" in this context. In general, sexual arousal is often considered to be an innate physiological response to certain stimuli, primarily driven by hormonal and neural mechanisms. In many species, including mammals, sexual arousal triggers instinctual behaviors related to reproduction, such as courtship displays, mounting,

and intromission. These behaviors are often genetically programmed and do not necessarily require prior learning or experience. However, while the basic physiological responses to sexual arousal may be innate, the specific patterns of sexual behavior can be influenced by experience, social learning, and environmental factors. Our data shows that the transition between behavioral motifs changes as male mice gain with consecutive sessions, suggesting that indeed they are learning with experience.

In contrast, we observed that for certain couples, the behavior that triggered the phase transition was the Mount without Intromission. It is believed that Mounts without Intromission may happen early in the appetitive to consummatory transition because as the male becomes experienced and initiates mounting sooner, the female might not be aroused enough to accept him by adopting the lordosis position. The fact that this mount type triggered the transition could be because both the male and the female were ready to initiate the copulatory stage, however, a combination of the female failing to acquire a good lordosis position, and the male to position correctly behind the female made it impossible for the intromission to happen. Alternatively, it could be that, once experienced, the Mount without Intromission is associated with the consummatory phase and is itself able to increase male arousal. Additionally, it might be that the Mount without Intromission might lead to consummatory feedback even though there is no penile insertion. Future studies should investigate the role of such copulatory act. It is worth mentioning that we did not see a reduction of this type of mount with experience or across the session. Therefore, this suggests that not all the Mounts without Intromission may be intended as mounts with intromission that failed due to an error in the positioning. It is important to alternatively consider that this type of mounts may be important for the copulatory act to be successful for both parties, as they may bring pleasure by themselves through the probing behavior.

It's crucial to note some limitations of our study. Firstly, our investigation didn't encompass a complete appetitive sequence due to the constraints of the laboratory setting where the behavior was observed. Secondly, our experimental setup was biased towards male behavior dominance, as the female had no means of avoiding the male's mount attempts, resulting in intermount intervals primarily dictated by the male. Consequently, our focus was primarily on male-driven behaviors. However, for a comprehensive understanding of the interaction, future experiments should incorporate the female perspective.

3.3.2 Experienced males require less excitatory ques

In order to explain the transition between these phases behavioral scientist have employed the term ‘drive’. The use of drive allows to create a intervening variable to parsimoniously explain and predict a behavior (Miller, 1971) In this context, thirst, hunger, and sexual arousal would be the drivers of drinking, eating, or mating behaviors. Thus, the drive provides a quantification that can be assessed through its associated impacts on behavioral dependent variables (Berridge, 2004). Anogenital investigation in the context of sexual behaviors are believed to increase the arousal of both the male and the female due to the volatile and non-volatile pheromones that are absorbed (Asaba et al., 2017; Neunuebel et al., 2015). One of the clearest results we obtained was the reduction of the anogenital investigations in the pre-copulatory phase (Figure 3-11 D top) (this result still hold when taking the motifs that happened in the pre-copulatory and copulatory). This suggest, that anogenital investigations can act as an associative cue between the sensory stimulus they are processing and the later sexual reward. Therefore, as they grow in experience, they are able to faster increase their arousal as an anticipation of what will come after. Additionally, the fact that the rate of

the investigations is unchanged suggest that the value that each of the motifs has does not change with experience. If naïve animals found anogenital investigations more appealing their rate would be higher in the early sessions and lower in the later ones. On the contrary, as the rate stays mostly unchanged, we believe that their role is more related to a conditioned stimulus (Moncho-Bogani et al., 2005).

3.3.3 Male experience crystalizes copulatory behaviors

Wild mice are predated by many animal species, praying birds such as eagles and cats among many others. Thus, they must constantly be on ward and alert of dangers coming from above or their surroundings. Mating puts them in a vulnerable situation. Thus, one would expect that they want the copulation to be as quick as possible. One way to make it quicker would be by learned strategies through their experience. However, we did not see any indication of a reduced latency to ejaculation with experience (Figure 3-11 C). In fact, the latency to ejaculation seems to be mouse specific, with some of them being over 30 minutes long. We also did not observe a reduction on the number of mounts (Figure 3-11 E top). Since the animals we used were breed in laboratory settings, they have not encountered real-life threats and thus it can be possible that such an adaptation would only be triggered by them experiencing predators. On the contrary, it could be that they use other mechanisms to protect themselves and they do not have to resort to a shortening of the copulatory period.

However, we must take into consideration that copulation does not only subserve fertilization. Sex can have many functions, as pregnancy induction, social bonding, or mate choice (Toates, 2009; Trezza et al., 2011; Pfaus et al., 2012; Fleischman, 2016; Werner et al., 2023). In fact, pregnancy in mice can be induced alone by mechanical stimulation in the house mouse (Stone & Srodulski, 2023) and as such a sufficient amount

of mechanical stimulation in the form of several mounts might be required by the female. Mate choice during copulation has also been observed in other rodent species, such as voles (Shapiro, 1986).

Instead, experience affected the organizational structure of the copulatory behaviors. As we have mentioned, we noted two types of mounts: Mounts with Intromission and Mounts without Intromission. As mounts without Intromission did not extinguish or decrease with experience, we believed that both mounts fulfill a particular role in the behavior. Additionally, male Genital grooming only occurs after a mount (of either type). The role of this motif is unclear, but it is speculated that it may be to clean the genital area of the male of pre-seminal fluid, or to lubricate it. Although genital grooming only happens after a mount (or after another genital grooming), not all the mounts are followed by a Genital grooming (75± 2% of Mounts with Intromission are followed by grooming. 12± 3% of Mounts without Intromission are followed by grooming). This ratio did not vary with experience, again suggesting that the presence of genital grooming may indicate something about the previous mount. In fact, it was the Mounts with Intromission that were followed by grooming the ones that were affected by experience.

This sequence not only became more common (Figure 3-10 F) (due to the increase of transition from Genital Grooming to Mount with Intromission), but it got shortened in time (Figure 3-13 A). Interestingly the intra-animal variance of the time interval between mounts that were followed by Genital Grooming decreased, not only shortening the interval between mounts but also making this interval more similar per animal and across animals. Further partition of this interval revealed that on one hand, the time the animals spent grooming decreased (Figure 3-13 D), which can be explained by an improvement in the execution of Genital grooming with experience. On the other hand, the time that took for the animal to go

from the Genital Grooming offset to the next mount (of any type) also decreased. This made the behavior of the male mouse more directed. Further analysis of this interval could reveal interesting microstructures of the learned behavior. Pose analysis of the male would help elucidate how does the Genital Grooming strategy changes with experience. Further, path analysis of the animal after Genital Grooming could reveal interesting insights into the different approaches naïve males and experienced males take.

Finally, to our surprise, while the decrease of the inter-mount interval for mounts followed by Genital Grooming was very noticeable and significant, the same interval for mounts that were not followed by grooming was unchanged. In our view this highlights the often-dismissed role that grooming has in the behavior. If we think of copulatory behavior as a cycle of Mounts and Intervals, where the drive to Mount is maximal at the beginning of the Mount and minimal at the end, the interval might be needed to regain the Mounting drive. The fact that the intervals with Genital Grooming become shorter and more stereotypical suggests that Genital Grooming might have an influence on the structuring of those cycles, to reinitiate the process that leads to the Mount threshold. The importance of Genital Grooming on the behavior not only begs for its function to be studied but also for taking into consideration when performing experiments that could impact the grooming capacity. For instance, optogenetic stimulation is done with a head mounted device that often impedes animal to groom, as their head is too heavy. This inability may affect the behavior and thus it is important to both think of experimental solutions to avoid this issue, and to understand what the role of Genital Grooming maybe.

3.3.4 Behavior across a sexual interaction

It is generally agreed that as the session progresses the sexual arousal of the couple progressively increases until it reaches the climax, and it terminates in the form of ejaculation for the male. As an alternative, arousal might be dynamically changing through the sexual interaction (for example, being high when the mount starts and minimal after grooming). To gain some insight into the arousal trajectory, and because in this study we did not perform direct measurements of sexual arousal, we tried to find proxies for it, by investigating behaviors that could be correlated with it. Two main behavioral variables can be thought as correlated with arousal: the intermount interval (the more aroused the male is we expect the intermount interval to be shorter, as the male should be more eager to reinitiate mounting); the thrusting rate (a more aroused male could perform pelvic thrusting with a higher rate, indicating higher vigor of the male which is believed to be correlated with arousal (Hull et al., 2002)). In a similar line the duration of the mount could also be an indication of the arousal level as it indicates their engagement with the copulative act. Finally, we also checked the latency to intromission. To check if there was any indication that arousal was increasing across the session, we checked how these variables evolved across a session. For that we compared the intermount interval, thrusting rate, mount duration and latency to intromission between the first events in the session and the same events towards the end of the session. While we saw no change in the intermount interval and the thrusting vigor, we saw an increase in mount duration and a decrease in the latency to intromission. Importantly, none of these variables changed with experience (figure 3-15). The first two variables show no evidence of arousal increase. However, the mount duration and latency to intromission may indicate an increase in the vigor of the male. However, these two variables are not male-only controlled, as mount duration and latency to intromission could be derived from an

increase in female receptivity as the session progresses, which might lead to a better lordosis posture and the female not interrupting the mount.

Overall, these results suggest that rather than a linear progression of increasing arousal during sex, arousal might be dynamically changing during the interaction. It might be that arousal works as a step function, increasing to the copulatory threshold and remaining stable through the interaction until the genital input provided during a mount is sufficient to drive ejaculation.

3.3.5 The value of employing statistical models

In this study we have used a novel layered HMM. While the employment of this particular model is new in the study of sexual behavior, the use of HMM of has been shown to be a powerful tool when modeling behavior (Franke et al., 2004; Marques et al., 2020). Behavior, like MMs is not deterministic (Schuster-Böckler & Bateman, 2007; Ramage, 2007). A large variability can be found in an individual, let alone a whole group. This variability makes it very hard to assess statistical differences between groups and treatments. By employing a HMM we maintained features of Markov processes, such as being able to mathematically compute the significance between different transition probabilities (Anderson & Goodman, 1957). This property allows to quantify first, whether there is a change in the number of visits to a given motif. Second whether the organization of the motif is significantly different. In our case we found that experience decreased the transition probability between grooming motifs and in turn increased the visits to Mount with Intromission. Such an intricate description of the behavioral changes would have been very difficult without employing Markov models.

Therefore, we believe, that this proposed model, or variations of it, could be a powerful tool to assess for organizational variations in the behavior between groups that would further help understand the neural correlates of the behavioral motifs.

3.3.6 Experience and sexual behavior

So far, we have described the changes that experience creates in the organization of sexual behavior. We would like to reiterate the importance of taking this into account when designing experiments. When looking at the latency to copulation, or anogenital investigation rate (Figure 3-11 B and C), one may think that there is a decrease if only looks at the first two sessions, however, when we look at all the sessions, the ANOVA is not significant, thus while certain aspect of the behavior may change from the first session to the second it is hard to assess which ones are due to the variability of the data or they are an actual effect of experience. Based on our LDA analysis, at least three sessions are needed for the male's behavior to stabilize (Figure 3-10 G). Thus, when doing withing animal perturbations, this should be considered.

3.3.7 Future work on behavioral organization

While our study brings interesting insights into mouse sexual behavior and understanding its structure may help future research design experiments and manipulations better, it has an important limitation as it is only focused on the male side. Doing a similar study where instead female behaviors are characterized and the effect of her experience in the behavior would be essential to have a more complete understanding of mouse sexual behavior and how male and female experience may affect different aspects of it.

In a similar line, in natural settings, the behavior does not take place in such a constrained space as the laboratory setting. In fact, the two animals meet in a common place for mounting, and as the dismount happens both animals hide in their respective corners. After a certain time, it is often the female that chases the male to continue with the behavior (Johansen et al., 2008). Therefore, it seems like female mice may have a central role in pacing the interaction (Lenschow et al., 2022). On the contrary, in laboratory settings it is often the male the one chasing the female and thus the one pacing the sexual encounter. It would be interesting to understand how the female lead may change the organizational structure and, in particular, the inter mount intervals. Perhaps looking at whether the ratio of Mounts followed by a genital grooming change, could help elucidate the role of genital grooming. In a female paced sexual encounter is likely the inter mount intervals would be longer. Thus, if the male would groom more it would suggest that their role is pleasure related or at least it might help him maintain his arousal level during the interval

Finally, this analysis was done by manually annotating behavioral motifs of recorded video. However, current tools allow us to track body parts of multiple animals at the same time (Lauer et al., 2022). The use of this tools would help us characterize micromovements and changes that are imperceptible by eye. Allowing for a much better characterization of the poses. Additionally, this gives us access to the path that the animal take, their distance and velocity. Adding this information would be very informative. In particular, (Pfaus,1996) suggested that appetitive and consummatory, not only do not have a clear boundary but they also interleaved. The addition of such information would be very useful to prove this. As perhaps, behaviors done in between two copulatory events resemble more the motifs observed during the appetitive phase.

Therefore, adding their distance, velocity, and angle to a model such as the HMM could provide with a richer state description.

3.3.7 Future work on neural correlates

Finally, it is important to understand the neural activity changes that underlie the observed effects of male experience on behavior. To study this, neural recordings should be conducted in relevant brain areas.

The first observed effect of male experience was in the pre-copulatory/appetitive phase of behavior, specifically in the reduction of anogenital investigations. As previously mentioned, these investigations are linked to the reception of volatile and non-volatile pheromones, mediated by the main olfactory bulb and accessory olfactory bulb. It is plausible that the activation of these areas is experience-dependent. The decrease in anogenital investigations may be associated with heightened activation of the olfactory bulbs upon initiation of such investigations. Given that anogenital investigations are rewarding behaviors, dopaminergic neurons may be particularly influenced by experience.

The second effect observed was in the copulatory/consummatory phase of behavior, where transitions between Mount with Intromission, Grooming, and back to Mount with Intromission became more pronounced. These copulatory behaviors are associated with activity in various hypothalamic areas (including VMH and MPOA) and the amygdala. Therefore, simultaneous measurement of activity in these regions would be valuable. Since male experience resulted in more stereotypical behavior, changes in neural activity may be related to increased pattern activation within these areas.

3.4 Materials and Methods

Adapted from de Costa Araujo, 2021

3.4.1 Animals

All experiments were approved by the Champalimaud Centre for the Unknown Bioethics Committee and by the Portuguese Veterinary General Board and in accordance with the European Union Directive 86/609/EEC.

All animals were bred in-house at the vivarium of the Champalimaud Research department. All male mice had the DAT:Cre genotype (Jax 006660) and females were C57BL/6J (Jax 000664). All animals were maintained on a 12h light/12h dark cycle.

Adult (12 weeks of age onwards) male and female mice were used. Male mice were single housed after 8 to 12 weeks of age, whereas female mice which were subjected to ovariectomy surgery between 8-12 weeks of age, were group housed and underwent regular estrogen and progesterone injections in order to induce sexual receptivity (Valente et al., 2021). Female mice were also sexually trained with male studs prior to being used in the experiments.

3.4.2 Sexual Behavior Setup

The behavioral arena was custom-made and consisted of a 35.5 x 13.4 x 21.5 cm box with transparent acrylic walls, two fixed point grey cameras (FL3-U3-13S2C-CS), and uniform and indirect illumination which was provided by one set of infra-red led lights placed around the arena.

3.4.3 Sexual behavior

All behavior experiments were performed during the night (mice were kept in reverse light cycle conditions, 8 am-8 pm).

The male was first placed in the behavioral arena and after a random period of habituation time to the box, a sexually experienced and receptive female mouse was introduced in the opposite place where the male was currently standing. The two animals were left to behave freely, until the male ejaculated, and the female was removed from the box. If after 1h, the male did not attempt to mount the female, the session was prematurely terminated. After a session with ejaculation, the time limit for waiting for a mount attempt was reduced to 30 min. After each session, regardless of the ejaculation outcome, the male was given one week before being tested again.

We allowed 10 sexually naive male mice to sexually interact with receptive females during 6 sessions where the male ejaculated. Other sessions when the male or the female did not engage in sexual behavior were discarded. The stimulus females were different for each session, except for sessions 4 to 6, where the female was the same to assess the variability due to the female sexual behavior.

3.4.4 Behavior recording

All the sessions of sexual behavior were recorded with two 30 fps cameras recording from above and from the wider side of the box. The videos were later manually annotated on a custom-made Bonsai workflow (Lopes et al., 2015) to identify the time of the following sexual behaviors.

3.4.5 Manual Annotations

For the appetitive phase: Time of first interaction between the male and the female, the male sniffing the female at close range, the male performing an anogenital investigation to the female and male and female touching noses. For the consummatory phase: Failed mount attempt,

Male mounting the female (the Mount-in and Mount-out times were annotated), Intromissions, Male grooming, and Ejaculation. Failed mount attempts correspond to the male standing on their back legs while leaning on the female, however the male body is not aligned to the female's. A Mount-in corresponds to the male putting his paws on the flank of the female, with his body aligned with her. The Mount-in was exactly annotated when the two bodies became aligned. Mounts can have intromissions or not. Intromissions were precisely annotated when the male pulled out the penis and his pelvis was furthest away from the female body.

We also analyzed the inter-mount intervals (IMI) which are defined as the time between the previous Mount-out and the next Mount-in. Likewise, we defined the inter-thrust interval (ITI) as the time between two consecutive thrusting events. The mating time, from first interaction with the female to ejaculation, was divided into the latency to first mount, where the first mount could be with or without intromission but not a failed mount attempt, and the ejaculation time, the time from first mount to ejaculation.

3.5 Data Analysis Methods

3.5.1 Markov Model

The Markov model was obtained by calculating the empirical probability between each pair of behavioral motifs. This probability was determined by calculating the ratio of a specific transition occurring within a given motif ($n_{i\to j}$) over all events associated with that motif (n_i).

$$P_{ij} = P(i|j) = \frac{n_{i\to j}}{n_i}$$

To calculate the transition probability matrix, we calculated the probability P_{ij} for each pair.

3.5.2 Hidden Markov Model

First, a Hidden Markov model with two hidden states was trained in the whole dataset using cross-validation (70% of the sessions were used for training and the remaining 30% for testing the model). The input data consisted of the following of events of each session: anogenital investigations, mounts without intromission, mounts with intromission, and ejaculation. Genital grooming was removed because their correlated occurrence with Mounts with Intromission avoided a good fit of the data. The cross-validation was repeated for 30 different permutations. The model selection was done based on the model that had the lowest BIC score in the test. Finally, the selected model was applied to the full dataset. This corresponded to the first layer of the HMM.

After the transition points were defined based on the outcome of the selected two-layer HMM, the transition probability between the events inside of each of the states was calculated, which corresponded to the second layer of the model.

When looking at the effect of experience in the event sequence, the same first layer model was applied to all cases – we observed no change in the results when different models were applied to each session. The second layer of the model was calculated independently for every level of experience.

3.5.3 Model Selection

To evaluate the best model between a single-state Markov model, a Markov model with fixed state transition, a 2 layered HMM with 2 hidden states, and a 2-layered HMM with 3 hidden states, we constructed each of the models and trained them in 70 percent of the data for 30 permutations and computed the log-likelihood of the reminding 30 percent of the data for each of the permutations.

Single-state Markov model
We calculated the transition matrix between all the different events in the training dataset without separating them into any states.

Markov model with fixed state-transition
We used the first mount with intromission as the transition point between the appetitive and consummatory phase and we calculated the transition probabilities within each of these states in the training dataset.

2 layered HMM with 2 or 3 hidden states
As explained in the previous section.

3.5.4 Linear Discriminant Analysis

We obtained the transition probability matrix using the 2-s 2-l HMM for every animal on each of the sessions. We transform each of the matrix into a one-dimensional vector and z-scored it. We then trained the LDA on the first and last session using leave one out cross validation method. This created an LDA eigenvector that separates maximally the first and the last session. We tested this eigenvector in the reminding animal that was not used in the creation of LDA. To do this we projected the z-scored transition probability vector of each of the session. This gave us a number for each session. If the number was negative, it means that it was labeled

as first session, if it was positive as the last session. The bigger the absolute value of this number the more confidence the algorithm had in the classification.

Using a leave one out cross-validation allowed us to obtain a LDA value per animal per session, the mean over all the animals was taken for each of the sessions.

3.5.5 Statistics

Statistical significance of the values

We used a repeated measures ANOVA to calculate whether there was a main effect of number of sessions. In case the ANOVA was significant we did a post-hoc test to check the difference between the first and the last session.

We used the same procedure to test across session effects, where the mount number was the main effect. To test the effect of experience and time in the session we did a two-way repeated measures ANOVA with the two main effects.

Statistical significance of the transition probability

To calculate the statistical significance of each of the transition probabilities between two events, we tested the transition probability computed from the observed sequence of events against the null hypothesis that the sequence of events we observed was stochastic. We randomized the sequence of events in each of the states. Then, we calculated the transition probability between the states. This measure gave us a stochastic transition probability distribution between every pair of events. We then computed the percentile of the observed transition probability concerning the stochastic transition probability distribution.

The observed transition probability was considered significant if it lay beyond 5 or 95 percentiles (*), 1 or 99 percentiles (**), 0.1 or 99.9 percentiles (***).

Statistical comparison between two transition probabilities

Using the properties of the Markov chain, we calculated the chi-square value between the transition probabilities matrixes T (base) and T^* (comparison) for each of the transition probability pairs (Anderson & Goodman, 1957).

$$X_{i,j}{}^2 = n_i \frac{\left(p_{i,j}{}^* - p_{i,j}\right)^2}{p_{i,j}}$$

where $p_{i,j}$ is the transition probability between states i and j in the base matrix and $p_{i,j}{}^*$ is the transition probability between states i and j in the matrix we want to make the comparison to and, $n_i$is the number of observations in state i in the base transition probability.

3.6 Tables

3.6.1 Mount duration

one-way ANOVA						
Source	**ddof1**	**ddof2**	**F**	**p-unc**	**ng2**	**eps**
epoch	3	30	3,830488	0,019575967	0,148867	0,835845

Post-hoc												
Contrast	**A**	**B**	**Paired**	**Parametric**	**T**	**dof**	**alternative**	**p-unc**	**p-corr**	**p-adjust**	**BF10**	**hedges**
epoch	first	first +1	TRUE	TRUE	-1,308	10	two-sided	0,22014	0,295691	fdr_bh	0.591	-0,35587
epoch	first	last -2	TRUE	TRUE	-2,82908	10	two-sided	0,01788	0,05364	fdr_bh	3.801	-0,9796
epoch	first	last -1	TRUE	TRUE	-3,37749	10	two-sided	0,007032	0,042193	fdr_bh	8.05	-0,92047
epoch	first +1	last -2	TRUE	TRUE	-1,23123	10	two-sided	0,246409	0,295691	fdr_bh	0.549	-0,45727
epoch	first +1	last -1	TRUE	TRUE	-1,62319	10	two-sided	0,135612	0,271224	fdr_bh	0.821	-0,55044
epoch	last -2	last -1	TRUE	TRUE	-0,71065	10	two-sided	0,493541	0,493541	fdr_bh	0.369	-0,23125

3.6.2 Inter Mount interval

One-way ANOVA						
Source	**ddof1**	**ddof2**	**F**	**p-unc**	**ng2**	**eps**
epoch	3	30	1,802822	0,167942225	0,106964	0,646172

Post-hoc												
Contrast	**A**	**B**	**Paired**	**Parametric**	**T**	**dof**	**alternative**	**p-unc**	**p-corr**	**p-adjust**	**BF10**	**hedges**
epoch	first	first +1	TRUE	TRUE	1,317731	10	two-sided	0,216983	0,433966	fdr_bh	0.596	0,531985
epoch	first	last -2	TRUE	TRUE	1,732654	10	two-sided	0,113826	0,433966	fdr_bh	0.929	0,766463
epoch	first	last -1	TRUE	TRUE	1,580197	10	two-sided	0,145143	0,433966	fdr_bh	0.783	0,744207
epoch	first +1	last -2	TRUE	TRUE	0,489038	10	two-sided	0,635363	0,857718	fdr_bh	0.33	0,12145
epoch	first +1	last -1	TRUE	TRUE	0,376008	10	two-sided	0,714765	0,857718	fdr_bh	0.316	0,128239
epoch	last -2	last -1	TRUE	TRUE	0,055796	10	two-sided	0,956604	0,956604	fdr_bh	0.298	0,017164

3.6.3 Latency to first thrust

One-way ANOVA						
Source	**ddof1**	**ddof2**	**F**	**p-unc**	**ng2**	**eps**
epoch	3	30	18,46615	5,6155E-07	0,607005	0,606351

Post-hoc												
Contrast	**A**	**B**	**Paired**	**Parametric**	**T**	**dof**	**alternative**	**p-unc**	**p-corr**	**p-adjust**	**BF10**	**hedges**
epoch	first	first +1	TRUE	TRUE	3,379719	10	two-sided	0,007006	0,014012	fdr_bh	8.075	1,488302
epoch	first	last -2	TRUE	TRUE	4,989925	10	two-sided	0,000545	0,001636	fdr_bh	67.53	2,291026
epoch	first	last -1	TRUE	TRUE	5,421796	10	two-sided	0,000292	0,001636	fdr_bh	114.736	2,327243
epoch	first +1	last -2	TRUE	TRUE	3,200155	10	two-sided	0,009489	0,014234	fdr_bh	6.314	1,276658
epoch	first +1	last -1	TRUE	TRUE	2,958607	10	two-sided	0,014322	0,017187	fdr_bh	4.536	1,329248
epoch	last -2	last -1	TRUE	TRUE	-0,13652	10	two-sided	0,894123	0,894123	fdr_bh	0.3	-0,04813

3.6.4 Inter thrust interval

One-way ANOVA						
Source	**ddof1**	**ddof2**	**F**	**p-unc**	**ng2**	**eps**
epoch	3	30	3,525327	0,02669193	0,224328	0,681031

Post-hoc												
Contrast	**A**	**B**	**Paired**	**Parametric**	**T**	**dof**	**alternative**	**p-unc**	**p-corr**	**p-adjust**	**BF10**	**hedges**
epoch	first	first +1	TRUE	TRUE	-0,33316	10	two-sided	0,745893	0,745893	fdr_bh	0.312	-0,13852
epoch	first	last -2	TRUE	TRUE	1,324809	10	two-sided	0,21471	0,322064	fdr_bh	0.6	0,616407
epoch	first	last -1	TRUE	TRUE	2,393769	10	two-sided	0,037715	0,113145	fdr_bh	2.119	1,010262
epoch	first +1	last -2	TRUE	TRUE	2,000338	10	two-sided	0,073347	0,146693	fdr_bh	1.28	0,912535
epoch	first +1	last -1	TRUE	TRUE	4,574925	10	two-sided	0,001019	0,006111	fdr_bh	39.868	1,605803
epoch	last -2	last -1	TRUE	TRUE	0,916528	10	two-sided	0,380962	0,457155	fdr_bh	0.422	0,359242

Chapter 4 – General discussion and conclusions

The work presented in this thesis was composed of two independent projects. The main analysis techniques of both projects relied on mathematical methods that revealed hidden structures in the data, called latent variables.

The first project aimed to elucidate the role of feedback from HVAs to V1. In particular, it attempted to characterize how the absence of feedback shaped the population stimulus representation for well-characterized drifting grating stimuli and for a naturalistic movie. The second project aimed to carefully describe mouse sexual behavior, both to understand what the main motifs of the behavior are and to learn how its organization changed with experience.

4.1 Latent variables in the representation of visual stimuli

In the first project, we investigated how the representations of visual stimuli of different characteristics were dependent on the presence of direct cortico-cortical FB from HVAs to V1. We showed that both the drifting grating stimuli and the naturalistic movie were represented on a manifold smaller than the stimulus dimensionality.

4.1.1 Population responses to drifting gratings lie along a 1D tuning axis

For the case of the drifting gratings, we showed how the population representation of each orientation created a one-dimensional tuning axis, embedded in a three-dimensional manifold (Figure 2-9). The tuning axis coded for the population strength of the stimulus. Thus, when a given orientation was very sharply represented by single neurons (the gOSI was high), the population response lied far away from the origin. In a similar manner, when the stimulus was weakly represented by the single neurons

(the gOSI was low), the population response lied close to the origin. Defining this one-dimensional latent vector that summarized the population responses allowed us to characterize how the population response changed when FB from HVAs to V1 was silenced. Indeed, it revealed that FB suppressed the population activity in response to drifting gratings, as the responses in the absence of FB lied farther away from the origin than when FB was present.

4.1.2 Population responses to the naturalistic movie lie in a low dimensional manifold

As mentioned, the population representation of the naturalistic movie was also bounded inside of a reduced subspace. The full variance of the data was captured using 35 dimensions, however after 10 dimensions, the variance explained by each of the components was very small. Because of the nature of the stimulus, its parametrization was trickier. We observed that the population coded the stimulus in a much more complex way. Figure 2-14 B shows an example projection into the first 3 PCs. In this figure one can notice, particularly for the hDM4(Gi)-FB example session, that the trajectories do not follow a straight line and they often cross and curve — this suggests that indeed, the population representation uses more than those three dimensions to represent the stimulus. For a more detailed characterization of the stimulus representation manifold, one would need access to the RFs of the neurons to understand the visual information they have access to via FF projections, and the visual flow and visual statistics of the movie of the RF and its surround.

However, only by looking at the latent dimensions obtained through PC, we already obtained insightful information about how naturalistic images and videos might be represented. Particularly, we saw that the activity along the first two PCs (the ones that carry the most variance), did not change so much upon the absence of FB (Figure 2-14 E), suggesting that

FF information may lie in a lower dimensional subspace that is invariant to the presence of FB. While this should be investigated more deeply, this preliminary result agrees with the results of FF information between primate V1 and V4 being shared inside of a low dimensional subspace (Semedo et al., 2018). The subsequent PCs, on the other hand, displayed quite a different pattern of activity, suggesting that FB indeed shapes the representations in the lower area. Further analysis in this direction will be interesting to understand the latent structure of FB information and its dimensionality.

4.2 Latent variables in mouse sexual behavior

Mouse sexual behavior consists of complex interactions between two individuals. In order to be able to characterize and study them, researchers have identified well defined behavioral motifs (anogenital investigations, genital grooming or mounts, …). Each time a behavior is performed, it is not done in exactly the same way — the posture, the orientation of the partner, and environmental and internal factors may account for the observed differences between repetitions of the same motif. However, the main properties of the motif are maintained; in fact, preliminary data shows that classification algorithms can learn these motifs using video tracking algorithms or accelerometer data (Brangers, 2023).

This suggests that, while the behavior is complex, high dimensional and variable, there are consistent structures that can be used to characterize it. Moreover, our study revealed that these behavioral motifs follow certain sequences that vary depending on the experience of the male. In particular, we showed that the sequence they follow changes across the behavior. Employing unbiased algorithms, we were able to identify two hidden states featuring different types of behavioral sequences. These

latent states could be mapped onto the previously described pre-copulatory and copulatory periods of sexual behaviors (Anderson & Perona, 2014). The analysis showed that the same behavioral motif may fulfill different roles during these two different states, hinting towards a more contextual understanding of the behavior.

4.3 Future directions

The two projects highlight the complexity of neural and behavioral data. However, as pointed out before (Krakauer et al., 2017) one cannot be understood without the other. Neural representation and behavior are two sides of the same coin; they relate to and influence each other in an endless loop. Therefore, it is important to relate neural data to behavior, and at the same time, to have a detailed understanding of the behavioral organization to be able to understand the neural data. Innate behaviors provide a particularly constrained relationship between the two. In contrast to learned behavior, we know that the neural circuitry is adapted to perform them. They naturally occur and are translatable between different species. This provides a robust framework in which the neural data can be understood.

Neuroscience research exists in a tight balance between controllability and ethological realism (Krakauer et al., 2017). A very controlled protocol may achieve low experimental noise and thus be fully reliable. However, the extent to which the obtained measurements are artificial, or how generalizable the conclusions are, may be unclear. On the other hand, a fully ethological study may err on the side of falling into a mere description, as manipulations, measurements, and repetitions may be hard to implement.

Biology excels in variability; its inherent changing nature has allowed for life to exist in all its multiple forms, shapes, and contexts. We live in a privileged time, in which technological advances allow for tracking of the posture and behavior of the animal (Mathis et al., 2018; Pereira et al., 2020). Moreover, current technology provides portable solutions to record neural activity while the animal is freely moving and doing the experiment. This technology has started to open the door to experimental designs that are relevant for the natural context of the animal (Rich et al., 2014; Zong et al., 2022; Forli & Yartsev, 2023), and therefore, could provide an ethological framework to understand the measured neural activity.

The realization that human-like complex behaviors were also observable in the non-human animal kingdom has changed the way we understand cognition, and allowed us to use animal models to study human-like abilities. Perhaps the next step is to reverse this relationship, and to understand the animality of humans. This would not only allow us to acknowledge the complexity of animal cognition in its own right, but also may shine a new light into our own. While the environmental context in which we evolved has changed a great deal, our brains still operate in the same way. Therefore, turning towards ethologically relevant protocols to understand different brain functions (including sensory processing) may provide an evolutionary and adaptive theoretical framework in which to interpret the data. Transitioning to these types of experimental settings is logistically challenging. Moreover, the data that would be acquired this way would be more complex and much more high-dimensional. Therefore, dimensionality reduction techniques that allow us to visualize and understand the data in lower dimensional latent manifolds will continue to be pivotal to be able to make sense of it.

References

Adamczak, B. (2016). On circlusion. *Mask Magazine*, *30*.

Ågmo, A., & Ellingsen, E. (2003). Relevance of non-human animal studies to the understanding of human sexuality. *Scandinavian Journal of Psychology*, *44*(3), 293–301. https://doi.org/10.1111/1467-9450.00348

Ågmo, A., & Snoeren, E. M. S. (2015). Silent or Vocalizing Rats Copulate in a Similar Manner. *PLOS ONE*, *10*(12), e0144164. https://doi.org/10.1371/journal.pone.0144164

Ågmo, A., & Snoeren, E. M. S. (2017). A cooperative function for multisensory stimuli in the induction of approach behavior of a potential mate. *PLOS ONE*, *12*(3), e0174339. https://doi.org/10.1371/journal.pone.0174339

Ahmavaara, Y., & Thurstone, L. L. (1954). *Transformation analysis of factorial data: And other new analytical methods of differential psychology with their application to Thurstone's basic studies*. Suomalaisen Kirjallisuuden Seuran Kirjapainon Oy.

Altmann, S. A. (1965). Sociobiology of rhesus monkeys. II: Stochastics of social communication. *Journal of Theoretical Biology*, *8*(3), 490–522. https://doi.org/10.1016/0022-5193(65)90024-X

Andermann, M. L., Kerlin, A. M., Roumis, D. K., Glickfeld, L. L., & Reid, R. C. (2011). Functional Specialization of Mouse Higher Visual Cortical Areas. *Neuron*, *72*(6), 1025–1039. https://doi.org/10.1016/j.neuron.2011.11.013

Anderson, D. J. (2016). Circuit modules linking internal states and social behaviour in flies and mice. *Nature Reviews Neuroscience*, *17*(11), 692–704. https://doi.org/10.1038/nrn.2016.125

Anderson, D. J., & Perona, P. (2014). Toward a Science of Computational Ethology. *Neuron*, *84*(1), 18–31. https://doi.org/10.1016/j.neuron.2014.09.005

Anderson, T. W., & Goodman, L. A. (1957). Statistical inference about Markov chains. *The Annals of Mathematical Statistics*, 89–110.

Andersson, M. (1994). *Sexual selection* (Vol. 72). Princeton University Press.

Angelucci, A., Bijanzadeh, M., Nurminen, L., Federer, F., Merlin, S., & Bressloff, P. C. (2017). Circuits and Mechanisms for Surround Modulation in Visual Cortex. *Annual Review of Neuroscience*, *40*(1), 425–451. https://doi.org/10.1146/annurev-neuro-072116-031418

Angelucci, A., & Bressloff, P. C. (2006). Contribution of feedforward, lateral and feedback connections to the classical receptive field center and extra-classical receptive field surround of primate V1 neurons. *Progress in Brain Research*, *154*(SUPPL. A), 93–120. https://doi.org/10.1016/S0079-6123(06)54005-1

Angelucci, A., & Bullier, J. (2003). Reaching beyond the classical receptive field of V1 neurons: Horizontal or feedback axons? *Journal of Physiology-Paris*, *97*(2–3), 141–154. https://doi.org/10.1016/j.jphysparis.2003.09.001

Angelucci, A., Levitt, J. B., Walton, E. J. S., Hupe, J. M., Bullier, J., & Lund, J. S. (2002). Circuits for local and global signal integration in primary visual cortex. *The Journal of Neuroscience*, *22*(19), 8633–8646.

Angoa-Pérez, M., & Kuhn, D. M. (2015). Neuroanatomical dichotomy of sexual behaviors in rodents: A special emphasis on brain serotonin. *Behavioural Pharmacology*, *26*(6 Special Issue Pharmacological Approaches to the Study of Social Behaviour-Part 1: Reviews), 595–606.

Archer, E. W., Koster, U., Pillow, J. W., & Macke, J. H. (2014). Low-dimensional models of neural population activity in sensory cortical circuits. *Advances in Neural Information Processing Systems*, *27*.

Armbruster, B. N., Li, X., Pausch, M. H., Herlitze, S., & Roth, B. L. (2007). Evolving the lock to fit the key to create a family of G protein-coupled receptors potently activated by an inert ligand. *Proceedings of the National Academy of Sciences of the United States of America*, *104*(12), 5163–5168. https://doi.org/10.1073/pnas.0700293104

Armbruster, B. N., & Roth, B. L. (2005). Mining the receptorome. *Journal of Biological Chemistry*, *280*(7), 5129–5132.

Arnold, A. P. (2009). The organizational–activational hypothesis as the foundation for a unified theory of sexual differentiation of all mammalian tissues. *Hormones and Behavior*, *55*(5), 570–578. https://doi.org/10.1016/j.yhbeh.2009.03.011

Asaba, A., Hattori, T., Mogi, K., & Kikusui, T. (2014). Sexual attractiveness of male chemicals and vocalizations in mice. *Frontiers in Neuroscience*, *8*, 99047.

Asaba, A., Osakada, T., Touhara, K., Kato, M., Mogi, K., & Kikusui, T. (2017). Male mice ultrasonic vocalizations enhance female sexual approach and hypothalamic kisspeptin neuron activity. *Hormones and Behavior*, *94*, 53–60. https://doi.org/10.1016/j.yhbeh.2017.06.006

Badre, D., Frank, M. J., & Moore, C. I. (2015). Interactionist Neuroscience. *Neuron*, *88*(5), 855–860. https://doi.org/10.1016/j.neuron.2015.10.021

Bagemihl, B. (1999). *Biological exuberance: Animal homosexuality and natural diversity*. First edition. New York : St. Martin's Press, 1999. https://search.library.wisc.edu/catalog/999881021602121

Baggini, J. (2002). David Hume: An Enquiry concerning Human Understanding (1748). In J. Baggini (Ed.), *Philosophy: Key Texts*

(pp. 61–84). Palgrave Macmillan UK. https://doi.org/10.1007/978-1-4039-1370-8_4

Bailey, N. W., & Zuk, M. (2009). Same-sex sexual behavior and evolution. *Trends in Ecology & Evolution*, *24*(8), 439–446. https://doi.org/10.1016/j.tree.2009.03.014

Baillarger, J. G. F. (1840). *Recherches sur la structure de la couche corticale des circonvolutions du cerveau*. chez J.-B. Baillière.

Baker, J. (1975). The DRAGON system—An overview. *IEEE Transactions on Acoustics, Speech, and Signal Processing*, *23*(1), 24–29.

Ball, G. F., & Balthazart, J. (2008). How useful is the appetitive and consummatory distinction for our understanding of the neuroendocrine control of sexual behavior? *Hormones and Behavior*, *53*(2), 307–311. https://doi.org/10.1016/j.yhbeh.2007.09.023

Bardy, C., Huang, J. Y., Wang, C., FitzGibbon, T., & Dreher, B. (2006). 'Simplification'of responses of complex cells in cat striate cortex: Suppressive surrounds and 'feedback'inactivation. *The Journal of Physiology*, *574*(3), 731–750.

Bardy, C., Huang, J. Y., Wang, C., FitzGibbon, T., & Dreher, B. (2009). 'Top-down'influences of ipsilateral or contralateral postero-temporal visual cortices on the extra-classical receptive fields of neurons in cat's striate cortex. *Neuroscience*, *158*(2), 951–968.

Barlow, H. B. (1972). Single units and sensation: A neuron doctrine for perceptual psychology? *Perception*, *1*(4), 371–394.

Barlow, H. B., & Foldiak, P. (1989). Adaptation and decorrelation in the cortex. In *The computing neuron* (pp. 54–72). Addison Wesley.

Bartholomew, D. J. (1995). Spearman and the origin and development of factor analysis. *British Journal of Mathematical and Statistical Psychology*, *48*(2), 211–220.

Bastock, M. (2018). *Courtship: An ethological study*. Routledge.

Baum, L. E. (1972). An inequality and associated maximization technique in statistical estimation for probabilistic functions of Markov processes. *Inequalities*, *3*(1), 1–8.

Baum, L. E., & Eagon, J. A. (1967). *An inequality with applications to statistical estimation for probabilistic functions of Markov processes and to a model for ecology*.

Baum, L. E., & Petrie, T. (1966). Statistical inference for probabilistic functions of finite state Markov chains. *The Annals of Mathematical Statistics*, *37*(6), 1554–1563.

Baum, L. E., Petrie, T., Soules, G., & Weiss, N. (1970). A maximization technique occurring in the statistical analysis of probabilistic functions of Markov chains. *The Annals of Mathematical Statistics*, *41*(1), 164–171.

Baum, L. E., & Sell, G. (1968a). Growth transformations for functions on manifolds. *Pacific Journal of Mathematics*, *27*(2), 211–227.

Baum, L. E., & Sell, G. (1968b). Growth transformations for functions on manifolds. *Pacific Journal of Mathematics*, *27*(2), 211–227.

Bayless, D. W., Davis, C. O., Yang, R., Wei, Y., De Andrade Carvalho, V. M., Knoedler, J. R., Yang, T., Livingston, O., Lomvardas, A., Martins, G. J., Vicente, A. M., Ding, J. B., Luo, L., & Shah, N. M. (2023). A neural circuit for male sexual behavior and reward. *Cell*, *186*(18), 3862-3881.e28. https://doi.org/10.1016/j.cell.2023.07.021

Beach, F. A. (1956). *Characteristics of masculine "sex drive." 4*(1), 32.

Beach, F. A. (1976). Sexual attractivity, proceptivity, and receptivity in female mammals. *Hormones and Behavior*, *7*(1), 105–138. https://doi.org/10.1016/0018-506X(76)90008-8

Bechtel, W. (2007). *Mental mechanisms: Philosophical perspectives on cognitive neuroscience*. Psychology Press.

Beer, C. (1964). Ethology-the zoologist's approach to behaviour-Part 2. *Tuatara*, *12*, 16–39.

Beer, C. G. (1983). Darwin, instinct, and ethology. *Journal of the History of the Behavioral Sciences*, *19*(1), 68–80.

Bensaude Vincent, B., & Loeve, S. (2018). Toward a Philosophy of Technosciences. In S. Loeve, X. Guchet, & B. Bensaude Vincent (Eds.), *French Philosophy of Technology* (Vol. 29, pp. 169–186). Springer International Publishing. https://doi.org/10.1007/978-3-319-89518-5_11

Bergan, J. F., Ben-Shaul, Y., & Dulac, C. (2014). Sex-specific processing of social cues in the medial amygdala. *eLife*, *3*, e02743. https://doi.org/10.7554/eLife.02743

Bernstein, J. (1871). *Untersuchungen über den Erregungsvorgang im Nerven-und Muskelsysteme*. Winter.

Berridge, K. C. (2004). Motivation concepts in behavioral neuroscience. *Physiology & Behavior*, *81*(2), 179–209. https://doi.org/10.1016/j.physbeh.2004.02.004

Birkhead, T. R., Moller, A., & Ridley, M. (1999). Sperm competition and sexual selection. *Nature*, *397*(6720), 576–576.

Blackless, M., Charuvastra, A., Derryck, A., Fausto-Sterling, A., Lauzanne, K., & Lee, E. (2000). How sexually dimorphic are we? Review and synthesis. *American Journal of Human Biology: The Official Journal of the Human Biology Association*, *12*(2), 151–166.

Bolz, J., & Gilbert, C. D. (1986). Generation of end-inhibition in the visual cortex via interlaminar connections. *Nature*, *320*(6060), 362–365.

Bonthuis, P. J., Cox, K. H., Searcy, B. T., Kumar, P., Tobet, S., & Rissman, E. F. (2010). Of mice and rats: Key species variations in the sexual differentiation of brain and behavior. *Frontiers in Neuroendocrinology*, *31*(3), 341–358. https://doi.org/10.1016/j.yfrne.2010.05.001

Boyd, M. A., & Lau, S. (1998). *An introduction to Markov modeling: Concepts and uses*. Annual Reliability and Maintainability Symposium.

Brainard, D. H. (1997). The Psychophysics Toolbox. *Spatial Vision*, *10*, 433–436.

Braitenberg, V., & Schüz, A. (2013). *Anatomy of the cortex: Statistics and geometry* (Vol. 18). Springer Science & Business Media.

Brangers, B.C., (2023). PhD Thesis. The Role of the Periaqueductal Gray in Female Sexual Behavior. http://hdl.handle.net/10362/153012

Brecht, M., Schneider, M., Sakmann, B., & Margrie, T. W. (2004). Whisker movements evoked by stimulation of single pyramidal cells in rat motor cortex. *Nature*, *427*(6976), 704–710.

Brennan, P. L. R., & Orbach, D. N. (2020). Copulatory behavior and its relationship to genital morphology. In *Advances in the Study of Behavior* (Vol. 52, pp. 65–122). Elsevier. https://doi.org/10.1016/bs.asb.2020.01.001

Broca, P. (1861). Perte de la parole, ramollissement chronique et destruction partielle du lobe antérieur gauche du cerveau. *Bull Soc Anthropol*, *2*(1), 235–238.

Brodmann, K. (1903). Beiträge zur histologischen Lokalisation der Grosshirnrinde. Erste Mitteilung: Die Regio Rolandica. *J Psychol Neurol*, *2*, 79–107.

Brodmann, K. (1905). Beitrage zur histologischen Lokalisation der Grosshirnrinde. *J Psychol Neurol*, *4*, 176–226.

Brodmann, K. (1909). *Vergleichende Lokalisationslehre der Grosshirnrinde in ihren Prinzipien dargestellt auf Grund des Zellenbaues*. Barth.

Brown, A. E. X., & De Bivort, B. (2018). Ethology as a physical science. *Nature Physics*, *14*(7), 653–657. https://doi.org/10.1038/s41567-018-0093-0

Brown, D. J. (2023). Nature, Artifice, and Discovery in Descartes' Mechanical Philosophy. *Philosophies*, *8*(5), 85. https://doi.org/10.3390/philosophies8050085

Bullier, J., Hupé, J., James, A., & Girard, P. (1996). Functional interactions between areas V1 and V2 in the monkey. *Journal of Physiology-Paris*, *90*(3–4), 217–220.

Bullock, T. H., Bennett, M. V., Johnston, D., Josephson, R., Marder, E., & Fields, R. D. (2005). The neuron doctrine, redux. *Science*, *310*(5749), 791–793.

Burkhalter, A., D'Souza, R. D., Ji, W., & Meier, A. M. (2023). Integration of Feedforward and Feedback Information Streams in the Modular Architecture of Mouse Visual Cortex. *Annual Review of Neuroscience*, *46*(1), 259–280. https://doi.org/10.1146/annurev-neuro-083122-021241

Burns-Cusato, M., Scordalakes, E. M., & Rissman, E. F. (2004). Of mice and missing data: What we know (and need to learn) about male

sexual behavior. *Physiology & Behavior*, *83*(2), 217–232. https://doi.org/10.1016/j.physbeh.2004.08.015

Cadena, S. A., Denfield, G. H., Walker, E. Y., Gatys, L. A., Tolias, A. S., Bethge, M., & Ecker, A. S. (2019). Deep convolutional models improve predictions of macaque V1 responses to natural images. *PLOS Computational Biology*, *15*(4), e1006897. https://doi.org/10.1371/journal.pcbi.1006897

Cadieu, C. F., Hong, H., Yamins, D. L., Pinto, N., Ardila, D., Solomon, E. A., Majaj, N. J., & DiCarlo, J. J. (2014). Deep neural networks rival the representation of primate IT cortex for core visual object recognition. *PLoS Computational Biology*, *10*(12), e1003963.

Cajal, R. (1899a). *La textura del sistema nerviosa del hombre y los vertebrados. 1st Moya*.

Cajal, R. (1899b). *La textura del sistema nerviosa del hombre y los vertebrados. 1st Moya*.

Calhoun, J. B. (1963). *The ecology and sociology of the Norway rat* (Issue 1008). US Department of Health, Education, and Welfare, Public Health Service.

Capalbo, M., Postma, E., & Goebel, R. (2008). Combining Structural Connectivity and Response Latencies to Model the Structure of the Visual System. *PLoS Computational Biology*, *4*(8), e1000159. https://doi.org/10.1371/journal.pcbi.1000159

Carandini, M. (2012). From circuits to behavior: A bridge too far? *Nature Neuroscience*, *15*(4), 507–509. https://doi.org/10.1038/nn.3043

Carandini, M., Demb, J. B., Mante, V., Tolhurst, D. J., Dan, Y., Olshausen, B. A., Gallant, J. L., & Rust, N. C. (2005). Do We Know What the Early Visual System Does? *The Journal of Neuroscience*, *25*(46), 10577–10597. https://doi.org/10.1523/JNEUROSCI.3726-05.2005

Carandini, M., & Heeger, D. J. (2012). Normalization as a canonical neural computation. *Nature Reviews Neuroscience*, *13*(1), 51–62. https://doi.org/10.1038/nrn3136

Castellani, G., Croese, T., Peralta Ramos, J. M., & Schwartz, M. (2023). Transforming the understanding of brain immunity. *Science*, *380*(6640), eabo7649. https://doi.org/10.1126/science.abo7649

Caviness, V. S., & Frost, D. O. (1980). Tangential organization of thalamic projections to the neocortex in the mouse. *Journal of Comparative Neurology*, *194*(2), 335–367. https://doi.org/10.1002/cne.901940205

Chapin, J. K., Moxon, K. A., Markowitz, R. S., & Nicolelis, M. A. (1999). Real-time control of a robot arm using simultaneously recorded neurons in the motor cortex. *Nature Neuroscience*, *2*(7), 664–670.

Chapin, J. K., & Nicolelis, M. A. L. (1999). Principal component analysis of neuronal ensemble activity reveals multidimensional somatosensory representations. *Journal of Neuroscience*

Methods, *94*(1), 121–140. https://doi.org/10.1016/S0165-0270(99)00130-2

Chen, S., Lee, A. Y., Bowens, N. M., Huber, R., & Kravitz, E. A. (2002). Fighting fruit flies: A model system for the study of aggression. *Proceedings of the National Academy of Sciences*, *99*(8), 5664–5668. https://doi.org/10.1073/pnas.082102599

Chu, X., & Ågmo, A. (2014). Sociosexual behaviours in cycling, intact female rats (Rattus norvegicus) housed in a seminatural environment. *Behaviour*, *151*(8), 1143–1184.

Chu, X., & Ågmo, A. (2015a). Sociosexual behaviors during the transition from non-receptivity to receptivity in rats housed in a seminatural environment. *Behavioural Processes*, *113*, 24–34.

Chu, X., & Ågmo, A. (2015b). Sociosexual behaviors of male rats (Rattus norvegicus) in a seminatural environment. *Journal of Comparative Psychology*, *129*(2), 132.

Chu, X., & Ågmo, A. (2016). Sociosexual interactions in rats: Are they relevant for understanding human sexual behavior? *International Journal of Psychological Research*, *9*(2), 76–95.

Chung, S., Lee, D. D., & Sompolinsky, H. (2018). Classification and geometry of general perceptual manifolds. *Physical Review X*, *8*(3), 031003.

Churchland, M. M., Cunningham, J. P., Kaufman, M. T., Foster, J. D., Nuyujukian, P., Ryu, S. I., & Shenoy, K. V. (2012). Neural population dynamics during reaching. *Nature*, *487*(7405), 51–56.

Cisek, P., & Green, A. M. (2024). Toward a neuroscience of natural behavior. *Current Opinion in Neurobiology*, *86*, 102859. https://doi.org/10.1016/j.conb.2024.102859

Cobb, M. (2002). Exorcizing the animal spirits: Jan Swammerdam on nerve function. *Nature Reviews Neuroscience*, *3*(5), 395–400. https://doi.org/10.1038/nrn806

Committee on Measuring Sex, Gender Identity, and Sexual Orientation, Committee on National Statistics, Division of Behavioral and Social Sciences and Education, & National Academies of Sciences, Engineering, and Medicine. (2022). *Measuring Sex, Gender Identity, and Sexual Orientation* (N. Bates, M. Chin, & T. Becker, Eds.; p. 26424). National Academies Press. https://doi.org/10.17226/26424

Cooper, R. P., & Peebles, D. (2015). Beyond Single-Level Accounts: The Role of Cognitive Architectures in Cognitive Scientific Explanation. *Topics in Cognitive Science*, *7*(2), 243–258. https://doi.org/10.1111/tops.12132

de Costa Araújo, S. (2021). PhD Thesis. Unravelling the activity patterns of midbrain dopaminergic neurons during male sexual behaviour. http://hdl.handle.net/10362/132857

Craig, W. (n.d.). *APPETITES AND AVERSIONS AS CONSTITUENTS OF INSTINCTS*.

Cronquist, A. (1969). ON THE RELATIONSHIP BETWEEN TAXONOMY AND EVOLUTION. *TAXON*, *18*(2), 177–187. https://doi.org/10.2307/1218675

Cryan, J. F., & Dinan, T. G. (2012). Mind-altering microorganisms: The impact of the gut microbiota on brain and behaviour. *Nature Reviews Neuroscience*, *13*(10), 701–712.

Cunningham, J. P., & Yu, B. M. (2014). Dimensionality reduction for large-scale neural recordings. *Nature Neuroscience*, *17*(11), 1500–1509. https://doi.org/10.1038/nn.3776

Cury, K. M., & Axel, R. (2023). Flexible neural control of transition points within the egg-laying behavioral sequence in Drosophila. *Nature Neuroscience*, *26*(6), 1054–1067. https://doi.org/10.1038/s41593-023-01332-5

Dantzer, R. (2018). Neuroimmune interactions: From the brain to the immune system and vice versa. *Physiological Reviews*, *98*(1), 477–504.

Darwin, C. (2016). *On the origin of species, 1859*.

Datta, S. R., Anderson, D. J., Branson, K., Perona, P., & Leifer, A. (2019). Computational neuroethology: A call to action. *Neuron*, *104*(1), 11–24.

Davis, M. H. (2018). *Markov models & optimization*. Routledge.

Dayan, P., & Balleine, B. W. (2002). Reward, Motivation, and Reinforcement Learning. *Neuron*, *36*(2), 285–298. https://doi.org/10.1016/S0896-6273(02)00963-7

de Vries, G. J., & Forger, N. G. (2015). Sex differences in the brain: A whole body perspective. *Biology of Sex Differences*, *6*, 1–15.

De Vries, S. E. J., Lecoq, J. A., Buice, M. A., Groblewski, P. A., Ocker, G. K., Oliver, M., Feng, D., Cain, N., Ledochowitsch, P., Millman, D., Roll, K., Garrett, M., Keenan, T., Kuan, L., Mihalas, S., Olsen, S., Thompson, C., Wakeman, W., Waters, J., … Koch, C. (2020). A large-scale standardized physiological survey reveals functional organization of the mouse visual cortex. *Nature Neuroscience*, *23*(1), 138–151. https://doi.org/10.1038/s41593-019-0550-9

De Winkel, K. N., Edel, E., Happee, R., & Bülthoff, H. H. (2021). Multisensory Interactions in Head and Body Centered Perception of Verticality. *Frontiers in Neuroscience*, *14*, 599226. https://doi.org/10.3389/fnins.2020.599226

Dean, M. D., Ardlie, K. G., & Nachman, M. W. (2006). The frequency of multiple paternity suggests that sperm competition is common in house mice (*Mus domesticus*). *Molecular Ecology*, *15*(13), 4141–4151. https://doi.org/10.1111/j.1365-294X.2006.03068.x

Deitch, D., Rubin, A., & Ziv, Y. (2021). Representational drift in the mouse visual cortex. *Current Biology*, *31*(19), 4327-4339.e6. https://doi.org/10.1016/j.cub.2021.07.062

Denker, J., & LeCun, Y. (1990). Transforming neural-net output levels to probability distributions. *Advances in Neural Information Processing Systems*, *3*.

Dennis, E. J., El Hady, A., Michaiel, A., Clemens, A., Tervo, D. R. G., Voigts, J., & Datta, S. R. (2021). Systems Neuroscience of Natural Behaviors in Rodents. *The Journal of Neuroscience*, *41*(5), 911–919. https://doi.org/10.1523/JNEUROSCI.1877-20.2020

Descartes, R., & Cress, D. A. (1998). *Discourse on method*. Hackett Publishing.

Deubel, H., & Schneider, W. X. (1996). Saccade target selection and object recognition: Evidence for a common attentional mechanism. *Vision Research*, *36*(12), 1827–1837. https://doi.org/10.1016/0042-6989(95)00294-4

Dewsbury, D. A. (1972). Patterns of Copulatory Behavior in Male Mammals. *The Quarterly Review of Biology*, *47*(1), 1–33. https://doi.org/10.1086/407097

Dewsbury, D. A. (1975). Diversity and Adaptation in Rodent Copulatory Behavior: Species differences provide ideal material for a broadened comparative psychology. *Science*, *190*(4218), 947–954.

DiCarlo, J. J., Zoccolan, D., & Rust, N. C. (2012). How Does the Brain Solve Visual Object Recognition? *Neuron*, *73*(3), 415–434. https://doi.org/10.1016/j.neuron.2012.01.010

Dingle, H. (1969). A statistical and information analysis of aggressive communication in the mantis shrimp Gonodactylus bredini Manning. *Animal Behaviour*, *17*, 561–575. https://doi.org/10.1016/0003-3472(69)90165-1

Doron, G., Shin, J. N., Takahashi, N., Drüke, M., Bocklisch, C., Skenderi, S., De Mont, L., Toumazou, M., Ledderose, J., Brecht, M., Naud, R., & Larkum, M. E. (2020). Perirhinal input to neocortical layer 1 controls learning. *Science*, *370*(6523), eaaz3136. https://doi.org/10.1126/science.aaz3136

Dosovitskiy, A., Beyer, L., Kolesnikov, A., Weissenborn, D., Zhai, X., Unterthiner, T., Dehghani, M., Minderer, M., Heigold, G., & Gelly, S. (2020). An image is worth 16x16 words: Transformers for image recognition at scale. *arXiv Preprint arXiv:2010.11929*.

Dow, B. M. (2002). Orientation and color columns in monkey visual cortex. *Cerebral Cortex*, *12*(10), 1005–1015.

D'Souza, R. D., Wang, Q., Ji, W., Meier, A. M., Kennedy, H., Knoblauch, K., & Burkhalter, A. (2022). Hierarchical and nonhierarchical features of the mouse visual cortical network. *Nature Communications*, *13*(1), 503. https://doi.org/10.1038/s41467-022-28035-y

Dulac, C., & Wagner, S. (2006). Genetic Analysis of Brain Circuits Underlying Pheromone Signaling. *Annual Review of Genetics*,

40(1), 449–467. https://doi.org/10.1146/annurev.genet.39.073003.093937
Eberhard, W. (1996). *Female control: Sexual selection by cryptic female choice* (Vol. 17). Princeton University Press.
Ebitz, R. B., & Hayden, B. Y. (2021). The population doctrine in cognitive neuroscience. *Neuron*, *109*(19), 3055–3068. https://doi.org/10.1016/j.neuron.2021.07.011
Edinger, L. (1900). *The anatomy of the central nervous system of man and of vertebrates in general* (Vol. 1931). Davis.
Edwards, D. A. (1970). Induction of estrus in female mice: Estrogen-progesterone interactions. *Hormones and Behavior*, *1*(4), 299–304. https://doi.org/10.1016/0018-506X(70)90022-X
Ellis, T. N., Hofer, J. M., Timmerman-Vaughan, G. M., Coyne, C. J., & Hellens, R. P. (2011). Mendel, 150 years on. *Trends in Plant Science*, *16*(11), 590–596.
Fairhall, A. (2014). The receptive field is dead. Long live the receptive field? *Current Opinion in Neurobiology*, *25*, ix–xii. https://doi.org/10.1016/j.conb.2014.02.001
Fausto-Sterling, A. (2000). *Sexing the body: Gender politics and the construction of sexuality*. Basic books.
Felleman, D. J., & Essen, D. C. V. (1991). Distributed hierarchical processing in the primate cerebral cortex. *Cerebral Cortex*, *1*(1), 1–47.
Ferster, D., & Miller, K. D. (2000). Neural mechanisms of orientation selectivity in the visual cortex. *Annual Review of Neuroscience*, *23*(1), 441–471.
Festa, D., Aschner, A., Davila, A., Kohn, A., & Coen-Cagli, R. (2021). Neuronal variability reflects probabilistic inference tuned to natural image statistics. *Nature Communications*, *12*(1), 3635. https://doi.org/10.1038/s41467-021-23838-x
Fetsch, C. R. (2016). The importance of task design and behavioral control for understanding the neural basis of cognitive functions. *Neurobiology of Cognitive Behavior*, *37*, 16–22. https://doi.org/10.1016/j.conb.2015.12.002
Field, D. J. (1987). Relations between the statistics of natural images and the response properties of cortical cells. *Josa a*, *4*(12), 2379–2394.
Field, D. J. (1994). What is the goal of sensory coding? *Neural Computation*, *6*(4), 559–601.
Finger, S. (2004). Paul Broca (1824–1880). *Journal of Neurology*, *251*(6).
Fioreze, G. T. (2022). PhD Thesis. The contribution of cortical feedback projections to sensory representations in the mouse primary visual cortex. http://hdl.handle.net/10362/145785
Firman, R. C., Gasparini, C., Manier, M. K., & Pizzari, T. (2017). Postmating female control: 20 years of cryptic female choice. *Trends in Ecology & Evolution*, *32*(5), 368–382.

Fischer, H. (1959). William Harvey's De motu locali animalium 1627. Edited, translated and introduced by Mrs. G. Whitteridge, D. Phil. Cambridge University Press, 4°. Published for The Royal College of Physicians, 1959. 60s. *Gesnerus*, *16*(1–2), 77–78.

Fleischman, D. S. (2016). An evolutionary behaviorist perspective on orgasm. *Socioaffective Neuroscience & Psychology*, *6*(1), 32130. https://doi.org/10.3402/snp.v6.32130

Font, E. (2023). 50 years of the Nobel Prize to Lorenz, Tinbergen, and von Frisch: Integrating behavioral function into an ethology for the 21st century. *Frontiers in Ethology*, *2*, 1270913.

Forli, A., & Yartsev, M. M. (2023). Hippocampal representation during collective spatial behaviour in bats. *Nature*, *621*(7980), 796–803.

Frank, M. J., & Badre, D. (2015). How cognitive theory guides neuroscience. *The Changing Face of Cognition*, *135*, 14–20. https://doi.org/10.1016/j.cognition.2014.11.009

Franke, A., Caelli, T., & Hudson, R. J. (2004). Analysis of movements and behavior of caribou (Rangifer tarandus) using hidden Markov models. *Ecological Modelling*, *173*(2), 259–270. https://doi.org/10.1016/j.ecolmodel.2003.06.004

Freeman, J., & Simoncelli, E. P. (2011). Metamers of the ventral stream. *Nature Neuroscience*, *14*(9), 1195–1201. https://doi.org/10.1038/nn.2889

Freeman, J., Ziemba, C. M., Heeger, D. J., Simoncelli, E. P., & Movshon, J. A. (2013). A functional and perceptual signature of the second visual area in primates. *Nature Neuroscience*, *16*(7), 974–981. https://doi.org/10.1038/nn.3402

Froudarakis, E., Berens, P., Ecker, A. S., Cotton, R. J., Sinz, F. H., Yatsenko, D., Saggau, P., Bethge, M., & Tolias, A. S. (2014). Population code in mouse V1 facilitates readout of natural scenes through increased sparseness. *Nature Neuroscience*, *17*(6), 851–857. https://doi.org/10.1038/nn.3707

Fukushima, K. (1980). Neocognitron: A self-organizing neural network model for a mechanism of pattern recognition unaffected by shift in position. *Biological Cybernetics*, *36*(4), 193–202. https://doi.org/10.1007/BF00344251

Fukushima, K., Miyake, S., & Ito, T. (1983). Neocognitron: A neural network model for a mechanism of visual pattern recognition. *IEEE Transactions on Systems, Man, and Cybernetics*, *5*, 826–834.

Fung, T. C. (2020). The microbiota-immune axis as a central mediator of gut-brain communication. *Neurobiology of Disease*, *136*, 104714. https://doi.org/10.1016/j.nbd.2019.104714

Galton, F. (1886). I. Family likeness in stature. *Proceedings of the Royal Society of London*, *40*(242–245), 42–73.

Galvani, L. (1792). *De viribus electricitatis in motu musculari commentarius*. Soc. Typogr.

Gao, P., Trautmann, E., Yu, B., Santhanam, G., Ryu, S., Shenoy, K., & Ganguli, S. (2017). A theory of multineuronal dimensionality, dynamics and measurement. *BioRxiv*, 214262.

Garrett, M. E., Nauhaus, I., Marshel, J. H., & Callaway, E. M. (2014). Topography and Areal Organization of Mouse Visual Cortex. *The Journal of Neuroscience*, *34*(37), 12587–12600. https://doi.org/10.1523/JNEUROSCI.1124-14.2014

Georgiadis, J. R., & Kringelbach, M. L. (2012). The human sexual response cycle: Brain imaging evidence linking sex to other pleasures. *Progress in Neurobiology*, *98*(1), 49–81.

Gibson, J. J. (1933). Adaptation, after-effect and contrast in the perception of curved lines. *Journal of Experimental Psychology*, *16*(1), 1.

Gilad, A., Gallero-Salas, Y., Groos, D., & Helmchen, F. (2018). Behavioral strategy determines frontal or posterior location of short-term memory in neocortex. *Neuron*, *99*(4), 814–828.

Glick, T. F. (1988). *The comparative reception of Darwinism*. University of Chicago Press.

Glickfeld, L. L., & Olsen, S. R. (2017). Higher-Order Areas of the Mouse Visual Cortex. *Annual Review of Vision Science*, *3*(1), 251–273. https://doi.org/10.1146/annurev-vision-102016-061331

Golgi, C. (1873). Sulla struttura della sostanza grigia dell cervello', Gazz. *Med Lombarda*, *33*, 224–246.

Gomez-Marin, A., & Ghazanfar, A. A. (2019). The Life of Behavior. *Neuron*, *104*(1), 25–36. https://doi.org/10.1016/j.neuron.2019.09.017

Gomez-Marin, A., Paton, J. J., Kampff, A. R., Costa, R. M., & Mainen, Z. F. (2014). Big behavioral data: Psychology, ethology and the foundations of neuroscience. *Nature Neuroscience*, *17*(11), 1455–1462. https://doi.org/10.1038/nn.3812

Guadarrama-Bazante, I. L., & Rodríguez-Manzo, G. (2019). Nucleus accumbens dopamine increases sexual motivation in sexually satiated male rats. *Psychopharmacology*, *236*, 1303–1312.

Güntürkün, O., & Bugnyar, T. (2016). Cognition without Cortex. *Trends in Cognitive Sciences*, *20*(4), 291–303. https://doi.org/10.1016/j.tics.2016.02.001

Guo, K., Robertson, R. G., Mahmoodi, S., & Young, M. P. (2005). Centre-surround interactions in response to natural scene stimulation in the primary visual cortex. *European Journal of Neuroscience*, *21*(2), 536–548. https://doi.org/10.1111/j.1460-9568.2005.03858.x

Guo, Z. V., Hires, S. A., Li, N., O'Connor, D. H., Komiyama, T., Ophir, E., Huber, D., Bonardi, C., Morandell, K., Gutnisky, D., Peron, S., Xu, N., Cox, J., & Svoboda, K. (2014). Procedures for Behavioral

Experiments in Head-Fixed Mice. *PLoS ONE*, *9*(2), e88678. https://doi.org/10.1371/journal.pone.0088678

Gutierrez-Castellanos, N., Husain, B. F. A., Dias, I. C., & Lima, S. Q. (2022). Neural and behavioral plasticity across the female reproductive cycle. *Trends in Endocrinology & Metabolism*, *33*(11), 769–785. https://doi.org/10.1016/j.tem.2022.09.001

Haga, S., Hattori, T., Sato, T., Sato, K., Matsuda, S., Kobayakawa, R., Sakano, H., Yoshihara, Y., Kikusui, T., & Touhara, K. (2010). The male mouse pheromone ESP1 enhances female sexual receptive behaviour through a specific vomeronasal receptor. *Nature*, *466*(7302), 118–122.

Hagerty, C. M., Lees, F. C., Tieman, S. B., & Hirsch, H. V. B. (1982). Principal components analysis of cells in cat visual cortex. *Brain Research*, *251*(1), 45–53. https://doi.org/10.1016/0006-8993(82)91272-0

Hamilton, W. D., & Zuk, M. (1982). Heritable true fitness and bright birds: A role for parasites? *Science*, *218*(4570), 384–387.

Han, X., Vermaercke, B., & Bonin, V. (2022). Diversity of spatiotemporal coding reveals specialized visual processing streams in the mouse cortex. *Nature Communications*, *13*(1), 3249. https://doi.org/10.1038/s41467-022-29656-z

Hanson, J. L., & Hurley, L. M. (2012). Female Presence and Estrous State Influence Mouse Ultrasonic Courtship Vocalizations. *PLOS ONE*, *7*(7), e40782. https://doi.org/10.1371/journal.pone.0040782

Haraway, D. (1988). Situated Knowledges: The Science Question in Feminism and the Privilege of Partial Perspective. *Feminist Studies*, *14*(3), 575. https://doi.org/10.2307/3178066

Harlow, H. F. (1949). The formation of learning sets. *Psychological Review*, *56*(1), 51.

Harris, J. A., Mihalas, S., Hirokawa, K. E., Whitesell, J. D., Choi, H., Bernard, A., Bohn, P., Caldejon, S., Casal, L., Cho, A., Feiner, A., Feng, D., Gaudreault, N., Gerfen, C. R., Graddis, N., Groblewski, P. A., Henry, A. M., Ho, A., Howard, R., … Zeng, H. (2019). Hierarchical organization of cortical and thalamic connectivity. *Nature*, *575*(7781), 195–202. https://doi.org/10.1038/s41586-019-1716-z

Harrison, P. (1992). Descartes on Animals. *The Philosophical Quarterly*, *42*(167), 219. https://doi.org/10.2307/2220217

Hartley, D. (1834). *Observations on Man, his Frame, his Duty, and his Expectations*. T. Tegg and son.

Hashikawa, K., Hashikawa, Y., Tremblay, R., Zhang, J., Feng, J. E., Sabol, A., Piper, W. T., Lee, H., Rudy, B., & Lin, D. (2017). Esr1+ cells in the ventromedial hypothalamus control female aggression. *Nature Neuroscience*, *20*(11), 1580–1590.

Hassabis, D., Kumaran, D., Summerfield, C., & Botvinick, M. (2017). Neuroscience-Inspired Artificial Intelligence. *Neuron*, *95*(2), 245–258. https://doi.org/10.1016/j.neuron.2017.06.011

Hebets, E. A., & Uetz, G. W. (1999). Female responses to isolated signals from multimodal male courtship displays in the wolf spider genusSchizocosa (Araneae: Lycosidae). *Animal Behaviour*, *57*(4), 865–872.

Hegdé, J., & Felleman, D. J. (2007). Reappraising the Functional Implications of the Primate Visual Anatomical Hierarchy. *The Neuroscientist*, *13*(5), 416–421. https://doi.org/10.1177/1073858407305201

Heijkoop, R., Huijgens, P. T., & Snoeren, E. M. S. (2018). Assessment of sexual behavior in rats: The potentials and pitfalls. *Animal Model of the Year 2036: Novel Perspectives in Behavioral Neuroscience*, *352*, 70–80. https://doi.org/10.1016/j.bbr.2017.10.029

Helmholtz, H. von. (1867). Handbook of physiological optics. *Voss, Leipzig*.

Hendrickson, A. E., & White, P. O. (1964a). Promax: A quick method for rotation to oblique simple structure. *British Journal of Statistical Psychology*, *17*(1), 65–70.

Hendrickson, A. E., & White, P. O. (1964b). Promax: A quick method for rotation to oblique simple structure. *British Journal of Statistical Psychology*, *17*(1), 65–70.

Hernandez, M. E., Soto-Cid, A., Rojas, F., Pascual, L. I., Aranda-Abreu, G. E., Toledo, R., Garcia, L. I., Quintanar-Stephano, A., & Manzo, J. (2006). Prostate response to prolactin in sexually active male rats. *Reproductive Biology and Endocrinology*, *4*, 1–12.

Hinde, R. A. (1956). Ethological models and the concept of 'drive.' *The British Journal for the Philosophy of Science*, *6*(24), 321–331.

Hinde, R. A. (1966). *Animal behavior: A synthesis of ethology and comparative psychology.*

Hishida, R., Horie, M., Tsukano, H., Tohmi, M., Yoshitake, K., Meguro, R., Takebayashi, H., Yanagawa, Y., & Shibuki, K. (2019). Feedback inhibition derived from the posterior parietal cortex regulates the neural properties of the mouse visual cortex. *European Journal of Neuroscience*, *January 2018*, ejn.14424. https://doi.org/10.1111/ejn.14424

Horn, B. K., & Schunck, B. G. (1981). Determining optical flow. *Artificial Intelligence*, *17*(1–3), 185–203.

Hotelling, H. (1933). Analysis of a complex of statistical variables into principal components. *Journal of Educational Psychology*, *24*(6), 417.

Hottois, G. (1980). SECONDARITY: A CENTRAL CONCEPT OF CONTEMPORARY PHILOSOPHY. *Metaphilosophy*, *11*(2), 134–137. https://doi.org/10.1111/j.1467-9973.1980.tb00102.x

Houweling, A. R., & Brecht, M. (2008). Behavioural report of single neuron stimulation in somatosensory cortex. *Nature*, *451*(7174), 65–68.
Hromádka, T., DeWeese, M. R., & Zador, A. M. (2008). Sparse representation of sounds in the unanesthetized auditory cortex. *PLoS Biology*, *6*(1), e16.
Huang, J. Y., Wang, C., & Dreher, B. (2007). The effects of reversible inactivation of postero-temporal visual cortex on neuronal activities in cat's area 17. *Brain Research*, *1138*, 111–128.
Huang, L., Chen, X., & Shou, T. (2004). Spatial frequency-dependent feedback of visual cortical area 21a modulating functional orientation column maps in areas 17 and 18 of the cat. *Brain Research*, *998*(2), 194–201.
Hubel, D. H., & Wiesel, T. N. (1962). Receptive fields, binocular interaction and functional architecture in the cat's visual cortex. *The Journal of Physiology*, *160*(1), 106–154. https://doi.org/10.1113/jphysiol.1962.sp006837
Hubel, D. H., & Wiesel, T. N. (1963). RECEPTIVE FIELDS OF CELLS IN STRIATE CORTEX OF VERY YOUNG, VISUALLY INEXPERIENCED KITTENS. *Journal of Neurophysiology*, *26*(6), 994–1002. https://doi.org/10.1152/jn.1963.26.6.994
Hubel, D. H., & Wiesel, T. N. (1968). Receptive fields and functional architecture of monkey striate cortex. *The Journal of Physiology*, *195*(1), 215–243.
Huberman, A. D., & Niell, C. M. (2011). What can mice tell us about how vision works? *Trends in Neurosciences*, *34*(9), 464–473. https://doi.org/10.1016/j.tins.2011.07.002
Huh, C. Y. L., Peach, J. P., Bennett, C., Vega, R. M., & Hestrin, S. (2018). Feature-Specific Organization of Feedback Pathways in Mouse Visual Cortex. *Current Biology*, *28*(1), 114-120.e5. https://doi.org/10.1016/j.cub.2017.11.056
Huijgens, P. T., Guarraci, F. A., Olivier, J. D. A., & Snoeren, E. M. S. (2021). Male rat sexual behavior: Insights from inter-copulatory intervals. *Behavioural Processes*, *190*, 104458. https://doi.org/10.1016/j.beproc.2021.104458
Hull, E. M., & Dominguez, J. M. (2007). SEXUAL BEHAVIOR IN MALE RODENTS. *Hormones and Behavior*, *52*(1), 45. https://doi.org/10.1016/j.yhbeh.2007.03.030
Hull, E. M., & Dominguez, J. M. (2015). Male sexual behavior. *Knobil and Neill's Physiology of Reproduction*, 2211–2285.
Hull, E. M., Meisel, R. L., & Sachs, B. D. (2002). Male sexual behavior. In *Hormones, brain and behavior* (pp. 3–137). Elsevier.
Hull, E. M., Wood, R. I., & McKenna, K. E. (2005). Neurobiology of male sexual behavior. In *Knobil and Neill's physiology of reproduction* (pp. 1729–1824). Elsevier.
Hull, E., & Rodriguez-Manzo, G. (2009). Male sexual behavior, Horm. *Brain Behav*, *1*, 5–65.

Hupé, J., James, A., Payne, B., Lomber, S., Girard, P., & Bullier, J. (1998). Cortical feedback improves discrimination between figure and background by V1, V2 and V3 neurons. *Nature*, *394*(6695), 784–787.

Hupe, J.-M., James, A. C., Girard, P., Lomber, S. G., Payne, B. R., & Bullier, J. (2001). Feedback connections act on the early part of the responses in monkey visual cortex. *Journal of Neurophysiology*, *85*(1), 134–145.

Hurley, J. R., & Cattell, R. B. (1962). The Procrustes program: Producing direct rotation to test a hypothesized factor structure. *Behavioral Science*, *7*(2), 258.

Hutmacher, F. (2019). Why Is There So Much More Research on Vision Than on Any Other Sensory Modality? *Frontiers in Psychology*, *10*, 2246. https://doi.org/10.3389/fpsyg.2019.02246

Ishii, K. K., Osakada, T., Mori, H., Miyasaka, N., Yoshihara, Y., Miyamichi, K., & Touhara, K. (2017). A labeled-line neural circuit for pheromone-mediated sexual behaviors in mice. *Neuron*, *95*(1), 123–137.

Javadzadeh, M., & Hofer, S. B. (2022). Dynamic causal communication channels between neocortical areas. *Neuron*, *110*(15), 2470-2483.e7. https://doi.org/10.1016/j.neuron.2022.05.011

Jean, A., Bonnet, P., Liere, P., Mhaouty-Kodja, S., & Hardin-Pouzet, H. (2017). Revisiting medial preoptic area plasticity induced in male mice by sexual experience. *Scientific Reports*, *7*(1), 17846.

Jean, A., Mhaouty-Kodja, S., & Hardin-Pouzet, H. (2021). Hypothalamic cellular and molecular plasticity linked to sexual experience in male rats and mice. *Frontiers in Neuroendocrinology*, *63*, 100949. https://doi.org/10.1016/j.yfrne.2021.100949

Jelinek, F., Bahl, L., & Mercer, R. (1975). Design of a linguistic statistical decoder for the recognition of continuous speech. *IEEE Transactions on Information Theory*, *21*(3), 250–256.

Jennings, K. J., & De Lecea, L. (2020). Neural and Hormonal Control of Sexual Behavior. *Endocrinology*, *161*(10), bqaa150. https://doi.org/10.1210/endocr/bqaa150

Ji, W., Gămănuţ, R., Bista, P., D'Souza, R. D., Wang, Q., & Burkhalter, A. (2015). Modularity in the Organization of Mouse Primary Visual Cortex. *Neuron*, *87*(3), 632–643. https://doi.org/10.1016/j.neuron.2015.07.004

Johansen, J. A., Clemens, L. G., & Nunez, A. A. (2008). Characterization of copulatory behavior in female mice: Evidence for paced mating. *Physiology & Behavior*, *95*(3), 425–429.

Johnson, A. W. (2018). Characterizing ingestive behavior through licking microstructure: Underlying neurobiology and its use in the study of obesity in animal models. *Special Issue: Developmental Perspectives on Obesity and Energy Balance*, *64*, 38–47. https://doi.org/10.1016/j.ijdevneu.2017.06.012

Juavinett, A. L., Erlich, J. C., & Churchland, A. K. (2018). Decision-making behaviors: Weighing ethology, complexity, and sensorimotor compatibility. *Current Opinion in Neurobiology*, *49*, 42–50.

Kaiser, H. F. (1958). The varimax criterion for analytic rotation in factor analysis. *Psychometrika*, *23*(3), 187–200.

Kalatsky, V. a, & Stryker, M. P. (2003). New paradigm for optical imaging: Temporally encoded maps of intrinsic signal. *Neuron*, *38*(4), 529–545.

Kalueff, A. V., Stewart, A. M., Song, C., Berridge, K. C., Graybiel, A. M., & Fentress, J. C. (2016). Neurobiology of rodent self-grooming and its value for translational neuroscience. *Nature Reviews Neuroscience*, *17*(1), 45–59. https://doi.org/10.1038/nrn.2015.8

Kanizsa, G., Legrenzi, P., & Bozzi, P. (1979). Organization in vision: Essays on Gestalt perception. *(No Title)*.

Karhunen, J., & Joutsensalo, J. (1995). Generalizations of principal component analysis, optimization problems, and neural networks. *Neural Networks*, *8*(4), 549–562.

Karigo, T., Kennedy, A., Yang, B., Liu, M., Tai, D., Wahle, I. A., & Anderson, D. J. (2021). Distinct hypothalamic control of same-and opposite-sex mounting behaviour in mice. *Nature*, *589*(7841), 258–263.

Katsara, M.-A., & Nothnagel, M. (2019). True colors: A literature review on the spatial distribution of eye and hair pigmentation. *Forensic Science International: Genetics*, *39*, 109–118.

Kayser, C., Einhäuser, W., & König, P. (2003). Temporal correlations of orientations in natural scenes. *Neurocomputing*, *52–54*, 117–123. https://doi.org/10.1016/S0925-2312(02)00789-0

Keller, A. J., Roth, M. M., & Scanziani, M. (2020). Feedback generates a second receptive field in neurons of the visual cortex. *Nature*, *582*(7813), 545–549. https://doi.org/10.1038/s41586-020-2319-4

Keller, M., Douhard, Q., Baum, M. J., & Bakker, J. (2006). Destruction of the main olfactory epithelium reduces female sexual behavior and olfactory investigation in female mice. *Chemical Senses*, *31*(4), 315–323.

Kirchberger, L., Mukherjee, S., Schnabel, U. H., Van Beest, E. H., Barsegyan, A., Levelt, C. N., Heimel, J. A., Lorteije, J. A. M., Van Der Togt, C., Self, M. W., & Roelfsema, P. R. (2021). The essential role of recurrent processing for figure-ground perception in mice. *Science Advances*, *7*(27), eabe1833. https://doi.org/10.1126/sciadv.abe1833

Kirchberger, L., Mukherjee, S., Self, M. W., & Roelfsema, P. R. (2023). Contextual drive of neuronal responses in mouse V1 in the absence of feedforward input. *Science Advances*, *9*(3), eadd2498. https://doi.org/10.1126/sciadv.add2498

Kjaer, T. W., Hertz, J. A., & Richmond, B. J. (1994). Decoding cortical neuronal signals: Network models, information estimation and

spatial tuning. *Journal of Computational Neuroscience*, *1*, 109–139.
Knoedler, J. R., & Shah, N. M. (2018). Molecular mechanisms underlying sexual differentiation of the nervous system. *Current Opinion in Neurobiology*, *53*, 192–197. https://doi.org/10.1016/j.conb.2018.09.005
Kobak, D., Brendel, W., Constantinidis, C., Feierstein, C. E., Kepecs, A., Mainen, Z. F., Qi, X.-L., Romo, R., Uchida, N., & Machens, C. K. (2016). Demixed principal component analysis of neural population data. *Elife*, *5*, e10989.
Kohn, A. (2007). Visual Adaptation: Physiology, Mechanisms, and Functional Benefits. *Journal of Neurophysiology*, *97*(5), 3155–3164. https://doi.org/10.1152/jn.00086.2007
Kondo, Y., Shinoda, A., Yamanouchi, K., & Arai, Y. (1990). Role of septum and preoptic area in regulating masculine and feminine sexual behavior in male rats. *Hormones and Behavior*, *24*(3), 421–434.
Kouemou, G. L., & Dymarski, D. P. (2011). History and theoretical basics of hidden Markov models. *Hidden Markov Models, Theory and Applications*, *1*.
Krakauer, J. W., Ghazanfar, A. A., Gomez-Marin, A., MacIver, M. A., & Poeppel, D. (2017). Neuroscience Needs Behavior: Correcting a Reductionist Bias. *Neuron*, *93*(3), 480–490. https://doi.org/10.1016/j.neuron.2016.12.041
Kringelbach, M. L. (2004). Food for thought: Hedonic experience beyond homeostasis in the human brain. *Neuroscience*, *126*(4), 807–819.
Kringelbach, M. L., Stein, A., & van Hartevelt, T. J. (2012). The functional human neuroanatomy of food pleasure cycles. *Physiology & Behavior*, *106*(3), 307–316.
Kumar, M. G., Hu, M., Ramanujan, A., Sur, M., & Murthy, H. A. (2021). Functional parcellation of mouse visual cortex using statistical techniques reveals response-dependent clustering of cortical processing areas. *PLOS Computational Biology*, *17*(2), e1008548. https://doi.org/10.1371/journal.pcbi.1008548
Kvalheim, O. M. (2012). History, philosophy and mathematical basis of the latent variable approach – from a peculiarity in psychology to a general method for analysis of multivariate data. *Journal of Chemometrics*, *26*(6), 210–217. https://doi.org/10.1002/cem.2427
Lauer, J., Zhou, M., Ye, S., Menegas, W., Schneider, S., Nath, T., Rahman, M. M., Di Santo, V., Soberanes, D., & Feng, G. (2022). Multi-animal pose estimation, identification and tracking with DeepLabCut. *Nature Methods*, *19*(4), 496–504.
Lecun, Y. (1998). Gradient-Based Learning Applied to Document Recognition. *PROCEEDINGS OF THE IEEE*, *86*(11).
LeCun, Y., Bengio, Y., & Hinton, G. (2015). Deep learning. *Nature*, *521*(7553), 436–444. https://doi.org/10.1038/nature14539

LeCun, Y., Boser, B., Denker, J. S., Henderson, D., Howard, R. E., Hubbard, W., & Jackel, L. D. (1989). Backpropagation Applied to Handwritten Zip Code Recognition. *Neural Computation*, *1*(4), 541–551. https://doi.org/10.1162/neco.1989.1.4.541

Lee, E., Rhim, I., Lee, J. W., Ghim, J.-W., Lee, S., Kim, E., & Jung, M. W. (2016). Enhanced Neuronal Activity in the Medial Prefrontal Cortex during Social Approach Behavior. *Journal of Neuroscience*, *36*(26), 6926–6936. https://doi.org/10.1523/JNEUROSCI.0307-16.2016

Lee, H., Kim, D.-W., Remedios, R., Anthony, T. E., Chang, A., Madisen, L., Zeng, H., & Anderson, D. J. (2014). Scalable control of mounting and attack by Esr1+ neurons in the ventromedial hypothalamus. *Nature*, *509*(7502), 627–632.

Lee, T. S., & Mumford, D. (2003). Hierarchical Bayesian inference in the visual cortex. *Journal of the Optical Society of America A*, *20*(7), 1434. https://doi.org/10.1364/JOSAA.20.001434

Lee, W., Fu, J., Bouwman, N., Farago, P., & Curley, J. P. (2019). Temporal microstructure of dyadic social behavior during relationship formation in mice. *PLOS ONE*, *14*(12), e0220596. https://doi.org/10.1371/journal.pone.0220596

Leinders-Zufall, T., Ishii, T., Chamero, P., Hendrix, P., Oboti, L., Schmid, A., Kircher, S., Pyrski, M., Akiyoshi, S., & Khan, M. (2014). A family of nonclassical class I MHC genes contributes to ultrasensitive chemodetection by mouse vomeronasal sensory neurons. *Journal of Neuroscience*, *34*(15), 5121–5133.

Leinweber, M., Ward, D. R., Sobczak, J. M., Attinger, A., & Keller, G. B. (2017a). A Sensorimotor Circuit in Mouse Cortex for Visual Flow Predictions. *Neuron*, *95*(6), 1420-1432.e5. https://doi.org/10.1016/j.neuron.2017.08.036

Leinweber, M., Ward, D. R., Sobczak, J. M., Attinger, A., & Keller, G. B. (2017b). A Sensorimotor Circuit in Mouse Cortex for Visual Flow Predictions. *Neuron*, *95*(6), 1420-1432.e5. https://doi.org/10.1016/j.neuron.2017.08.036

Lenschow, C., & Lima, S. Q. (2020). In the mood for sex: Neural circuits for reproduction. *Current Opinion in Neurobiology*, *60*, 155–168. https://doi.org/10.1016/j.conb.2019.12.001

Lenschow, C., Mendes, A. R. P., & Lima, S. Q. (2022). Hearing, touching, and multisensory integration during mate choice. *Frontiers in Neural Circuits*, *16*, 943888. https://doi.org/10.3389/fncir.2022.943888

Lettvin, J. Y., Maturana, H. R., McCulloch, W. S., & Pitts, W. H. (1959). What the frog's eye tells the frog's brain. *Proceedings of the IRE*, *47*(11), 1940–1951.

Leventhal, A., Thompson, K., Liu, D., Zhou, Y., & Ault, S. (1995). Concomitant sensitivity to orientation, direction, and color of cells

in layers 2, 3, and 4 of monkey striate cortex. *Journal of Neuroscience*, *15*(3), 1808–1818.

Levin, D. M. (1993). *Modernity and the Hegemony of Vision*. Univ of California Press.

Levin, R. J. (2009). Revisiting post-ejaculation refractory time—What we know and what we do not know in males and in females. *The Journal of Sexual Medicine*, *6*(9), 2376–2389.

Levitis, D. A., Lidicker, W. Z., & Freund, G. (2009). Behavioural biologists do not agree on what constitutes behaviour. *Animal Behaviour*, *78*(1), 103–110. https://doi.org/10.1016/j.anbehav.2009.03.018

Li, Y., Mathis, A., Grewe, B. F., Osterhout, J. A., Ahanonu, B., Schnitzer, M. J., Murthy, V. N., & Dulac, C. (2017). Neuronal representation of social information in the medial amygdala of awake behaving mice. *Cell*, *171*(5), 1176–1190.

Liang, F., Li, H., Chou, X., Zhou, M., Zhang, N. K., Xiao, Z., Zhang, K. K., Tao, H. W., & Zhang, L. I. (2019). Sparse representation in awake auditory cortex: Cell-type dependence, synaptic mechanisms, developmental emergence, and modulation. *Cerebral Cortex*, *29*(9), 3796–3812.

Lindsay, G. W. (2020). Attention in psychology, neuroscience, and machine learning. *Frontiers in Computational Neuroscience*, *14*, 516985.

Liu, L., She, L., Chen, M., Liu, T., Lu, H. D., Dan, Y., & Poo, M. (2016). Spatial structure of neuronal receptive field in awake monkey secondary visual cortex (V2). *Proceedings of the National Academy of Sciences*, *113*(7), 1913–1918. https://doi.org/10.1073/pnas.1525505113

Liu, Z.-W., Jiang, N., Tao, X., Wang, X.-P., Liu, X.-M., & Xiao, S.-Y. (2020). Assessment of Sexual Behavior of Male Mice. *Journal of Visualized Experiments*, *157*, 60154. https://doi.org/10.3791/60154

Lohuis, M. N. O., Canton, A. C., Pennartz, C. M. a, & Olcese, U. (2022). Higher order visual areas enhance stimulus responsiveness in mouse primary visual cortex. *Cerebral Cortex*, *32*(15), 3269–3288. https://doi.org/10.1093/cercor/bhab414

Lopes, G., Bonacchi, N., Frazão, J., Neto, J. P., Atallah, B. V., Soares, S., Moreira, L., Matias, S., Itskov, P. M., & Correia, P. A. (2015). Bonsai: An event-based framework for processing and controlling data streams. *Frontiers in Neuroinformatics*, *9*, 7.

Lorenz, K. Z. (1937). The companion in the bird's world. *The Auk*, *54*(3), 245–273.

Lorenz, K. Z. (1950). *The comparative method in studying innate behavior patterns.*

Lorrain, D. S., Matuszewich, L., Friedman, R. D., & Hull, E. M. (1997). Extracellular serotonin in the lateral hypothalamic area is increased during the postejaculatory interval and impairs

copulation in male rats. *Journal of Neuroscience*, *17*(23), 9361–9366.
Lorrain, D. S., Riolo, J. V., Matuszewich, L., & Hull, E. M. (1999). Lateral hypothalamic serotonin inhibits nucleus accumbens dopamine: Implications for sexual satiety. *Journal of Neuroscience*, *19*(17), 7648–7652.
Machens, C. K., Romo, R., & Brody, C. D. (2010). Functional, but not anatomical, separation of “what” and “when” in prefrontal cortex. *Journal of Neuroscience*, *30*(1), 350–360.
MacKay, D. J. (2003). *Information theory, inference and learning algorithms*. Cambridge university press.
Macpherson, T., Churchland, A., Sejnowski, T., DiCarlo, J., Kamitani, Y., Takahashi, H., & Hikida, T. (2021). Natural and Artificial Intelligence: A brief introduction to the interplay between AI and neuroscience research. *Neural Networks*, *144*, 603–613. https://doi.org/10.1016/j.neunet.2021.09.018
Magnhagen, C. (1991a). Predation risk as a cost of reproduction. *Trends in Ecology & Evolution*, *6*(6), 183–186.
Magnhagen, C. (1991b). Predation risk as a cost of reproduction. *Trends in Ecology & Evolution*, *6*(6), 183–186.
Manning, A., & Dawkins, M. S. (2012). *An introduction to animal behaviour*. Cambridge University Press.
Mante, V., Sussillo, D., Shenoy, K. V., & Newsome, W. T. (2013). Context-dependent computation by recurrent dynamics in prefrontal cortex. *Nature*, *503*(7474), 78–84.
Marblestone, A. H., Wayne, G., & Kording, K. P. (2016). Toward an Integration of Deep Learning and Neuroscience. *Frontiers in Computational Neuroscience*, *10*. https://doi.org/10.3389/fncom.2016.00094
Markov, A. (2004). The extension of the law of large numbers onto quantities depending on each other. *Probability and Statistics*, 143–158.
Marks, T. D., & Goard, M. J. (2021). Stimulus-dependent representational drift in primary visual cortex. *Nature Communications*, *12*(1), 5169.
Marler, P., & Griffin, D. R. (1973). The 1973 Nobel prize for physiology or medicine. *Science*, *182*(4111), 464–466.
Marques, J. C., Li, M., Schaak, D., Robson, D. N., & Li, J. M. (2020). Internal state dynamics shape brainwide activity and foraging behaviour. *Nature*, *577*(7789), 239–243. https://doi.org/10.1038/s41586-019-1858-z
Marques, T., Nguyen, J., Fioreze, G., & Petreanu, L. (2018). The functional organization of cortical feedback inputs to primary visual cortex. *Nature Neuroscience*, *21*(5), 757–764. https://doi.org/10.1038/s41593-018-0135-z
Marr, D. (2010). *Vision: A computational investigation into the human representation and processing of visual information*. MIT press.

Marshel, J. H., Garrett, M. E., Nauhaus, I., & Callaway, E. M. (2011). Functional Specialization of Seven Mouse Visual Cortical Areas. *Neuron*, *72*(6), 1040–1054. https://doi.org/10.1016/j.neuron.2011.12.004

Martinez-Conde, S., Otero-Millan, J., & Macknik, S. L. (2013). The impact of microsaccades on vision: Towards a unified theory of saccadic function. *Nature Reviews Neuroscience*, *14*(2), 83–96. https://doi.org/10.1038/nrn3405

Martínez-García, F., Martínez-Ricós, J., Agustín-Pavón, C., Martínez-Hernández, J., Novejarque, A., & Lanuza, E. (2009). Refining the dual olfactory hypothesis: Pheromone reward and odour experience. *Behavioural Brain Research*, *200*(2), 277–286.

Martínez-Ricós, J., Agustín-Pavón, C., Lanuza, E., & Martinez-Garcia, F. (2008). Role of the vomeronasal system in intersexual attraction in female mice. *Neuroscience*, *153*(2), 383–395.

Masters, W. H., & Johnson, V. E. (1966). *Human sexual response.*

Mathis, M. W., & Mathis, A. (2020). Deep learning tools for the measurement of animal behavior in neuroscience. *Current Opinion in Neurobiology*, *60*, 1–11. https://doi.org/10.1016/j.conb.2019.10.008

Maunsell, J. H. R., & Essen, D. C. V. (1983). The Connections of the Middel Temporal Visual Area (MT) and Their Relationship to a Cortical Hie. *Journal of Neuroscience*, *3*(12), 2563–2586.

Mayrhofer, J. M., Haiss, F., Helmchen, F., & Weber, B. (2015). Sparse, reliable, and long-term stable representation of periodic whisker deflections in the mouse barrel cortex. *Neuroimage*, *115*, 52–63.

Mazo, C., Baeta, M., & Petreanu, L. (2024). Auditory cortex conveys non-topographic sound localization signals to visual cortex. *Nature Communications*, *15*(1), 3116.

Mazor, O., & Laurent, G. (2005). Transient dynamics versus fixed points in odor representations by locust antennal lobe projection neurons. *Neuron*, *48*(4), 661–673.

Mazurek, M., Kager, M., & Van Hooser, S. D. (2014). Robust quantification of orientation selectivity and direction selectivity. *Frontiers in Neural Circuits*, *8*. https://doi.org/10.3389/fncir.2014.00092

Mc Gill, T. E. (1962). Reduction in “head-mounts” in the sexual behavior of the mouse as a function of experience. *Psychological Reports*, *10*(1), 284–284.

McCarthy, M. M., & Arnold, A. P. (2011). Reframing sexual differentiation of the brain. *Nature Neuroscience*, *14*(6), 677–683. https://doi.org/10.1038/nn.2834

McClurkin, J. W., Optican, L. M., Richmond, B. J., & Gawne, T. J. (1991). Concurrent processing and complexity of temporally encoded neuronal messages in visual perception. *Science*, *253*(5020), 675–677.

McGill, T. E. (1962). Sexual Behavior in Three Inbred Strains of Mice. *Behaviour*, *19*(4), 341–350. https://doi.org/10.1163/156853962X00087

McGill, T. E. (1963). Sexual behavior of the mouse after long-term and short-term postejaculatory recovery periods. *The Journal of Genetic Psychology*, *103*(1), 53–57.

McGill, T. E., & Blight, W. C. (1963). The sexual behaviour of hybrid male mice compared with the sexual behaviour of males of the inbred parent strains. *Animal Behaviour*, *11*(4), 480–483. https://doi.org/10.1016/0003-3472(63)90265-3

Mignard, M., & Malpeli, J. G. (1991). Paths of Information Flow Through Visual Cortex. *Science*, *251*(4998), 1249–1251. https://doi.org/10.1126/science.1848727

Mill, J. S. (1843). Of the laws of the mind. *Collected Works of John Stuart Mill—A System of Logic: Book VI: On the Logic of the Moral Sciences*, 24–36.

Miller, G. A. (1952). Finite markov processes in psychology. *Psychometrika*, *17*(2), 149–167. https://doi.org/10.1007/BF02288779

Miller, N. E. (1971). Neal E. Miller: Selected papers. *(No Title)*.

Mobbs, D., Trimmer, P. C., Blumstein, D. T., & Dayan, P. (2018). Foraging for foundations in decision neuroscience: Insights from ethology. *Nature Reviews Neuroscience*, *19*(7), 419–427.

Moncho-Bogani, J., Lanuza, E., Hernandez, A., Novejarque, A., & Martınez-Garcıa, F. (2002). *Attractive properties of sexual pheromones in mice: Innate or learned?*

Moncho-Bogani, J., Martinez-Garcia, F., Novejarque, A., & Lanuza, E. (2005). Attraction to sexual pheromones and associated odorants in female mice involves activation of the reward system and basolateral amygdala. *European Journal of Neuroscience*, *21*(8), 2186–2198.

Morimoto, M. M., Uchishiba, E., & Saleem, A. B. (2021). Organization of feedback projections to mouse primary visual cortex. *iScience*, *24*(5), 102450. https://doi.org/10.1016/j.isci.2021.102450

Mosig, D. W., & Dewsbury, D. A. (1976). Studies of the copulatory behavior of house mice (Mus musculus). *Behavioral Biology*, *16*(4), 463–473. https://doi.org/10.1016/S0091-6773(76)91635-7

Mosteller, F. (1958). Stochastic Models for the Learning Process. *Proceedings of the American Philosophical Society*, *102*(1), 53–59.

Musall, S., Kaufman, M. T., Juavinett, A. L., Gluf, S., & Churchland, A. K. (2019). Single-trial neural dynamics are dominated by richly varied movements. *Nature Neuroscience*, *22*(10), 1677–1686.

Nassi, J. J., Lomber, S. G., & Born, R. T. (2013). Corticocortical Feedback Contributes to Surround Suppression in V1 of the Alert Primate.

The Journal of Neuroscience, *33*(19), 8504–8517. https://doi.org/10.1523/JNEUROSCI.5124-12.2013

Nastase, S. A., Goldstein, A., & Hasson, U. (2020). Keep it real: Rethinking the primacy of experimental control in cognitive neuroscience. *NeuroImage*, *222*, 117254. https://doi.org/10.1016/j.neuroimage.2020.117254

Nelson, R. J. (2005). *An introduction to behavioral endocrinology*. Sinauer Associates.

Niell, C. M., & Scanziani, M. (2021). How Cortical Circuits Implement Cortical Computations: Mouse Visual Cortex as a Model. *Annual Review of Neuroscience*, *44*(1), 517–546. https://doi.org/10.1146/annurev-neuro-102320-085825

Niell, C. M., & Stryker, M. P. (2008). Highly Selective Receptive Fields in Mouse Visual Cortex. *The Journal of Neuroscience*, *28*(30), 7520–7536. https://doi.org/10.1523/JNEUROSCI.0623-08.2008

Nomoto, K., & Lima, S. Q. (2015). Enhanced Male-Evoked Responses in the Ventromedial Hypothalamus of Sexually Receptive Female Mice. *Current Biology*, *25*(5), 589–594. https://doi.org/10.1016/j.cub.2014.12.048

Nowak, L., Munk, M., James, A., Girard, P., & Bullier, J. (1999). Cross-correlation study of the temporal interactions between areas V1 and V2 of the macaque monkey. *Journal of Neurophysiology*, *81*(3), 1057–1074.

Nurminen, L., Merlin, S., Bijanzadeh, M., Federer, F., & Angelucci, A. (2018). Top-down feedback controls spatial summation and response amplitude in primate visual cortex. *Nature Communications*, *9*(1), 2281. https://doi.org/10.1038/s41467-018-04500-5

Nutsch, V. L., Will, R. G., Robison, C. L., Martz, J. R., Tobiansky, D. J., & Dominguez, J. M. (2016). Colocalization of Mating-Induced Fos and D2-Like Dopamine Receptors in the Medial Preoptic Area: Influence of Sexual Experience. *Frontiers in Behavioral Neuroscience*, *10*. https://www.frontiersin.org/articles/10.3389/fnbeh.2016.00075

Nyby, J. (1983). Ultrasonic vocalizations during sex behavior of male house mice (Mus musculus): A description. *Behavioral and Neural Biology*, *39*(1), 128–134. https://doi.org/10.1016/S0163-1047(83)90722-7

Oboti, L., Pérez-Gómez, A., Keller, M., Jacobi, E., Birnbaumer, L., Leinders-Zufall, T., Zufall, F., & Chamero, P. (2014). A wide range of pheromone-stimulated sexual and reproductive behaviors in female mice depend on G protein Gαo. *BMC Biology*, *12*, 1–17.

Oh, S. W., Harris, J. A., Ng, L., Winslow, B., Cain, N., Mihalas, S., Wang, Q., Lau, C., Kuan, L., Henry, A. M., Mortrud, M. T., Ouellette, B., Nguyen, T. N., Sorensen, S. A., Slaughterbeck, C. R., Wakeman, W., Li, Y., Feng, D., Ho, A., … Zeng, H. (2014). A mesoscale

connectome of the mouse brain. *Nature*, *508*(7495), 207–214. https://doi.org/10.1038/nature13186

Ohki, K., Chung, S., Ch'ng, Y. H., Kara, P., & Reid, R. C. (2005). Functional imaging with cellular resolution reveals precise micro-architecture in visual cortex. *Nature*, *433*(7026), 597–603. https://doi.org/10.1038/nature03274

Oie, K. S., Kiemel, T., & Jeka, J. J. (2002). Multisensory fusion: Simultaneous re-weighting of vision and touch for the control of human posture. *Cognitive Brain Research*, *14*(1), 164–176. https://doi.org/10.1016/S0926-6410(02)00071-X

Olavarria, J., & Montero, V. M. (1989). Organization of visual cortex in the mouse revealed by correlating callosal and striate-extrastriate connections. *Visual Neuroscience*, *3*(1), 59–69.

Olshausen, B. A., & Field, D. J. (1996). Emergence of simple-cell receptive field properties by learning a sparse code for natural images. *Nature*, *381*(6583), 607–609.

Olsson, K. H., Kvarnemo, C., & Svensson, O. (2009). Relative costs of courtship behaviours in nest-building sand gobies. *Animal Behaviour*, *77*(2), 541–546.

Ong, W. J., & Hartley, J. (2013). *Orality and literacy*. Routledge.

Pachitariu, M., Stringer, C., Dipoppa, M., Schröder, S., Rossi, L. F., Dalgleish, H., Carandini, M., & Harris, K. D. (2017). Suite2p: Beyond 10,000 neurons with standard two-photon microscopy. *bioRxiv*, 061507. https://doi.org/10.1101/061507

Pafundo, D. E., Nicholas, M. A., Zhang, R., & Kuhlman, S. J. (2016). Top-Down-Mediated Facilitation in the Visual Cortex Is Gated by Subcortical Neuromodulation. *The Journal of Neuroscience*, *36*(10), 2904–2914. https://doi.org/10.1523/JNEUROSCI.2909-15.2016

Pak, A., Ryu, E., Li, C., & Chubykin, A. A. (2020). Top-Down Feedback Controls the Cortical Representation of Illusory Contours in Mouse Primary Visual Cortex. *The Journal of Neuroscience*, *40*(3), 648–660. https://doi.org/10.1523/JNEUROSCI.1998-19.2019

Park, J. H. (2011). Assessment of Male Sexual Behavior in Mice. In T. D. Gould (Ed.), *Mood and Anxiety Related Phenotypes in Mice* (Vol. 63, pp. 357–373). Humana Press. https://doi.org/10.1007/978-1-61779-313-4_22

Parker, P. R., Brown, M. A., Smear, M. C., & Niell, C. M. (2020). Movement-related signals in sensory areas: Roles in natural behavior. *Trends in Neurosciences*, *43*(8), 581–595.

Patton, P. (2015). Ludwig Edinger: The Vertebrate Series and Comparative Neuroanatomy. *Journal of the History of the Neurosciences*, *24*(1), 26–57. https://doi.org/10.1080/0964704X.2014.917251

Pearson, K. (1901). LIII. On lines and planes of closest fit to systems of points in space. *The London, Edinburgh, and Dublin Philosophical Magazine and Journal of Science*, *2*(11), 559–572.

Pennartz, C. M. A., Oude Lohuis, M. N., & Olcese, U. (2023). How 'visual' is the visual cortex? The interactions between the visual cortex and other sensory, motivational and motor systems as enabling factors for visual perception. *Philosophical Transactions of the Royal Society B: Biological Sciences*, *378*(1886), 20220336. https://doi.org/10.1098/rstb.2022.0336

Pereira, T. D., Shaevitz, J. W., & Murthy, M. (2020). Quantifying behavior to understand the brain. *Nature Neuroscience*, *23*(12), 1537–1549. https://doi.org/10.1038/s41593-020-00734-z

Peterka, R. J. (2002). Sensorimotor Integration in Human Postural Control. *Journal of Neurophysiology*, *88*(3), 1097–1118. https://doi.org/10.1152/jn.2002.88.3.1097

Pfaff, D., & Sakuma, Y. (1979). Facilitation of the lordosis reflex of female rats from the ventromedial nucleus of the hypothalamus. *The Journal of Physiology*, *288*(1), 189–202.

Pfaff, D. W., & Sakuma, Y. (1979). Deficit in the lordosis reflex of female rats caused by lesions in the ventromedial nucleus of the hypothalamus. *The Journal of Physiology*, *288*(1), 203–210.

Pfaus, J. G. (1996). Frank A. Beach award: Homologies of animal and human sexual behaviors. *Hormones and Behavior*, *30*(3), 187–200.

Pfaus, J. G. (2009). Pathways of Sexual Desire. *The Journal of Sexual Medicine*, *6*(6), 1506–1533. https://doi.org/10.1111/j.1743-6109.2009.01309.x

Pfaus, J. G., Kippin, T. E., Coria-Avila, G. A., Gelez, H., Afonso, V. M., Ismail, N., & Parada, M. (2012). Who, What, Where, When (and Maybe Even Why)? How the Experience of Sexual Reward Connects Sexual Desire, Preference, and Performance. *Archives of Sexual Behavior*, *41*(1), 31–62. https://doi.org/10.1007/s10508-012-9935-5

Phelps, S. M., Lydon, J. P., O'Malley, B. W., & Crews, D. (1998). Regulation of male sexual behavior by progesterone receptor, sexual experience, and androgen. *Hormones and Behavior*, *34*(3), 294–302.

Piccolino, M. (1997). Luigi Galvani and animal electricity: Two centuries after the foundation of electrophysiology. *Trends in Neurosciences*, *20*(10), 443–448. https://doi.org/10.1016/S0166-2236(97)01101-6

Picot, M., Naulé, L., Marie-Luce, C., Martini, M., Raskin, K., Grange-Messent, V., Franceschini, I., Keller, M., & Mhaouty-Kodja, S. (2014). Vulnerability of the neural circuitry underlying sexual behavior to chronic adult exposure to oral bisphenol a in male mice. *Endocrinology*, *155*(2), 502–512.

Pillmann, F. (2003). Carl Wernicke (1848–1905). *Journal of Neurology*, *250*, 1390–1391.

Plant, T. M., & Zeleznik, A. J. (2014). *Knobil and Neill's physiology of reproduction*. Academic Press.

Pologruto, T. A., Sabatini, B. L., & Svoboda, K. (2003). ScanImage: Flexible software for operating laser scanning microscopes. *BioMedical Engineering OnLine*, *2*(1), 13. https://doi.org/10.1186/1475-925X-2-13

Poo, C., & Isaacson, J. S. (2009). Odor representations in olfactory cortex:"sparse" coding, global inhibition, and oscillations. *Neuron*, *62*(6), 850–861.

Poort, J., Self, M. W., Van Vugt, B., Malkki, H., & Roelfsema, P. R. (2016). Texture segregation causes early figure enhancement and later ground suppression in areas V1 and V4 of visual cortex. *Cerebral Cortex*, *26*(10), 3964–3976.

Quan, N., & Banks, W. A. (2007). Brain-immune communication pathways. *Brain, Behavior, and Immunity*, *21*(6), 727–735. https://doi.org/10.1016/j.bbi.2007.05.005

Quiroga, R. Q., Reddy, L., Kreiman, G., Koch, C., & Fried, I. (2005). Invariant visual representation by single neurons in the human brain. *Nature*, *435*(7045), 1102–1107.

Raam, T., & Hong, W. (2021). Organization of neural circuits underlying social behavior: A consideration of the medial amygdala. *The Social Brain*, *68*, 124–136. https://doi.org/10.1016/j.conb.2021.02.008

Rabiner, L. R. (1989). A tutorial on hidden Markov models and selected applications in speech recognition. *Proceedings of the IEEE*, *77*(2), 257–286.

Rabiner, L. R., Wilpon, J. G., & Juang, B. (1986). A segmental k-means training procedure for connected word recognition. *AT&T Technical Journal*, *65*(3), 21–31.

Rabiner, 2015 https://ethw.org/First-Hand:The_Hidden_Markov_Model

Rahwan, I., Cebrian, M., Obradovich, N., Bongard, J., Bonnefon, J.-F., Breazeal, C., Crandall, J. W., Christakis, N. A., Couzin, I. D., Jackson, M. O., Jennings, N. R., Kamar, E., Kloumann, I. M., Larochelle, H., Lazer, D., McElreath, R., Mislove, A., Parkes, D. C., Pentland, A. 'Sandy,' … Wellman, M. (2019). Machine behaviour. *Nature*, *568*(7753), 477–486. https://doi.org/10.1038/s41586-019-1138-y

Ramage, D. (2007). Hidden Markov models fundamentals. *CS229 Section Notes*, *1*.

Ramon y Cajal, S. (1888). *Estructura de los centros nerviosos de las aves*.

Rao, R. P. N., & Ballard, D. H. (1999). Predictive coding in the visual cortex: A functional interpretation of some extra-classical

receptive-field effects. *Nature Neuroscience*, *2*(1), 79–87. https://doi.org/10.1038/4580

Ratiu, P., Talos, I.-F., Haker, S., Lieberman, D., & Everett, P. (2004). The tale of Phineas Gage, digitally remastered. *Journal of Neurotrauma*, *21*(5), 637–643.

Renart, A., De La Rocha, J., Bartho, P., Hollender, L., Parga, N., Reyes, A., & Harris, K. D. (2010). The asynchronous state in cortical circuits. *Science*, *327*(5965), 587–590.

Rigotti, M., Barak, O., Warden, M. R., Wang, X.-J., Daw, N. D., Miller, E. K., & Fusi, S. (2013). The importance of mixed selectivity in complex cognitive tasks. *Nature*, *497*(7451), 585–590.

Rikhye, R. V., & Sur, M. (2015). Spatial Correlations in Natural Scenes Modulate Response Reliability in Mouse Visual Cortex. *The Journal of Neuroscience*, *35*(43), 14661–14680. https://doi.org/10.1523/JNEUROSCI.1660-15.2015

Rinberg, D., Koulakov, A., & Gelperin, A. (2006). Sparse odor coding in awake behaving mice. *Journal of Neuroscience*, *26*(34), 8857–8865.

Roberts, M. J., Lowet, E., Brunet, N. M., Ter Wal, M., Tiesinga, P., Fries, P., & De Weerd, P. (2013). Robust gamma coherence between macaque V1 and V2 by dynamic frequency matching. *Neuron*, *78*(3), 523–536.

Rockland, K. S., & Pandya, D. N. (1979). Laminar origins and terminations of cortical connections of the occipital lobe in the rhesus monkey. *Brain Research*, *179*(1), 3–20.

Rodriguez-Manzo, G. (1999). Blockade of the establishment of the sexual inhibition resulting from sexual exhaustion by the Coolidge effect. *Behavioural Brain Research*, *100*(1–2), 245–254.

Rodríguez-Manzo, G., & Canseco-Alba, A. (2014). A Role for Learning and Memory in the Expression of an Innate Behavior. In *Identification of Neural Markers Accompanying Memory* (pp. 135–147). Elsevier. https://doi.org/10.1016/B978-0-12-408139-0.00009-2

Rojas-Durán, F., Pascual-Mathey, L. I., Serrano, K., Aranda-Abreu, G. E., Manzo, J., Soto-Cid, A. H., & Hernandez, M. E. (2015). Correlation of prolactin levels and PRL-receptor expression with Stat and Mapk cell signaling in the prostate of long-term sexually active rats. *Physiology & Behavior*, *138*, 188–192.

Rosenblatt, F. (1958). The perceptron: A probabilistic model for information storage and organization in the brain. *Psychological Review*, *65*(6), 386–408. https://doi.org/10.1037/h0042519

Rosenblatt, F. (1961). Principles of neurodynamics. Perceptrons and the theory of brain mechanisms," Cornell Aeronautical Lab Inc Buffalo NY. *Azerbaijan Journal of High Performance Computing*, *5*(2), 2022.

Rosenblatt, F. (1962). *Principles of neurodynamics: Perceptrons and the theory of brain mechanisms* (Vol. 55). Spartan books Washington, DC.

Rosenthal, G. G. (2017). *Mate choice: The evolution of sexual decision making from microbes to humans*. Princeton University Press.

Roughgarden, J. (2013). *Evolution's rainbow: Diversity, gender, and sexuality in nature and people*. Univ of California Press.

Rowan, W. (1952a). *The Study of Instinct*.

Rowan, W. (1952b). *The Study of Instinct*.

Rutsch, A., Kantsjö, J. B., & Ronchi, F. (2020). The Gut-Brain Axis: How Microbiota and Host Inflammasome Influence Brain Physiology and Pathology. *Frontiers in Immunology*, *11*, 604179. https://doi.org/10.3389/fimmu.2020.604179

Ryu, S., & De Marco, R. J. (2017). Performance on innate behaviour during early development as a function of stress level. *Scientific Reports*, *7*(1), 7840. https://doi.org/10.1038/s41598-017-08400-4

Sachdev, R. N., Krause, M. R., & Mazer, J. A. (2012). Surround suppression and sparse coding in visual and barrel cortices. *Frontiers in Neural Circuits*, *6*, 43.

Sachs, B. D. (2007). A contextual definition of male sexual arousal. *Hormones and Behavior*, *51*(5), 569–578. https://doi.org/10.1016/j.yhbeh.2007.03.011

Sadtler, P. T., Quick, K. M., Golub, M. D., Chase, S. M., Ryu, S. I., Tyler-Kabara, E. C., Yu, B. M., & Batista, A. P. (2014). Neural constraints on learning. *Nature*, *512*(7515), 423–426.

Sakuma, Y., & Pfaff, D. W. (1979). Facilitation of female reproductive behavior from mesensephalic central gray in the rat. *American Journal of Physiology-Regulatory, Integrative and Comparative Physiology*, *237*(5), R278–R284.

Saleem, A. B., Ayaz, A., Jeffery, K. J., Harris, K. D., & Carandini, M. (2013). Integration of visual motion and locomotion in mouse visual cortex. *Nature Neuroscience*, *16*(12), 1864–1869. https://doi.org/10.1038/nn.3567

Salzman, C. D., & Newsome, W. T. (1994). Neural mechanisms for forming a perceptual decision. *Science*, *264*(5156), 231–237.

Sandell, J. H., & Schiller, P. H. (1982). Effect of cooling area 18 on striate cortex cells in the squirrel monkey. *Journal of Neurophysiology*, *48*(1), 38–48.

Saxe, A., Nelli, S., & Summerfield, C. (2021). If deep learning is the answer, what is the question? *Nature Reviews Neuroscience*, *22*(1), 55–67. https://doi.org/10.1038/s41583-020-00395-8

Saxena, S., & Cunningham, J. P. (2019). Towards the neural population doctrine. *Current Opinion in Neurobiology*, *55*, 103–111. https://doi.org/10.1016/j.conb.2019.02.002

Schall, J. D. (2004). On building a bridge between brain and behavior. *Annu. Rev. Psychol.*, *55*, 23–50.

Schärer, L., Littlewood, D. T. J., Waeschenbach, A., Yoshida, W., & Vizoso, D. B. (2011). Mating behavior and the evolution of sperm design. *Proceedings of the National Academy of Sciences*, *108*(4), 1490–1495. https://doi.org/10.1073/pnas.1013892108

Schnabel, U. H., Bossens, C., Lorteije, J. A. M., Self, M. W., Op De Beeck, H., & Roelfsema, P. R. (2018). Figure-ground perception in the awake mouse and neuronal activity elicited by figure-ground stimuli in primary visual cortex. *Scientific Reports*, *8*(1), 17800. https://doi.org/10.1038/s41598-018-36087-8

Schulz, K. M., Molenda-Figueira, H. A., & Sisk, C. L. (2009). Back to the future: The organizational–activational hypothesis adapted to puberty and adolescence. *Hormones and Behavior*, *55*(5), 597–604. https://doi.org/10.1016/j.yhbeh.2009.03.010

Schuster-Böckler, B., & Bateman, A. (2007). An introduction to hidden Markov models. *Current Protocols in Bioinformatics*, *18*(1), A-3A.

Sebeok, T. A. (1965). *A communication network model for languages is applied to signaling behavior in animals. 147*.

Seizert, C. A. (2018). The neurobiology of the male sexual refractory period. *Neuroscience & Biobehavioral Reviews*, *92*, 350–377.

Self, M. W., Lorteije, J. A. M., Vangeneugden, J., Van Beest, E. H., Grigore, M. E., Levelt, C. N., Heimel, J. A., & Roelfsema, P. R. (2014). Orientation-Tuned Surround Suppression in Mouse Visual Cortex. *Journal of Neuroscience*, *34*(28), 9290–9304. https://doi.org/10.1523/JNEUROSCI.5051-13.2014

Semedo, J. D., Zandvakili, A., Machens, C. K., Byron, M. Y., & Kohn, A. (2019). Cortical areas interact through a communication subspace. *Neuron*, *102*(1), 249–259.

Shapiro, L. E., Austin, D., Ward, S. E., & Dewsbury, D. A. (1986). Familiarity and female mate choice in two species of voles (Microtus ochrogaster and Microtus montanus). *Animal Behaviour*, *34*, 90–97. https://doi.org/10.1016/0003-3472(86)90010-2

Shepherd, G. M. (2003). *The synaptic organization of the brain*. Oxford university press.

Sherrington, C. S. (1906). Observations on the scratch-reflex in the spinal dog. *The Journal of Physiology*, *34*(1–2), 1.

Shipp, S. (2016). Neural Elements for Predictive Coding. *Frontiers in Psychology*, *7*. https://doi.org/10.3389/fpsyg.2016.01792

Siegle, J. H., Jia, X., Durand, S., Gale, S., Bennett, C., Graddis, N., Heller, G., Ramirez, T. K., Choi, H., Luviano, J. A., Groblewski, P. A., Ahmed, R., Arkhipov, A., Bernard, A., Billeh, Y. N., Brown, D., Buice, M. A., Cain, N., Caldejon, S., … Koch, C. (2021). Survey of spiking in the mouse visual system reveals functional hierarchy. *Nature*, *592*(7852), 86–92. https://doi.org/10.1038/s41586-020-03171-x

Simmons, L. W. (2001). The evolution of polyandry: An examination of the genetic incompatibility and good-sperm hypotheses. *Journal of Evolutionary Biology*, *14*(4), 585–594. https://doi.org/10.1046/j.1420-9101.2001.00309.x

Skinner, B. F. (2014). *Contingencies of reinforcement: A theoretical analysis* (Vol. 3). BF Skinner Foundation.

Snider, A. (2022). Machine in Renaissance Sciences. In M. Sgarbi (Ed.), *Encyclopedia of Renaissance Philosophy* (pp. 2011–2020). Springer International Publishing. https://doi.org/10.1007/978-3-319-14169-5_942

Sofroniew, N. J., Flickinger, D., King, J., & Svoboda, K. (2016). A large field of view two-photon mesoscope with subcellular resolution for in vivo imaging. *eLife*, *5*, e14472. https://doi.org/10.7554/eLife.14472

Spearman, C. (1987). The proof and measurement of association between two things. *The American Journal of Psychology*, *100*(3/4), 441–471.

Stachniak, T. J., Ghosh, A., & Sternson, S. M. (2014). Chemogenetic Synaptic Silencing of Neural Circuits Localizes a Hypothalamus→Midbrain Pathway for Feeding Behavior. *Neuron*, *82*(4), 797–808. https://doi.org/10.1016/j.neuron.2014.04.008

Steinmetz, N. A., Aydin, C., Lebedeva, A., Okun, M., Pachitariu, M., Bauza, M., Beau, M., Bhagat, J., Böhm, C., & Broux, M. (2021). Neuropixels 2.0: A miniaturized high-density probe for stable, long-term brain recordings. *Science*, *372*(6539), eabf4588.

Stone, B. J., & Srodulski, S. J. (2023). Inducing Pseudopregnancy in Female Mice Without the Need for Vasectomized Males Prior to Non-Surgical Embryo Transfer or Artificial Insemination. *JoVE (Journal of Visualized Experiments)*, *197*, e65477.

Stringer, C., Michaelos, M., Tsyboulski, D., Lindo, S. E., & Pachitariu, M. (2021). High-precision coding in visual cortex. *Cell*, *184*(10), 2767-2778.e15. https://doi.org/10.1016/j.cell.2021.03.042

Stringer, C., Pachitariu, M., Steinmetz, N., Carandini, M., & Harris, K. D. (2019). High-dimensional geometry of population responses in visual cortex. *Nature*, *571*(7765), 361–365. https://doi.org/10.1038/s41586-019-1346-5

Suter, B. (2010). Ephus: Multipurpose data acquisition software for neuroscience experiments. *Frontiers in Neural Circuits*, *4*. https://doi.org/10.3389/fncir.2010.00100

Sutter, A., & Lindholm, A. K. (2016). The copulatory plug delays ejaculation by rival males and affects sperm competition outcome in house mice. *Journal of Evolutionary Biology*, *29*(8), 1617–1630. https://doi.org/10.1111/jeb.12898

Swammerdam, J. (1758). The Book of Nature II. *London (UK): Seyffert*, 122–132.

Swaney, W. T., Dubose, B. N., Curley, J. P., & Champagne, F. A. (2012). Sexual experience affects reproductive behavior and preoptic androgen receptors in male mice. *Hormones and Behavior*, *61*(4), 472–478. https://doi.org/10.1016/j.yhbeh.2012.01.001

Taziaux, M., Keller, M., Bakker, J., & Balthazart, J. (2007). Sexual behavior activity tracks rapid changes in brain estrogen concentrations. *Journal of Neuroscience*, *27*(24), 6563–6572.

Tetzlaff, T., Helias, M., Einevoll, G. T., & Diesmann, M. (2012). *Decorrelation of neural-network activity by inhibitory feedback*.

Thompson, S. M., Berkowitz, L. E., & Clark, B. J. (2017). Behavioral and neural subsystems of rodent exploration. *SI: Ethological Approaches*, *61*, 3–15. https://doi.org/10.1016/j.lmot.2017.03.009

Thurstone, L. L. (1931). Multiple factor analysis. *Psychological Review*, *38*(5), 406.

Thurstone, L. L. (1947). *Multiple-factor analysis; a development and expansion of The Vectors of Mind.*

Tinbergen, N. (1963). On aims and methods of ethology. *Zeitschrift Für Tierpsychologie*, *20*(4), 410–433.

Tinbergen, N. (2020). *The study of instinct*. Pygmalion Press, an imprint of Plunkett Lake Press.

Toates, F. (2009). An Integrative Theoretical Framework for Understanding Sexual Motivation, Arousal, and Behavior. *Journal of Sex Research*, *46*(2–3), 168–193. https://doi.org/10.1080/00224490902747768

Tohmi, M., Meguro, R., Tsukano, H., Hishida, R., & Shibuki, K. (2014). The Extrageniculate Visual Pathway Generates Distinct Response Properties in the Higher Visual Areas of Mice. *Current Biology*, *24*(6), 587–597. https://doi.org/10.1016/j.cub.2014.01.061

Trezza, V., Campolongo, P., & Vanderschuren, L. J. M. J. (2011). Evaluating the rewarding nature of social interactions in laboratory animals. *Developmental Cognitive Neuroscience*, *1*(4), 444–458. https://doi.org/10.1016/j.dcn.2011.05.007

Ts'o, D., & Gilbert, C. D. (1988). The organization of chromatic and spatial interactions in the primate striate cortex. *Journal of Neuroscience*, *8*(5), 1712–1727.

Ubeda-Bañon, I., Novejarque, A., Mohedano-Moriano, A., Pro-Sistiaga, P., De La Rosa-Prieto, C., Insausti, R., Martinez-Garcia, F., Lanuza, E., & Martinez-Marcos, A. (2007). Projections from the posterolateral olfactory amygdala to the ventral striatum: Neural basis for reinforcing properties of chemical stimuli. *BMC Neuroscience*, *8*(1), 103. https://doi.org/10.1186/1471-2202-8-103

Uphouse, L. L., Wilson, J. R., & Schlesinger, K. (1970). Induction of estrus in mice: The possible role of adrenal progesterone. *Hormones and Behavior*, *1*(4), 255–264. https://doi.org/10.1016/0018-506X(70)90019-X

Vaiceliunaite, A., Erisken, S., Franzen, F., Katzner, S., & Busse, L. (2013). Spatial integration in mouse primary visual cortex. *Journal of Neurophysiology*, *110*(4), 964–972. https://doi.org/10.1152/jn.00138.2013

Valente, S., Marques, T., & Lima, S. Q. (2021). No evidence for prolactin's involvement in the post-ejaculatory refractory period. *Communications Biology*, *4*(1), 10. https://doi.org/10.1038/s42003-020-01570-4

Van Horn, S. C., Erişir, A., & Sherman, S. M. (2000). Relative distribution of synapses in the A-laminae of the lateral geniculate nucleus of the cat. *Journal of Comparative Neurology*, *416*(4), 509–520.

Ventura-Aquino, E., & Paredes, R. G. (2017). Animal Models in Sexual Medicine: The Need and Importance of Studying Sexual Motivation. *Sexual Medicine Reviews*, *5*(1), 5–19. https://doi.org/10.1016/j.sxmr.2016.07.003

Von Frisch, K. (1953). *The dancing bees*. A Harvest.

Voulodimos, A., Doulamis, N., Doulamis, A., & Protopapadakis, E. (2018). Deep Learning for Computer Vision: A Brief Review. *Computational Intelligence and Neuroscience*, *2018*, 1–13. https://doi.org/10.1155/2018/7068349

Wagor, E., Mangini, N. J., & Pearlman, A. L. (1980). Retinotopic organization of striate and extrastriate visual cortex in the mouse. *Journal of Comparative Neurology*, *193*(1), 187–202. https://doi.org/10.1002/cne.901930113

Wallen, K. (2005). Hormonal influences on sexually differentiated behavior in nonhuman primates. *Frontiers in Neuroendocrinology*, *26*(1), 7–26. https://doi.org/10.1016/j.yfrne.2005.02.001

Wang, C., Huang, J. Y., Bardy, C., FitzGibbon, T., & Dreher, B. (2010). Influence of 'feedback'signals on spatial integration in receptive fields of cat area 17 neurons. *Brain Research*, *1328*, 34–48.

Wang, C., Waleszczyk, W., Burke, W., & Dreher, B. (2000). Modulatory influence of feedback projections from area 21a on neuronal activities in striate cortex of the cat. *Cerebral Cortex*, *10*(12), 1217–1232.

Wang, Q., & Burkhalter, A. (2007). Area map of mouse visual cortex. *Journal of Comparative Neurology*, *502*(3), 339–357. https://doi.org/10.1002/cne.21286

Wang, Q., Sporns, O., & Burkhalter, A. (2012). Network Analysis of Corticocortical Connections Reveals Ventral and Dorsal Processing Streams in Mouse Visual Cortex. *The Journal of Neuroscience*, *32*(13), 4386–4399. https://doi.org/10.1523/JNEUROSCI.6063-11.2012

Weber, A. I., Krishnamurthy, K., & Fairhall, A. L. (2019). Coding Principles in Adaptation. *Annual Review of Vision Science*, *5*(1), 427–449. https://doi.org/10.1146/annurev-vision-091718-014818

Weber, E. M., & Olsson, I. A. S. (2008). Maternal behaviour in Mus musculus sp.: An ethological review. *Applied Animal Behaviour Science*, *114*(1), 1–22. https://doi.org/10.1016/j.applanim.2008.06.006

Wei, D., Talwar, V., & Lin, D. (2021). Neural circuits of social behaviors: Innate yet flexible. *Neuron*, *109*(10), 1600–1620. https://doi.org/10.1016/j.neuron.2021.02.012

Wei, Y.-C., Wang, S.-R., Jiao, Z.-L., Zhang, W., Lin, J.-K., Li, X.-Y., Li, S.-S., Zhang, X., & Xu, X.-H. (2018). Medial preoptic area in mice is capable of mediating sexually dimorphic behaviors regardless of gender. *Nature Communications*, *9*(1), 279.

Werbos, P. (1974). Beyond regression: New tools for prediction and analysis in the behavioral sciences. *PhD Thesis, Committee on Applied Mathematics, Harvard University, Cambridge, MA*.

Werner, M., Borgmann, M., & Laan, E. (2023). Sexual Pleasure Matters – and How to Define and Assess It Too. A Conceptual Framework of Sexual Pleasure and the Sexual Response. *International Journal of Sexual Health*, *35*(3), 313–340. https://doi.org/10.1080/19317611.2023.2212663

Wernicke, C. (1969). *The symptom complex of aphasia: A psychological study on an anatomical basis*. 34–97.

Wilson, J. R., Kuehn, R. E., & Beach, F. A. (1963). Modification in the sexual behavior of male rats produced by changing the stimulus female. *Journal of Comparative and Physiological Psychology*, *56*(3), 636.

Wolff, S. B., & Ölveczky, B. P. (2018). The promise and perils of causal circuit manipulations. *Current Opinion in Neurobiology*, *49*, 84–94.

Wu, M. V., & Shah, N. M. (2011). Control of masculinization of the brain and behavior. *Current Opinion in Neurobiology*, *21*(1), 116–123.

Xia, J., Marks, T. D., Goard, M. J., & Wessel, R. (2021). Stable representation of a naturalistic movie emerges from episodic activity with gain variability. *Nature Communications*, *12*(1). https://doi.org/10.1038/s41467-021-25437-2

Yamins, D. L., & DiCarlo, J. J. (2016). Eight open questions in the computational modeling of higher sensory cortex. *Current Opinion in Neurobiology*, *37*, 114–120. https://doi.org/10.1016/j.conb.2016.02.001

Yamins, D. L., Hong, H., Cadieu, C. F., Solomon, E. A., Seibert, D., & DiCarlo, J. J. (2014). Performance-optimized hierarchical models predict neural responses in higher visual cortex. *Proceedings of the National Academy of Sciences of the United States of America*, *111*(23), 8619–8624. https://doi.org/10.1073/pnas.1403112111

Yang, C. F., Chiang, M. C., Gray, D. C., Prabhakaran, M., Alvarado, M., Juntti, S. A., Unger, E. K., Wells, J. A., & Shah, N. M. (2013). Sexually dimorphic neurons in the ventromedial hypothalamus

govern mating in both sexes and aggression in males. *Cell*, *153*(4), 896–909.
Yoshida, T., & Ohki, K. (2020). Natural images are reliably represented by sparse and variable populations of neurons in visual cortex. *Nature Communications*, *11*(1), 872. https://doi.org/10.1038/s41467-020-14645-x
Young, H., Belbut, B., Baeta, M., & Petreanu, L. (2021). Laminar-specific cortico-cortical loops in mouse visual cortex. *eLife*, *10*, 1–25. https://doi.org/10.7554/eLife.59551
Yuste, R. (2015). From the neuron doctrine to neural networks. *Nature Reviews Neuroscience*, *16*(8), 487–497. https://doi.org/10.1038/nrn3962
Zhang, S. X., Lutas, A., Yang, S., Diaz, A., Fluhr, H., Nagel, G., Gao, S., & Andermann, M. L. (2021). Hypothalamic dopamine neurons motivate mating through persistent cAMP signalling. *Nature*, *597*(7875), 245–249.
Zilles, K. (2018). Brodmann: A pioneer of human brain mapping—his impact on concepts of cortical organization. *Brain*, *141*(11), 3262–3278. https://doi.org/10.1093/brain/awy273
Zong, W., Obenhaus, H. A., Skytøen, E. R., Eneqvist, H., de Jong, N. L., Vale, R., Jorge, M. R., Moser, M.-B., & Moser, E. I. (2022). Large-scale two-photon calcium imaging in freely moving mice. *Cell*, *185*(7), 1240–1256.

ITQB NOVA, Avenida da República, 2780-157 Oeiras, Portugal | Tel +351 214 469 100 | itqb.unl.pt